Consequence of FA2H Deficiency and FA2H Interaction Partners Revealed by Proteomic Analyses

Dissertation

zur

Erlangung des Doktorgrades (Dr. rer. nat.)

der

Mathematisch-Naturwissenschaftlichen Fakultät

der

Rheinischen Friedrich-Wilhelms-Universität Bonn

vorgelegt von

Robert Hardt

aus

Bonn

Bonn, 2014

Angefertigt mit Genehmigung der Mathematisch-Naturwissenschaftlichen Fakultät der Rheinischen Friedrich-Wilhelms-Universität Bonn.

1. Gutachter: PD Dr. Matthias Eckhardt

2. Gutachter: Prof. Dr. Michael Hoch

Tag der Promotion: 10.02.2015

Erscheinungsjahr: 2015

Table of contents

1 Abstract

Fatty acid-2 hydroxylase (FA2H) is a 43 kDa transmembrane protein residing in the endoplasmic reticulum. As a monooxygenase it is responsible for the alpha–hydroxylation of fatty acids, which are later incorporated into sphingolipids, thereby generating 2-OH sphingolipids. FA2H and 2-OH sphingolipids show a quite ubiquitous tissue distribution, with high amounts detectable in brain, spinal cord, skin, testis, ovary, kidney, stomach and intestine. Especially important is their role in myelin, where up to 60% of the total amount of galactoylceramide and sulfatide are alpha-hydroxylated. The importance of this modification is emphasized by the observation that humans with a FA2H deficiency develop a spastic paraplegia (autosomal recessive spastic paraplegia 35 (SPG35)). Moreover, aged FA2H-KO mice present with a similar phenotype, showing an axonal and myelin sheath degeneration in spinal cord and later also in sciatic nerves. While the symptoms of FA2H deficiency have been well described, so far almost nothing is known about the exact disease mechanisms. Furthermore, there is no knowledge about the proteins biological regulation and its protein microenvironment.

Thus, in the first part of the thesis FA2H-KO mice of different ages (6, 13 & 17 months) were examined for changes in their CNS- and PNS-myelin protein composition, which might help to better understand the observed pathology. This was achieved using a TMT 6-plex gel-free quantitative mass spectrometry approach. In the CNS this led to the identification of various protein alterations, of which some were already present in 6-month-old mice. The most prominent ones, which were also verified by Western blot, were upregulations of C1qb, C4b, ApoE, GFAP, tau protein, hinting at previously unknown roles of inflammation, astrogliosis and tau aggregation in the pathology of FA2H deficiency. In addition, a strong upregulation of one structural myelin membrane protein, Opalin/TMEM10, was observed as well. Because not much is known about this protein's function so far, its possible role in the pathology of FA2H deficiency should be elucidated by further experiments. The PNS-myelin analysis also allowed for the identification of various protein changes. Those were mainly restricted to 13- and 17-month-old animals, which is in line with the late onset of PNS-demyelination. Unfortunately, because many of the measured changes were not consistent and thus less confident, further experiments are still needed for verification.

The second part of this thesis concentrated on the discovery of protein interaction partners of FA2H. This was done, because the pathology may not be caused by the absence of 2-OH sphingolipids, but rather the loss of certain protein interactions of FA2H. For the identification, two complementary affinity purification-based screening strategies were applied in combination with quantitative mass spectrometry (SILAC-lP). In addition, a selection of the interaction partners was afterwards

successfully verified by Western blotting and bimolecular fluorescence complementation (BiFC). Finally, this for the first time allowed a description of FA2H interaction partners in mammals. Interestingly, many are involved in metabolism, transport and regulation of synthesis of sphingolipids, indicating a tight coupling of enzymes participating in these processes. Furthermore, with PGRMC1 and 2, two promising regulators of FA2H's activity were identified.

2 Introduction

2.1 Sphingolipids

2.1.1 Overview

Sphingolipids are one of the major lipid constituents of cellular membranes besides glycerolipids and sterols with an exceptional high abundance in myelin. Sphingolipids are characterized by containing a sphingoid base backbone, which in mammals usually is sphingosine (2-amino-4-octadecene-1,3-diol) (Figure 2-1B). Based on sphingosine, other sphingolipids are derived by adding a fatty acid chain via an N-amide linkage at the C_2-position and/or other molecules via the OH-group at the C_1-position (Figure 2-1A).

One of the simplest sphingolipids is ceramide, consisting only of sphingosine and a N-linked fatty acid chain. Ceramide itself is the basis for the generation of more complex sphingolipid classes, like sphingomyelins (SM) and glycosphingolipids (GSL). This is achieved by the addition of various O-linked headgroups by specific enzymes (see below). For sphingomyelins this headgroup is a phosphocholine or phosphoethanolamine, while for GSLs it is one or more sugar molecules. The simplest GSLs with only one sugar are glucosylceramide (GlcCer) and galactosylceramide (GalCer). Both can be further modified to generate other sphingolipids. From GalCer, two derivatives are derived, sulfatide (3-Sulfo-GalCer) and the ganglioside GM4. In contrast, many more different gangliosides and other complex GSLs can be produced from GlcCer. These gangliosides have headgroups consisting of larger sugar chains (≥2) and include at least one N-acetylneuraminic acid molecule (Figure 2-1C).

Another layer of complexity is given by the length, desaturation and hydroxylation of the N-linked fatty acid chain. In mammals the acid chain lengths usually vary from C_{16} to C_{36}. Desaturation can occur at various positions, while hydroxylation is mainly found at the C2-position (alpha-hydroxylation) or the last C-atom (omega-hydroxylation). The one enzyme identified so far, which is responsible for the alpha-hydroxylation, is fatty acid 2-hydroxylase (FA2H) (see: 2.3 Fatty acid 2-hydroxylase). The additional hydroxyl group is thought to allow sphingolipids to build up more hydrogen bonds with other lipids, thus increasing membrane stability (Pascher 1976; Boggs et al. 1988). The corresponding 2-OH sphingolipids are especially abundant in epidermal and nervous tissue, but they can also be found in many other tissues and culture cells (Hama 2010).

A

R group	Sphingolipid class
H	Ceramide
Phosphocholine/Phosphoethanolamine	Sphingomyelin
Sugar(s)	Glycosphingolipid

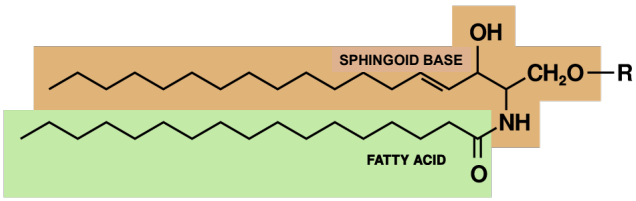

B **C**

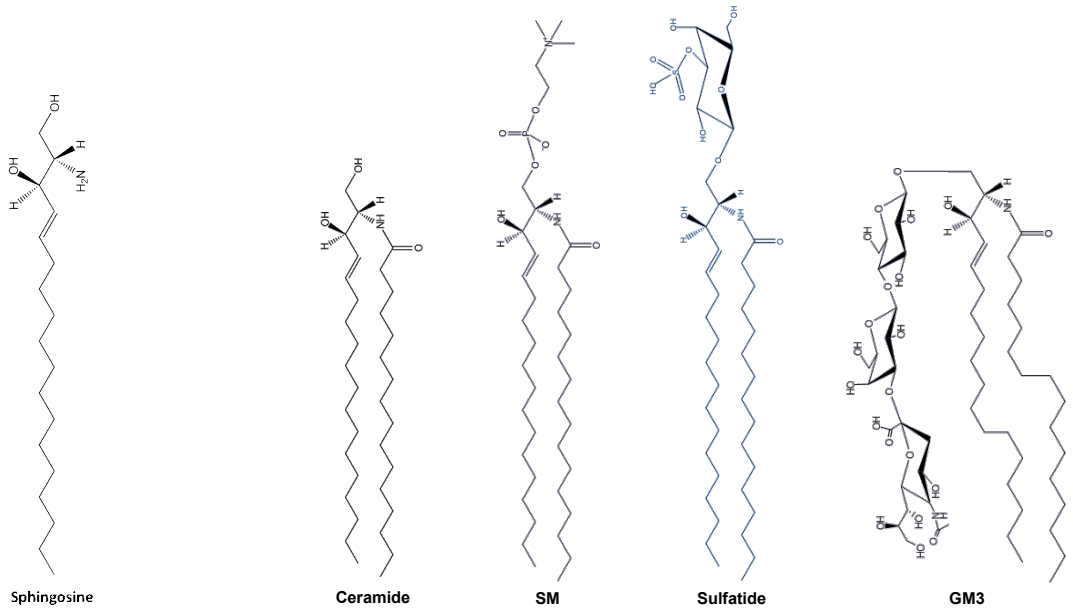

Figure 2-1: Structures of sphingosine and some sphingolipids. **(A)** General structure of various sphingolipid classes (Picture based on: http://commons.wikimedia.org/wiki/File%3ASphingolipid.png). **(B)** Molecular structure of sphingosine the most common sphingoid base in mammals. **(C)** Some common sphingolipids found in mammals. Shown are always the d18:1/d12:0-isoforms of each lipid. SM = sphingomyelin, GM3 = ganglioside GM3.

2.1.2 Sphingolipid metabolism

2.1.2.1 Synthesis

The synthesis of sphingolipids (Figure 2-2A) begins with the four-stage generation of ceramide by specific enzyme complexes at the outer leaflet of the endoplasmic reticulum (ER). First, one molecule of serine and palmitoyl-CoA are condensated by the serine palmitoyltransferase complex (SPT-complex) forming the sphingoid base 3-keto-dihydrosphingosine. The complex was initially described as a heterodimer composed of SPTLC1 together with SPTLC2 or SPTLC3, but more recent findings point at a high molecular weight complex containing also other proteins (Hanada 2003; Hornemann et al. 2007). This product is then reduced by 3-ketodihydrosphingosine reductase to dihydrosphingosine (Kihara & Igarashi 2004). Subsequently, dihydrosphingosine is acylated by one of six mammalian ceramide synthases (CerS1-6), giving rise to dihydroceramide. These six synthases mostly differ in tissue expression and the chain length of the preferred acyl-CoA substrates (Mullen

et al. 2012). Moreover, recent findings have shown that active CerS function as dimers composed of either identical or different CerS-proteins (Laviad et al. 2012). To finally obtain ceramide, dihydroceramide is subsequently reduced by a desaturase, inserting a 4,5-double bound into the sphingolipid backbone (Michel et al. 1997). As mentioned above, ceramide can then be further modified by the addition of various headgroups, giving rise to all other major sphingolipid classes.

Since most ceramide modifications are achieved by Golgi apparatus-localized enzymes, ceramide has to be transported to this compartment. This happens either by anterograde vesicular transport or by a specific cytosolic ceramide-transfer protein (CERT). Experiments indicate that both ways of transport preferentially lead to the synthesis of different ceramide derivatives. While ceramide delivered by vesicular transport is mainly used for glycosphingolipid synthesis, CERT-transported ceramide seems to be largely destined for sphingomyelin synthesis (Hanada et al. 2003).

Sphingomyelins are produced by sphingomyelin synthases of which two isoforms (SMS1 and SMS2) are so far known in mammals sphingomyelin (Huitema et al. 2004; Tafesse et al. 2006). While SMS1 seems to be restricted to the trans-Golgi compartment, SMS2 is also found at the plasma membrane (PM), with the enzymes' active sites facing the Golgi-lumen or the extracellular space, respectively. The enzymes transfer the phosphocholine or phosphoethanolamine headgroup from the corresponding glycerolipid to ceramide. Thus, one molecule of diacylglycerol is generated together with each molecule of sphingomyelin.

The Golgi-located enzyme responsible for GlcCer-synthesis, ceramide glucosyltransferase, has been known for years, but the exact mechanisms of synthesis are still under discussion. It is generally accepted that the enzymes' active site is facing the cytosol, therefore restricting GlcCer-synthesis to the outer leaflet of the Golgi apparatus (Jeckel et al. 1992). Furthermore, the various glycosyltransferases, responsible for complex GSL-synthesis, are also located to the Golgi apparatus with their catalytic sites directed to the organelles' lumen. But there are conflicting experimental results regarding the enzyme's exact location within the Golgi system and the mode of GlcCer-delivery to the Golgi lumen for complex GSL-synthesis. While one group showed that GlcCer is produced at the cis-Golgi, transported to the trans-Golgi via the lipid-binding protein FAPP2 and then flipped to the Golgi lumen (D'Angelo et al. 2007), another group postulated a trans-Golgi synthesis followed by GlcCer-redelivery to the ER, flipping into the ER and finally vesicular transport to the Golgi (Halter et al. 2007).

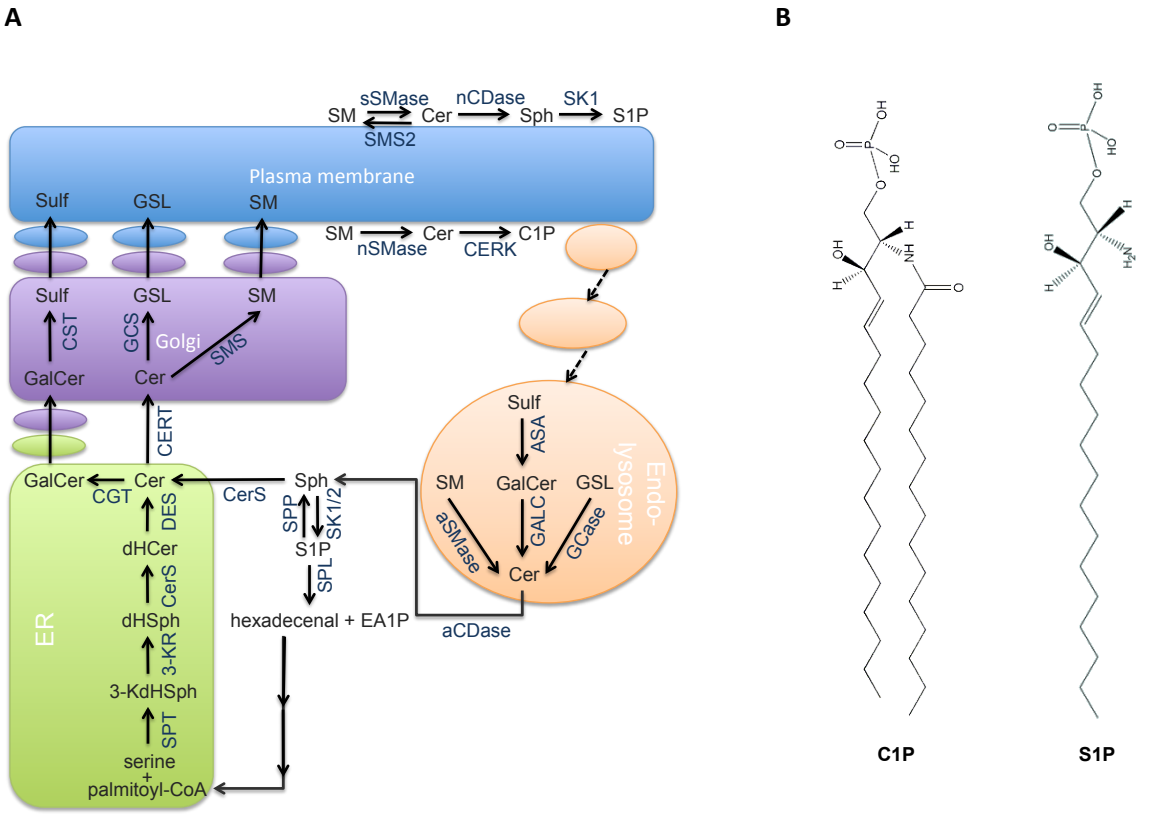

Figure 2-2: Mammalian sphingolipid metabolism. (A) Scheme of the sphingolipid metabolism within a mammalian cell. Sphingolipid synthesis starts in the ER with the condensation of serine and palmitoyl-CoA by the serine palmitoyl transferase complex (SPT). The product 3-keto-dihydrosphingosine (3-KdHSph) is then reduced by 3-keto-dihydrosphingosine reductase (3-KR) to dihydrosphingosine (dHSph), which is rapidly acylated to dihydroceramide (dHCer) by one of six ceramide synthases (CerS). Finally, dHCer is reduced by dihydroceramide desaturase (DES) to ceramide (Cer). Ceramide can afterwards be modified by the addition of various headgroups. In the ER, galactosylceramide (GalCer) can be produced by ceramide galactosyltransferase (CGT). After vesicular transport to the Golgi apparatus, GalCer can then be sulfated by cerebroside sulfotransferase (CST), thereby producing sulfatide (Sulf). Alternatively, ceramide is transported to the Golgi apparatus by ceramide transfer protein (CERT), where it is converted either to sphingomyelin (SM) by sphingomyelin synthases (SMS) or to glycosphingolipids (GSL) by a variety of glycosphingolipid synthase (GCS). In addition, ceramide kinase (CERK) in the Golgi or at the plasma membrane can phosphorylate ceramide to ceramide1-phosphate (C1P), an important signaling molecule. The degradation of sphingolipids mostly ensues at the Golgi, PM or within the endolysosome. At the plasma membrane, SM is converted back to ceramide by secretory (sSMase) or neutral sphingomyelinase (nSMase), while in the lysosome this is achieved by acidic SNmase (aSMase). Sulf and GalCer are degraded in the endolysosome. First Sulf is desulfated by arylsulfatase A (ASA), followed by GalCer's breakdown by galactosyl ceramidase (GALC). Furthermore, GSLs are broken down by different endolysosomal glycosidases (GCase). The produced ceramide can subsequently be further degraded to sphingosine (Sph) by ceramidases (CDase), neutral CDase at the PM and acidic CDase in the endolysosome. Thereafter, sphingosine can be either reused by ceramide synthases or phosphorylated by sphingosine kinases (SK1 &2). The resulting sphingosine 1-phosphate (S1P), also an important signaling molecule, can be dephosphorylated by S1P-phosphatases (SPP) or cleaved into ethanolamine 1-phosphate (EA1P) and hexadecanal by S1P lyase (SPL). Hexadecanal can then be recycled to palmitoyl-CoA in a multistep enzymatic process. (Picture modified from: (Mullen et al. 2012)). **(B)** Structures of phosphorylated sphingolipid derivatives ceramide 1-phosphate (C1P) and sphingosine 1-phosphate (S1P).

In contrast to SM, GlcCer and complex GSLs, GalCer is synthesized by ceramide galactosyltransferase (CGalT) in the lumen of the ER. The enzyme is abundantly expressed in oligodendrocytes of the central and peripheral nervous system, but can also be found in some other tissues. Correspondingly a huge amount (27%) of total myelin lipids is composed of GalCer and its sulfated derivative sulfatide

(Coetzee et al. 1996). The sulfation of GalCer is achieved in the Golgi by the enzyme cerebroside sulfotransferase (CST).

Besides being a substrate for SM- and GSL-synthesis, ceramide can also be phosphorylated to ceramide 1-phosphate (C1P) (Figure 2-2B) by ceramide kinase (CERK) at the trans-Golgi or the plasma membrane. C1P is a signaling molecule which numerous functions e.g. inhibiting apoptosis, promoting cell survival and inducing inflammatory responses. Its cellular levels are regulated trough its synthesis by CERK and breakdown by C1P-phosphatases and lipid phosphate phosphatases (Arana et al. 2010).

2.1.2.2 Degradation

The degradation of sphingolipids (Figure 2-2A) is also conducted by a variety of enzymes. Sphingomyelins are degraded by sphingomyelinases (SMase), also called sphingomyelin phosphodiesterases (SMPD), to phosphocholin and ceramide. Three major subgroups of these enzymes exist: the alkaline, acidic and neutral SMases. While alkaline SMase is only expressed in intestine and liver, where it mainly degrades extracellular SM, both ubiquitously expressed acidic and neutral SMases target endogenous SM. Acidic SMase (SMPD1) is either located in the endolysosome (aSMase) or secreted into the extracellular space (sSMase). Neutral SMases (nSMase), of which three enzymes (SMPD2, SMPD3 and SMPD4) are known, can be found at the ER, Golgi and/or PM. Defects in SMase enzymes can lead to severe diseases. For example, defects in SMPD1 lead to the accumulation of SM in the lysosome, thereby causing the lysosomal storage disorders Niemann-Pick type A and B (National Library of Medicine 2014).

The complex sugar-structures of GSLs are usually degraded in a sequential manner by different acidic glycosidases within the endolysosome. The failure of one of these enzymes normally leads to the accumulation of the respective substrate within the cell, giving rise to a so-called lipid storage disease. An overview of the numerous lysosomal lipid storage diseases can be found in the following two review articles by Ballabio & Gieselmann and Schulze & Sandhoff (Ballabio & Gieselmann 2009; Schulze & Sandhoff 2011).

Sulfatide and GalCer are also degraded to ceramide in the lysosome. First, sulfatide is desulfated to GalCer by arylsulfatase A (ASA), followed by the degalactosylation of GalCer by galactosylceramidase (GALC). The importance of these enzymes for normal cellular function is emphasized by lipid storage diseases caused by defective ASA or GALC, metachromatic leukodystrophy (see Gieselmann & Krägeloh-Mann 2010 and the references therein) or Krabbe disease (Sakai 2009).

All of the sphingolipid degradation pathways mentioned above produce ceramide. Ceramide itself is then deacylated to sphingosine by different ceramidases (CDase). These are either neutral CDase at

the outer leaflet of the PM, acidic CDase in the lysosome or one of three alkaline CDases located in ER and/or Golgi (Mao & Obeid 2008). Sphingosine is subsequently either reused for ceramide production in the so-called salvage pathway or phosphorylated by one of two ubiquitous sphingosine kinases (SK1&2) in cytosol and ER. Afterwards, sphingosine 1-phosphate (S1P) (Figure 2-2B), a very important lipid signaling molecule (Pyne & Pyne 2000; Maceyka et al. 2012), is irreversibly broken down by S1P-lyase (SPL) at the cytosolic face of the ER, yielding ethanolamine 1-phosphate (EA1P) and hexadecenal. Hexadecenal can then be converted back to palmitoyl-CoA by in a series of enzymatic reactions and subsequently used again for lipid synthesis (Nakahara et al. 2012). Alternatively S1P can be reverted back to sphingosine by certain phosphatases, which are lipid phosphate phosphatases (LPP1-3) at the cell surface or S1P-phosphatases (SSP1&2) at the cytosolic side of the ER.

2-OH sphingolipids are degraded by the same processes described above, finally leading to the release of sphingosine and 2-OH fatty acids by CDases. Afterwards, the 2-OH fatty acids may potentially be reused for sphingolipid synthesis by an unknown salvage pathway. Alternatively, they are activated to acyl-CoAs and subsequently transported to the peroxisome by an unknown process. In the peroxisome they are cleaved to formyl-CoA and n-1 aldehyde by the enzyme 2-hydroxyacyl-CoA lyase, in a process called peroxisomal α-oxidation (Foulon et al. 2005). Ultimately, the n-1 aldehyde is further degraded via peroxisomal β-oxidation to acetyl-CoA, NADH and FADH.

2.2 Myelin and demyelinating diseases

2.2.1 Overview

Myelin is the insulating material surrounding an axon, thus allowing fast saltatory signal transduction. It consists of multiple layers of plasma membrane of specialized glial cells, which are tightly wrapped around the axons in an interspaced fashion. This leads to the segmentation of axons in isolated (=internodal) and non-isolated (=nodal) regions. The glial cells responsible are oligodendrocytes in the central (CNS) and Schwann cells in the peripheral nervous system (PNS) (Figure 2-3A). While oligodendrocytes are capable of enwrapping multiple axons at a time, Schwann cells are restricted to a single axon. The segmentation enables the very rapid movement of action potentials along the axon by “jumping” from one node to the other. Therefore, this mode of signal propagation is called saltatory transmission and usually at least 10X faster than the transmission along unmyelinated axons (Hartline & Colman 2007). Myelin and saltatory transmission were initially thought to be an exclusive evolutionary achievement of vertebrates, but later discoveries showed a parallel evolution in some invertebrate species (Hartline 2008).

Besides nodes and internodes the myelinated axon can be further separated into specialized regions (Figure 2-3b). Between both regions there is a transitional area consisting of the juxtaparanode and the paranode. In addition, there are differences between CNS and PNS. In the PNS the outermost myelin layers are covered by a basal lamina and the nodes by Schwann cell microvilli. In contrast, no basal lamina is evident in the CNS and the nodes are covered by perinodal astrocytes. Detailed informations regarding these specialized regions and differences between CNS and PNS can be found in a review article by Poliak and Pelles (Poliak & Peles 2003).

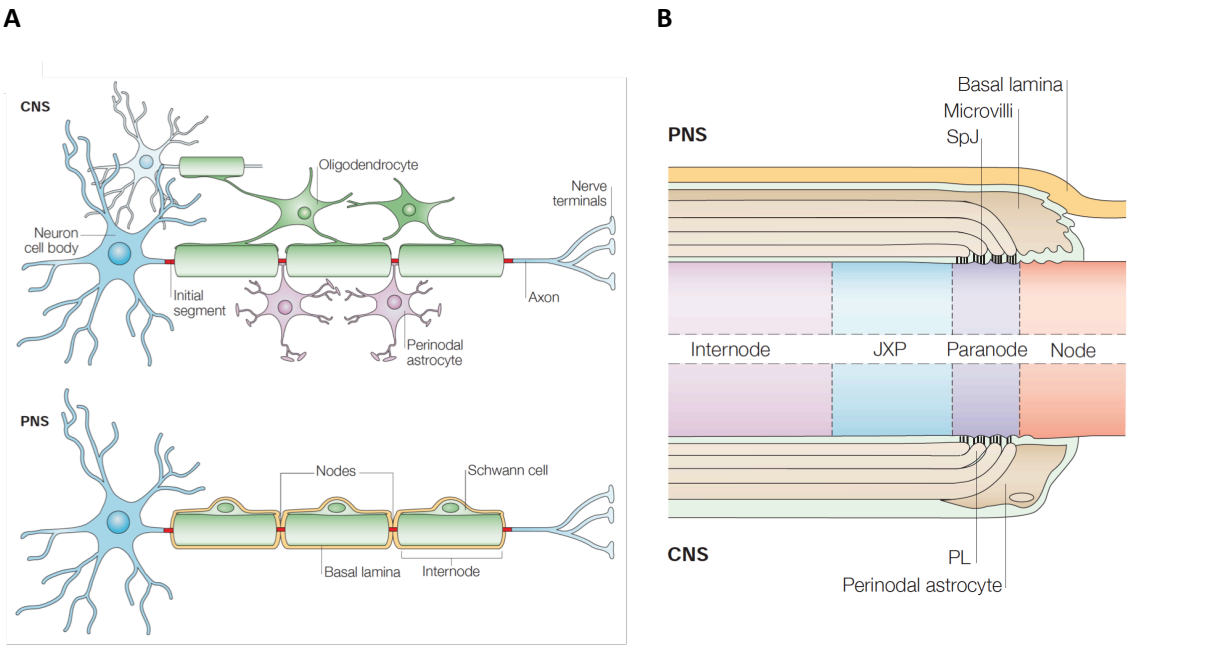

Figure 2-3: Structure of myelinated axons in CNS and PNS. (A) Myelinating glia cells, oligodendrocytes in the central nervous system (CNS) and Schwann cells in the peripheral nervous system (PNS), wrap their membrane around the axon of neurons. This segments axons in isolated (internodes) and non-isolated areas (nodes of Ranvier). While in the CNS one oligodendrocyte can engulf multiple axons with its membrane extensions, Schwann cells myelinate only a single axon. **(B)** Schematic of a longitudinal section through a myelinated axon in CNS (below) and PNS (above). Visible are the internode, followed by the adjacent juxtaparanode (JXP), paranode and the non-isolated node. Reprinted by permission from Macmillan Publishers Ltd: NATURE REVIEWS NEUROSCIENCE The local differentiation of myelinated axons at nodes of Ranvier, copyright 2003 (Poliak & Peles 2003).

Since myelin is mainly made up of plasma membrane tightly wrapped around a neurons axon, its lipid and protein composition are significantly different from the whole brain (see Table 2-1). Myelin exhibits a very high lipid content of 70% and only 30% protein, respectively. The lipids consist of ~28% cholesterol, ~43% phospholipids and a very high amount of ~28% galactolipids. These 28% galactolipids can be mainly subdivided in 23% galactosylceramide, the predominant cerebroside of the brain, and 4% sulfatide, its sulfated derivative (see also: 2.1 Sphingolipids). Considering that the phospholipid sphingomyelin is also a sphingolipid, about 35% of myelin lipids are sphingolipids. Notably as much as 60% of galactolipids can be hydroxylated at the C2-position of their N-linked fatty acid chain. This is the highest amount of 2-hydroxyacylsphingolipids (2-OH sphingolipids) found in

any mammalian tissue (Maldonado et al. 2008). Further information regarding the role of 2-OH sphingolipids and their functions in myelin is discussed below (see chapter 2.3 Fatty acid 2-hydroxylase).

Table 2-1: Lipid and protein composition of myelin, grey matter and whole brain in various mammals. Protein and lipid numbers are given in percentage dry weight, while all others are given as percentage of total lipid weight. Table adapted from: (Siegel et al. 2005).

	Myelin				
Substance*	**Human**	**Bovine**	**Rat**	**Gray matter (human)**	**Whole brain (rat)**
Protein	30	24.7	29.5	55.3	56.9
Lipid	70	75.3	70.5	32.7	37
Cholesterol	27.7	28.1	27.3	22	23
Cerebroside	22.7	24	23.7	5.4	14.6
Sulfatide	3.8	3.6	7.1	1.7	4.8
Total galactolipid	27.5	29.3	31.5	7.3	21.3
Phosphatidyethanolamine	15.6	17.4	16.7	22.7	19.8
Phosphatidylcholine	11.2	10.9	11.3	26.7	22
Sphingomyelin	7.9	7.1	3.2	6.9	3.8
Phosphatidylserine	4.8	6.5	7	8.7	7.2
Phosphatidylinositol	0.6	0.8	1.2	2.7	2.4
Total phospholipid	43.1	43	44	69.5	57.6

Recent mass spectrometry (MS) based experiments have shown that CNS- and PNS-myelin contain at least 1300 and 550 different proteins, respectively (de Monasterio-Schrader et al. 2012; Patzig et al. 2011). Still, this numbers are expected to increase due to advances in mass spectrometry sample processing and instrument performance. Accordingly, a very recent paper, comparing the human and mouse CNS-myelin proteome, documented again ~1000 proteins in mouse, but up to ~2300 proteins in humans (Gopalakrishnan et al. 2013). Intriguingly, of these many proteins only a few exhibit high abundances, being already visible after Coomassie-staining of SDS-PAGE separated myelin proteins, while the majority have very low abundances (see Figure 2-4 and (Jahn et al. 2009)). In CNS-myelin the three most abundant ones are PLP (proteolipid protein, 17%), MBP (myelin basic protein, 8%) and CNP (cyclic nucleotide phosphodiesterase, 4%), which together constitute 29% of all myelin proteins according to recent quantitative mass spectrometry measurements (Jahn et al. 2009). Interestingly, older estimations based on conventional stained SDS-PAGE gels showed even higher numbers for these three proteins: 30 – 45% PLP, 22 – 35% MBP and 4 – 15% CNPase (Jahn et al. 2009). For PNS-myelin the situation is quite similar. According to quantitative mass spectrometry data, only three proteins account for 45% of all PNS-myelin proteins. These are P0 (protein P0, 21%), Periaxin (16%) and MBP (8%). Again, previous estimations, based on densitometry measurements of conventionally stained gels, differed significantly from these findings: 45 – 70% P0, 2 – 26% MBP and 2 – 15% P2/PMP2 (myelin P2 protein) (Patzig et al. 2011).

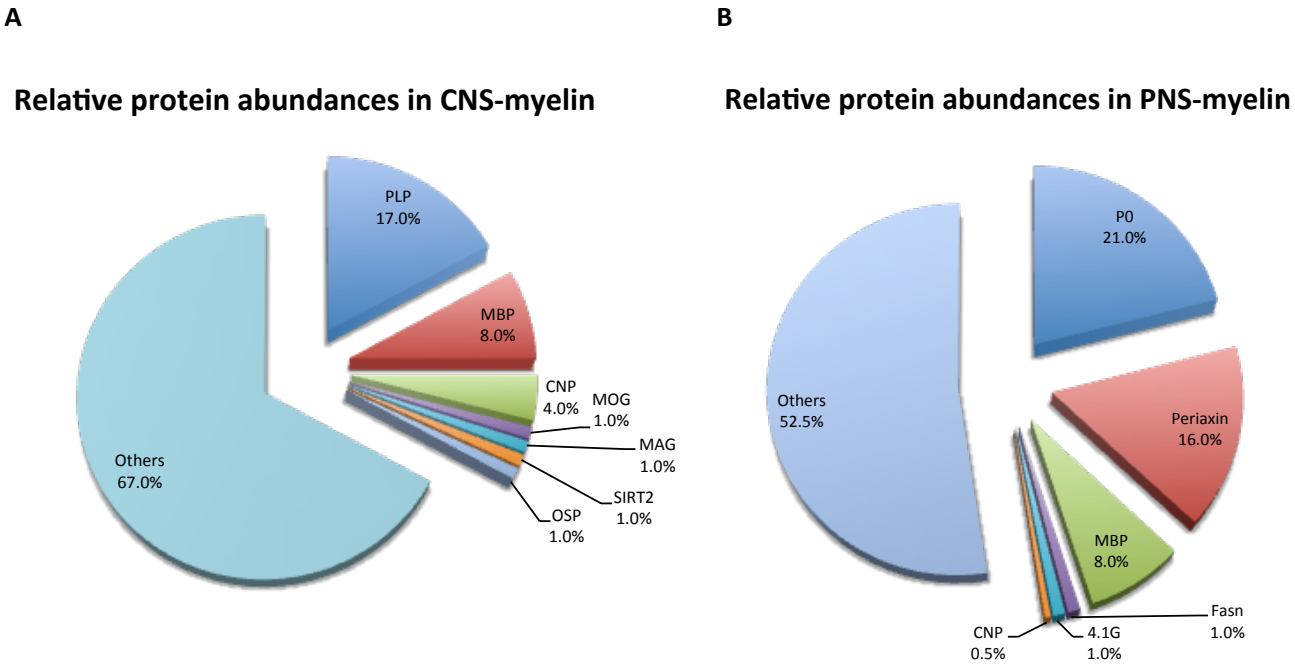

Figure 2-4: Protein composition of CNS- and PNS-myelin. (A) Pie chart depicting the relative abundances (%) of the major CNS-myelin proteins according to the LC-MS^E data published by Jahn and colleagues (Jahn et al. 2009). **(B)** Pie chart depicting the relative abundances (%) of the major PNS-myelin proteins according to the LC-MS^E data published by Patzig and colleagues (Patzig et al. 2011). PLP = myelin proteolipid protein; MBP = myelin basic protein; CNP = 2',3'-cyclic nucleotide 3'-phosphodiesterase; MOG = Myelin oligodendrocyte glycoprotein; MAG = myelin-associated glycoprotein; Sirt2 = Sirtuin2; OSP = oligodendrocyte-specific protein; P0 = myelin protein P0.; Fasn = fatty acid synthase; 4.1G = band 4.1 G-protein.

2.2.2 Demyelinating diseases

The insulation of axons by myelin is essential for effective neuronal signal propagation. Therefore, various often severe and/or lethal diseases exist, which are caused by damaged or structurally altered myelin. Demyelination can be inflicted by infectious agents, certain chemicals, autoimmune diseases or genetically inherited causes.

Important examples for demyelinating autoimmune diseases are multiple sclerosis, Guillain-Barré syndrome, transverse myelitis and acute disseminated encephalomyelitis. Examples for genetically caused diseases are Charcot-Marie-Tooth disease and the large group of leukodystrophies (Kohlschütter et al. 2010). Not surprisingly the causative genes are often coding for important structural myelin components or lipid metabolism enzymes. For example, in Pelizaeus–Merzbacher disease the most frequent mutations are causing an overexpression of the structural myelin protein PLP. Since PLP is important for the cohesion of opposing myelin membranes, deregulation of it cellular levels lead to myelin instability. Another example is metachromatic leukodystrophy, caused by a defective arylsulfatase A (ASA) enzyme. Since ASA is responsible for the degradation of the sphingolipid sulfatide, this leads to the lysosomal accumulation of sulfatide. Similarly in Krabbe disease the GalCer degrading enzyme galactosylceramidase is affected, causing lysosomal GalCer

accumulation. In both diseases the accumulation of excess amounts of sphingolipids finally leads to demyelination by mechanisms still unknown.

2.3 Fatty acid 2-hydroxylase

2.3.1 Overview

Fatty acid 2-hydroxylase (FA2H) is a 43 kDa monooxygenase residing in the ER-membrane and responsible for the synthesis of 2-hydroxyacylsphingolipids (Figure 2-5) (Hama 2010). The enzyme does not hydroxylate ceramides directly, but utilizes fatty acids. These are then incorporated into sphingolipids by the different ceramide synthases, which show the same preferences for certain acyl-chain lengths regardless of the presence or absence of a 2-OH group (Mizutani et al. 2008).

The human enzyme was first discovered in 2004 by Alderson and colleagues (Alderson et al. 2004) by searching for proteins homologues to the known yeast FA2H (FAH1/Scs7p). Using Northern blotting they also determined its expression pattern, with the highest expression in brain and colon and lower expression in testis, prostate, pancreas and kidney. One year later our group identified the highly similar murine homolog (Eckhardt et al. 2005) and allocated its expression to brain, stomach, skin, kidney and testis. In addition, a time-course analysis of its brain expression revealed an expression pattern very similar to known myelin genes.

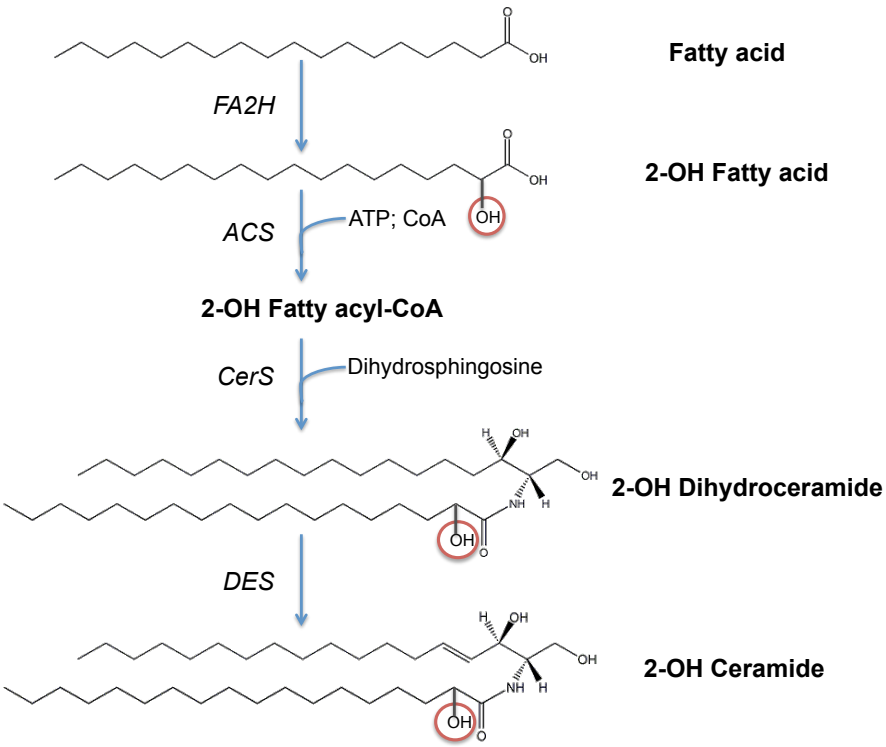

Figure 2-5: Pathway of 2-OH sphingolipid generation. The synthesis of 2-OH sphingolipids is achieved by the same enzymes responsible for non-hydroxylated sphingolipids. The only difference is that 2-OH fatty acids, generated by FA2H, are used by the ceramide synthases instead of their non-hydroxy counterparts. Shortly, free fatty acids are first hydroxylated by FA2H and subsequently activated by acyl-CoA synthethases (ACS). The activated 2-OH fatty acyl-CoAs are then linked to dihydrosphingosine by ceramide synthases (CerS) forming 2-OH dihydroceramide. This is subsequently desaturated by dihydroceramide desaturase (DES) to form 2-OH ceramide. 2-OH ceramide can then be further modified by various enzymes to form the different sphingolipid classes like sphingomyelins, glycosphingolipids, galactosylceramides and sulfatides (see Figure 2-2).

The 372 amino acids (aa) long enzyme is anchored in the ER via four transmembrane domains, with both protein termini localized to the cytosolic side of the membrane (Figure 2-6). It also contains a conserved cytochrome b_5 heme-binding domain at its N-terminus (aa 8-86), probably an electron acceptor-domain, which is essential for full enzyme activity. A catalytic sterol desaturase domain, typical for membrane-located desaturases and hydroxylases (Shanklin & Cahoon 1998), is located at the C-terminus. It encloses four conserved histidine-rich motifs ($HX_{(2-3)}(XH)H$), which are thought to bind iron. This domain probably transfers electrons, initially supplied by a reductase via the $cytb_5$-domain, to fatty acids. In addition, an ER-retention signal can be found at the enzymes C-terminus. While the enzyme can hydroxylate free fatty acids in vitro, at the moment it is still unclear, if the enzyme also does so in vivo or rather uses activated fatty acids (Alderson et al. 2005).

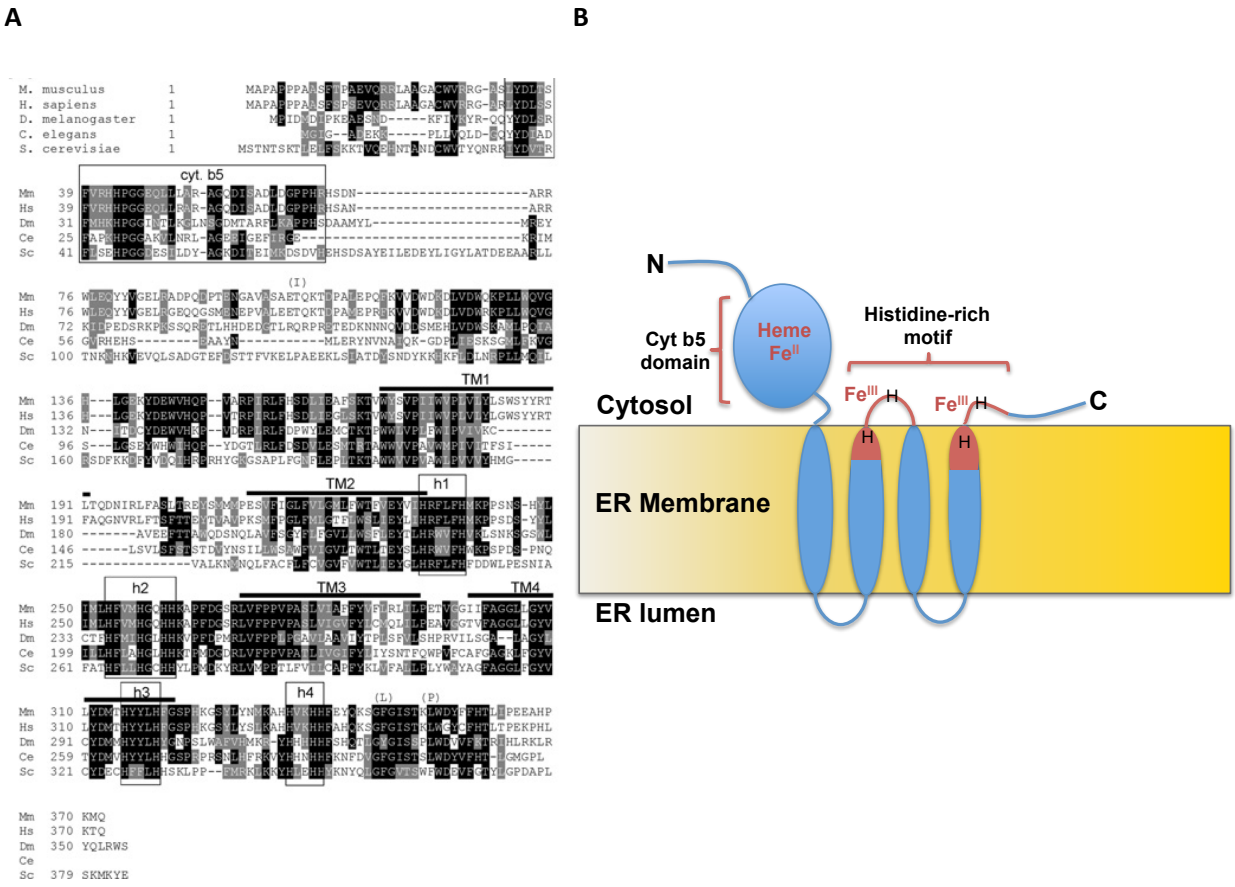

Figure 2-6: Structure of FA2H. (A) Sequence alignment of FA2H protein sequences from different species**.** Mus musculus (Mm; FVB/N strain; GenBank® AY660882), Homo sapiens (Hs; GenBank® accession no. AAH04263), Drosophila melanogaster (Dm; GenBank® AAL68319), Caenorhabditis elegans (Ce; GenBank® accession no. NP 492678) and S. cerevisiae (Sc; GenBank® NP013999). Sequence similarities are highlighted using the BOXSHADE program. Conserved domains (cytochrome b5 = cytb$_5$; histidine-rich motifs = H1-4) are indicated by boxes and putative transmembrane domains (TM1-4) by black bars on top of the protein sequences. The amino acid sequence of C57BL/6J mice (GenBank® NP 835187) differs at three positions from that of FVB/N mice. Letters on top of the mouse sequence indicate three sequence differences between FVB/N and C57BL/6J mice (GenBank® NP 835187). Picture from: (Eckhardt et al. 2005). **(B)** General structure and topology of FA2H. The protein is anchored in the ER by four transmembrane domains with its N- and C-terminus facing the cytosol. The N-terminus contains a cytochrome b5 domain, which is thought to be important for the transfer of electrons from a reductase to the enzyme. The C-terminal part of FA2H contains four transmembrane domains, which itself contain four conserved histidine-rich motifs (H). These motifs are thought to coordinate iron thereby representing the catalytic desaturase domain of the enzyme. Picture modified from: (Hama 2010).

2.3.2 FA2H-associated diseases

In the last years various mutations in the human FA2H gene have been described, causing a type of spastic paraplegia called autosomal recessive spastic paraplegia-35 (SPG35). Spastic paraplegia is a collective term for several diseases, of distinct genetic causes, which all lead to progressive lower extremity spasticity and weakness.

Patients with SPG35 (MIM: 612319), also more generally termed fatty acid hydrolase-associated neurodegeneration (FAHN), present with variable symptoms, which also vary in severity, depending on the kind of mutation in the FA2H gene. Possible symptoms are: progressive spastic paraparesis,

dysarthria, varying degrees of cognitive decline, leukodystrophy, dystonia, optic atrophy and seizures. In addition, a couple of patients exhibited neurodegeneration with brain iron accumulation (NBIA). The disease usually manifests in childhood and progresses rapidly with many patients becoming wheelchair bound until reaching adulthood.

The first study linking FA2H-mutations with spastic paraplegia was published by Edvardson and colleagues (Edvardson et al. 2008). They reported two different mutations leading to differentially severe phenotypes. One group of patients exhibited progressive spasticity combined with ataxia, dystonia, and cognitive decline, while another showed just walking difficulties and mild spasticity. The first group carried an intronic G-A transition in the FA2H gene, which leads to missplicing and therefore the production of a shortened catalytically inactive enzyme (Δaa 204–346). The mutation found in the second patient group led to a single amino acid substitution (D35Y). An in-vitro activity assay revealed that this mutation abolished the enzyme's activity. Surprisingly, subsequent analysis of fibroblast from both patient groups revealed no decrease in fatty acid 2-hydroxylase activity. This, together with findings by our group (Maier et al. 2011), hints at the existence of a second enzyme with fatty acid 2-hydroxylase activity.

The next mutations, found in two unrelated families, were reported by Dick and colleagues (Dick et al. 2008; Dick et al. 2010). These patients presented classical progressing spastic paraplegia symptoms. In addition, in some patients MRI scans revealed a leukodystrophy. The first family carried a mutation that led to amino acid exchange (R235C). Interestingly, an in-vitro functional activity assay showed that this mutant enzyme still synthesized 60 - 80% of the 2-OH ceramide levels compared to the wildtype enzyme. The second family carried an 18bp-deletion in exon 1, leading to the deletion of 6 amino acids (Δaa 53-58) within the cytochrome b5 domain. The in-vitro assay showed that this deletion totally abolished the enzyme's activity.

Until now, more than 30 FAHN-cases have been described, with patients carrying additional FA2H-mutations (Kruer et al. 2010; Garone et al. 2011; Tonelli et al. 2012; Cao et al. 2013; Rupps et al. 2013; Donkervoort et al. 2014).

2.3.3 FA2H-KO mouse models

To further elucidate the functions of FA2H, our group generated KO-mouse ($FA2H^{-/-}$) deficient for FA2H in all tissues (Zöller et al. 2008). While the animals totally lacked 2-OH sphingolipids in central and peripheral nervous system, oligodendrocyte differentiation, myelin structure and peripheral nerve conduction velocities were unaffected in up to five-month-old animals. Only very old animals (~18 months) showed signs of axonal and myelin sheath degeneration in the spinal cord and sciatic nerves. Moreover, animals older then 22 month of age developed a progressing hindlimb paralysis.

Therefore, it was concluded that 2-OH sphingolipids are not necessary for initial myelin development, but essential for its long-term stability and maintenance. Furthermore, the animals exhibited a skin phenotype, which included hyperproliferation of sebocytes with enlarged sebaceous glands, an altered sebum composition and a cycling alopecia (Maier et al. 2011). Interestingly, despite the total loss of FA2H, 2-OH sphingolipids were still present in the animals' epidermis, strongly suggesting that at least one additional fatty acid 2-hydroxylase exist.

Additional information, focusing on the CNS-function of FA2H, comes from a second mouse model deficient for FA2H only in myelinating cells ($FA2H^{flox/flox}$ Cnp1-Cre) published by Potter and colleagues (Potter et al. 2011). Using the Cre-lox system the group generated total ($FA2H^{-/-}$), as well as oligodendrocyte & Schwann cell specific FA2H-KO mice. 12-month-old mice from both types of KO-animals exhibited demyelination and axonal degeneration in the CNS. Furthermore, only minor alterations were observable in the PNS. Together with the results published by our group this indicates that the CNS-pathology manifest earlier than the PNS-pathology. In addition, in both models they also observed a previously unreported cerebrellar dysfunction manifesting with significant motor deficits. Interestingly, when assessing spatial learning and memory by behavioral testing, only $FA2H^{-/-}$ animals showed impairments, while $FA2H^{flox/flox}$ Cnp1-Cre animals performed as WT ones. This finding suggests, that the existence of 2-OH sphingolipids in other cells than oligodendrocytes is essential for memory and learning.

2.3.4 Cell signaling by 2-OH sphingolipids

While the signaling functions of ceramide and ceramide derivatives, for example ceramide 1-phosphate (reviewed in Arana et al. 2010) and sphingosine 1-phosphate (reviewed in Maceyka et al. 2012), have been studied for several years, little is known about a specific role of 2-OH sphingolipids in signal transduction. But in the last 5 - 6 years increasing evidence emerged, pointing at a role in cell differentiation and apoptosis.

First evidence linking cell differentiation and 2-OH sphingolipids came from a study on keratinocyte differentiation (Uchida et al. 2007). It was shown that FA2H and 2-OH sphingolipids, mainly ceramide and GlcCer, increased during differentiation of cultured human keratinocytes. Furthermore, FA2H-knock down (FA2H-KD) by siRNA interfered with this process by impairing the generation of epidermal lamellar membranes. Further evidence was provided by the group of Hiroko Hama when studying differentiation after dibutyryl cAMP-administration (dcAMP) in rat Schwann and in D6P2T Schwannoma cells (Maldonado et al. 2008; Alderson & Hama 2009). dcAMP, a known inductor of cell cycle exit and Schwann cell differentiation, led to the upregulation of FA2H in both cell types. This cell cycle exit could be inhibited by siRNA-mediated KD of FA2H. Interestingly, two cyclin dependent kinase inhibitors (CDKi), known to be involved in this process, were downregulated after FA2H-KD.

The latest evidence for a role of 2-OH sphingolipids in cell differentiation came from a report investigating differentiation and lipogenesis in 3T3-L1 adipocytes (Guo et al. 2010). Again, a significant increase in FA2H expression accompanied cell differentiation and this process could be blocked by siRNA-mediated FA2H-KD. In addition, in mature adipocytes FA2H-KD decreased basal and insulin-mediated glucose uptake and lipogenesis. While some results could be explained by an accelerated GLUT4 transporter endocytosis caused by increased mobility of raft lipids, a contribution by direct signaling via 2-OH sphingolipids seemed also plausible.

Regarding apoptosis, first evidence was given by Kyogashima and colleagues (Kyogashima et al. 2008), proving that fractions of kidney extract containing 2-OH ceramides induced apoptosis more strongly in three tested human tumor cell lines, than 2-OH ceramide free fractions. Two years later another group evaluated the influence of different C6 ceramides on cell growth in breast carcinoma MCF7 cells (Szulc et al. 2010). They tested both stereoisomers of 2-OH-C6 ceramide/dihydroceramide as well as non-hydroxy-C6 ceramide/dihydroceramide. Again, 2-OH ceramides exhibited a stronger growth inhibitory effect than their non-hydroxy counterparts, with the strongest generated by the natural occurring R-stereoisomeric forms. In a follow-up study by Kota et al., R- and S-sterioisomers of C16 ceramides, which are more similar to natural occurring ceramides, were tested on C6 glioma cells (Kota et al. 2013). Classical apoptosis assays and comparative mass spectrometric proteomic analysis revealed that treatment with (2'R)-2-OH-C16 ceramide lead to a strong apoptotic response, which was not observable when using the S-stereoisomer or non-hydroxy-C16 ceramide. In detail, analysis of the proteomic data and verifications by Western blot (WB) further revealed an involvement of Akt and MAP kinase pathways in the tumor cells' response to (2'R)-2-OH ceramide.

2.4 Aim of this study

The goal of this thesis was to get detailed insights into the mechanisms governing the pathology of FA2H deficiency, with the help of two mass spectrometry-based proteomic approaches.

FA2H deficiency leads to long-term myelin instability. This might be explained by the fact that non-hydroxylated sphingolipids can form less hydrogen bonds with other lipids (Pascher 1976; Boggs et al. 1988). Thus, FA2H deficiency results in less stable lipid-lipid interactions. However, myelin stability is also dependent on various proteins. For example, the presence of structural myelin proteins, like MBP or PLP, is usually indispensible for forming and maintaining a stable myelin sheath, as becomes evident by animals carrying defects in such proteins (Readhead & Hood 1990; Klugmann et al. 1997). In addition, the targeting of some myelin proteins, like MOG, MAG, CNPase, neurofascin 155 and neural cell adhesion molecule 120, seems to be largely dependent on the lipid-protein interactions

found in specialized cholesterol and sphingolipid-rich membrane microdomains called lipid-rafts (Simons & Trotter 2007; Dupree & Pomicter 2010). Intriguingly, FA2H has been shown to modulate lipid raft fluidity in adipocytes (Guo et al. 2010). Therefore, one could assume that the changed lipid composition, caused by FA2H deficiency, leads to a wrong localization of myelin proteins, which in turn elicits the long-term myelin stability. Although if such changes exist, they either seem to be more subtle or occur at later stages of life, because initial analysis of young (three-month-old) FA2H-KO mice have shown no differences in the amount of the major myelin proteins MBP, CNP, L-MAG, NCAM and MAL (Zöller et al. 2008). Thus, to clarify the role of myelin protein alterations in the pathology of FA2H deficiency, a large-scale quantitative mass spectrometry screening approach was employed. Moreover, since it was unclear when changes might occur, relatively young (6 months) as well as old (13 months) and very old mice (17 months) were analyzed in parallel.

Alternatively, it may be the case that the pathology is not caused by the absence of 2-OH sphingolipids, but instead the FA2H-protein itself. FA2H may interact with other proteins in or at the ER, as has been described for its plant homolog, which functionaly associates with the cell death suppressor protein Bax inhibitor-1 (Nagano et al. 2009). Therefore, the potential loss of one or more interactions might cause the pathology, for example by leading to a wrong localization of the interactor. Intriguingly, this could also potentially explain SPG35 patient mutations, which showed strong residual (Dick et al. 2010) or even full enzymatic activity (Kruer et al. 2010). Moreover, there is almost no information available regarding mammalian FA2H interaction partners so far. The protein-protein interactions (PPI), found in public interaction partner databases, are mostly generated automatically and not verified individually. Thus, in the second approach mammalian FA2H protein interaction partners should be identified by different co-immunoprecipitation (Co-IP) experiments in combination with quantitative mass spectrometry.

3 Material & Methods

An overview of the instruments, equipment, chemicals, solutions, buffers, antibodies and cell lines used in this thesis is given in the following sub-sections.

3.1 Material

3.1.1 Instruments

The following table gives an overview of the instruments used in this thesis' research.

Table 3-1: Alphabetical instrument list.

Application	Name/Type	Manufacturer
Centrifuges		
	Allegra X-15R	BeckmanCoulter
	Centrifuge 5415D with F45-24-11 rotor	Eppendorf
	Centrifuge 5810R with rotors • F34-6-38 • A-4-62 (swing)	Eppendorf
	L7-65 Ultracentrifuge with SW-41 rotor	BeckmanCoulter
	Optima-TLX Benchtop Ultracentrifuge with TLS-55 rotor	BeckmanCoulter
	Centrifuge 5417R	Eppendorf
	Heraeus Pico17	ThermoScientific
Cell culture		
	37 °C incubator	New Brunswick Scientific
	Laminar flow workbench	Clean Air
	Axio microscope	Zeiss
	Water bath	GFL
Chromatographic instruments		
	Easy-nLC 1000	ThermoScientific
General equipment		
	Vortex Genie 2	Scientific Industries
	Analytic scale CP 124S-OCE	Sartorius
	Digital pH-Meter 761 Calimatic	Knick
	Dry block heater	STAR LAB
	Freezer -20 °C	AEG
	Freezer -80 °C Ultra Low	Sanyo
	GENios Microplate reader	TECAN
	Hot water bath 1083	GFL
	Ice machine	Ziegra
	Infinite 200 Pro	TECAN
	Magnetic stirrer	IKA
	Mini incubator INCU-line	VWR
	Mithras LB 940 Multimode Microplate Reader	Berthold Technologies
	Motor pump	
	PC 4400 scale	Mettler
	Refrigerator	AEG
	RS-TR05 roller mixer	Phoenix Instruments
	Rotamax 120 orbital shaker	Heidolph
	Scan Speed 40 vacuum concentrator	SCANVAC
	Thermomixer Comfort 1.5 ml	Eppendorf

	Ultrasonic bath	Branson
	Ultra-Turrax homogenizer	IKA
Nucleid acid handling		
	Agarose gel casting system	Peqlab
	Electrophoresis gel system	Peqlab
	NanoDrop 2000 spectrophotometer	ThermoScientific
	Thermocycler	Biometra
	UV-imaging system	Biometra
Protein/peptide electrophoresis & Western blotting		
	Curix 60 image processor	AGFA
	FUSION-Solo chemiluminescence detection system	Peqlab/Vilber Lourmat
	PerfectBlue™ 'Semi-Dry'-Electroblotter (SEDEC M)	Peqlab
	Mini PROTEAN 3 electrophoresis system	BioRad
	Power Pac 200 power supply	BioRad
	Mini-PROTEAN® Tetra Cell electrophoresis system	BioRad
	G3100A OFFGEL Fractionator	Agilent Technologies
	Odyssey Infrared Imaging System	Licor
Mass spectrometers		
	Autoflex III smartbeam MALDI TOF/TOF	Bruker Daltonics
	LTQ Orbitrap Velos	ThermoScientific

3.1.2 Equipment

An overview of the equipment used in the presented work is given below:

Table 3-2: Alphabetical equipment list.

Application	Type	Manufacturer
Chromatography		
	Capillary column (length 15-20cm, ID 100 µm, self packed) containing Bruker-Michrom Magic C18 5 µm particles	
General		
	Filter paper	Whatman
	Dounce glas homogenisator	
	Glass flasks 50, 100, 200, 500 and 1000 ml	Schott
	Nitrocellulose blotting membrane	Whatman
	Pasteur pipettes 15 and 20 cm	Brand
	Plastic tubes 15 & 50 ml	Sarstedt
	PVDF blotting membrane	Merck Millipore
	Reaction micro tubes	Sarstedt
	Sterile filter	Sarstedt

3.1.3 Software

Table 3-3: Alphabetical software list

Application	Name	Producer	URL
Mass spectrometry data analysis			
	MaxQuant 1.4.1.2	Max Planck Institute of Biochemistry (Martinsried, Germany)	http://MaxQuant.org
	Perseus 1.4.0.12	Max Planck Institute of Biochemistry (Martinsried, Germany)	http://www.perseus-framework.org
	GOrilla (Gene Ontology enRIchment anaLysis and visuaLizAtion tool)	Weizmann Institute of Science (Tel-Aviv, Israel)	http://cbl-gorilla.cs.technion.ac.il
	PANTHER 9.0	University of Southern California, laboratory Prof. Thomas (Los Angeles, USA)	http://www.pantherdb.org
	GO Slimmer of AmiGO 1.8	Gene Ontology Consortium	http://amigo1.geneontology.org/cgi-bin/amigo/slimmer
Western blot quantification	Odyssey 3.0	Licor (USA)	
	FUSION-Capt Advance Solo 4 software	Vilber Lourmat	

3.1.4 Chemicals, Solutions and Buffers

The following table names the chemicals, solutions and buffers used in this thesis research.

Table 3-4: Alphabetical chemical, solution and buffer list.

Application	Name/Type	Supplier	Contents
Agarose gel electrophoresis			
	10X TAE		400 mM Tris base 200 mM acetic acid 12.7 mM EDTA
	Agarose UltraPure	LifeTechnologies	
	Ethidium bromide solution		5 mg/ml
BlueNative-PAGE			
	3X Gel buffer		200 mM 6-aminohexanoic acid 150 mM Bis-Tris

			pH 7.0
	10X Anode buffer		500 mM Bis-Tris pH 7.0
	10X BlueNative loading dye		5% w/v Coomassie brilliant blue G 500 mM 6-aminohexanoic acid 100 mM Bis-Tris pH 7.0
	10X Cathode buffer		150 mM Bis-Tris 500 mM Tricine pH 7.0
	Acrylamide-bisacrylamide mix (49.5% T, 3% C)		96 g acrylamide 3 g bisacrylamide In 200 ml ddH_2O
	Coomassie solution		0.2% (w/v) Coomassie brilliant blue G in ddH_2O
	NativeMARK™ Unstained Protein Standard	Life Technologies	
Cell lysis			
	BioID-lysis buffer		2% (v/v) Triton X-100 0.4% (w/v) SDS 500 mM NaCl 5 mM EDTA 1 mM DTT 50 mM Tris pH 7.4
	100X Halt Protease Inhibitor Cocktail	Thermo Scientific	
	RIPA buffer		0.1% (w/v) SDS 0.5% (w/v) sodium deoxycholate 1% (v/v) Nonidet-P40 150 mM NaCl 50 mM Tris pH 8.0
	StrepTag lysis buffer		1% (v/v) Triton X-100 150 mM NaCl 7.5% (v/v) glycerol 2 mM $CaCl_2$ 2 mM $MgCl_2$ 50 mM Tris pH7.4
Chromatography			
	Acetonitrile MS-grade	Biosolve BV	
	Formic acid MS-grade	Sigma Aldrich	
	Trifluoro acetic acid MS grade	Sigma Aldrich	
	Water MS-grade	Biosolve BV	

Cloning			
	Phusion High Fidelity DNA Polymerase Kit	NEB	
	QIAprep Midiprep Kit	Qiagen	
	QIAprep Miniprep Kit	Qiagen	
	QIAquick Gel Extraction Kit	Qiagen	
	QIAquick PCR Purification Kit	Qiagen	
	REDTaq Ready Mix	Sigma Aldrich	
	Restriction enzymes incl. buffers	Thermo Scientific	
	StarGate® Twin-Strep® Cloning Kit, mammalian	IBA lifesciences	
	T4-DNA ligase	Thermo Scientific	
Immunofluorescence staining			
	1000X 4',6-diamidino-2-phenylindole (DAPI) solution		1 mg/ml in ddH_2O
	4% PFA solution		4% (w/v) PFA in 1X PBS
	Ammoniumchloride solution		50 mM NH_4Cl in 1X PBS
	Blocking solution		1% (w/v) BSA in 1X TBS
	Permeablization solution		0.3% (v/v) Triton X-100 in 1X TBS
	ProLong® Gold	Life Technologies	
Mass spectrometric sample preparation			
	RapiGest surfactant	Waters	
	Trypsin from porcine pancreas (Proteomics grade)	Sigma Aldrich	
Miscellaneous			
	1X PBS		137 mM NaCl 2.7 mM KCl 10 mM Na_2HPO_4 2 mM KH_2PO_4 pH 7.4
	1X TBS pH 8.0		100 mM Tris 150 mM NaCl pH 8.0
	StrepTag washing buffer		0.1% (v/v) Triton X-100 150 mM NaCl 7.5% (v/v) glycerol 2 mM $CaCl_2$ 2 mM $MgCl_2$

			50 mM Tris pH8.0
Mouse genotyping			
	Genotyping lysis buffer		150 mM NaCl 2 mM EDTA 1% (w/v) SDS 20 mM Tris pH 8.0
	Proteinase K		10 mg/ml in ddH_20
	saturated NaCl		~6 M NaCl in ddH_20
Myelin preparation			
	10.5% sucrose solution		10.5 g sucrose 1 mM EDTA add 100 ml H_2O
	30% sucrose solution		30 g sucrose 1 mM EDTA add 100 ml H_2O
	EDTA (ethylenediaminetetraacetic acid) solution		1 mM EDTA in ddH_20
	cOmplete™ protease inhibitor cocktail tablets	Roche	
Protein content estimation			
	BioRad D_C Protein Assay	Biorad	
Protein precipitation			
	Acetone	Carl Roth	
	Chloroform/Methanol (CHCl3/MeOH) mix		2 volumes chloroform (CarlRoth) 1 volumes methanol (CarlRoth)
	Methanol	CarlRoth	
SDS-PAGE & Western blotting			
	10X SDS running buffer		0.25 M Tris-Base 14.5% (v/v) glycerol 1% (w/v) SDS
	4X sample buffer (Laemmli buffer)		8% SDS 40% (v/v) glycerol 240 mM Tris-HCl pH 6.8 4% (w/v) bromphenolblue 4% (v/v) ß-mercaptoethanol
	Blotting buffer		48 mM Tris-Base 39 mM glycine 0.037% (w/v) SDS 20% (v/v) methanol pH 8.3

	PageBlue Protein Staining Solution (Coomassie-staining solution)	ThermoScientific	
	Pierce ECL Western Blotting Substrate	Thermo Scientific	
	PonceauS staining solution		0.2% (w/v) Ponceau S 3% (w/v) trichloroacetic acid (TCA)
	Strep-Tactin®-HRP conjugate	IBA lifesciences	
	Stripping buffer (Acidic)		200 mM glycine 0.1% (w/v) SDS 1% (v/v) Tween 20 pH 2.2
	TBS-T		1 X TBS 0.05% (v/v) Tween 20
Whole brain lysate			
	High-SDS buffer		8% (w/v) SDS 300 mM NaCl 100 mM Tris pH 8.0

3.1.5 Antibodies

The following table states the antibodies and their dilutions for Western blotting used in this study.

Table 3-5: Antibody list.

Type	Target name	Host species	Dilution in Western blot	Manufacturer	Product number	Misc.
Primary						
	ACSL3	rabbit	1:1000	ThermoScientific	PA5-29507	
	ALDH3A2	rabbit	1:1000	Abcam	ab113111	
	ApoE	goat	1:500	Santa Cruz Biotechnology	sc-6384	
	Biotin		1:15,000	ThermoScientific		no antibody but Streptavidin-HRP conjugate
	C1q	mouse	1:500	Hycult biotechnology b.v.	HM1096	clone JL-1
	FA2H	rabbit	1:800	Pineda (Berlin)	-	serum #2, affinity purified
	GFAP	mouse	1:1000	MP Biomedicals Immuno	691102	
	GFP	rabbit	1:5000 – 10,000	Abcam	ab290	

	MAPT (Tau)	mouse	1:1000	Dianova	DLN-08565	Ab2, clone TAU-5
	MBP	rabbit	1:10,000	Millipore	AB980	
	NF-H (NF200)	rabbit	1:1000	SigmaAldrich	N4142	
	Opalin	mouse	1:500	Santa Cruz Biotechnology	sc-374490	H12
	Periaxin (N-term.)	rabbit	1:20,000	Kindly provided by Prof. Brophy (Edinburgh)		Detects both periaxin isoforms
	PGRMC1	rabbit	1:1000	Abcam	ab80941	
	SACM1L	rabbit	1:500	ThermoScientific	PA5-26565	
	SPTLC1	rabbit	1:2000	Kindly provided by Prof. Hornemann (Zurich)		
	StrepTag	-	1:5000	IBA lifesciences	2-1502-001	no antibody but StrepTactin-HRP conjugate
Secondary						
	α-goat-DyLight800	donkey	1:10,000	ThermoScientific	SA5-10092	
	α-goat-HRP	chicken	1:5000	Dianova		
	α-mouse-DyLight649	goat	1:10,000	ThermoScientific		
	α-mouse-DyLight800	goat	1:10,000	ThermoScientific		
	α-mouse-HRP	goat	1:5000	Dianova		
	α-rabbit-DyLight649	goat	1:10,000	ThermoScientific		
	α-rabbit-DyLight800	goat	1:10,000	ThermoScientific		
	α-rabbit-HRP	goat	1:5000	Dianova		

3.1.6 Bacterial strains

The table bellow lists the bacterial strains used.

Table 3-6: Bacterial strains used in this thesis work.

Name	Description
XL1 blue	*E.coli* XL1 blue strain
***dam*- K12**	*dam* negative *E.coli* strain

3.1.7 Eukaryotic cell lines

The following cell lines were used and cultured in the indicated media.

Table 3-7: Cell lines used in alphabetical order.

Name	Description	Culture conditions
BHK	Baby hamster kidney cells	DMEM-GlutaMAX™ containing 100 U/ml Penicillin, 100 µg/ml Streptomycin and 5% FCS (heat inactivated)
HEK293	Human embryonic kidney cells 293	DMEM-GlutaMAX™ containing 100 U/ml Penicillin, 100 µg/ml Streptomycin and 10% FCS (heat inactivated)
HEK293+Twin-Strep-mFA2H stable clone A3	Human embryonic kidney cells 293 stably transfected with Twin-Strep-mFA2H	DMEM-GlutaMAX™ containing 100 U/ml Penicillin, 100 µg/ml Streptomycin and 10% FCS (heat inactivated), 500 µg/ml G418
HEK293-T	Derivative of HEK293 cells stably transfected with SV40 Large T-antigen	DMEM-GlutaMAX™ containing 100 U/ml Penicillin, 100 µg/ml Streptomycin and 10% FCS (heat inactivated)
HeLa	Immortalized cell line isolated from cervical cancer **He**nrietta **La**cks	DMEM-GlutaMAX™ containing 100 U/ml Penicillin, 100 µg/ml Streptomycin and 10% FCS (heat inactivated)

3.1.8 Mice strains

All animals were obtained from our in-house animal facility. The wildtype and FA2H-KO animals used in all experiments had either a mixed 129Ola/C57BL/6 or a C57BL/6 genetic background. All mice were raised in accordance with the instructions of local and state authorities regarding animal welfare.

3.1.9 Oligonucleotides

All used oligonucleotides were ordered at Eurofins MWG Operon.

Table 3-8: Oligonucleotides used for cloning and PCR.

Name	Sequence (5→3)
BiFC mFA2H_C (ClaI) RV	TC-ATCGAT-CTGCATCTTCGGGTGGGC
BiFC mFA2H_C (EcoRI) FW	AT-GAATTC-ATGGCCCCCGCTCCGC
BiFC mCerS2_C (ClaI) RV	TC-ATCGAT-GTCATTCTTAGGATGATTGTTAT
BiFC mCerS2_C (EcoRI) FW	AT-GAATTC-ATGCTCCAGACCTTGTATG
BiFC-hACSL3_C (ClaI) RV	TC-ATCGAT-TTTTCTTCCATACATTCGCTCAA
BiFC-hACSL3_C (EcoRI) FW	AT-GAATTC-ATGAATAACCACGTGTCTTCAAA
BiFC-hPGRMC1_C (ClaI) RV	TC-ATCGAT-ATCATTTTTCCGGGCACTCTCATC
BiFC-hPGRMC1_C (EcoRI) FW	AT-GAATTC-ATGGCTGCCGAGGATGTGGT

BiFC-hSPTLC1_C (EcoRI) FW	CT-GAATTC-ATG GCG ACC GCC ACG GAG
BiFC-hSPTLC1_C (ClaI) RV	TT-ATCGAT- GAGCAGGACGGCCTGGG
BioID-mFA2H (EcoRI) FW	AT-GAATTC-ATGGCCCCCGCTCCGC
BioID-mFA2H (KpnI) RV	TG-GGTACC-TCACTGCATCTTCGGGTG
FA2Hanti (genotyping primer)	GCTCTTCTTCAAGAGCCATCC
FA2Hneo (genotyping primer)	ATTCGCAGCGCATCGCCTTCTATC
FA2Hwtsense (genotyping primer)	GTGCTGTACCTCAGCTGGTC
Twin-Strep-mFA2H 1-163 RV	AGCGGCTCTTCTCCC-GGCCTCGATGAGGTCTGAG
Twin-Strep-mFA2H FW	AGCGGCTCTTCAATG-GCCCCCGCTCCGCCC
Twin-Strep-mFA2H RV	AGCGGCTCTTCTCCC-CTGCATCTTCGGGTGGGC

3.1.10 Plasmids

The table bellow list the plasmids utilized in this thesis.

Table 3-9: Plasmids cloned and/or used in this thesis.

Name	Insert/protein product	Source	Remarks
pcDNA3	-	Invitrogen	
pcDNA3-hACSL3-cYFP1	Human ACSL3 with C-terminal citrine YFP1-tag for BiFC	-	PCR copied from pEGFP-hACSL3-HA. Inserted via EcoRI and ClaI.
pcDNA3-hACSL3-YFP2	Human ACSL3 with C-terminal citrine YFP2-tag for BiFC	-	PCR copied from pEGFP-hACSL3-HA. Inserted via EcoRI and ClaI.
pcDNA3-hPGRMC1-cYFP1	Human PGRMC1 with C-terminal citrine YFP1-tag for BiFC	-	PCR copied from pCMV-SPORT6-hPGRMC1. Inserted via EcoRI and ClaI.
pcDNA3-hPGRMC1-YFP2	Human PGRMC1 with C-terminal citrine YFP2-tag for BiFC	-	PCR copied from pCMV-SPORT6-hPGRMC1. Inserted via EcoRI and ClaI.
pcDNA3-mCerS2-cYFP1	Murine CerS2 (Lass2) with C-terminal citrine YFP1-tag for BiFC	-	PCR copied from pCMV-SPORT6-mCerS2. Inserted via EcoRI and ClaI.
pcDNA3-mCerS2-YFP2	Murine CerS2 (Lass2) with C-terminal citrine YFP2-tag for BiFC	-	PCR copied from pCMV-SPORT6-mCerS2. Inserted via EcoRI and ClaI.
pcDNA3-[ClaI…EcoRI]-cYFP1 (linearized vector)	C-terminal citrine YFP1-tag for BiFC	Kindly provided by Dr. Reiterer/Prof. Hauri (Nyfeler et al. 2005)	ClaI + EcoRi cut pcDNA3-MCFD2-cYFP1
pcDNA3-[ClaI…EcoRI]-YFP2 (linearized vector)	C-terminal citrine YFP2-tag for BiFC	Kindly provided by Dr. Reiterer/Prof. Hauri (Nyfeler et al. 2005)	ClaI + EcoRi cut pcDNA3-MCFD2-YFP2
pcDNA3-mFA2H-cYFP1	Murine FA2H with C-	-	PCR copied from

	terminal citrine YFP1-tag for BiFC		pcDNA3.1/zeo/mFA2H. Inserted via EcoRI and ClaI.
pcDNA3-mFA2H-YFP2	Murine FA2H with C-terminal citrine YFP2-tag for BiFC	-	PCR copied from pcDNA3.1/zeo/mFA2H. Inserted via EcoRI and ClaI.
pcDNA3-sscYFP1-ERGIC53	Human ERGIC53 with N-terminal ER-targeting sequence (ss) followed by citrine YFP1	Kindly provided by Dr. Reiterer/Prof. Hauri (Nyfeler et al. 2005)	
pcDNA3-hSPTLC1-cYFP1	Human SPTLC1 with C-terminal citrine YFP1-tag for BiFC	-	PCR copied from pcDNA3.1-SPTLC1-his. Inserted via EcoRI and ClaI.
pcDNA3-hSPTLC1-YFP2	Human SPTLC1 with C-terminal citrine YFP2-tag for BiFC	-	PCR copied from pcDNA3.1his-SPTLC1. Inserted via EcoRI and ClaI.
pcDNA3-ssYFP2-ERGIC53	Human ERGIC53 with N-terminal ER-targeting sequence (ss) followed by citrine YFP2	Kindly provided by Dr. Reiterer/Prof. Hauri (Nyfeler et al. 2005)	
pcDNA3.1/zeo/mFA2H	Murine FA2H in mammalian expression vector with Zeocin-resistance cassette	RZPD	
pcDNA3.1-mycBioID	myc-taged *E.coli* biotin-ligase	Kind gift from Kyle Roux (Roux et al. 2012)	
pcDNA3.1-mycBioID-mFA2H	Fusion protein of myc-taged *E.coli* biotin-ligase with murine FA2H	-	PCR copied from pcDNA3.1/zeo/mFA2H. Inserted via KpnI and EcoRI.
pCMV-SPORT6-hPGRMC1	Human PGRMC1 cDNA in mammalian expression vector	Source BioScience LifeSciences	
pCMV-SPORT6-mCerS2	Murine CerS2 (Lass2) in mammalian expression vector	Source BioScience LifeSciences	
pEGFP-hACSL3-HA	Human ACSL3 with N-terminal EGFP and C-terminal HA-tag	Kind gift from Dr. J. Füllekrug	
pENTRY-IBA51		iba GmbH (part of StarGate® cloning kit)	
pENTRY-IBA51-mFA2H	Murine FA2H	-	
pESG-IBA103-mFA2H	Murine FA2H with C-terminal Twin-Strep-tag®	Cloned via StarGate® cloning kit (iba GmbH), mFA2H-insert copied from pcDNA3.1-mFA2H (PCR)	PCR copied from pcDNA3.1/zeo/mFA2H. Inserted via recombination sites.

pESG-IBA103-mFA2H1-163	Murine FA2H amino acids 1-163 with C-terminal Twin-Strep-tag®	Cloned via StarGate® cloning kit (iba GmbH), mFA2H-insert copied from pcDNA3.1-mFA2H (PCR)	PCR copied from pcDNA3.1/zeo/mFA2H. Inserted via recombination sites.
pESG-IBA105-mFA2H	Murine FA2H with N-terminal Twin-Strep-tag®	Cloned via StarGate® cloning kit (iba GmbH), mFA2H-insert from copied pcDNA3.1-mFA2H (PCR)	PCR copied from pcDNA3.1/zeo/mFA2H. Inserted via recombination sites.
pESG-IBA105-mFA2H1-163	Murine FA2H amino acids 1-163 with N-terminal Twin-Strep-tag®	Cloned via StarGate® cloning kit (iba GmbH), mFA2H-insert copied from pcDNA3.1-mFA2H (PCR)	PCR copied from pcDNA3.1/zeo/mFA2H. Inserted via recombination sites.
pcDNA3.1his-SPTLC1	Human SPTLC1 with N-terminal His-tag	Kindly provided by Prof. Hornemann (Zurich, Switzerland)	

3.2 Methods

3.2.1 Animal work & mouse tissue preparation

3.2.1.1 Genotyping

The mice used in this thesis research were genotyped via polymerase chain reaction (PCR) using genomic DNA derived from a very small tissue biopsy (tail tip or piece of earlobe).

The tissue was first digested overnight at 55 °C in 750 µl genotyping lysis buffer containing Proteinase K (20 µg/ml). Next morning, 250 µl saturated NaCl solution (~6 M) was added followed by another 5 min incubation to precipitate proteins. Afterwards, the samples were centrifuged 10 min at 18,000 g and 4 °C to remove insoluble material. Subsequently, 750 µl of the supernatant was transferred to a new microtube and the DNA precipitated by the addition of 500 µl isopropanol. The genomic DNA was then pelleted for 20 min at 4 °C and 10,000 g, washed once in 500 µl 70% (v/v) ethanol and air-dried for 5-10 min. For solvation the pellet was resupended in 200 - 500 µl ddH_2O and incubated for 2-4 h at room temperature. 1 µl of the genomic DNA was thereafter used in the PCR. The primers used for FA2H-KO project animals are defined in Table 3-8 (p.27) and the PCR-program is depicted in the table below:

Table 3-10: PCR-program for FA2H-KO genotyping PCR.

Step	Temperature	Time	Repeat
1	94 °C	5 min	
2	95 °C	30 s	
3	59°C	45 s	
4	72 °C	1.5 min	Go to step 2, Repeat 29x
5	72 °C	10 min	
6	4 °C	hold	

3.2.1.2 Myelin preparation

3.2.1.2.1 Central nervous system (CNS) myelin preparation (brain)

Myelin from the central nervous system i.e. brain was isolated by a protocol, which is based on a publication by Caroni and Schwab (Caroni & Schwab 1988).

It is important to note that all purification steps were carried out at 4 °C. In addition, all solutions used until the first water wash contained complete protease inhibitor cocktail (Roche). First, mouse brains were homogenized in 10.5% isotonic sucrose solution using an Ultra-Turrax homogenizer (3X intervals: 20 s homogenization, 1 min pause on ice). This led to the detachment of the myelin sheath from the axon and the generation of myelin vesicles. Then, to obtain a crude density separation, the

homogenates were centrifuged at 18,000 g for 45 min. Material with a density equal or higher than the 10.5% sucrose solution pelleted, whereas less dense constituents remained in the supernatants. Subsequently, the supernatants were aspirated and the pellets dissolved in 10 ml 30% sucrose solution. Afterwards, the suspensions were transferred to a 12 ml ultracentrifugation tube and overlaid carefully with 2 ml of 10.5% sucrose. This was followed by 50 min ultracentrifugation at 68,000 g using a SW-41 rotor. During this the myelin membrane vesicles accumulated as a clearly visible interphase between the 10.5 and 30 % sucrose solution. Thereafter, the interphase was transferred to a new ultracentifugation tube and washed two times with ddH_2O (containing 1 mM EDTA) at 68,000 g for 30 min (SW-41 rotor). This way, excess axolemmal contaminants were removed. To gain higher myelin purity with less contaminants, the washed myelin pellets were again subjected to the same sucrose density gradient and the two ddH_2O-washing steps. In the end, the purified myelin samples were resuspended in 100 µl ddH_2O (containing 1 mM EDTA) and stored at -80 °C until analysis.

3.2.1.2.2 Peripheral nervous system (PNS) myelin preparation (sciatic nerves)

The preparation of PNS-myelin was done in a similar way as the CNS-myelin preparation with some important alterations, because the raw tissue material was significantly less (one pair of sciatic nerves). First, the sciatic nerves were homogenized using a Dounce homogenizer instead of an UltraTurrax. Second, the whole procedure was scaled down i.e. microtubes (normal and ultracentrifugal) and a benchtop ultracentrifuge (TLS-55 rotor) were used. Accordingly, smaller buffer volumes were used. Third, myelin was not subjected to a second density gradient followed by two ddH_2O-washing steps. While this would lead to purer PNS-myelin, it would also cause a very high and thus not desirable myelin loss. In addition, the sucrose contents of both gradient solutions were slightly altered to 9.2% and 28.4%, because PNS-myelin exhibits a lower density than its CNS counterpart (Larocca & Norton 2007).

3.2.1.3 Whole brain lysate preparation

For preparation of whole brain lysates, 750 µl of the brain homogenates produced during CNS-myelin purification were transferred to a microtube and mixed with 750 µl High-SDS buffer (8% SDS, 300 mM NaCl, 100 mM Tris, pH 8.0). The samples were heated to 99 °C for 5 min, followed by DNA shearing via ultrasonification (3X 10 s) and another 5 min heating at 99 °C. Subsequently, the protein amount was determined and the samples stored at -80 °C. Furthermore, 150 µl of each lysate was mixed with 50 µl 4X Laemmli-buffer, denatured 5 min at 95 °C and also stored at -80 °C.

3.2.2 Bacterial culture techniques

3.2.2.1 Cell maintenance

For liquid culture, bacteria were usually grown overnight in a shaking incubator in LB-medium containing an appropriate antibiotic at 37 °C and 200 rpm. To obtain single colonies, e.g. after transformation, cells were spread onto LB-agarose plates containing an appropriate antibiotic and grown at 37 °C overnight.

3.2.2.2 Transformation of chemical competent bacteria

The delivery of plasmids into a bacterial cell is called transformation. It is generally used to either achieve plasmid amplification or recombinant protein expression. One method uses a chemical treatment in combination with heat-shocking. While the first prevents the electrostatic repulsion of the foreign DNA by the cell membrane, using high concentrations of calcium, the second opens up pores in it, thereby allowing plasmid entry.

For this thesis ready-made chemical competent bacteria were used. For transformation ~1 ng of plasmid-DNA was mixed with 100 µl of chemically competent cells pre-thawed on ice and incubated for 30 min. To achieve plasmid uptake, they were heat shocked afterwards for 1 min at 42°C and subsequently put back on ice for 2 min. In the case of a kanamycin-resistance containing plasmid, this was follow by the addition of 900 µl pre-warmed LB-medium and incubation at 37 °C and 600 rpm for 1 h. For ampicillin-resistance plasmids this step was omitted. In the end, the transformed bacteria were spread onto LB-plates containing the appropriate antibiotic and grown overnight at 37 °C.

3.2.3 Eukaryotic cell culture techniques

3.2.3.1 Cell maintenance

Cells were handled under sterile conditions using laminar airflow workbenches and heat-sterilized or autoclaved materials. Cells were grown in an incubator in standard cell culture vessels in a water-saturated atmosphere at 37 °C and 5% CO_2.

3.2.3.2 Cell passaging

For cell passaging the cell medium was drawn out of the vessel and replaced with 37 °C warm 1X PBS to wash the cells. Afterwards, PBS was removed and an appropriate amount of 0.05% (w/v) trypsin solution added to cover the whole vessel. The cells were then placed back into a 37 °C incubator for 2 - 5 min to allow enzymatic cell detachment. Subsequently, the cells were resuspended in cell culture medium containing 5 - 10% FCS to stop the enzymatic reaction. For simple cell maintenance, 1/5 – 1/10 of the cell suspension was seeded onto a new culture vessel and filled up with medium. If a

precise amount of cells was needed the cell number was determined before using a Neubauer cell counting chamber. Thereafter, cells were placed back into the 37 °C incubator.

3.2.3.3 Cryo preservation

First, cold preservation medium had to be prepared by mixing 9 volumes of the cell culture medium the cells normally grow in with 1 volume of DMSO. Then the cells were detached as described before (3.2.3.2 Cell passaging), pelleted by centrifugation and resuspended in cold preservation medium. Finally, they were transferred into cryotubes, immediately put on ice to minimize DMSO-mediated cytotoxicity and slowly pre-frozen in a Styrofoam block overnight to -80 °C. At the next day the cryotubes were relocated into a liquid nitrogen tank for long-term storage.

3.2.3.4 Cell revival from cryo preservation

Cryotubes were thawed until a small ice core remained, their content transferred to a sterile conical tube containing ice-cold cell culture medium and everything mixed by inversion. Next, the cells were pelleted by centrifugation and the supernatant aspirated to remove toxic DMSO-remains. In the end they were resuspended in warm culture medium, transferred to a new cell culture vessel and put into the 37 °C incubator.

3.2.3.5 Stable isotope labeling by amino acids in cell culture (SILAC)

In “stable isotope labeling by amino acids in cell culture” (SILAC), all proteins of a cell are metabolically labeled by growing them for at least 6 cell divisions in media containing either light or heavy isotopes of amino acids (usually arginine and lysine). This later allows a very robust relative protein quantitation by mass spectrometry between differently labeled samples (Ong et al. 2002) (Figure 3-1).

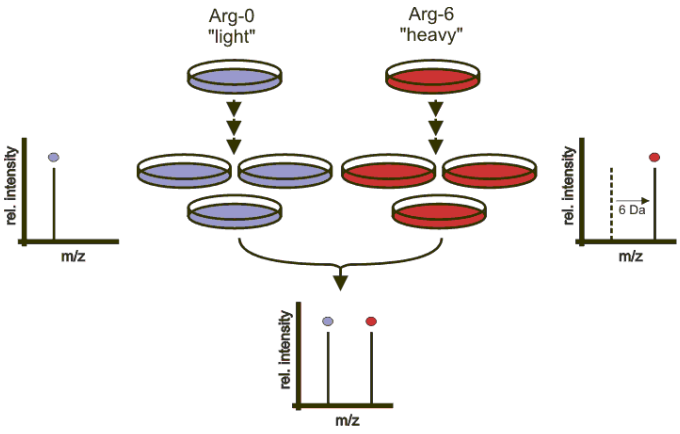

Figure 3-1: Principle of SILAC. Cellular proteins are labeled by growing cells for some passages in culture medium containing light or heavy isotopes of certain amino acids (usually arginine and/or lysine). After at least six passages most of the proteins are labeled. Subsequent mass spectrometric processing allows the comparison of protein abundances between differentially labeled and treated samples. Picture from: https://commons.wikimedia.org/wiki/File:Silac.gif

In this study cells were labeled for at least 6 passages (=98.4% incorporation rate) with either a light (natural lysine and arginine) or a heavy amino acid mix ($^{15}N_2{}^{13}C_6$-lysine and $^{15}N_4{}^{13}C_6$-arginine) in DMEM. In this process the cells were split each day 1:1 into fresh medium. In the end the success of label incorporation was assessed by MALDI-TOF/TOF protein analysis after cell lysis and in-gel digestion.

3.2.3.6 Transfection

In this thesis the following two methods were used for delivering plasmid into eukaryotic cells.

3.2.3.6.1 Calcium phosphate method ($CaPO_4$-method)

This method for the delivery of plasmid DNA into eukaryotic cells is especially effective for HEK293/HEK293-T cells. Usually transfection efficiencies of ≥90% are achieved. The principle of this method is that the plasmid DNA is precipitated together with calcium and phosphate, thereby giving rise to DNA-calcium phosphate precipitates. These precipitates are then spread on the cells and probably taken up by endocytosis. After one round of mitosis, during which the nuclear membrane is broken down, the plasmid DNA can finally reach the cell nucleus. A detailed description of the method is given below. Table 3-11 gives the seeding densities and transfection reagent volumes used for different culture plate formats.

Table 3-11: Cell densities and transfection reagent volumes for different culture plate formats.

Plate format	Seeding density	2M $CaCl_2$ volume (µl)	Plasmid DNA amount (µg)	Fill up volume ddH_2O (µl)	2X HBS volume (µl)
6 well	5x 10^5	13	2	100	100
6 cm plate	3-4x 10^6	26	4	200	200
10 cm plate	3x 10^6	65	10	500	500
15 cm plate	8x 10^6	130	20	1000	1000

First, the cells were seeded one day prior to transfection at the appropriate cell density. At the next step the transfection mixture was prepared by first diluting the plasmid together with $CaCl_2$ in sterile ddH_2O. Then this mixture was added drop-by-drop under constant shaking to the indicated amount of sterile 2X HBS (50 mM HEPES, 280 mM NaCl, 1.5 mM Na_2HPO_4, pH 7.0). To allow efficient precipitate formation the mixture was kept at room temperature for 30 min. Afterwards, it was mixed once by pipetting up and down and evenly spread onto the cells in a drop wise matter. In addition, the culture plate was carefully tilted to achieve uniform complex distribution. The cells were then incubated at 37 °C and 5% CO_2 for 24 or 48 h depending on the intended construct expression strength.

3.2.3.6.2 TurboFect™

BHK and HeLa cells were transfected using the commercial available cationic polymeric reagent TurboFect™ according to the manufacturers protocol. Shortly, cells were seeded one day prior to transfection so that they showed about 90% confluence the next day (6 well =~$2.5x10^5$ cells/well). For transfection the plasmid DNA (6 well = 4 µg/well) was first diluted in an appropriate amount of fresh serum- and antibiotic-free growth medium (6 well = 400 µl/well). Afterwards, TurboFect™-reagent was added (6 well = 5 µl/well) and everything mixed thoroughly. After 15 - 20 min incubation at room temperature the transfection mixture was pipetted onto the cells and evenly distributed by mild shaking. Cells were then put back into a 37 °C incubator and incubated for 24 or 48 h. Usually for 48 h-expressions the cell culture medium was replaced with fresh one after 24 h to reduce cytotoxicity evoked by prolonged TurboFect™ exposure.

3.2.3.7 Stable cell line generation

To obtain cell lines, which stably express the transgene of choice, cells were first transfected with an appropriate plasmid containing both the transgene and a selectable marker gene, i.e. puromycin or neomycin resistance gene. Therefore, at a first step the limiting concentration of the antibiotic inducing cell death had to be determined for each cell line individually. Afterwards, the cells of choice were seeded onto a 10 cm culture plate and transfected. Approximately 24 h later the respective antibiotic was added to the cells at a concentration slightly over the limiting concentration determined before. The cells were now grown for ~14 days under constant selective pressure and the medium replaced every 2nd – 3rd day. Subsequently, single colonies, derived from cells that integrated the plasmid or parts of it stably into their genome, were picked under a microscope using pipette tips. The clones were transferred to individual wells of a 24 well plate and cultivated under constant selective pressure until reaching confluency. This was followed by further passages to well plates of increasing sizes. At the 6 well stage all clones still viable were tested for transgene

expression by WB. Then positive clones were further propagated on 10 cm dishes and finally stored by cryo preservation until further usage.

3.2.4 Protein techniques

3.2.4.1 Proximity-dependent protein biotinylation & identification (BioID)

An recently published method (Roux et al. 2012) to identify interaction partners of a protein uses the fusion of a constitutively active *E.coli* biotin ligase (BirA mutant R118G = BirA*) to it. When expressed in cells, neighboring proteins are biotinylated at their N-terminus and lysine residues, thereby allowing their identification by mass spectrometry after affinity purification (Figure 3-2).

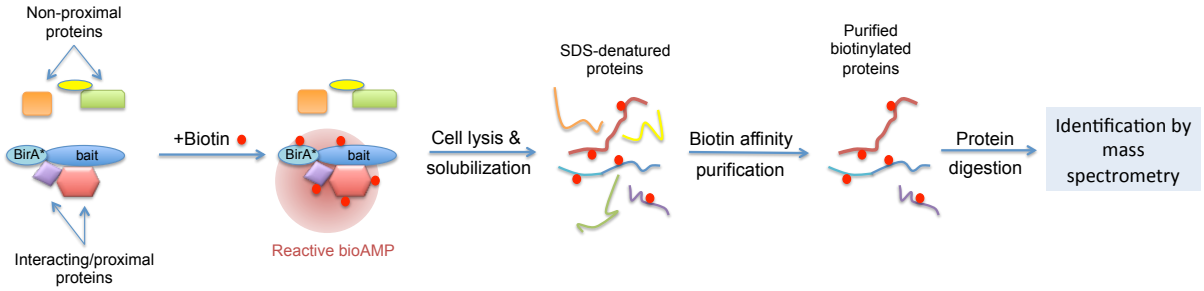

Figure 3-2: Schematic model of BioID-method. The protein of interest is expressed fused to a promiscuous biotin ligase (BirA*), leading to biotinylation of proximal proteins. After stringent cell lysis, biotin-marked proteins are selectively enriched, digested to peptides and finally identified by mass spectrometry. Picture adapted from: (Roux et al. 2012).

For this assay, cells grown in a culture medium without biotin were first transfected with a plasmid containing the fusion protein. About 24 h later, 50 µM biotin was added to the cells, followed by another 24 h of incubation. Afterwards, cells were harvested and either lysed directly or stored at -20 °C.

3.2.4.2 Paraformaldehyde (PFA)-crosslinking

Another method for the identification of protein interaction partners is paraformaldehyde-crosslinking (PFA-crosslinking). While strong interactions can be elucidated using complex affinity purification and subsequent mass spectrometry analysis, weak or transient interactions can be interrupted during sample lysis or purification. To overcome this, the cells expressing the proteins of interest are treated with PFA before cell lysis, which leads to the covalent but reversible crosslinking of proteins with their interacting and neighboring proteins (indirect interactors). Transient and weak interactions are therefore preserved throughout lysis and affinity purification. During mass spectrometric sample preparation the covalent bounds are again removed by sample boiling in a reducing sample buffer (Vasilescu et al. 2004; Klockenbusch & Kast 2010).

First, the cells expressing the protein of interest were pelleted and washed thrice with 1X PBS to remove all cell culture media remains. Then the cells were resuspended in 1 ml of 37 °C warm PFA solution (0.25 - 1% in 1X PBS) per $1x10^7$ cells and incubated at room temperature under constant agitation for 15 min. Subsequently, they were pelleted at 2000 g for 5 min and the crosslinking stopped by resuspension in 1 ml of ice-cold stopping solution (1.25 M glycine in PBS) per $1x10^7$ cells. Pelletizing and washing the cells once again with stopping solution finished the procedure. Afterwards, the cell pellets were either lysed directly or stored at -20 °C.

3.2.4.3 Cell lysis

The cells were mixed with the appropriate amount (see Table 3-12) of the desired ice cold lysis buffer (see 3.1.4 Chemicals, Solutions and Buffers) containing 1X Protease Inhibitor Cocktail (ThermoScientific) and resuspended by pipetting up and down. Afterwards, they were incubated for 30 min on an overhead tumbling incubator at 4 °C, followed by 30 min centrifugation at 18,000 g and 4 °C. The lysate was then transferred to a precooled microtube.

Table 3-12: Lysis buffer volumes used for cell pellets derived from different culture vessel sizes.

Cell culture vessel size	Volume of lysis buffer
6 well plate	~50 - 100µl
10 cm plate	~150 - 250 µl
15 cm plate	~250 - 500 µl

3.2.4.4 Protein precipitation

To remove excess amounts of lipids and to concentrate protein samples, both of the following protein precipitations were employed.

3.2.4.4.1 Ice cold acetone

The protein samples were mixed with ice cold acetone at a ratio of 1:4 (vol/vol) and then placed overnight at -20 °C to allow complete protein precipitation. At the next day, the samples were centrifuged at 20,000 g and 4 °C for 30 min. Subsequently, the supernatants were aspirated carefully and the pellet air-dried for ~5 min.

3.2.4.4.2 Chloroform-Methanol

For $CHCl_3$/MeOH-precipitation the samples were mixed with ice-cold chloroform/methanol 2/1 (vol/vol) solution at a 5:1 ratio and vortexed thoroughly. This was followed by a 20,000 g centrifugation at 4 °C for 30 min, which led to a phase separation with the precipitated proteins contained in the interphase. Afterwards, the lower and upper phase were both carefully extracted with a Hammilton syringe and the pellets washed with ice-cold methanol. Therefore, 1 ml methanol was added to each pellet, followed by 15 min centrifugation and drying in a vacuum centrifuge.

3.2.4.5 Protein concentration determination

Protein concentrations were determined using the commercially available two-step colorimetric BioRad-DC Protein Assay, which works similarly as the established Lowry assay (Lowry et al. 1951). In the assay proteins react first with an alkaline copper tartrate solution and then with the later added Folin's reagent, giving rise to a blue colored complex. The addition of the copper containing alkaline medium leads to an interaction of copper and certain amino acid side chains (tyrosine and tryptophane, cystine, cysteine, and histidine). Afterwards, these copper-bound proteins reduce the added Folin's reagent leading to the blue-colored compound, which has a maximum absorbance at 750 nm. Because the absorbance intensity is proportional to the protein content of the solution, measuring and comparing it to known values of a calibration solution allows the determination of it's protein concentration.

In this thesis experiments, BSA calibration dilutions of six concentrations (2, 1, 0.5, 0.25, 0.125 and 0.0625 µg/µl), always dissolved in the same buffer as the samples, were used. 5 µl of each standard or sample were pipetted in triplicates or quadruplicates into wells of a 96-well microplate. This was followed by addition of 25 µl alkaline copper tartrate solution (solution A', produced by mixing 1 ml solution A with 20 µl solution S) and finally 200 µl Folin reagent (solution B). After 15 min incubation at room temperature the absorbance was measured with a GENios microplate reader. In the end the samples protein content was calculated using the linear equation of the standards regression line.

3.2.4.6 Protein electrophoresis

3.2.4.6.1 SDS-PAGE

In sodium dodecyl sulfate polyacryalamide gel electrophoresis (SDS-PAGE) proteins are separated by size, while wandering through a SDS-rich polyacrylamide gel matrix towards the anode. The separation capability depends on the gels pore size, which is determined by the acrylamide concentration. SDS used in this system binds to proteins, thereby disrupting non-covalent bonds within and unfolding them. This gives each protein a net negative charge, which is proportional to its size. Further endogenous protein charges are masked allowing a true separation by molecular weight. In addition, protein samples are denatured in reducing sample buffer under heating to fully unfold proteins before electrophoretic separation.

Table 3-13: Composition of SDS-Polyacrylamide gels.

	stacking gel	7.5% separating gel	10% separating gel	12.5% separating gel	15% separating gel
Total volume	1 ml	5 ml	5 ml	5 ml	5 ml
H_2O	0.604 ml	2.707 ml	2.395 ml	2.082 ml	1.770 ml
40 % Acrylamide	0.125 ml	0.938 ml	1.25 ml	1.563 ml	1.875 ml

Tris HCl	0.250 ml (pH 6.8)	1.250 ml (pH 8.8)	1.250 ml (pH 8.8)	1.250 ml (pH 8.8)	1.250 ml (pH 8.8)
10% SDS	10 µl	50 µl	50 µl	50 µl	50 µl
APS	10 µl	50 µl	50 µl	50 µl	50 µl
TEMED	1 µl	5 µl	5 µl	5 µl	5 µl

In this thesis 0.75 and 1 mm mini gels were used casted with the Mini-PROTEAN® system (BioRad). The different gel compositions used are given in Table 3-13. Before loading, protein samples were mixed with 4X Laemmli buffer, containing SDS and the strong reducing agent β-mercaptoethanol, and denatured at 95 °C for 5 min. For some heat sensitive proteins this heating was replaced by a 20 min incubation at room temperature. After cool down, the samples were loaded into the gel pockets together with a protein molecular weight marker (PageRuler Prestained Protein Marker). The gels were run at a constant voltage of 200 V to achieve protein separation.

3.2.4.6.2 BlueNative-PAGE

In blue native polyacrylamide gel electrophoresis (BlueNative-PAGE) whole protein-complexes and not just single proteins are separated by size within a polyacrylamide gel matrix. This is achieved by lysing the cells with a non-denaturing buffer and replacing SDS in all buffers with Coomassie brilliant blue. Like SDS, it binds to proteins giving them a net negative charge proportional to their size.

Table 3-14: Composition of 8% BlueNative-gel.

Name	Volume
3X Gel buffer	666.6 µl
Acrylamide-bisacrylamide mix (49.5% T, 3% C)	324.4 µl
10% APS	6.7 µl
TEMED	0.67 µl
ddH_2O	1001.6 µl
total	2 ml

The BlueNative-gels were also prepared with the Mini-PROTEAN® system (BioRad). Before usage, all equipment was thoroughly washed in water, to remove any traces of SDS. In addition, all buffers were pre-cooled to 4 °C. In this thesis 8% gels were used for native protein separation (see Table 3-14). Before loading, the protein samples as well as the molecular weight marker (NativeMARK™ Unstained Protein Standard) they were mixed with 10X BlueNative loading dye. Furthermore, all empty gel pockets were filled with 1X loading dye diluted in lysis buffer without detergent. After loading, all samples were overlaid with 0.2% Coomassie solution and the gel run at 100 V for 1 h followed by 200 V until complete separation. If a WB was done afterwards, the gel had to be incubated in 1X SDS running buffer for 5 min to allow protein transfer.

3.2.4.7 Silver staining of SDS-Gels

Sensitive silver staining was performed according to the protocol published by Heukeshoven and Dernick (Heukeshoven & Dernick 1986).

After SDS-PAGE, gels were fixed for at least 30 min or overnight in fixing solution (30% EtOH, 10% acetic acid). Afterwards, gels were incubated in fresh sensitizer solution (30% EtOH, 500 mM sodium acetat, 0.5% (w/v) glutaraldehyde, 0.2% (w/v) sodium thiosulfate) for 30 min – 2h, followed by three 20-30 min washes in ddH_2O. Then silver solution (0.1% (w/v) $AgNO_3$, 0.01% (v/v) formaldehyde) was added and left on the gels for 30 min. Excess silver ions were removed by short (1-2 min) washing with ddH_2O and lastly developer (2.5% (w/v) $NaCO_3$, 0.01% formaldehyde) was added. The solution was replaced once with fresh developer to remove silver precipitates. When sufficient staining was achieved, incubating the gels in 50 mM glycine solution for 5 – 10 min stopped the staining. Finally, gels were washed in ddH_2O and digitalized with an image scanner.

3.2.4.8 Western blot

Western blotting (WB) is the transfer of all proteins separated by gel electrophoresis onto a protein binding polymeric membrane (usually nitrocellulose or PVDF) followed by protein detection using protein-specific antibodies. The transfer could be achieved by capillary forces but is usually accelerated by applying an electric current.

In this thesis, WB was done with a semi-dry blotter and the following setup. First, three thin Whatman papers were soaked in blotting buffer and placed onto the blotters anode. On these papers the blotting membrane presoaked in buffer was placed followed by the gel from the electrophoresis. The gel was covered with three additional presoaked papers and finally the whole assembly covered with the blotters cathode lid. Blotting was then carried out for 70 – 90 min at 75 mA per gel. Subsequently, the immunogenic detection was accomplished as follows: First the membrane was placed in a vessel together with blocking solution (5% filtered skim milk in TBS-T) for 30 – 60 min at room temperature to saturate all parts of the membrane without bound protein. Then the primary antibody, specific to the protein of interest, was added diluted in blocking solution. This was followed either by incubation for 2 h at room temperature or overnight at 4 °C. Afterwards, the membrane was washed thrice for 5 min in TBS-T and the incubated with the secondary antibody diluted in blocking solution. Depending on the detection system used, fluorescence or chemiluminescence, the incubation lasted 45 or 60 min, respectively. In the end, the membrane was washed again thrice in TBS-T for 5 min and one time in 1X TBS before signal detection. In the case of fluorescent secondary antibodies, an Odyssey near-infrared scanner (Licor) was employed. For chemiluminescent WBs the membrane was covered with ECL substrate (ThermoScientific) and the signals visualized by either a photographic film or a CCD-camera system (Peqlab). Quantification was

done with the standard software package of the respective detection system (fluorescence = Odyssey V1.2, chemiluminescence =).

3.2.4.9 Western blot stripping

For the removal of antibodies from a WB for detection with other antibodies two protocols were employed, a mild and a harsh treatment, depending on the antibodies binding strength.

For the mild treatment, an acidic (pH 2.2) stripping buffer containing 200 mM glycine, 0.1% (w/v) SDS and 10% (v/v) Tween 20 was used. The blot was washed twice for 5 – 10 min with this buffer, then twice with 1X PBS for 5 - 10 min and finally twice with TBS-T for 5 min. Subsequently, the blot had to be blocked again with blocking solution before detection with a new antibody.

The harsh treatment required a buffer consisting of 2% (w/v) SDS, 0.75% (v/v) β-mercaptoethanol, and 62.5 mM (Tris pH 7.0). Before stripping, the buffer was heated to 50 °C. Next, it was added to the membrane and incubated under constant agitation for 30 min. Afterwards, the stripping solution was decanted, the blot rinsed 2 - 3 times with ddH_2O followed by two 5 min TBS-T washes. Finally, it had to be blocked again with blocking solution.

3.2.4.10 Twin-Strep-tag® affinity purification

The Twin-Strep-tag®–StrepTactin® affinity purification system (Schmidt et al. 2013) was employed to purify FA2H and its interacting proteins, thereby allowing their identification by mass spectrometry. The Twin-Strep-tag® is an improved version of the StrepTag and mainly consists of two tags connected by a short glycine-rich amino acid linker sequence. The Twin-Strep-tag shows a higher specificity and stronger affinity to StrepTactin®, being suitable for the rapid purification of intact protein complexes under mild buffer conditions.

Twin-Strep-FA2H was purified directly from cell lysates using StrepTactin® coupled to MacroPrep® (polymethacrylate) beads. All purification steps were carried out at 4 °C to minimize protein degradation. For the purification the beads, supplied as a 50% slurry, were directly added to the cell lysate and incubated overnight on a tumbling incubator. 25 µl bead slurry were used per cell lysate derived from one confluent 15 cm cell culture plate. After incubation, the beads were spun down shortly at 3000 g and the supernatant, containing the unbound proteins, removed. Then the beads were washed thrice with 1 ml of StrepTag washing buffer. Finally, the bound Twin-Strep-FA2H and its interacting partners were eluted 3-4 times with 50 µl washing buffer containing 2.5 mM biotin. For this, the beads were shaken with the buffer at 1100 rpm for 5 min, followed by 2 min centrifugation at 10,000 g and transfer of the supernatant (=eluate) to a new microtube.

3.2.4.11 NeutrAvidin affinity purification

NeutrAvidin is produced from avidin via deglycosylation. It retains the same high binding affinity to biotin that avidin exhibits, but has a reduced unspecific binding activity, allowing a cleaner purification of biotinylated molecules. In this thesis, NeutrAvidin affinity purification was used for the purification of proteins biotinylated in BioID-assays.

Biotinylated proteins were directly purified from cell lysates by adding NeutrAvidin-agarose beads (supplied as 50% slurry). 200 µl bead slurry, pre-conditioned by washing three times with one bead volume of lysis buffer, were used per cell lysate derived from one confluent 15 cm cell culture plate. The whole purification process was done at 4 °C and all centrifugations to pellet the beads at 500 g. After the addition of beads, the samples were incubated on a tumbling incubator overnight, thereby guaranteeing complete protein binding. At the next day, the beads were washed thoroughly with four different buffers to reduce unspecific binding. The washing was always carried out by incubating for 5 min with 1 ml washing solution under mild agitation and subsequent solution removal by a short centrifugation (500 g). First, the beads were washed 2X with 2% SDS, then 1X with 0.1% sodium deoxycholat, 1% TX-100, 500 mM NaCl, 1 mM EDTA, 50 mM Hepes, pH 7.5, afterwards 1X with 250 mM LiCl, 0.5% NP-40, 0.5% sodium deoxycholat, 1 mM EDTA, 10mM Tris-HCl, pH 8.1 and finally 2X in 50 mM Tris, 50 mM NaCl, pH 7.4. Since the NeutrAvidin-biotin-bond is to strong for efficient and complete protein elution, peptides for mass spectrometry analysis were generated by the direct addition of trypsin to the beads (see: 3.2.4.12.1.2 On-bead digest).

3.2.4.12 Mass spectrometry sample preparation

3.2.4.12.1 Generation of peptides

3.2.4.12.1.1 In-gel digest

First, each protein band or gel region of interest from a Coomassie-stained gel was excised using a clean scalpel, cut into small pieces (1x1 mm) and transferred into a 1.5 ml microtube. Afterwards, the gel was destained by adding 500 µl of 30% ACN in 100 mM NH_4HCO_3, incubating on a thermomixer at 25°C and 1000 rpm for 30 min and subsequently removing the solution. If there was still staining left, the destaining procedure was repeated.

Destaining was succeeded by gel-shrinking. For this, 500 µl 100% ACN were pipetted to the gel pieces, followed by a 15 min incubation at 1000 rpm 25°C, removal of the ACN-solution and finally vacuum centrifugation at 60°C to complete dryness.

Thereafter, 10 µl of trypsin solution (50 ng/µl in 50 mM NH_4HCO_3) were added to each dried gel sample and let become soaked up for ~1 min. Then 50 µl 100 mM NH_4HCO_3 were added and

incubated for 10 min to allow gel swelling. If samples were not completely covered afterwards, additional 100 mM NH_4HCO_3 was transferred into each tube. The tubes were subsequently placed overnight into a 37 °C-incubator to achieve protein digestion.

At the next day, the peptide solution was transferred to a fresh microtube. Subsequently, the peptides remaining in the gel matrix were extracted in three steps. First, 50 µl extraction solution 1 (0.1% TFA 50% ACN in H_2O) were added to each tube, incubated at 1000 rpm 25 °C for 15 min and then transferred to the peptide solution of the overnight digest. Second, 5 µl of extraction solution 2 (100 mM NH_4HCO_3) were put onto each sample and incubated as before. Third, without removing solution 2, 100 µl solution 3 (100% ACN) were added followed by another 15 min incubation. Finally, this extract was combined with the one from before and dried in a vacuum centrifuge at 60 °C to complete dryness. Usually, the dried peptides were then resuspended and cleaned up using StageTips before mass spectrometry analysis (see 3.2.4.12.6 Peptide cleanup by StageTips).

3.2.4.12.1.2 On-bead digest

Proteins bound to an affinity matrix can also be digested with trypsin directly instead of eluting, running on a SDS-PAGE and digesting in gel. This can be especially beneficial, if a complete elution is hindered by very strong protein binding (see: 3.2.4.11 NeutrAvidin affinity purification). The procedure applied in this thesis is described below:

The beads with the bound proteins, already washed in a buffer suitable for the subsequent tryptic digestion, were first treated with 10 mM DTT in 100 mM NH_4HCO_3 and heated to 56 °C for 30 min to accomplish protein reduction. Afterwards, the reduced disulfide bridges were alkylated by adding acrylamide to a final concentration of ~56 mM and incubating at room temperature for 30 min under constant agitation. Thereafter, the whole supernatant was removed by centrifugation (800 g, 1 min) and residual reduction and alkylation reagents eliminated by washing thrice with 1 ml 100 mM NH_4HCO_3. At last 1 µg trypsin, diluted in 300 µl 100 mM NH_4HCO_3, were added to each sample and digested overnight at 37 °C. At the next morning the solution containing the peptides was transferred to a clean microtube. Then, remaining peptides still bound to the beads were extracted by incubating twice with 300 µl of 5% ACN 0.1% FA (15 min, 800 rpm). The digests and extracts were combined afterwards and ready to be processed further (see: 3.2.4.12.4 Peptide cleanup by solid phase extraction (SPE).

3.2.4.12.1.3 RapiGest-assisted digest

RapiGest is a commercially available acid-cleavable detergent. It is used to solubilize and thereby improve the tryptic digestion of hydrophobic proteins (e.g. membrane proteins), which are normally less accessible by proteases. After the digestion, RapiGest can be easily cleaved and precipitated by

acidification, thereby allowing its complete removal before LC/MS-analysis, where it would interfere. RapiGest was used in this thesis as follows:

50 µl of 0.1% RapiGest (diluted in 100 mM TEAB) were added to each protein pellet, obtained by protein precipitation (see 3.2.4.4 Protein precipitation). The samples were mixed thoroughly and then boiled at 100 °C for 5 min to improve pellet resolubilisation. After sample cool down, DTT (diluted in 100 mM TEAB) was added to a final concentration of 5 mM and incubated 45 min at 60 °C for protein reduction. Subsequently, the samples were cooled down to room temperature and acrylamide added for cystein alkylation (final concentration 50 mM) followed by 20 min incubation. In the end, trypsin was added at a 1:100 trypsin:protein ratio, the sample filled up to 100 µl with 100 mM TEAB and everything digested overnight at 37 °C.

3.2.4.12.2 Tandem mass tags (TMT)-labeling of peptides

TMT-labeling allows the relative protein quantification between up to six samples in a single experiment (Figure 3-3A). Thus, peptides from different samples, for example cells or tissue lysate, are covalently linked to isobaric mass tags via their amine groups. This is achieved by an amine-reactive NHS-ester group contained in the tags. Afterwards, the samples can be mixed and processed together for downstream mass spectrometry analysis. The isobaric mass tags have an identical structure and mass, differing only in their isotopic composition (Figure 3-3B), therefore peptides from each sample co-elute during liquid chromatography. During fragmentation in the mass spectrometer each tag gives rise to a specific reporter ion of a defined mass. This subsequently allows to relatively quantify the amount of the fragmented peptide contributed by each sample (Figure 3-3C).

First, the TMT label reagents were removed from the freezer and equilibrated to room temperature. Afterwards, 123 µl of 100% acetonitrile were added to each tube and allowed to dissolve the reagent for 5 minutes assisted by intermittent mixing. Then it was split into three 40 µl fractions, allowing the parallel labeling of 3 samples. For this, the 40 µl were transferred to the sample vial containing the peptides destined to be labeled. The vial was mixed for 5 minutes at 600 rpm on thermomixer and then incubated for 1.5 h at room temperature to enable complete peptide labeling. This was stopped by adding 8 µl quenching reagent (5% hydroxylamine in 100 mM TEAB), which contains an excess of amine groups, mixing and incubating for 15 min at room temperature.

A

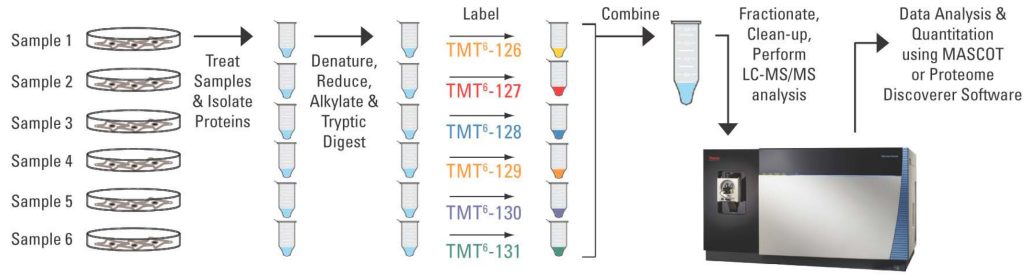

B

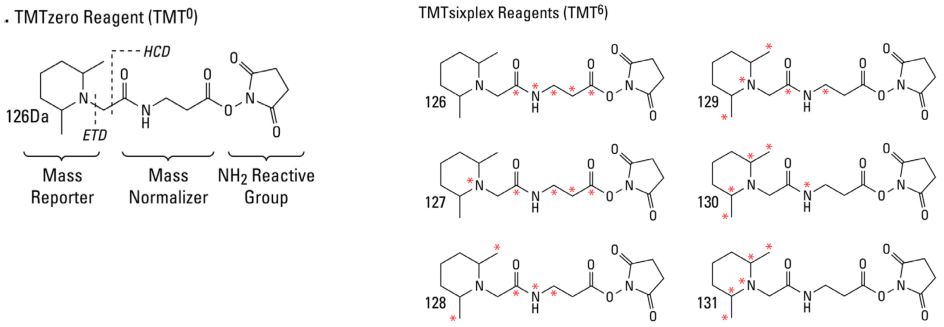

C

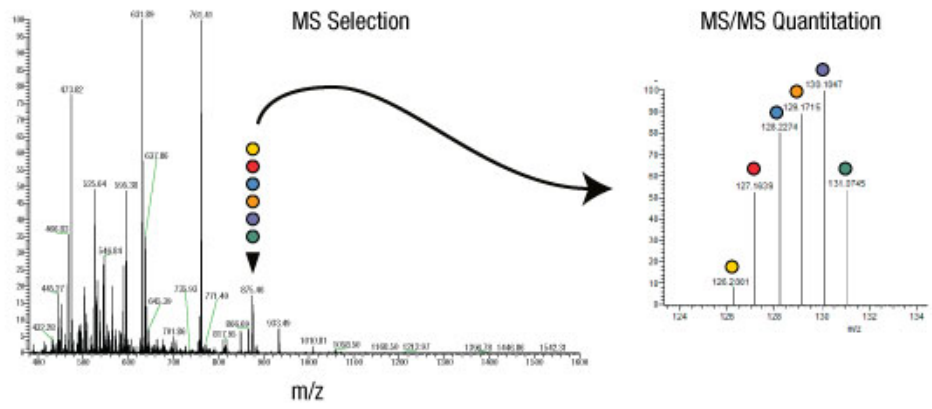

Figure 3-3: Principle of TMT-labeling. (A) Simplified experimental workflow of TMTsixplex™-labeling experiment. **(B)** Chemical structures of TMTzero (left) and TMTsixplex reagents (right). The TMTzero molecule is marked with the important structural components contained in all isobaric-labeling molecules. The mass reporter region is the part of the tag that breaks apart during HCD (higher-energy collisional dissociation)- or ETD (electron-transfer dissociation)-fragmentation in the mass spectrometer, thereby giving rise to a reporter ion. By varying the presence of heavy isotopes (red asteriskes) within this region, each tag produces a differentially sized reporter ion (HCD: 126, 127, 128, 129, 130 or 131 Da). This is counterbalanced by the isotope composition within the mass normalizer region, because all TMT-tags exhibit the same molecule mass. In addition, there is an amino-reactive NHS-group, needed for the covalent attachment to peptides. **(C)** Representative MS1-spectrum with labeled precursor peptide (left) and exemplary fragment spectrum of TMT reporter ions (right). Pictures from ThermoScientific: http://www.piercenet.com/product/amine-reactive-6-plex-tandem-mass-tag-reagents.

3.2.4.12.3 RapiGest removal by precipitation

RapiGest was removed by acidic cleavage and subsequent centrifugation. Accordingly, each sample was first acidified with TFA to a final concentration of 5% (v/v) and incubated for 45 min at 37 °C under constant agitation (800 rpm). Afterwards, the samples were centrifuged for 30 min at 20,000 g and the cleared supernatant transferred to a new microtube.

3.2.4.12.4 Peptide cleanup by solid phase extraction (SPE)

High peptide amounts, usually products of an in-solution digest, were desalted via solid phase extraction (SPE) using Oasis HLB cartridges (Waters). First, before sample loading the cartridge was activated 3x with 1 ml 70% ACN in 0.1% formic acid (FA) and subsequently equilibrated by flushing it 4x with 1 ml 0.1% FA. In addition, the peptide samples had to be conditioned to allow cartridge binding. For this, they were reduced to ~200 µl in a vacuum centrifugator to evaporate excess amounts of organic solvent, which would prevent column binding. Afterwards, they were filled up to 1 ml with 0.1% FA and acidified with 10 µl 100% FA.

Then they were loaded onto the HLB cartridges by pushing the solutions 3X trough. This was followed by 10 column washes with 1 ml 0.1% FA each. Finally, desalted peptides were eluted in two steps. First with 500 µl 30% ACN, followed by 300 µl 70% ACN. Both eluates were combined and dried at 60° C in a vacuum centrifuge afterwards.

3.2.4.12.5 Isoelectric fractionation of peptides (OFFGEL)

To obtain higher peptide and therefore protein identifications of complex samples via mass spectrometry, it can be useful to fractionate these samples before analysis by various methods. In isoelectric focusing, peptides are fractionated according to their isoelectric point within a pH gradient.

To accomplish this, an Agilent OFFGEL fractionation system with ready-made immobilized pH gradient (IPG) gel strips was used. In the first step, the IPG strip (12-well gel pH 3 - 10) was assembled into the sample tray according to the manufacturers instructions and rehydrated with rehydration buffer (0.2 % ampholyte solution pH 3-10 in H_2O). Afterwards, the vacuum dried peptide sample was resuspended in rehydration buffer and equally loaded onto the sample tray. The sample was the separated into 12 fractions by applying a high voltage overnight. Detailed instrument settings are given in Table 3-15. At the next morning the fractions were transferred to microtubes. 150 µl 0.1% TFA were added to each well and incubated for 15 min for extraction of remaining peptides. Then the extracts were combined with their respective fractions and cleaned up using StageTips.

Table 3-15: OFFGEL instrument settings for 12-well peptide separation.

Step	Volt Hour (kVh)	Voltage (V)	Current (µA)	Power (mW)	Time (h)
Focussing	20	4500	50	200	100
Hold	-	500	20	50	-

3.2.4.12.6 Peptide cleanup by StageTips

Small peptide amounts, usually peptides of a single gel band or OFFGEL-fraction, had to be desalted and concentrated before mass spectrometric measurement. For this purpose, so called StageTips (stop-and-go-extraction tips) were self prepared from standard 20 µl laboratory pipette tips, stuffed with a small amount of Empore C18 mesh material (Rappsilber et al. 2007). The tips were put in self-made adaptors, which themselves fitted into standard 1.5 ml microtubes. Thereby, solutions could be passed trough the tips by short centrifugations at low g-forces.

The cleanup procedure was as follows. First, the tips were activated by passing trough 20 µl methanol, followed by 20 µl 0.5% acetic acid in 80% acetonitrile. This was followed by an equilibration step with 20 µl 0.5% acetic acid. Thereafter, peptide samples could be directly loaded onto the tips, if they contained less than 5% ACN. Otherwise they had to be diluted first with water. Afterwards, the StageTips were washed once with 20 µl 0.5% acetic acid. Subsequently, the washed and desalted peptides were eluated in two steps of 10 µl 0.5% acetic acid in 80% acetonitrile each into a fresh microtube. In addition, the excess of organic solvent, which would prevent binding to the analytical column during MS-analysis, had to be removed by vacuum centrifugation. The dried peptides were stored at -80 °C before MS-analysis.

3.2.4.13 Mass spectometric measurements

Peptides were analyzed by a LC-MS/MS setup consisting of an Easy-nLC 1000 nano liquid chromatography device (ThermoScientific) coupled to an Orbitrap Velos mass spectrometer (ThermoScientific).

The solvents for LC-analysis were: solvent A: 0.1% FA in ddH_2O, solvent B: 0.1% FA in ACN. Separation of peptides was achieved on self-prepared C18-reversed phase capillary columns (Magic C18, 5 µm, 100 µm X 150-200 mm, Bruker-Michrom) via linear 30 or 60 min gradients at a flowrate of 400 nl/min. The linear gradients were always followed by two short column washes at 95% solvent B and a column equilibration of 10 min (Table 3-16).

Table 3-16: Profile of gradients used for LC-MS/MS separation of peptides.

Gradient type	Time (min)	Percentage of solvent B (%)
30 min	0	1
	30	35
	31	95
	34	1
	37	95
	40	1
	50	1
60 min	0	1
	60	35
	61	95
	64	1
	67	95
	70	1
	80	1

The mass spectrometer was set to acquire Orbitrap survey spectra in a mass range of 400 – 1200 m/z with a resolution of 30,000. For MS/MS peptides, fragmented by CID, were analyzed in the LTQ ion trap (minimal ion population: 5000, isolation width: 2 m/z, normalized collision energy: 35%) whereas HCD-fragmented peptides were measured in the Orbitrap (minimal ion population: 5000, isolation width: 2 m/z, normalized collision energy: 42%). In both cases, the ten most intense peaks from each survey scan were chosen for fragmentation. To reduce repeated fragmentation of the same peptides, dynamic exclusion was enabled (repeat count: 1, repeat duration: 30 s, excl. list size: 500, excl. duration: 30 s, excl. mass width relative to mass, excl. mass width relative to low/high: 10.00 ppm, expiration count: 1, expiration S/N threshold: 3.0).

3.2.4.14 Mass spectrometry data analysis

3.2.4.14.1 MaxQuant protein identification

Raw MS-data from the SILAC-IP interaction partner experiments was processed and searched against a modified human UniProtKB database (HUMAN.fasta from 06/2013) with added murine FA2H-sequence (Q5MPP0)) using the MaxQuant 1.4.1.2 software package (http://MaxQuant.org, (Cox & Mann 2008; Cox et al. 2011)). Note that all raw files of one experiment were included in a single search. The following search settings were used: Precursor tol. = 4.5 ppm, MS/MS tol. (FTMS) = 20 ppm, Top MS/MS peaks per 100 Da. (FTMS) = 12, MS/MS tol. (ITMS) = 0.5 Da, Top MS/MS peaks per 100 Da. (ITMS) = 8, PSM FDR = 0.01, Protein FDR = 0.01, Site FDR = 0.01, Min. peptide Length = 7, Min. score for unmodified peptides = 0, Min. score for modified peptides = 40, Min. delta score for

unmodified peptides = 0, Min. delta score for modified peptides = 17, Min. unique peptides = 0, Min. razor peptides = 1, Min. peptides = 1, Variable modifications = Acetyl (Protein N-term); Oxidation (M), Fixed modifications = Propionamide (C); Match between runs = enabled, Matching time window [min] = 2, Alignment time window [min] = 20. For SILAC-quantification the standard method with of 2 labeling states was selected. For the light channel no isotope labels were selected and for the heavy state Arg+10 and Lys+8. The quantification parameters were: Use only unmodified peptides = enabled, Modifications included in protein quantification = Acetyl (Protein N-term); Oxidation (M), Peptides used for protein quantification = Razor, Discard unmodified counterpart peptides = Enabled, Min. ratio count = 2, Site quantification = Use least modified peptide. The BioID-experiment data were searched with the same settings with the addition of Biotin (+226.077598 Da, N-terminus, K) as variable modification.

Data from TMT-experiments was analyzed with MaxQuant 1.4.1.2 against a murine UniProtKB database (MOUSE.fasta from 11/2013). The search settings were the same as for the interaction partner experiments (see above) with the exception of the selected quantification method, where the preset reporter ion quantification method TMT 6-plex was selected with default settings. Note that all raw files of one experiment were always combined in a single search.

3.2.4.14.2 Statistical analysis

3.2.4.14.2.1 Perseus

The protein result lists of all experiments were further analyzed and statistically evaluated with Perseus 1.4.0.12 (http://www.perseus-framework.org, (Cox & Mann 2012)) as follows:

For the SILAC-IP experiments, protein groups identified by MaxQuant as contaminants, reverse hits or identified by site hits were first filtered out. Subsequently, the normalized H/L-expression ratios of each protein group were linearized by log2-transformation, followed by an one sample t-test. It was tested, if the log2-expression ratios (log2 fold change) differed significantly from 0 (= log2(1) = no change). Afterwards, a volcano plot was produced, by plotting the average log2 fold change of each protein group against its –log-transformed p-value (-log10 p-value). This plot is a frequently used method to visualize the results of an interaction partner search. Protein groups enriched in the bait-containing sample should have a high log2 fold change (=enrichment) in combination with a large –log p-value (=significance), therefore appearing in the upper right part of the plot. In contrast, background proteins contributed by control and bait sample, should cluster around a log2 fold change of 0. Finally protein groups were deemed significantly enriched, if they exhibited a log2 fold change ≥ 0.585 (fold change ≥ 1.5) and a –log p-value > 1.301 (p-value < 0.05).

For the TMT experiments, protein groups identified by MaxQuant as contaminants, reverse hits or identified by site hits were first filtered out. Next, the expression values of each TMT-channel were normalized by dividing them through the respective summed TMT-channel intensity. Thereafter, FA2H-KO/WT expression ratios were calculated for each timepoint and subsequently linearized by log2-transformation. This was followed by filtering out every protein group with less then two expression values for at least one timepoint. Afterwards a one sample t-test was performed, testing if the log2-expression ratios differed significantly from 0. Finally, protein groups were deemed significantly upregulated, if they exhibited a log2 fold change ≥ 0.585 (fold change ≥ 1.5) and a –log p-value > 1.301 (p-value < 0.05). Conversely, the criteria for a significant downregulation were a log2 fold change ≤ -0.585 (fold change ≤ 0.667) and a –log p-value > 1.301 (p-value < 0.05).

3.2.4.14.2.2 GOrilla

Large scale gene function analysis was carried out with GOrilla (http://cbl-gorilla.cs.technion.ac.il, (Eden et al. 2009)), using its internal GO-term database (release May 17, 2014). GOrilla compares the GO-terms associated with entries of target list with the ones of a background list. By using hypergeometric testing, it calculates a p-value for each GO-terms, which indicates its degree of enrichment in the target list (Figure 3-4A). Accordingly, in the SILAC-IP experiments, the significantly enriched protein groups (target list) were searched against the whole list of identified protein groups (background list), using each groups first corresponding gene name. A significance threshold was applied filtering out all entries with p-values > 0.001. Furthermore, GOrilla calculates an error-corrected p-value (FDR q-value) by multiple testing using the Benjamini and Hochberg method (Benjamini & Hochberg 1995), and a simple enrichment factor (Figure 3-4B).

A **B**

$$\mathrm{Prob}(X \geq b) = \mathrm{HGT}(b; N, B, n) = \sum_{i=b}^{\min(n,B)} \frac{\binom{n}{i}\binom{N-n}{B-i}}{\binom{N}{B}}, \qquad enrichment = \frac{b/n}{B/N}$$

Figure 3-4: Formulas used by GOrilla to calculate p-values and enrichment factors.
(A) Formula using hypergeometric testing for p-value calculation. **(B)** Equation for calculation of enrichment factor. N = number of protein groups in ID list; B = number of protein groups associated with a specific GO term in ID list; n = number of protein groups in target list; b = number of protein groups associated with a specific GO term in target list.

3.2.4.14.2.3 Other statistical software

Alternatively, large scale annotation analysis was done using the PANTHER classification system 9.0 (http://www.pantherdb.org, (Mi et al. 2013)) and the GOSlimmer tool in the AmiGO 1.8 database (http://amigo1.geneontology.org/cgi-bin/amigo/slimmer, annotations from: Tue Jun 3 16:12:02 2014), without applying any statistical enrichment analysis.

3.2.4.15 Immunofluorescence staining and microscopy of cells

For immunofluorescent stainings, cells grown on glass coverslips were first fixed with 37 °C-prewarmed 4% PFA in PBS for 10 min at room temperature. Subsequently, they were once washed in PBS, incubated 20 min in 50 mM NH_4Cl in PBS, and washed twice with TBS. Next, cells were permeabilized via 10 min incubation in 0.3% Triton X-100 in TBS, succeeded by two TBS washes. These steps were omitted if only cell surface staining was desired. Afterwards, blocking of non-specific sites was performed with 1% BSA in TBS for 30 min at room temperature. This was followed by incubation with the primary antibodies in blocking solution for 60 – 120 min in a humid chamber. Thereafter, excess antibodies were removed by washing three times for 5 min in TBS before the secondary antibodies solutions were applied. In addition, 4',6-diamidino-2-phenylindole (DAPI) was added (dilution 1:1000) to these solutions to achieve nuclear staining. The incubations were performed 60 – 120 min in a dark humid chamber to avoid photobleaching of the fluorescent secondary antibodies. Afterwards the coverslips were washed twice for 5 min with TBS, shortly rinsed in ddH_2O followed by ethanol, and finally air dried for 10 min. The dried coverslips were mounted on glass coverslides in ProLong® Gold mounting medium and incubated overnight at room temperature. Hence, they were ready for fluorescent microscopy or stored at 4 °C. For fluorescent microscopy an AxioVert 100 M (Zeiss) equipped with a CCD camera (AxioCamHR) was used. Pictures were acquired and evaluated with the AxioVert 4.8 software.

3.2.4.16 Bimolecular fluorescence complementation (BiFC)

Bimolecular fluorescence complementation (BiFC) is a technique to verify protein-protein interactions previously identified in screening approaches in living cells (Kerppola 2008). Complementary fragments of a fluorescent protein, which are not fluorescent themself, are fused to potentially interacting proteins and transiently expressed in cells. If the proteins do interact, their attached protein fragments can reconstitute a functional fluorescent protein. This can be excited by its respective wavelength, thereby allowing an immediate visualization and quantitative read-out of the interaction. A variety of different fluorescent proteins can be used for BiFC, which are mostly ECFP- and EYFP-variants.

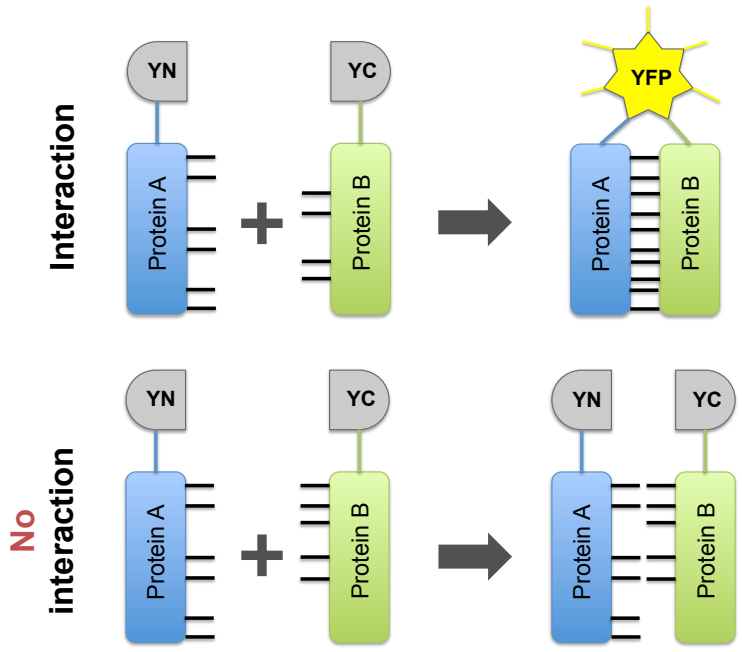

Figure 3-5: Schematic illustration of BiFC-principle.
Complementary fragments of a fluorescent protein (YFP-N-term. = YN; YFP-C-term. = YC), which are not fluorescent themself, are fused to putative protein interaction partners (Protein A & B) and expressed in cells. If the proteins actually interact they come in close contact, leading to the reconstitution of a functional fluorescent protein out of the two fragments. This can be visualized and quantitatively measured by fluorescent microscopy and related methods. In contrast, if they do not interact, no functional fluorescent protein is reconstituted and thus no fluorescent signal measurable. Picture adapted from: (Kerppola 2006).

In this thesis work, fluorescent fragments of the YFP Q69M-variant called citrine were used. The fragments were cYFP1 (amino acids 1-158) and YFP2 (amino acids 159-239), which were attached N- or C-terminally via a short linker sequence $(GGGGS)_2$. In addition, to the YFP-fragment sequences the N-terminal tagging plasmids also contained the signal sequence of calreticulin (SS_{cal}) to maintain protein ER-translocation (Nyfeler et al. 2005). The plasmids were kindly provided by Dr. V. Reiterer (Biotechnologie Institut Thurgau - Switzerland).

BiFC was performed as follows: First cells were seeded in appropriate culture vessels. For immunofluorescence microscopy these were coverslips within 12-well plates, whereas for quantitative measurements 6-well plates were used. After overnight attachment, the cells were transfected with the respective plasmid combinations and grown for 48 h. Subsequently, either immunofluorescence microscopy was performed (see 3.2.4.15 Immunofluorescence staining and microscopy of cells) or the cells fluorescence (BiFC-signal) was measured with a plate reader after transfer to a 96-well plate. For this, the cells were detached using trypsin, washed two times in 1X PBS, resuspended in 200 µl 1X PBS, and transferred to a black 96 well plate. Afterwards, the measurement was performed using one of the following devices: (A) Mithras LB 940 plate reader (Berthold Technologies) equipped with an excitation filter of 510/10 and an emission filter of 535 nm. (B) Infinite 200 PRO (TECAN) equipped with a monochromator set to an excitation of 505/9 and

emission of 540/20. The raw data obtained was evaluated with Microsoft Excel. Note that a positive control was included for the quantitative measurements. For this, cells were co-transfected with cYFP1- and YFP2-taged ER-Golgi intermediate compartment 53 kDa protein (ERGIC53), a lectin that oligomerizes in the ER and produces a strong BiFC-signal. Each other interaction's BiFC-signal was subsequently normalized to the positive control to compensate for variations in transfection efficiency.

3.2.5 Lipid analytic techniques

3.2.5.1 Bligh-Dyer lipid extraction

Lipids were extracted from cells by a protocol based on the rapid extraction method published by Bligh & Dyer (Bligh & Dyer 1959). Shortly, cells from one confluent well of a 6 well plate were harvested and washed once in 1X PBS. Afterwards, they were resuspended in 200 µl 1X PBS followed by successive addition and mixing with 750 µl chloroform-methanol (1:2, v/v), 250 µl chloroform ($CHCl_3$) and 250 µl ddH_2O. Finally, a phase separation was achieved by centrifuging for 2 min at 3000 g. The extracted lipids, contained in the lower chloroform-rich phase, were subsequently transferred to a microtube and dried in a vacuum centrifuge at 60°C. If the lipids were not further processed, they were stored at -20 °C. If larger or smaller amounts of cells were processed, the volumes of all buffers were adjusted accordingly, thereby maintaining the same proportions of chloroform, methanol and water during the extraction process.

3.2.5.2 Alkaline methanolysis of glycerolipids

Alkaline methanolysis of glycerolipids was done according to the method published by Bodennec and colleagues (Bodennec et al. 2000). First, the already extracted and dried lipids, derived from one well of a 6 well plate, were dissolved in a 400 µl 1:1-solution (v/v) of chloroform/0.6 M NaOH in methanol and incubated at RT for 2 h. Subsequently 160 µl of ddH_2O were added and the sample mixed vigorously. Then the mixture was centrifuged at 3000 g for 1 min to achieve phase separation. The upper phase was aspirated and the lower phase washed with a theoretical upper phase of 98 µl chloroform-methanol-ddH2O (3:48:47, v/v/v). After another short centrifugation, the lower lipophilic phase was removed to a microtube, dried in a vacuum centrifuge at 60°C and stored at -20 °C.

3.2.5.3 Thin-layer chromatography (TLC)

In thin layer chromatography substances are separated while migrating trough a solid matrix made of an adsorbent material called the stationary phase. Usually, the matrix material is spread onto a solid support glass plate (TLC plate). To achieve analyte separation, it is applied to the stationary phase. Afterwards, the plate is put into a solvent mixture, the mobile phase. The mobile phase is drawn up

by capillary forces taking the analyte with it, thereby achieving separation due to different migration rates.

In this thesis work, HPTLC silica plates (Merck) were used for lipid analytics. Before sample loading the plates were activated at 180 °C for 10 min. As the standard mobile phase for sphingo- and phospholipid separation a mixture of chloroform-methanol-water (70:30:4, v/v/v) was used. After chromatographic separation the plates were dried completely. Finally, for lipid visualization, the plates were sprayed with cupric sulfate solution, dried completely, and charred for 5 min at 180 °C. In the end, the TLC plates were digitalized with an image scanner.

3.2.6 Nucleic acid and cloning techniques

3.2.6.1 Polymerase chain reaction

Polymerase chain reaction (PCR) is a method to specifically amplify regions of DNA using short sequence-complementary oligonucleotides (primers) and a heat-resistant DNA-dependent DNA-polymerase. The PCR reaction consists of three phases. First, the DNA is denatured at 95-98 °C for 20 – 30 s to separate all double stranded DNA. Then the temperature is lowered for ~30 s to a value, which allows binding of the primers to their complementary target sequence. This step is called annealing and its temperature is dependent on the primers sequence (~50 – 68 °C). Afterwards, the temperature is risen to 72 °C at which the polymerase starts amplifying the DNA from the 3' end of the primer. The time of the amplification step depends on the length of DNA to be amplified. To obtain high amounts of amplified DNA, the three steps are generally repeated in 20 -35 cycles.

In this thesis two different DNA-polymerases were used: For genotyping of mice REDTaq® DNA Polymerase (SigmaAldrich) and for all cloning purposes Phusion® High-Fidelity DNA Polymerase (NEB). While REDTaq® DNA Polymerase was provided in a ready-to-use mix already containing buffer and dNTPs, for Phusion® PCRs all constituents had to be mixed before. The pipetting schemes for both PCR reactions are given below (Table 3-18 and Table 3-18). The PCRs were conducted on a Biometra Thermocycler 2000 with a heated lid. After PCR, the samples were cleaned for subsequent reactions using a QIAquick PCR Purification Kit® (Qiagen) according to the manufacturers protocol. Alternatively, the samples were first separated by agarose gel electrophoresis followed by gel-cutting and nucleotide-extraction using a QIAquick Gel Extraction Kit® (Qiagen).

Table 3-17: Pipetting scheme for REDTaq® PCR reactions.

	20 µl reaction	50 µl reaction
Name	**Volume/amount**	**Volume/amount**
REDTaq® Ready Mix	10 µl	25 µl
100 µM Forward primer	0.1 µl	0.25 µl
100 µM Reverse primer	0.1 µl	0.25 µl
Template DNA	1-10 ng	1-10 ng
Nuclease free H_2O	Fill up to 20 µl	Fill up to 50 µl

Table 3-18: Pipetting scheme for Phusion® PCR reactions.

	20 µl reaction	50 µl reaction
Name	**Volume/amount**	**Volume/amount**
5X HF or GC buffer	4 µl	10 µl
100 µM Forward primer	0.1 µl	0.25 µl
100 µM Reverse primer	0.1 µl	0.25 µl
Template DNA	1-10 ng	1-10 ng
2mM dNTPs	2 µl	5 µl
Phusion DNA Polymerase	0.2 µl	0.5 µl
Nuclease free H_2O	Fill up to 20 µl	Fill up to 50 µl

3.2.6.2 Isolation of plasmid DNA

Plasmid DNA was isolated from transformed bacteria using Qiagen MiniPrep or Midiprep Kits® depending on the size of the bacterial starting material. For mini scale preparations a single colony was picked from a-plate, inoculated into 5 ml liquid LB-medium (including appropriate antibiotic) and incubated over night at 250 rpm 37 °C. In the case of a midi preparation 50 ml medium were used. At the next day, the cells were pelleted and resuspended with the provided resuspension buffer containing RNAse in a volume according to the manufacturers manual. Afterwards, alkaline lysis buffer containing SDS was added to break up the cells. The lysis was stopped and proteins precipitated by adding acidic neutralization buffer. Then the samples were centrifuged to remove any precipitated material and the clear supernatant loaded onto positively charged nucleic acid binding columns. The columns were spun and afterwards washed with the provided washing buffers. In the end, the bound plasmids were eluted with either ddH_2O (mini kit) or elution buffer (midi kit). When a midi kit was used, three additional steps followed. First, the plasmid-DNA was precipitated from the eluate with isopropanol. Second, the pellet was washed once in 70% ethanol. In the end, the DNA was resuspended in ddH_2O. The plasmid obtained by both kits were finally evaluated regarding DNA-content and purity with a NanoDrop spectrophotometer and stored at -20 °C until further usage.

3.2.6.3 Restriction digest

DNA was digested with restriction endonucleases, which cleave the phosphodiester bound of DNA at specific recognition sites. This technique was on the one hand used for subcloning of DNA-fragments and on the other hand for the verification of plasmid identities. The digestion was usually done for 1-2 h at 37 °C in 20 µl reactions according to the following table:

Table 3-19: Reaction volumes for restriction digest.

Name	Volume/amount
10X restriction buffer	2 µl
DNA	1-2 µg
Restriction enzyme (10 units/µl)	0.5 - 1 µl
ddH_2O	Fill up to 20 µl

3.2.6.4 Agarose gel electrophoresis

Agarose gel electrophoresis is used to separate nucleotides by size, thereby allowing the determination of their molecular weight when run in parallel with a DNA-concentration standard. In addition, it can also be applied in a preparative manner to purify certain nucleotides out of a nucleotide mixture e.g. after restriction digest or PCR. The separation is achieved by applying an electric field to a polymeric agarose matrix with the nucleotide samples loaded onto it. Because of their negatively charges they move towards the anode. While small molecules can pass the gel matrix more easily larger molecules are slowed down by it, leading to a separation by size. The matrix separation capabilities are directly given by its composition, so depending of the molecules to be separated agarose gels of different percentages have to be used.

In this thesis 0.5 – 2% agarose mini-gels in 1X TAE buffer supplemented with ethidium bromide (1:200 from stock solution) were used. Samples were premixed with 6X loading dye and run at 120 – 140 V for 30 - 45 min depending on the gels agarose composition. Usually, a GeneRuler 1 kb DNA ladder (ThermoScientific) was used. The visualization of nucleotides was achieved by UV-excitation and gel images were acquired with a CCD-based camera system.

3.2.6.5 Nucleotide-extraction from agarose gels

Nucleotides were extracted after gel electrophoresis by using a QIAquick Gel Extraction Kit® (Qiagen) according to the manufacturers protocol. Shortly, the bands of interest were cut out with a clean scalpel, weighted, and melted for 10 - 15 min at 50 °C after mixing with 3 gel volumes of gel solubilization buffer. Thereafter, 1 gel volume of isopropanol was added and the mixture loaded onto positively charged spin columns for nucleotide retrieval. The columns were centrifuged 1 min at 16,000 g, the flow through discarded, and the columns washed once with 500 µl ethanol-containing

washing buffer. In the end, residual ethanol was removed by another centrifugation and the cleaned nucleotides eluted with 30-50µl ddH_2O to fresh microtubes. If not used directly the eluates were stored at -20 °C.

3.2.6.6 DNA-concentration determination

3.2.6.6.1 Exact determination via spectrophotometry

DNA shows a high absorbance of UV-light at 260 nm, which is proportional to its amount (50 ng/µl dsDNA & 1cm light path = 1 absorbance unit). Therefore, a sample's DNA-concentration can be estimated by measuring its absorbance at 260 nm via a spectrophotometer. In this work, a NanoDrop spectrophotometer was used which only needs 0.5 -1 µl of a sample to determine its DNA-concentration.

3.2.6.6.2 Determination via agarose gel

The DNA-concentration of a sample can also be determined by separating it on an agarose gel together with a size standard of known concentration. The comparison of the sample's nucleotide band intensity with the ones of the standard finally allows a determination of its DNA-concentration.

3.2.6.7 DNA-Ligation

DNA-ligation is the enzymatic joining of DNA ends by phosphodiester bonds. In this thesis work T4 DNA ligase (ThermoScientific) was used. Depending if DNA fragments with blunt or sticky ends were present, one of the following procedures was applied.

For sticky end ligations a 20 µl ligation reaction was mixed according to Table 3-20 and incubated for 1 h at room temperature.

Table 3-20: Reaction mixture for sticky end ligation.

Name	Volume/amount
10X T4 DNA ligase buffer	2 µl
T4 DNA ligase (1 unit/µl)	1 µl
Linear vector DNA	20 ng
Insert DNA	3:1 molar ratio over vector
ddH_2O	Fill up to 20 µl

Blunt end ligation reactions were pipetted as described in Table 3-21 and incubated for 2 h - overnight at room temperature.

Table 3-21: Reaction mixture for blunt end ligation.

Name	Volume/amount
10X T4 DNA ligase buffer	2 µl
T4 DNA ligase (1 unit/µl)	5 µl
Linear vector DNA	20 ng
Insert DNA	3:1 molar ratio over vector
ddH_2O	Fill up to 20 µl

After ligation, 5 µl of the mixture were transformed into competent bacteria (see 3.2.2.2 Transformation of chemical competent bacteria).

3.2.6.8 StarGate® cloning

Directional cloning of Twin-Strep constructs into mammalian expression vectors was achieved by the StarGate® combinatorial cloning system (IBA lifesciences). This system utilizes two types of vectors, a universal donor and various acceptor vectors. Initially, the gene of interest is amplified via PCR thereby adding recombinase recognition sites, which allow directional subcloning into the donor vector. From this, donor vector the gene of interest can than be subcloned in a variety of different acceptor vectors by another recombinase-mediated reaction. For a detailed description of the cloning procedure consult the manufactures manual. The primers used for donor generation are detailed in Table 3-8.

4 Results

4.1 Comparative quantitative myelin proteome analysis of FA2H-KO mice

Changes in the myelin protein composition of FA2H-KO compared to WT mice were measured using a reporter ion-based quantification approach (see 3.2.4.12.2 Tandem mass tags (TMT)-labeling of peptides). The assay was done separately for myelin originating from two different tissues e.g. brain (=CNS myelin) and sciatic nerves (=PNS myelin) and from animals at 6, 13 and 17 months of age. Furthermore, each assay was conducted in three biological replicates. Note that no technical replicates were conducted due to the high cost of labeling reagents and the limited amount of PNS-myelin available per animal. A schematic depicting the analysis workflow is given in Figure 4-1.

Myelin was purified from the different animals and tissues by density gradient purification. After a quality assessment by SDS-PAGE and silver staining, myelin from both tissues was processed as follows. First, equal protein amounts of myelin were tryptically digested. Afterwards, the resulting peptides of each genotype and animal age were individually labeled with a distinct isobaric label (TMT 6-plex). Following labeling, the six samples were combined and the sample complexity reduced by 12-well OFFGEL fractionation. Thereafter, each fraction was analyzed by LC-MS/MS in a high resolution Orbitrap Velos hybrid mass spectrometer. During fragmentation in the mass spectrometer each isobaric tag leads to the generation of a specific fragment (reporter ion), allowing the determination of each peptide's relative abundance in comparison to the five others. For each protein the relative protein amount can thus be easily calculated from the sum of its peptide values.

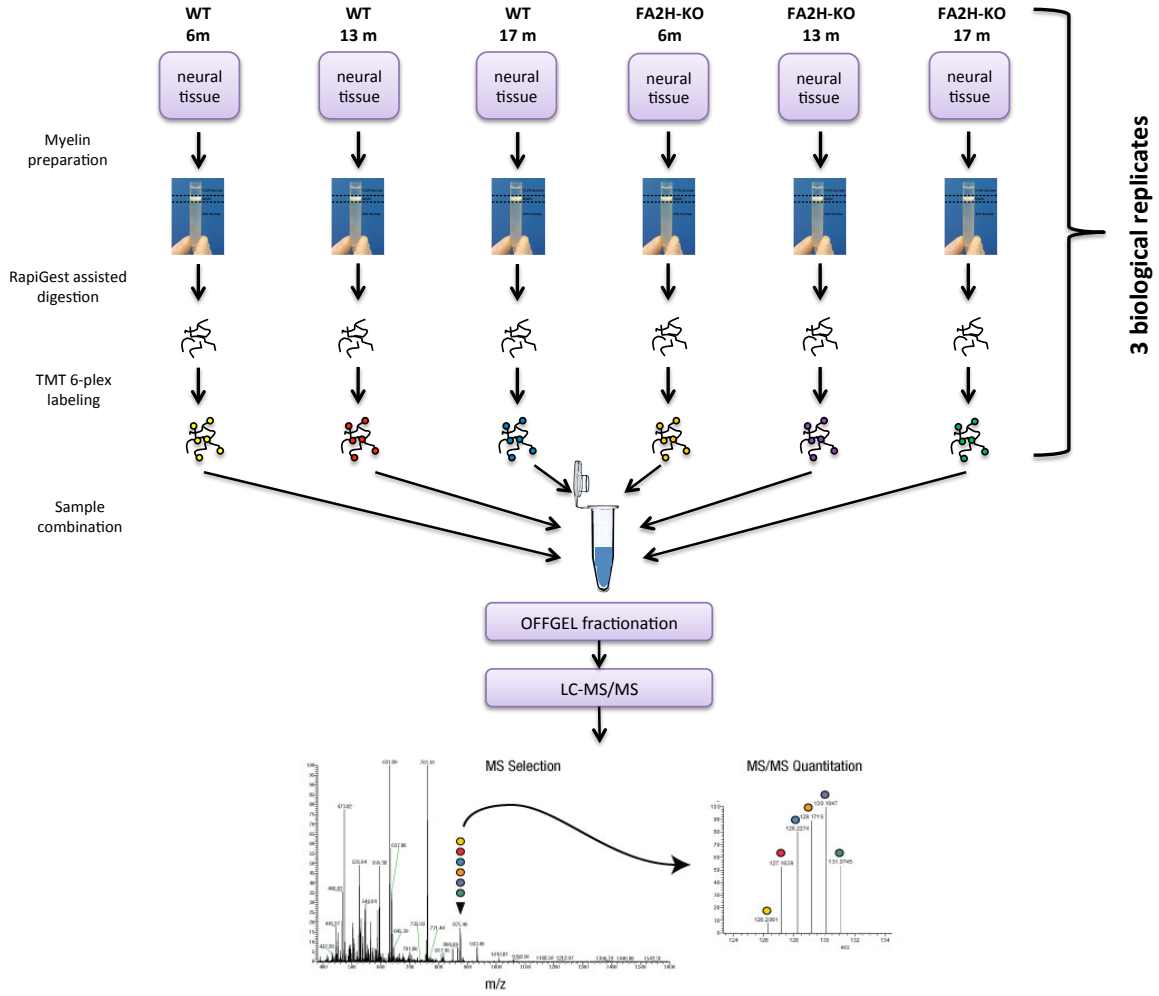

Figure 4-1: Scheme of quantitative myelin proteome analysis by TMT-labeling approach.
Myelin containing neural tissues, i.e. brain and sciatic nerves of WT and FA2H-KO mice, of three stages of age (6, 13 and 17 months) were obtained and myelin was individually purified from each tissue by density gradient centrifugation. Equal protein amounts of myelin from one tissue type were tryptically digested, assisted by the acid-labile and mass spectrometry compatible detergent RapiGest. Subsequently, the resulting peptides of each sample were differentially labeled with one of six TMT 6-plex tags followed by sample combination. The combined peptides were then desalted, the sample complexity reduced by isoelectric peptide focusing (OFFGEL) and all fractions finally analyzed by LC-MS/MS. The acquired spectra were finally processed by MaxQuant, allowing the identification and relative quantification of myelin proteins based on reporter ion intensities. The experiment was repeated three times using animals of the same age and genotype (3 biological replicates).

4.1.1 Myelin purification & quality assessment

Myelin from WT and FA2H-KO animals was prepared by the well-established sucrose density gradient centrifugation method (see 3.2.1.2 Myelin preparation). Because of its relatively unique density, a reasonably pure myelin enriched-fraction can be obtained by this method. After preparation, the myelin quality was examined by separating small amounts via SDS-PAGE and performing a subsequent silver staining.

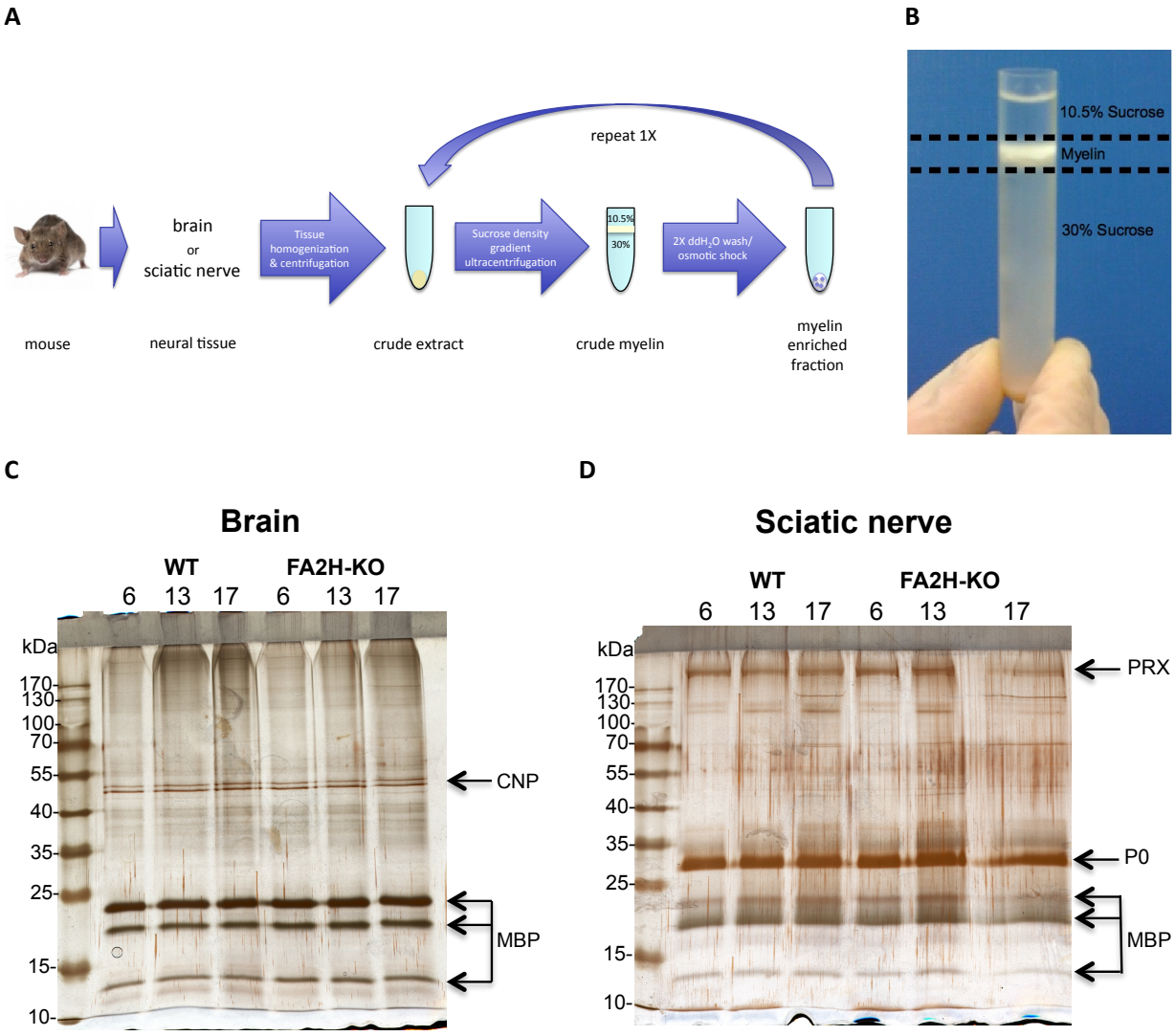

Figure 4-2: Isolation of myelin from brains and sciatic nerves.
(A) Scheme depicting myelin purification procedure by sucrose density gradient. **(B)** Example picture for myelin-enriched fraction (from brain) obtained by sucrose density gradient centrifugation. Myelin is clearly visible as a distinct white layer between the two differentially concentrated sucrose solutions (10.5 and 30%). Note that for sciatic nerve myelin, sucrose solutions of slightly altered concentrations (9.2% and 28.4%,) were used. **(C) and (D)** 1 µg of brain/sciatic nerve myelin from one animal of each genotype (WT and FA2H-KO) and age (6, 13 and 17 months) was separated by 12.5% SDS-PAGE and proteins subsequently visualized by silver staining. Myelin from the same animals was used for all gels. Strongly stained protein bands representing some known myelin proteins are marked with arrows. CNP = 2',3'-cyclic-nucleotide 3'-phosphodiesterase; PLP = proteolipid protein; MBP = myelin basic protein; PRX = periaxin; P0 = myelin protein zero.

The silver stained gels (Figure 4-2C and D) indicated that myelin was successfully purified from brains and sciatic nerves of 6, 13 and 17 months old WT and FA2H-KO animals. The protein pattern was similar to the one described in the literature (Larocca & Norton 2007). Typical major protein bands usually found in CNS- (MBP, CNP) and PNS-myelin (MBP, P0, PRX) were visible. Surprisingly, the PLP-signal (~35 kDa) was absent in the brain samples for unknown reasons. However, the following mass spectrometry analyzes clearly showed its presence in the myelin preparations (Figure 4-4). Overall, there were only minor differences in the protein band patterns, emphasizing the consistency of the

purification procedure. Furthermore, there were no apparent differences between WT and FA2H-KO animals at any given time point, indicating that the high abundant myelin proteins are unchanged.

4.1.2 Identification of myelin proteome alterations in FA2H-KO mice

For the quantitative analysis of myelin proteome changes in FA2H-KO mice the samples were processed as follows. For each tissue (brain or sciatic nerves) 40 µg of myelin from 6-, 13- and 17-month-old WT and FA2H-KO mice were first delipidated by aceton precipitation. Afterwards, each sample was resolubilized in 0.1% RapiGest containing buffer, reduced and alkylated, digested with trypsin and the peptides TMT-6plex labeled. The labeled peptides were then combined, RapiGest removed by acidic-cleavage and precipitation, and the combined samples desalted by solid-phase extraction (SPE). Subsequently, the complexity of the sample was reduced by isoelectric peptide fractionation (OFFGEL). Thereafter, the resulting 12 fractions were desalted using C18-StageTips and analyzed by LC-MS/MS. Finally, the 36 raw data files (12 fractions X 3 biological replicates) were combined and protein groups identified by searching against a murine Uniprot database using MaxQuant. The identifications are given as protein groups and not single proteins. A protein group is an identifier, which includes all proteins, protein isoforms and protein sequence variants that can be explained by the same detected peptides. A protein group can also contain one single protein, but only if peptides unique for it were found. Additionally, MaxQuant calculated reporter ion intensities for each protein. Afterwards, the resulting protein group lists were further processed using Perseus. Shortly, the data were normalized, FA2H-KO/WT expression ratios calculated, entries with insufficient quantitative values removed, and significantly changed protein groups identified by one-sample t-tests. Moreover, annotation analyses of significantly changed protein groups were conducted using AmiGO and PANTHER. The results for each tissue are given in the sections below. The details of the data analysis are described in the method section (3.2.4.14 Mass spectrometry data analysis).

4.1.2.1 Brain myelin analysis

4.1.2.1.1 Mass spectrometric analysis using TMT-labeling

The comparative brain myelin proteome analysis was carried out as described above. A first overview of its results and a comparison to previously published CNS-myelin data is given in Figure 4-3. Note that the original MaxQuant result files and the processed protein group list can be found on the supplemental DVD.

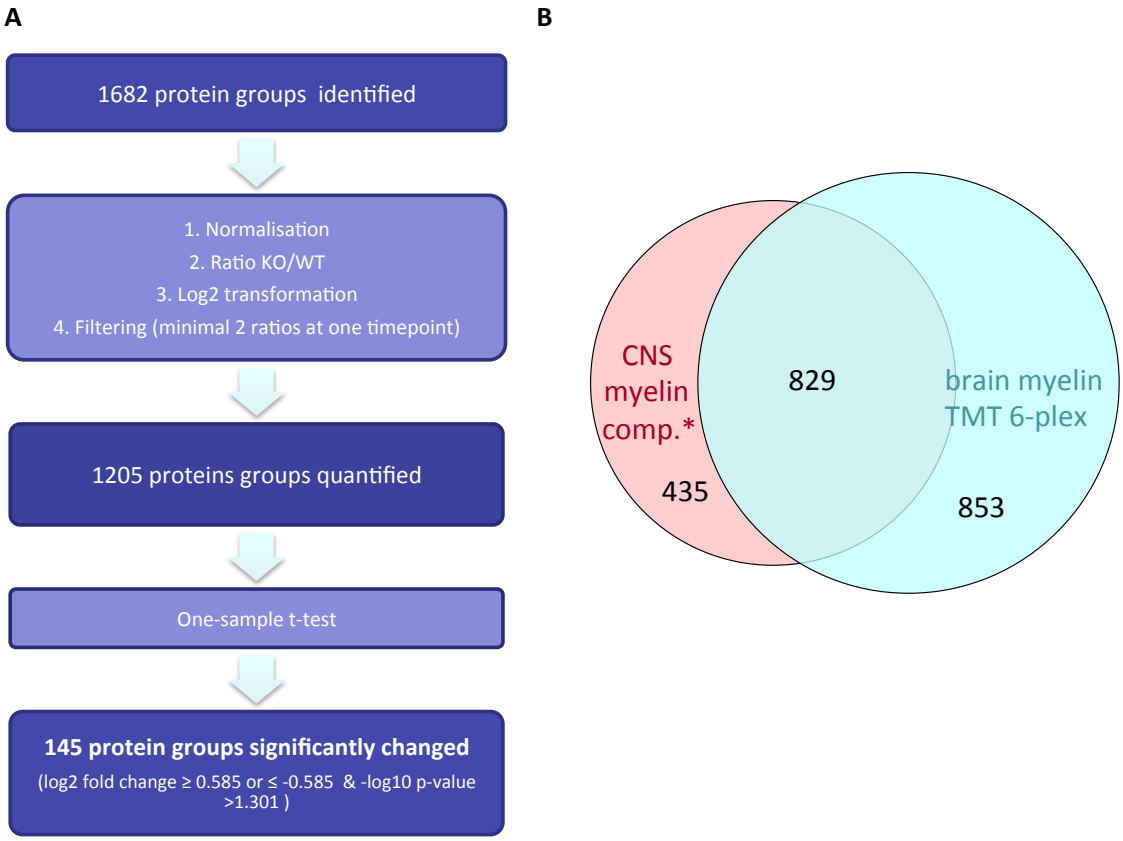

Figure 4-3: Quantitative brain myelin (CNS) proteome analysis.
(A) Diagram depicting the workflow of protein group results processing. MaxQuant identified 1682 protein groups after combined analysis of all raw files (matched against murine Uniprot database). The data were then normalized (each reporter intensity divided by summed reporter channel intensity) and log2 FA2H-KO/WT expression ratios (log2 fold change) calculated for each timepoint. Subsequently, the data were filtered for protein groups with at least two expression ratios at one timepoint leaving 1205. To assess proteins, which had a significantly changed expression in FA2H-KO mice, the log2 transformed expression values were evaluated by a one-sample t-test against 0 (log2(1) = 0 = no change) for each timepoint. This resulted in the identification of 145 significantly changed protein groups. **(B)** Proportional Venn diagram comparing the proteins identified with TMT 6-plex brain myelin proteome analysis in this thesis with the published CNS myelin reference list (de Monasterio-Schrader et al. 2012). The first gene name of each protein group was used as identifier. A list, containing all gene names related to the overlapping areas, can be found on the supplemental DVD.

1682 protein groups were identified by MaxQuant (razor or unique peptides ≥ 1; false discovery rate (FDR) = 0.01) in the brain myelin dataset (Figure 4-3A), thereby significantly exceeding the number of ~1300 currently known CNS-myelin proteins (de Monasterio-Schrader et al. 2012). Still, when comparing the brain myelin dataset with the reference list, there was a large congruency of 829 protein groups identified in both, as becomes obvious from the Venn diagram (Figure 4-3B). This further proved the successful myelin preparation by the sucrose density gradient protocol.

To identify protein abundance differences between WT and FA2H-KO mice, the data were further processed (Figure 4-3A). Therefore, after normalization, expression ratios FA2H-KO/WT were calculated for each timepoint (6, 13 and 17 months), which were afterwards linearized by a log2-transformation (log2 fold change). Because quantitative information was not available for all protein groups, due to weak reporter ion signals, protein groups, which had less than two expression ratios

at at least one timepoint, were filtered out. This reduced the list to 1205 entries. To assess protein groups, which had a significantly changed expression in FA2H-KO mice, a one-sample t-test was performed for each timepoint. On the basis of the generated –log10-transformed p-values and the magnitude of the log2 fold change, the protein groups were filtered for being significantly upregulated and downregulated. Protein groups were deemed significantly upregulated, if they exhibited a relevant, i.e. sufficiently large enough, log2 fold change ≥ 0.585 (fold change ≥ 1.5) and a –log10 p-value > 1.301 (p-value < 0.05). Conversely, the criteria for a significant downregulation were a log2 fold change ≤ -0.585 (fold change ≤ 0.667) and a –log10 p-value > 1.301 (p-value < 0.05). This led to 145 protein groups, which were significantly changed at at least one timepoint. Note that some of these were changed at more than one timepoint.

Before analyzing this relatively large number of changed protein groups in more detail, it was first evaluated if major CNS-myelin proteins, e.g. MBP, CNP, MOG etc., were not changed between FA2H-KO and WT at all three timepoints. As mentioned before (see: 2.4 Aim of this study), initial analyses of young FA2H-KO CNS-myelin had shown no differences in such proteins, therefore arguing for more subtle changes causing the FA2H deficiency phenotype. In the figure below (Figure 4-4) the mean log2 fold changes for some major CNS-myelin proteins are plotted against the animal ages. Within these plot dashed black lines mark the borders for a log2 fold change to be deemed relevant. Further note that MaxQuant had possible MBP-isoforms and sequence variants subdivided into three separate protein groups.

The plot revealed that the examined major CNS-myelin proteins were not substantially changed between FA2H-KO and WT at all three timepoints. Only for MBP, two of its three protein groups showed a log2 fold change close to the lower border. Accordingly, a slight downregulation of some MBP-isoforms could not be excluded completely.

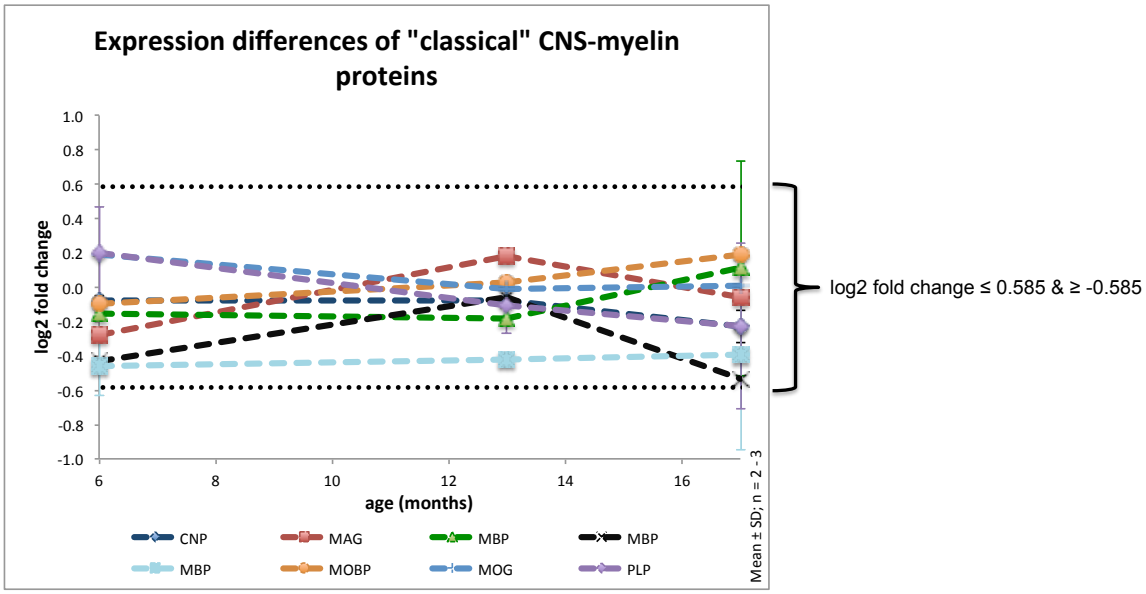

Figure 4-4: Expression differences of major CNS-myelin proteins between FA2H-KO and WT mice in brain myelin. Each protein group's mean log2 transformed KO/WT expression ratios (log2 fold change) are plotted against the mice age in month. For each line the standard deviation at each time point is given by error bars, if it was calculable (n = 2-3). Horizontal doted black lines mark the borders for relevant, i.e. sufficiently large enough, log2 fold changes (log2 fold change ≥ 0.585 & ≤ -0.585). Note that MaxQuant assigned different MBP-isoforms and sequence variants to three separate protein group entries, with all had slightly different mean log2 fold changes. CNP = cyclic nucleotide phosphodiesterase; MAG = myelin-associated glycoprotein; MBP = myelin basic protein; MOBP = myelin-associated oligodendrocyte basic protein; MOG = myelin-oligodendrocyte glycoprotein; PLP = proteolipid protein.

After showing no relevant change in major CNS-myelin proteins, the 145 significantly changed protein groups were evaluated in more detail. At each single timepoint between 50 and 71 protein groups were significantly up- or downregulated (Figure 4-5A). Moreover, a trend was observable showing that the number of significantly upregulated proteins increased, while the number of significantly downregulated protein groups decreased over time. While the increase in upregulations can be likely attributed to the aggravating pathology of the FA2H-KO deficiency, the decrease in downregulations cannot be explained conclusively. Potentially, it may reflect compensatory reactions within the organisms of the KO-mice, which tried to restore the amounts of the affected proteins to WT-levels.

Next, for assessing the persistence of an expression change, the protein group identifications were compared to each other between the three timepoints. This was done separately for the up- and downregulated protein groups and depicted in proportional Venn diagrams (Figure 4-5B). The respective Venn diagrams showed that the majority of protein groups significantly up- or downregulated were unique for one timepoint, thereby further supporting the possible influence of compensatory effects mentioned above. Still, for the upregulated ones there were also three protein groups displaying a constant significant change from the first to the last timepoint. In contrast, others were up- or downregulated constantly only at timepoints 6 and 13M (up = 3; down = 8) or timepoints

13 and 17M (up = 11). Moreover, no protein groups were significantly downregulated between the last two timepoints. For the upregulations the greatest congruency was observable for the later timepoints (13 & 17M), thus emphasizing that at least some upregulations were persistent. The opposite was true for the downregulations, with the biggest congruency between timepoints 6 and 13M. Accordingly, the majority of downregulations were only temporary and reverted back to the WT-level in older mice, again speaking for compensatory reactions in the KO-animals.

A

	Up*	Down**
6 months	15	35
13 months	34	19
17 months	61	10

*Upregulated in KO = log2 fold change ≥ 0.585 & -log10 p-value > 1.301
**Downregulated in KO = log2 fold change ≤ -0.585 & -log10 p-value > 1.301

B

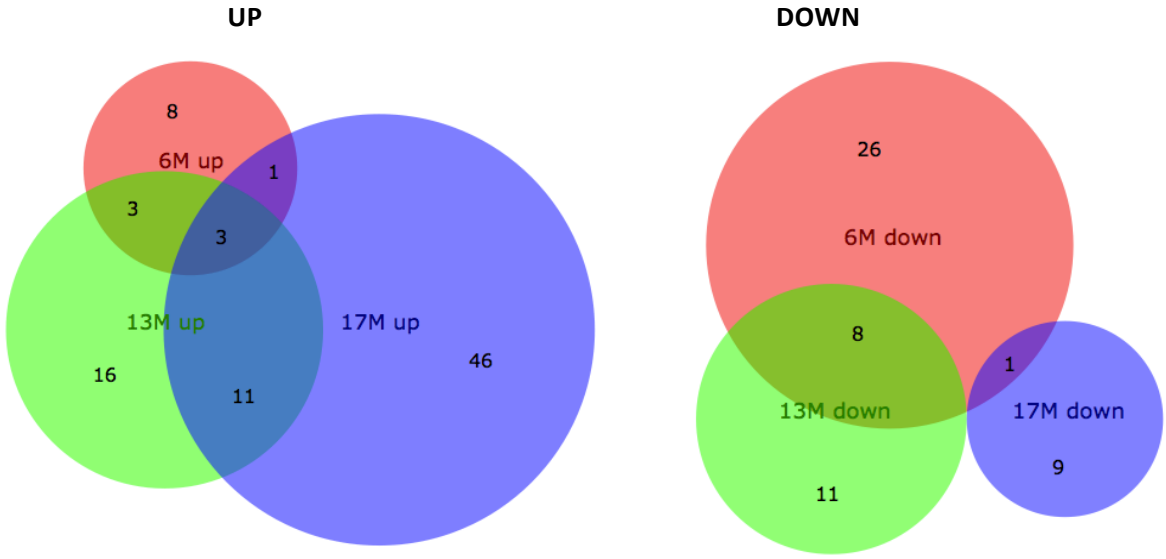

Figure 4-5: The 145 protein groups significantly up- and downregulated in FA2H-KO brain myelin.
(A) Number of significantly up- and downregulated protein groups at each time point. Note that the same proteins can be changed at more than one timepoint. **(B)** Comparison of the significantly upregulated (left) or downregulated (right) protein group identifications at the three timepoints by area-proportional Venn diagrams. The first gene name of each protein group was used as identifier. The identities of the protein groups behind each number are given in Table 4-1 and Table 4-2.

To get an overview about the identity of the relatively large number of significantly changed protein groups, tables were generated for the upregulated (Table 4-1) and downregulated (Table 4-2) protein groups. In each table the protein groups (indicated by their respective gene names) are given with their log2 fold change for each timepoint. Log2 fold changes, which were significant (-log10 p-value >1.301), are highlighted by red (upregulated) or green (downregulated) shading, respectively.

Table 4-1: Protein groups significantly upregulated in brain myelin at at least one timepoint.
The table contains the proteins groups, indicated by their respective gene games, which showed a significant upregulation at one timepoint or more. Besides each gene name the log2 fold change (log2 ratio FA2H-KO/WT) is given for each timepoint. Significant changes (log2 fold change ≥ 0.585 & -log10 p > 1.301) are shaded in red.

Gene names	log2 fold change 6M	log2 fold change 13M	log2 fold change 17M	Gene names	log2 fold change 6M	log2 fold change 13M	log2 fold change 17M
Acta1;Actc1;Actg2; Acta2	-0.0720	0.2839	0.6950	Map4	0.2376	0.5922	0.6228
Actr1a	-0.1490	0.1302	0.7189	Mapt	0.6290	0.9679	0.8513
Amph	0.0955	0.3769	0.6115	Mark1	0.2406	0.1035	0.8548
Ank3	0.5887	0.2829	0.2405	Mcam	0.7237	0.7853	0.4283
Apoe	0.7043	0.9555	0.8848	Mink1	0.6205	0.6720	0.2816
Asap1	0.3882	0.7889	0.9565	Msn	0.3920	0.6559	0.7229
Aspa	-0.5010	0.3926	0.6325	Mvp	0.2602	0.4356	0.7386
Atpif1	0.5085	0.7005	0.4411	Myo18a	0.5086	0.5106	0.7845
Bcr;Abr	-0.4705	0.2027	0.5948	Myo6	0.2016	0.2955	0.5923
C1qb	0.8778	1.3776	1.8911	Nefh	-0.1186	-0.1319	0.8063
C4b	0.8363	2.2834	2.2925	Nefl	-0.2225	-0.0120	0.8806
Cadm4	0.4227	0.5109	0.5865	Nefm	-0.1590	0.0074	0.9354
Ccdc124	0.4023	0.9786	1.0150	Opalin	0.9294	0.7626	1.0055
Ckap5	0.3293	0.8913	0.6070	Pacsin2	-0.0391	0.7413	0.8693
Clasp2	0.3196	0.7513	0.8451	Pcbp1;Pcbp3;Pcbp2	-0.3535	0.0142	0.6486
Crocc	-0.2277	0.4888	0.8973	Pclo	0.5574	0.5999	0.5811
Ctsd	-0.1608	-0.3405	0.7346	Phgdh	-0.4710	0.2983	0.6935
Dctn2	-0.1720	0.1688	0.8316	Plcb3	0.3215	0.6531	0.7000
Ddc	-0.3853	-0.1371	1.2003	Ppib	0.6318	0.6871	0.3067
Dhrs1	0.5075	0.6540	0.3471	Ppp2r2d;Ppp2r2a	-0.3603	0.1090	0.7866
Dnm1	0.0991	0.6994	0.7395	Prkag2	0.0326	-0.1270	0.6919
Dnm1;Dnm2	0.3480	0.8480	0.8157	Prkcb	0.1015	0.1065	0.8838
Dnm3	0.1777	0.6094	0.6263	Ptn	0.9249	0.9370	1.1389
Dock5	0.5089	0.2775	0.6296	Qdpr	-0.1557	0.3143	0.8409
Dstn	-0.4120	0.0149	0.7185	Rras2	0.6441	0.2492	0.3820
Edil3	0.5759	0.7566	0.5890	Scamp4	0.5675	0.6194	0.6117
Erbb2ip	0.5556	0.8849	1.0746	Scrn1	-0.4814	-0.3127	0.6217
Fabp5	-0.0659	0.3053	0.9348	Sirpa	0.6224	0.2730	0.4804
Fasn	-0.1297	0.2606	0.7930	Slk	0.5733	0.7763	0.4949
Fnbp1	-0.0046	0.6370	0.9081	Stk39	-0.3923	0.0483	0.6105
Gfap	0.7495	1.2719	1.3426	Synj1	0.5233	0.2845	0.6140
Glul	-0.2428	-0.0898	0.6266	Sypl;Sypl1	0.6302	0.0889	-0.0907
Gpd1	-0.3174	0.3608	0.7428	Taok1	0.6467	0.5343	0.1024
Gprc5b	1.1533	0.5885	0.0125	Taok2	0.6946	0.7244	0.3054
Grn	-0.1810	0.8560	1.2189	Tbc1d10b	0.6993	0.5429	0.1998
Hip1r	-0.0294	0.6531	0.8620	Tjp2	0.1258	0.2978	0.7369
Hmgn1	0.7984	1.6866	1.7496	Tollip	-0.0211	0.5463	0.7647
Hmgn2	0.8473	0.8366	1.2773	Tom1l2	-0.2676	0.1462	0.6152
Hspa2	-0.0844	0.6976	0.4684	Trim2	0.2501	0.6443	0.6697

Htra1	0.6387	0.7627	0.8122	Tubb4a	-0.3010	-0.0226	0.7120
Ina	-0.1040	0.0648	0.7080	Ubc;Ubb;Uba52;Rps27a;Kxd 1;Gm7866;Gm7808;Gm5239	0.1421	0.4133	0.5903
Kif5b	0.0281	0.4120	0.8226	Unc5b;Unc5c	0.3316	0.6333	0.4732
Lap3	-0.2801	0.2666	0.9373	Wasl	0.4393	0.9207	1.1548
Lyz2	0.7505	2.7104	2.5483	Wdr37	0.0063	0.1217	0.7047
Map2	0.6758	1.0630	0.8366				
Map4	0.2265	0.4813	0.8030				

From the table, it is possible to immediately identify the 3 constantly significantly upregulated protein groups as C1q (complement C1q subcomponent subunit B), Gfap (glial fibrillary acidic protein) and Htra1 (high-temperature requirement A serine peptidase 1). The information in the table furthermore suggests that other protein groups, like Apoe (apolipoprotein E), C4b (complement C4-B), Map2 (microtubule-associated protein 2) and Ptn (pleiotrophin), presumably exhibited a relevant (log2 fold changes ≥ 0.585) constant upregulation as well, but the measured log2 fold change was not significant at one of the timepoints. The same seemed to be the case for the protein groups, Hmgn1 and Hmgn2 (high mobility group nucleosome binding domain 1 and 2), Lyz2 (lysozyme 2), Mapt (microtubule-associated protein tau) and Opalin, whose log2 fold change was significant at just one timepoint.

Table 4-2: Protein groups significantly downregulated in brain myelin at at least one timepoint.
The table contains the proteins groups, indicated by their respective gene games, which showed a significant upregulation at one timepoint or more. Besides each gene name the log2 fold change (log2 ratio FA2H-KO/WT) is given for each timepoint. Significant changes (log2 fold change ≤ -0.585 & -log10 p > 1.301) are shaded in green.

Gene names	log2 fold change 6M	log2 fold change 13M	log2 fold change 17M	Gene names	log2 fold change 6M	log2 fold change 13M	log2 fold change 17M
Abhd4	-0.5925	-0.6092	0.4023	Kiaa1045	-0.7019	-0.7071	-0.5826
Acot7	-1.2128	-0.5868	0.2210	Ldhb	-1.0794	-0.6953	-0.0277
Ak1	-0.6498	-0.2080	0.0317	Mgll	-0.8237	-0.3642	-0.6474
Alb	-0.4564	-0.7814	-1.0302	Mif	-0.8627	-0.9866	-0.6688
Anln	-1.4509	-0.7394	-0.1650	Mtm1	-0.5302	-0.0827	-0.6154
Arf1	-0.6650	-0.5018	-0.0926	Ndrg1	-0.4332	-0.7046	-0.4743
Ass1	-0.9718	-1.0498	-1.0878	Nme2	-0.6253	-0.3788	-0.0773
Atp6v1a	-0.7774	-0.8999	-0.4470	Osbpl1a	-0.4199	-1.0502	-0.3687
Atp6v1b2	-0.7630	-0.8421	-0.4614	Otub1	-0.5923	-0.4805	0.4450
Calb2	-0.9340	-0.5588	-0.1104	Pea15	-0.6085	0.0680	0.5501
Cd59a	-0.2263	0.0700	-1.5964	Pebp1	-0.8469	-0.3353	0.0185
Eci1	-0.9595	-1.0367	-0.7363	Pfn2	-0.8564	-0.5189	0.1678
Eno2	-0.9176	-0.7428	0.2245	Pkm	-0.8415	-0.5933	-0.0293
Esyt2	0.2264	0.2598	-4.0012	Rheb	-0.7894	-0.4185	-0.2079
Etfa	-0.5757	-0.9288	-0.4890	Sept4	-1.1114	-0.7994	-0.1521

Fam177a1	-0.1735	-0.9156	0.5258	Sept7	-0.6701	-0.3843	-0.0654
Fam65a	-1.0919	-0.8042	-0.9517	Sept8	-0.6604	-0.2637	0.0320
Fyco1	-0.9593	-0.6965	-0.8515	Sh3bgrl3	-0.7466	-0.2425	0.3845
Gdi2	-1.0315	-0.5867	-0.2466	Slc38a3	0.0915	0.1123	-1.5563
Gng11	-0.8004	-0.3230	0.1118	Sod2	-0.3777	-0.6764	-0.0969
Got1	-0.8329	-0.8483	-0.2828	Tbc1d24	0.3491	-0.5494	-0.7648
Got2	-0.8063	-0.6099	-0.8573	Tpi1	-0.7629	-0.5181	0.1142
Gstm5	-0.5899	-0.2790	-0.0843	Tubb3	-0.6201	-0.1562	0.0822
Hadha	0.3959	0.1597	-0.6310	Txn	-0.5970	-0.4495	0.0646
Hba-a1	-0.7853	-1.2451	-1.3723	Ube2n	-0.5733	-0.7180	-0.3655
Hsd17b11	-1.0919	-0.4842	-0.2682	Vat1	-1.0215	-0.4316	-0.1652
Igsf8	-0.2213	-0.4264	-0.5899	Vsnl1	-0.6109	-0.4655	-0.2883
Ist1	-0.7412	-0.4349	-0.0049				

The table further emphasized that no single protein group was constantly significantly downregulated in FA2H-KO mice. Still, when considering also the non significant but sufficient log 2 fold changes (log2 fold change ≤ -0.585), it seemed that at least some protein groups were potentially downregulated at all three timepoints. These were Ass1 (argininosuccinate synthase 1), Eci1 (enoyl-CoA delta isomerase 1), Fam65a (enoyl-CoA delta isomerase 1), Fyco1 (FYVE and coiled-coil domain containing 1), Got2 (glutamic-oxaloacetic transaminase 2), Hba-a1 (hemoglobin alpha, adult chain 1) and Mif (macrophage migration inhibitory factor). In addition, as described in Figure 4-5, many protein groups were downregulated only in younger mice (6 and 13 months), but reverted back to WT-levels in the older animals (17 months).

To also get a general functional idea about the protein groups up- or downregulated at each timepoint, annotation analyses were conducted by AmiGO (http://tools.bioso.org/cgi-bin/amigo/slimmer) and PANTHER (pantherdb.org) using each group's first gene name. The two terms "Cellular Component" (GOslim by AmiGO) and "Protein Classification" (PANTHER classification) were evaluated and the results depicted in the bar charts (Figure 4-6). Detailed tables with the absolute numbers of the assigned annotations can be found on the supplemental DVD. In addition, PANTHER-generated gene lists, containing information for each of the submitted gene names, can also be found on the DVD.

A

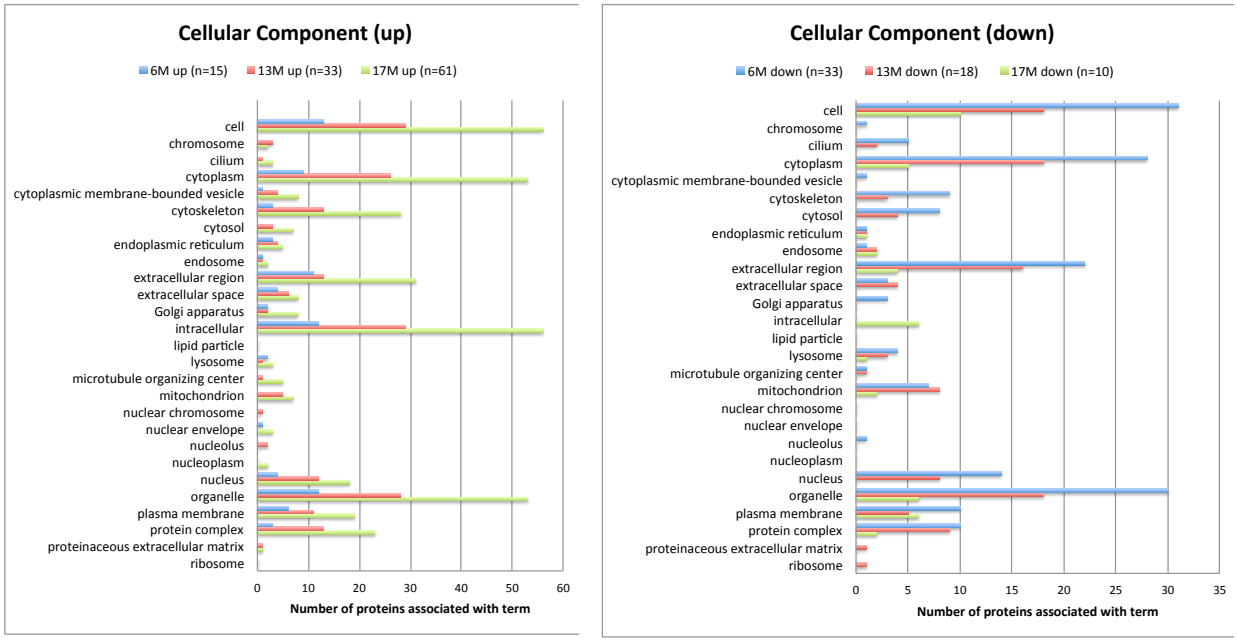

B

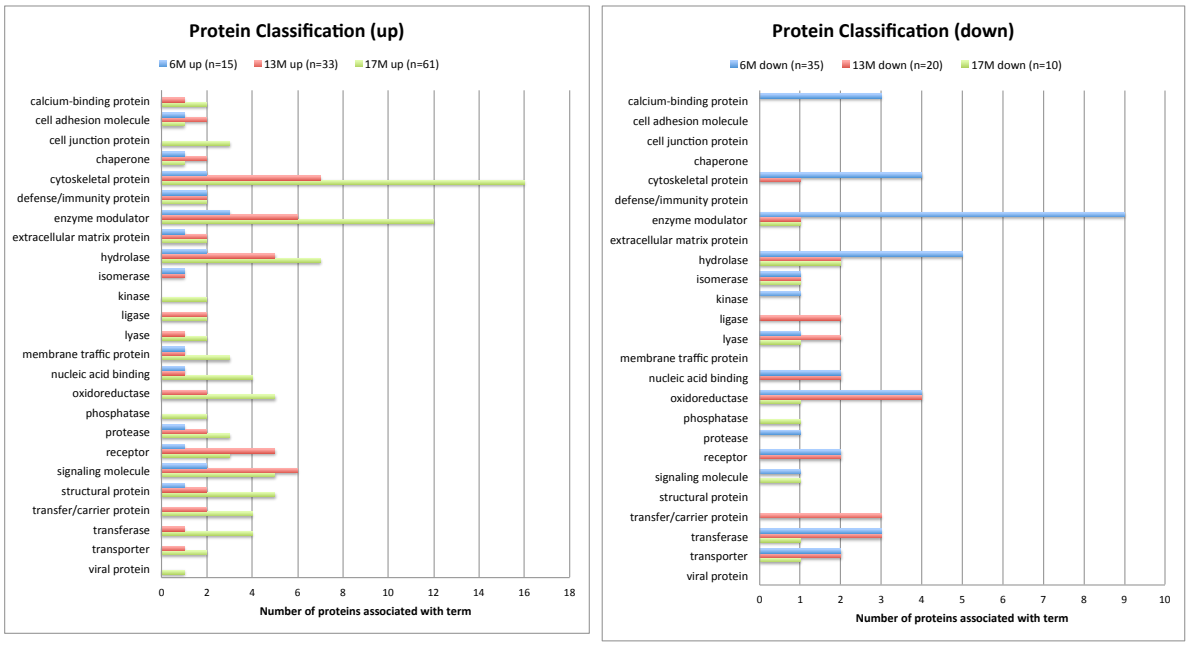

Figure 4-6: Annotation analysis of protein groups up- or downregulated in brain myelin of FA2H-KO mice at each timepoint. The protein groups significantly up- or downregulated in brain myelin of FA2H-KO mice at each timepoint (6M, 13M, 17M = 6, 13 and 17 months) were analyzed for annotation terms using AmiGO and PANTHER. As an identifier the first major gene name for each protein group was used and the up- and downregulated protein groups were evaluated separately. The results for the two assessed categories ("Cellular Component", "Protein Classification") are given in bar charts (left = downregulated; right = upregulated). In the charts each bar indicates the number of protein groups at a given timepoint associated with a certain annotation subcategory. Note that every protein group can be associated with more than one subcategory. In the chart legends n signifies the number of significantly changed proteins at that specific timepoint, which could be annotated by the annotation tool. **(A) Cellular Compartment chart.** Result of AmiGO GOslim analysis. **(B**) **Protein Classification chart.** Result of PANTHER analysis.

In line with the observations made above, regarding the changes in protein up- and downregulations in CNS-myelin of FA2H-KO mice, the "Cellular Component" annotation analysis (Figure 4-6A) showed

that the number of protein groups in almost all of the assessed subcategories increased over time for the upregulated protein groups. The opposite was true for the downregulated protein groups, which showed a decrease in all subcategories. Considering the upregulated protein groups, the majority were linked to an intracellular cytoplasmic and known organelle localization. In regard to organelles, the largest numbers were found for nuclear proteins. Nevertheless, at the later timepoints, 13M and 17M (13 and 17 months), there was also a relatively large group of protein groups with a plasma membrane localization. In addition, one could also observe a strong increase in the number of cytoskeletal-related protein groups over time. Regarding solely the downregulated protein groups, it became obvious that they were largely localized intracellulary in the cytoplasm with known organelle localization. Regarding organelles, protein groups containing mitochondrial, nuclear and plasma membrane proteins made up the biggest groups of the downregulated ones.

The “Protein Classification” analysis (Figure 4-6B) provided a more detailed overview of the protein classes the changed protein groups belong to. For the upregulated protein groups the number of proteins within almost all protein classes increased over time. The most striking change was seen for cytoskeletal proteins. While only two were upregulated at timepoint 6M, seven were upregulated at timepoint 13M and fourteen at timepoint 17M. The second strongest increase was observed for enzyme modulators. Furthermore, hydrolases, receptors, signaling molecules and structural proteins also increased strongly. Last, there was a small group of upregulated defense/immunity related protein groups. The downregulated protein groups belonged to many different protein classes with the number of entries within each class changing quite drastically over time. At the earliest timepoint (6M) the largest protein classes were enzyme modulators (9), followed by hydrolases (5), cytoskeletal proteins (4) and oxidoreductases (4). In comparison, at timepoint 13M the majority were oxidoreductases (4), transferases (3) and transfer/carrier proteins (3). At timepoint 17M, in contrast, only a very small number of 10 potein groups were significantly changed, which showed no tendency in belonging to certain protein classes.

In summary, a quite large number of up- and downregulated protein groups existed in FA2H-KO mice, which had diverse localizations and functions. Additionally, the strongest and the largest number of upregulations were found in very old animals (timepoint 17M), with a noticeable incidence of cytoskeletal and immune system related proteins groups.

Consequently, a selection of seven protein groups, strongly upregulated at timepoint 17M and mainly linked to these processes, was reviewed in more detail. Figure 4-7A depicts a line plot of all the 145 significantly changed protein groups by plotting each proteins expression ratios (log2 fold changes) against its respective timepoint. The seven protein groups are depicted in an additional line plot (Figure 4-7B) including standard deviations.

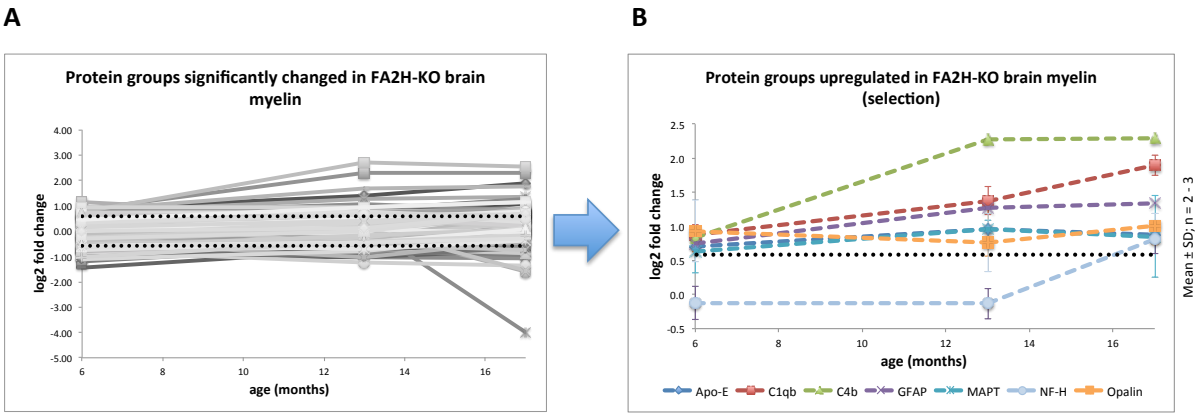

Figure 4-7: Line plot of proteins groups significantly changed in FA2H-KO mice at at least one timepoint. **(A)** Line plot of the 145 significantly changed protein groups. Each protein group's mean log2 transformed KO/WT expression ratios (log2 fold change) are plotted against the mice age in month. Horizontal doted black lines indicate the borders for relevant log2 fold changes (log2 fold change ≥ 0.585 & ≤ -0.585). **(B)** Additional line plot showing only a selection of strongly upregulated protein groups. For each line the standard deviation at each time point is given by error bars, if it was calculable (n = 2-3). A horizontal doted black line indicates the border for relevant upregulations (log2 fold change ≥ 0.585). MAPT = Microtubule-associated protein tau; C1qb = Complement C1q subcomponent subunit B; GFAP = Glial fibrillary acidic protein; C4b = Complement C4-B; Apo-E = Apolipoprotein E, NF-H = Neurofilament heavy.

The protein groups selected contained three cytoskeletal related polypeptides: Microtubule-associated protein tau (MAPT), glial fibrillary acidic protein (GFAP) and neurofilament heavy (NF-H). Of the three, MAPT and GFAP were already upregulated at timepoint 6M increasing even more towards timepoint 13M and/or 17M, while NF-H was only significantly increased in 17M old FA2H-KO animals. Moreover, of the three protein groups GFAP presented with the strongest upregulation at all timepoints. Interestingly, MAPT and GFAP are also linked to immunological processes. Regarding proteins directly involved in immunological processes, Complement C1q subcomponent subunit B (C1qb), Complement C4-B (C4b) and apolipoprotein E (Apo-E) were chosen. Both complement proteins showed an about 2-fold (log2 fold change = 1) upregulation at 6 months, and increased even more at the later timepoints. Especially C4b was already upregulated almost 5-fold (log2 fold change ≈ 2.3) at timepoint 13M, staying at that high level until timepoint 17M. Moreover, Apo-E, well known for its role in cholesterol transport, was also integrated into the selection, because it also plays a role in neuroinflammation and neurodegenerative diseases. Its upregulation was very similar to the one of MAPT being about 2-fold increased at the later timepoints. Lastly, the structural myelin membrane protein Opalin, which is not linked to the cytoskeleton or immune system processes, was included into the selection. This was done, because Opalin was the only potential structural myelin membrane protein being upregulated (~2-fold at all timepoints) and might explain the myelin phenotype caused by FA2H deficiency. Fittingly, Opalin's corresponding gene is found in a locus linked to spastic paraplegia, which is a hallmark feature of FA2H-deficient patients.

4.1.2.1.2 Verifications by Western Blot analyses

To verify some of the upregulations observed in brain myelin of very old FA2H-KO (17M) compared to WT mice, quantitative WB-analyses were conducted. For this, myelin and whole brain lysates were prepared from another independent group of four WT and four FA2H-KO animals of advanced age (21 - 23 months). These were probed with antibodies against MBP, MAPT, GFAP, NF-H, C1q, ApoE, and Opalin. MBP was included, because its mass spectrometric quantitative analysis results were inconsistent. MaxQuant had different MBP-isoforms and sequence variants, which are contained in the used Uniprot database, subdivided into three separate protein groups. These differed in their expression ratios, with two almost reaching the threshold for a relevant change in expression (log2 fold change ≤ 0.585). Thus, the WB should clarify this issue. Furthermore, an antibody against α-Tubulin was included as loading control in all lysate samples. In the myelin samples a loading control was not possible, because the level of each myelin protein could potentially be altered. After detection, the acquired WB-signals were quantified with the respective software depending on the detection system used (fluorescence = Odyssey 3.0; chemiluminescence = FUSION-Capt Advance Solo 4).

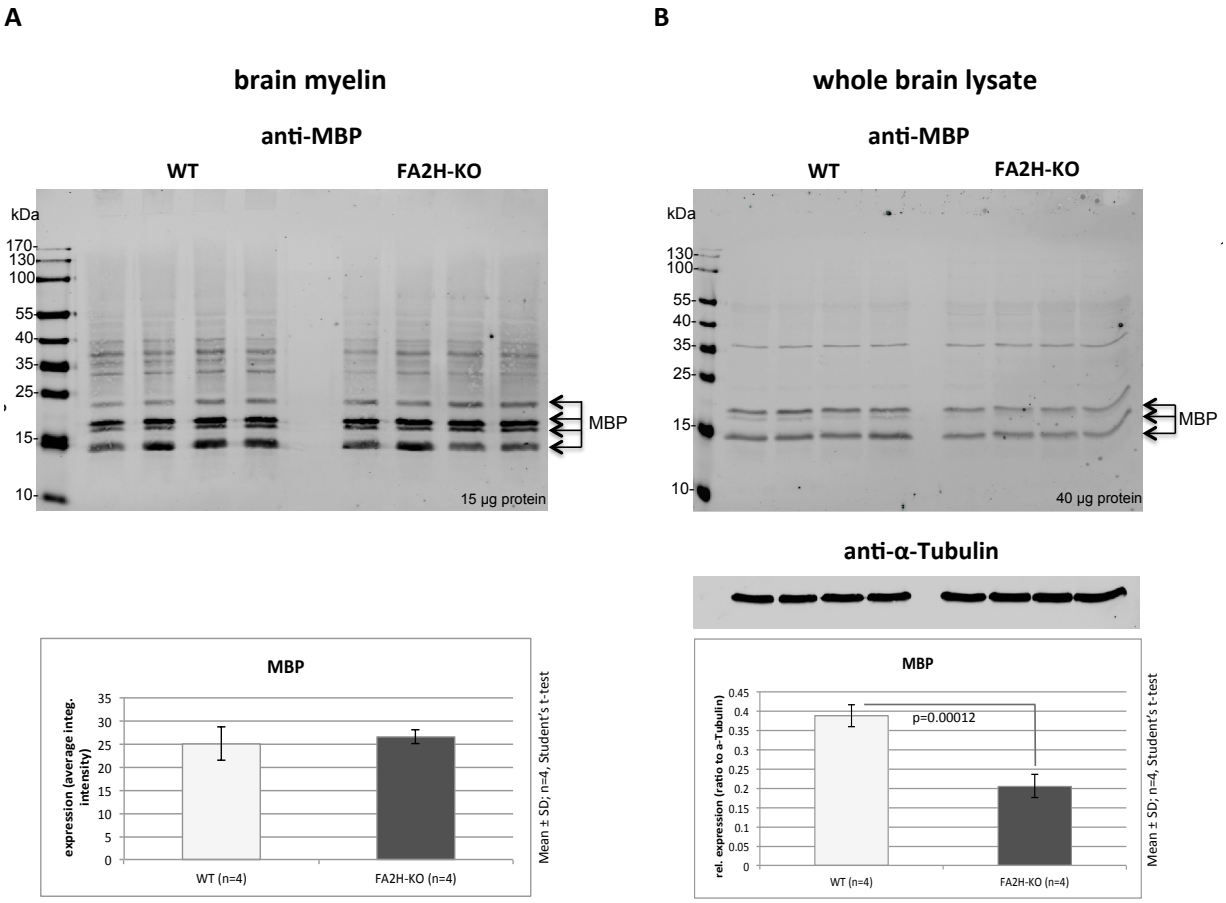

Figure 4-8: MBP-WB analyses of brain myelin and whole tissue lysate from 21- to 23-month-old WT and FA2H-KO mice. The indicated amount (protein content) of brain myelin or whole brain lysate from each animal were separated by SDS-PAGE and blotted onto nitrocellulose. Afterwards, proteins were detected using appropriate primary antibodies in combination with fluorescent secondary antibodies. Signals were visualized and quantified using the near-infrared Odyssey detection system. Expression differences were statistically evaluated by Student's t- test and plotted in bar charts with significant changes marked with p-values. **(A)** Brain myelin analysis acquired by incubation with MBP antibody (rabbit, 1:10000, ON, 4 °C) followed by anti-rabbit-DyLight649 secondary antibody incubation (1:5000, 1 h, RT). Black arrows indicate the four major MBP isoform protein bands. The absolute MBP-expression for both genotypes is given in a bar chart (below) as average integrated intensity (+/- standard deviation) of the indicated MBP-signals. **(B)** Whole brain lysate analysis obtained by concomitant incubation with MBP (rabbit, 1:10000, ON, 4°C) and α-Tubulin (mouse, 1:5000, ON, 4°C) antibodies. Secondary antibodies were anti-rabbit-DyLight649 and anti-mouse-DyLight800 (both 1:5000, 1 h, RT). Black arrows indicate major MBP-isoforms. The quantification results are given in a bar chart (below) depicting the mean relative MBP-expression (ratio to α-Tubulin) for both genotypes (+/- standard deviation).

While the WB clearly showed the four major MBP protein bands (14, 17, 18.5 and 21.5 kDa) in purified myelin, only three of them (14, 17, 18.5 kDa) were detectable in the whole brain lysate (Figure 4-8). The quantification of these bands proved no difference in the brain myelin MBP-expression between 21- to 23-month-old WT and FA2H-KO animals. In contrast, a strong (about 2-fold) and significant reduction of MBP was evident in FA2H-KO mice, when looking at the whole brain lysate WB. This implied that brains of aged FA2H-KO mice have a reduced myelin amount. When solely analyzing purified myelin this effect is overseen, because equal protein amounts are loaded.

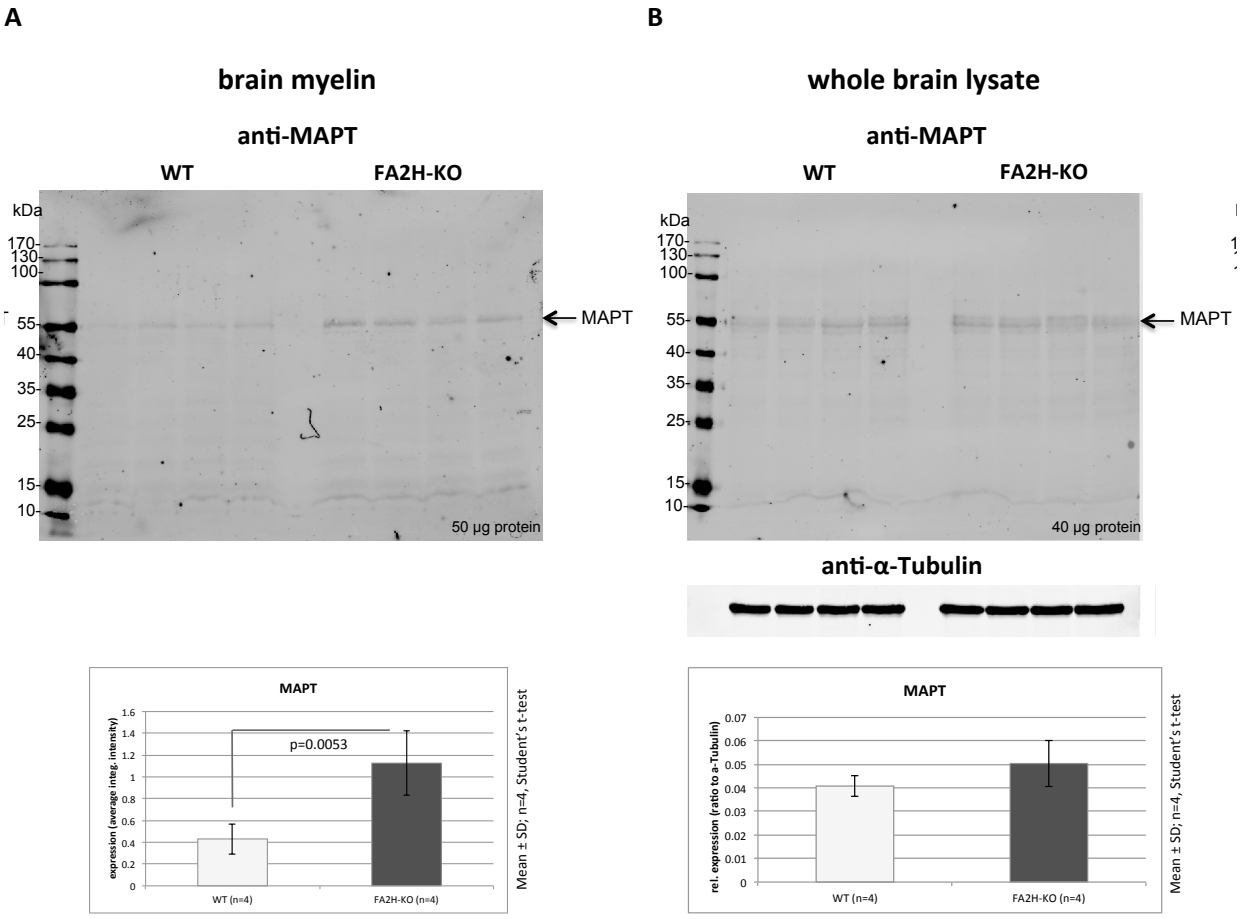

Figure 4-9: MAPT-WB analyses of brain myelin and whole tissue lysate from 21- to 23-month-old WT and FA2H-KO mice. The indicated amount (protein content) of brain myelin or whole brain lysate from each animal were separated by SDS-PAGE and blotted onto nitrocellulose. Afterwards, proteins were detected using appropriate primary antibodies in combination with fluorescent secondary antibodies. Signals were visualized and quantified using the near-infrared Odyssey detection system. Expression differences were statistically evaluated by Student's t-test and plotted in bar charts with significant changes marked with p-values. **(A)** Brain myelin analysis obtained by incubation with MAPT antibody (mouse, 1:1000, ON, 4 °C) followed by anti-mouse-DyLight649 secondary antibody incubation (1:5000, 1 h, RT). The black arrow indicates the MAPT protein band. The absolute MAPT-expression for both genotypes is given in a bar chart (below) as average integrated intensity (+/- standard deviation). **(B)** Whole brain lysate analysis obtained by simultaneous incubation with MAPT (mouse, 1:1000, ON, 4°C) and α-Tubulin (rabbit, 1:5000, ON, 4°C) antibodies. Secondary antibodies were anti-mouse-DyLight649 and anti-rabbit-DyLight800 (both 1:5000, 1 h, RT). The black arrow points at the MAPT-signal. The quantification results are given in a bar chart (below) depicting the mean relative MAPT-expression (ratio to α-Tubulin) for both genotypes (+/- standard deviation).

In the MAPT-WBs of purified myelin and whole brain of 21- to 23-month-old mice (Figure 4-9) the protein became visible as a relatively weak but still quantifiable signal at 55 kDa. Considering myelin, a significant ~3-fold upregulation of MAPT was observed in FA2H-KO mice, thus being a little higher then value obtained for the younger 17-month-old animals analyzed by mass spectrometry (~2-fold). In the whole brain the average MAPT-expression was also higher in the KO compared to the WT mice, but the difference was not significant. This difference between myelin and whole brain is probably explained by the observation made above, that FA2H-KO mice have a reduced myelin amount. Consequently, upregulations visible in myelin normalized to the same protein amount will be smaller in the whole brain.

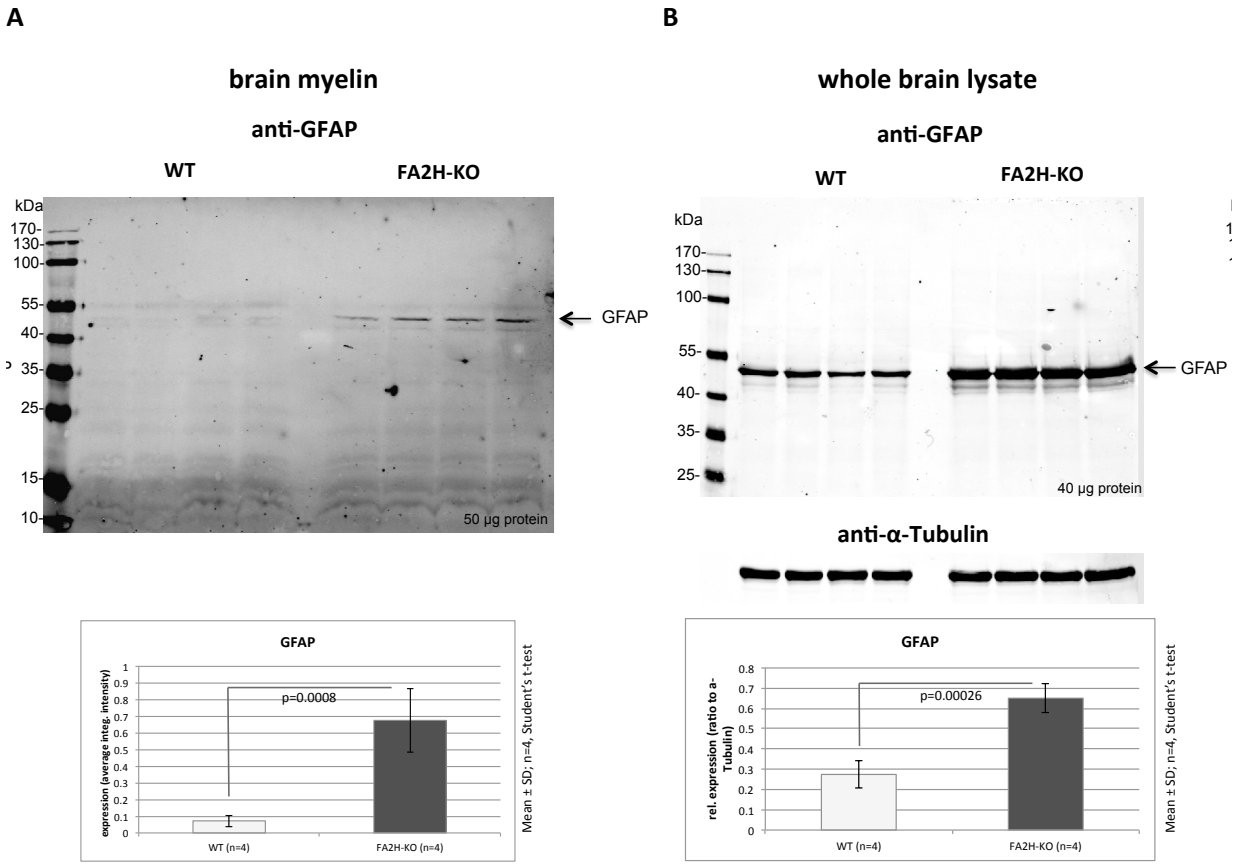

Figure 4-10: GFAP-WB analyses of brain myelin and whole tissue lysate from 21- to 23-month-old WT and FA2H-KO mice. The indicated amount (protein content) of brain myelin or whole brain lysate from each animal were separated by SDS-PAGE and blotted onto nitrocellulose. Afterwards, proteins were detected using appropriate primary antibodies in combination with fluorescent secondary antibodies. Signals were visualized and quantified using the near-infrared Odyssey detection system. Expression differences were statistically evaluated by Student's t-test and plotted in bar charts with significant changes marked with p-values. **(A)** Brain myelin analysis obtained by incubation with GFAP antibody (mouse, 1:1000, ON, 4 °C) followed by anti-mouse-DyLight649 secondary antibody incubation (1:5000, 1 h, RT). The black arrow indicates the GFAP protein band. The absolute GFAP-expression for both genotypes is given in a bar chart (below) as average integrated intensity (+/- standard deviation). **(B)** Whole brain lysate analysis obtained by concomitant incubation with GFAP (mouse, 1:1000, ON, 4°C) and α-Tubulin (rabbit, 1:5000, ON, 4°C) antibodies. Secondary antibodies were anti-mouse-DyLight649 and anti-rabbit-DyLight800 (both 1:5000, 1 h, RT). The black arrow points at the GFAP-signal. The quantification results are given in a bar chart (below) depicting the mean relative GFAP-expression (ratio to α-Tubulin) for both genotypes (+/- standard deviation).

The GFAP-WBs of brain myelin and whole brain lysate from 21- to 23-month-old mice (Figure 4-10) showed a single protein band of 50 kDa, corresponding to the protein's expected size. Quantification of this band revealed a significant upregulation of GFAP in brain myelin and whole brain of FA2H-KO compared to WT mice. In myelin it was ~6-fold and in whole brain about 2-fold. As mentioned before, this difference can be explained by the generally reduced myelin amount in FA2H-KO mice. Furthermore, the ~6-fold upregulation of GFAP in myelin of 21- to 23-month-old FA2H-KO mice was markedly higher than the one measured by mass spectrometry in younger 17-month-old KO-animals (~2.5-fold).

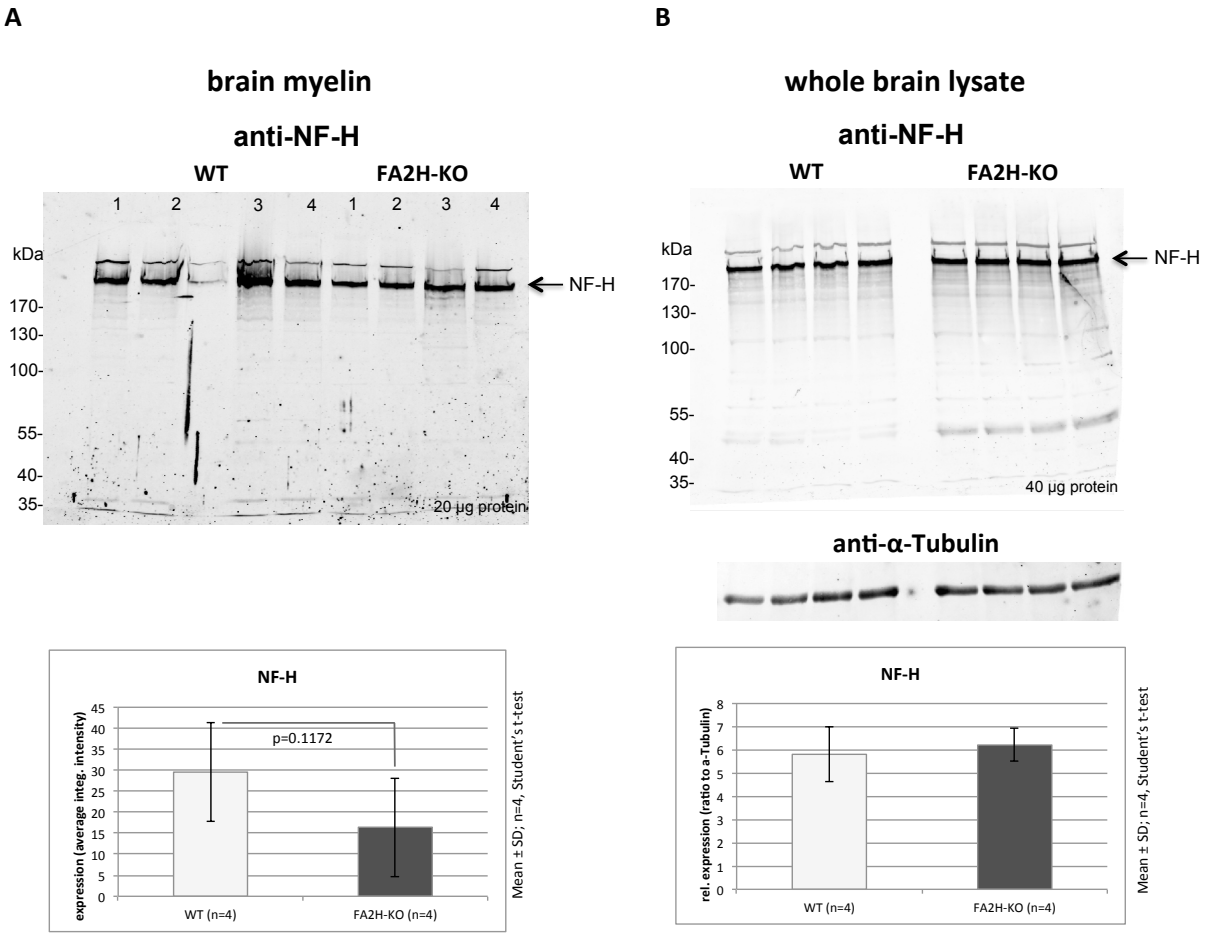

Figure 4-11: NF-H-WB analyses of brain myelin and whole tissue lysate from 21- to 23-month-old WT and FA2H-KO mice. The indicated amount (protein content) of brain myelin or whole brain lysate from each animal were separated by SDS-PAGE and blotted onto nitrocellulose. Afterwards, proteins were detected using appropriate primary antibodies in combination with fluorescent secondary antibodies. Signals were visualized and quantified using the near-infrared Odyssey detection system. Expression differences were statistically evaluated by Student's t-test and plotted in bar charts with significant changes marked with p-values. **(A)** Brain myelin analysis obtained by incubation with NF-H antibody (rabbit, 1:500, ON, 4 °C) followed by anti-rabbit-DyLight649 secondary antibody incubation (1:5000, 1 h, RT). The black arrow indicates the NF-H-protein. The absolute NF-H-expression for both genotypes is given in a bar chart (below) as average integrated intensity (+/- standard deviation). **(B)** Whole brain lysate analysis obtained by simultaneous incubation with NF-H (rabbit, 1:500, ON, 4°C) and α-Tubulin (mouse, 1:5000, ON, 4°C) antibodies. Secondary antibodies were anti-mouse-DyLight649 and anti-rabbit-DyLight800 (both 1:5000, 1 h, RT). The black arrow points at the NF-H-signal. The quantification results are given in a bar chart (below) depicting the mean relative NF-H-expression (ratio to α-Tubulin) for both genotypes (+/- standard deviation).

NF-H became visible in the WB as a prominent band corresponding to the expected molecular weight of ~200 kDa. In brain myelin of 21- to 23-month-old mice the intensity of this band varied strongly between each animal regardless of its genotype. The signal quantification showed that the average expression was lower in the KO-animals, but the expression difference was not significant due to the high signal variance. Thus, the mass spectrometric measured ~2-fold upregulation of NF-H in myelin of old FA2H-KO animals could not be verified by WB. In the whole brain lysate WB the signal intensities were constant, but the quantification showed again no significant difference between WT and FA2H-KO.

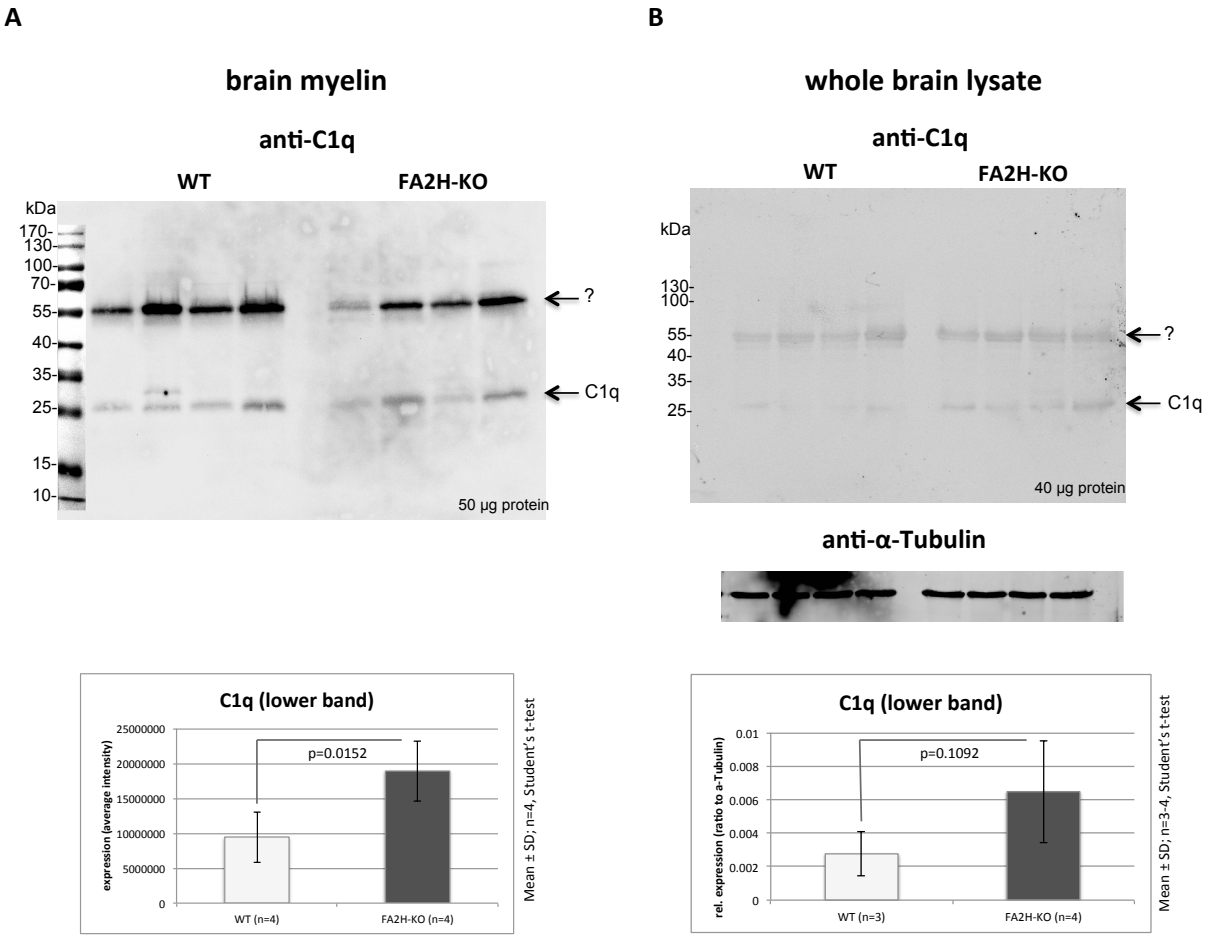

Figure 4-12: C1q-WB analyses of brain myelin and whole tissue lysate from 21- to 23-month-old WT and FA2H-KO mice. The indicated amount (protein content) of brain myelin or whole brain lysate from each animal were separated by SDS-PAGE and blotted onto nitrocellulose. Afterwards, proteins were detected using appropriate primary antibodies in combination with fluorescent or HRP-coupled secondary antibodies. Signals were visualized and quantified using the appropriate detection system. Expression differences were statistically evaluated by Student's t-test and plotted in bar charts with significant changes marked with p-values. **(A)** Brain myelin analysis obtained by incubation with C1q antibody (mouse, 1:500, ON, 4 °C) followed by anti-mouse-HRP secondary antibody incubation (1:5000, 1 h, RT). The C1q-protein band and an additional band of unknown identity are marked with an arrow. The absolute C1q-expression for both genotypes is given in a bar chart (below) as average intensity (+/- standard deviation). **(B)** Whole brain lysate analysis obtained by concomitant incubation with C1q (mouse, 1:500, ON, 4°C) and α-Tubulin (rabbit, 1:5000, ON, 4°C) antibodies. Secondary antibodies were anti-mouse-DyLight649 and anti-rabbit-DyLight800 (both 1:5000, 1 h, RT). Black arrows point at the C1q-signal and an additional signal of unknown identity. The quantification results are given in a bar chart (below) depicting the mean relative C1q-expression (ratio to α-Tubulin) for both genotypes (+/- standard deviation).

The C1q-WB showed two polypeptides, one at ~25 and the other at ~55 kDa respectively, of which only the lower band agrees with the proteins known molecular weight. Therefore, the quantification was solely based on this signal. Furthermore, because a strong unspecific background staining was overlapping with parts of the α-Tubulin signal, WT animal #2 was left out of the quantification (WT n=3). The quantification demonstrated that a significant larger amount of C1q was present in brain myelin of 21- to 23-month-old FA2H-KO mice compared to the WT-controls. Interestingly, this increase was only ~2-fold and thus less strong than the ~4-fold increase determined by mass spectrometry in significantly younger animals (17-month-old). In the whole brain, the average

expression was higher in the KO-animals as well, but this difference was not statistically significant. Consequently, no upregulation could be observed in the whole brain. As mentioned before, the difference between myelin and whole brain can be explained by the generally reduced myelin amount observed in older FA2H-KO mice.

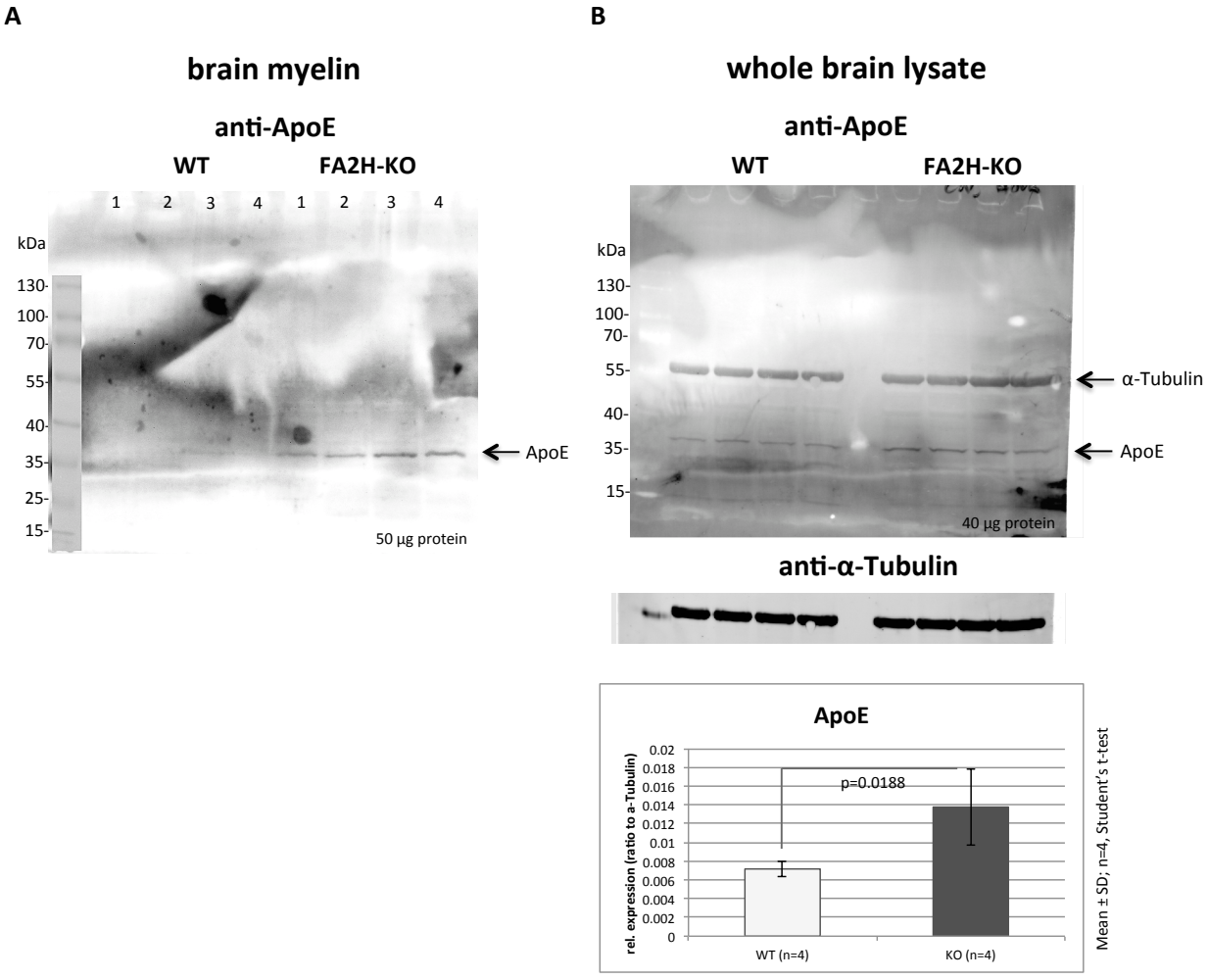

Figure 4-13: ApoE-WB analyses of brain myelin and whole tissue lysate from 21- to 23-month-old WT and FA2H-KO mice. The indicated amount (protein content) of brain myelin or whole brain lysate from each animal were separated by SDS-PAGE and blotted onto PVDF. Afterwards, proteins were detected using appropriate primary antibodies in combination with fluorescent or HRP-coupled secondary antibodies. Signals were visualized and quantified using the appropriate detection system. Expression differences were statistically evaluated by Student's t-test and plotted in bar charts with significant changes marked with p-values. **(A)** Brain myelin analysis obtained by incubation with ApoE antibody (goat, 1:500, ON, 4 °C) followed by anti-goat-HRP secondary antibody incubation (1:5000, 1 h, RT). The ApoE protein band is marked with an arrow. Because ApoE was only detectable in one WT, but in all four FA2H-KO samples, a quantification and statistical evaluation was not feasible. **(B)** Whole brain lysate analysis obtained by simultaneous incubation with ApoE (goat, 1:500, ON, 4°C) and α-Tubulin (mouse, 1:5000, ON, 4°C) antibodies. Secondary antibodies were anti-mouse-DyLight649 and anti-goat-DyLight800 (both 1:5000, 45 min, RT). Black arrows indicate the ApoE and the α-Tubulin protein band. α-Tubulin was also visible in the 800 nm channel, because the anti-goat-DyLight800 secondary antibody also bound to the secondary anti-mouse antibody. Quantification results are given in a bar chart (below) depicting the mean relative ApoE-expression (ratio to α-Tubulin) for both genotypes (+/- standard deviation).

The ApoE-WB gave a signal of ~36 kDa, which is in line with the protein's molecular weight. In addition, an unspecific background staining of the whole blotting area was visible as well, which was especially intense in the brain myelin WB. In brain myelin, one WT sample exhibited a relatively weak ApoE signal, while no ApoE was detectable in the three others. On the other hand, a stronger ApoE signal was observable in all four FA2H-KO samples, signifing increased ApoE amounts in myelin of FA2H-KO mice. The whole brain WB analysis revealed ApoE signals in all animals assessed, with generally stronger signals in the FA2H-KO mice. Accordingly, the quantification of the signals revealed a significant ~2-fold elevation of the protein in FA2H-KO animals.

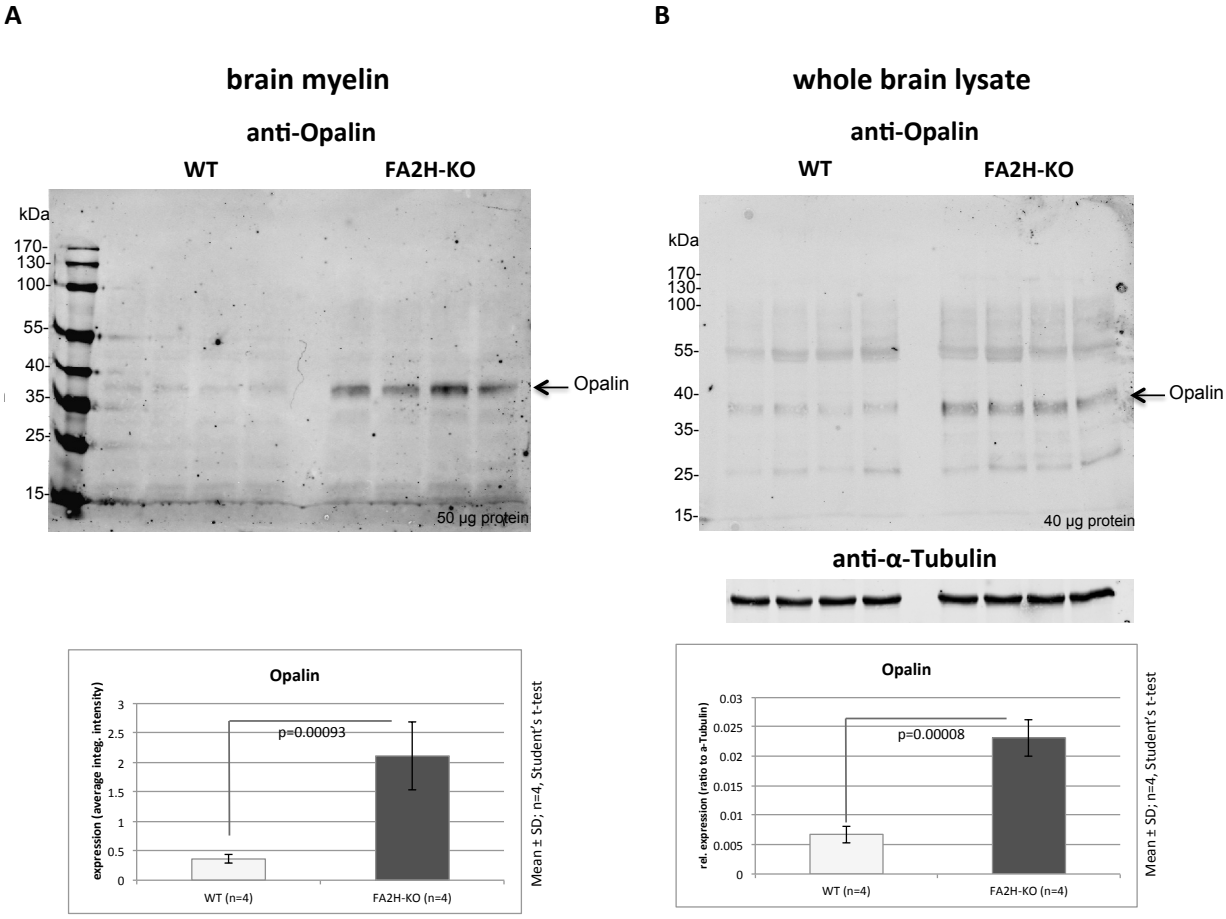

Figure 4-14: Opalin-WB analyses of brain myelin and whole tissue lysate from 21- to 23-month-old WT and FA2H-KO mice. The indicated amount (protein content) of brain myelin or whole brain lysate from each animal were separated by SDS-PAGE and blotted onto nitrocellulose. Afterwards, proteins were detected using appropriate primary antibodies in combination with fluorescent secondary antibodies. Signals were visualized and quantified using the near-infrared Odyssey detection system. Expression differences were statistically evaluated by Student's t-test and plotted in bar charts with significant changes marked with p-values. **(A)** Brain myelin analysis obtained by incubation with Opalin antibody (mouse, 1:500, ON, 4 °C) followed by anti-mouse-DyLight649 secondary antibody incubation (1:5000, 1 h, RT). The black arrow indicates the Opalin-protein. The absolute Opalin-expression for both genotypes is given in a bar chart (below) as average integrated intensity (+/- standard deviation). **(B)** Whole brain lysate analysis obtained by concomitant incubation with Opalin (mouse, 1:500, ON, 4°C) and α-Tubulin (rabbit, 1:5000, ON, 4°C) antibodies. Secondary antibodies were anti-mouse-DyLight649 and anti-rabbit-DyLight800 (both 1:5000, 1 h, RT). The black arrow points at the Opalin-signal. The quantification results are given in a bar chart (below) depicting the mean relative Opalin-expression (ratio to α-Tubulin) for both genotypes (+/- standard deviation).

The antibody against Opalin gave a signal of 34 - 39 kDa, corresponding with the glycosylated protein's molecular weight. In addition, some background bands of various sizes were visible. Quantification of the Opalin-signals in brain myelin and whole brain lysate of 21- to 23-month-old mice proved the protein's significant upregulation in FA2H-KO compared to WT. It was upregulated ~5-fold in myelin and only ~3-fold in the whole brain. As argued above, this was probably due to the reduced myelin amount in FA2H-KO mice. Furthermore, with a ~5-fold increase the upregulation in

FA2H-KO myelin was significantly higher than the ~2-fold increase determined in 17-month-old animals by mass spectrometry.

Altogether, the different WB-verifications using very old mice could confirm the upregulation of MAPT, GFAP, C1q, ApoE and Opalin found in the mass spectrometric brain myelin analysis. Intriguingly, for MAPT, GFAP and Opalin the measured upregulation was even stronger than the one determined by mass spectrometry. This can be explained by the age difference between the animals used in the two analyses. Apparently, the four- to six-month-older mice used in the WB analyses had an aggravated phenotype reflected by the increase in the three proteins. Moreover, for GFAP and Opalin the upregulation was also detectable in whole brain lysates, but to a lesser extent. In contrast, no significant change was evident for MAPT and C1q in the whole brain. Furthermore, the upregulation of NF-H could neither be verified in myelin nor in the total brain of FA2H-KO mice by WB. The amount of NF-H in myelin was very variable in all eight animals assessed. Finally, the uncertain quantification status of MBP in myelin could be cleared. The myelin MBP-levels were not changed between the two genotypes. On the other hand, a previously not described significant reduction of MBP in FA2H-KO mice was observed in the total brain analysis.

4.1.2.2 Sciatic nerve myelin analysis

4.1.2.2.1 Mass spectrometric analysis using TMT-labeling

Analogous to the comparative brain myelin analysis, the sciatic nerve myelin of the same animals was analyzed to see if similar proteome alterations are also present in PNS-myelin. An overview of the analysis results and a comparison to previously published PNS-myelin data is depicted in Figure 4-15. Note that the original MaxQuant result files and the processed protein group list can be found on the supplemental DVD.

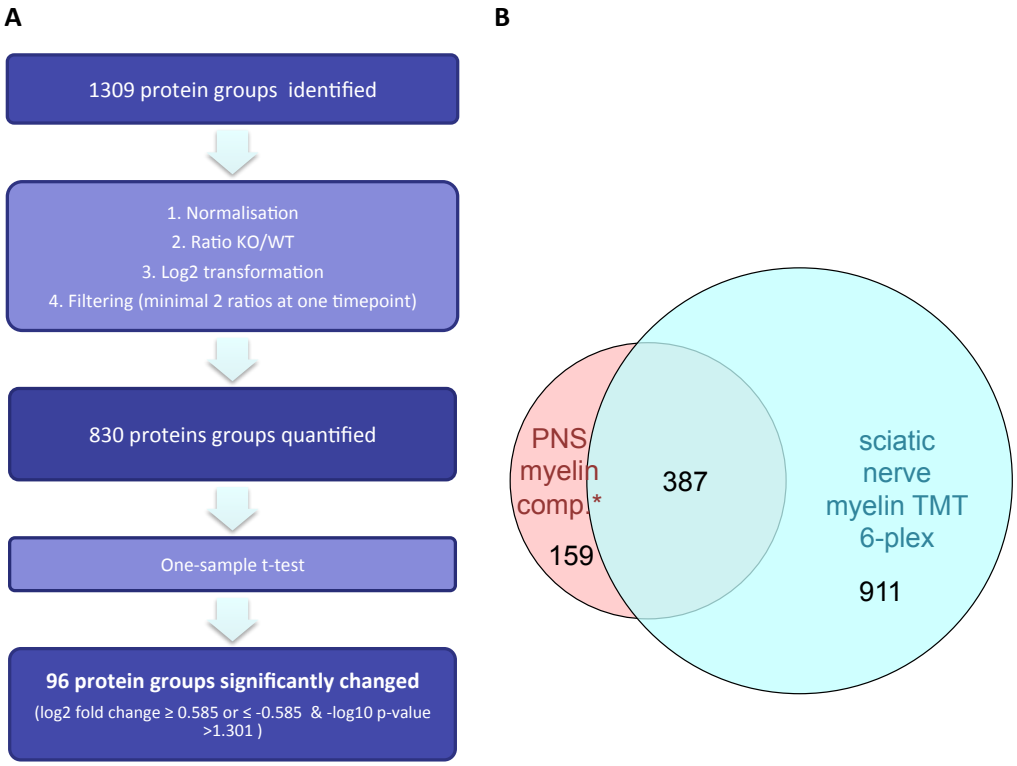

Figure 4-15: Quantitative sciatic nerve myelin (PNS) proteome analysis.
(A) Diagram depicting the workflow of protein group results processing. MaxQuant identified 1309 protein groups after combined analysis of all raw files (matched against murine Uniprot database). The data were then normalized (each reporter intensity divided by summed reporter channel intensity) and log2 FA2H-KO/WT expression ratios (log2 fold change) calculated for each timepoint. Subsequently, the data were filtered for protein groups with at least two expression ratios at one timepoint leaving 830. To assess proteins, which had a significantly changed expression in FA2H-KO mice, the log2 transformed expression values were evaluated by an one-sample t-test against 0 (log2(1) = 0 = no change) for each timepoint. This resulted in the identification of 96 significantly changed protein groups. **(B)** Venn diagram comparing the protein groups identified with TMT 6-plex brain myelin proteome analysis in this thesis with the published PNS myelin reference list (Patzig et al. 2011). The first gene name of each protein group was used as identifier. A list containing all gene names related to the overlapping areas can be found on the supplemental DVD.

With the help of MaxQuant, 1309 protein groups were identified in the combined analysis of all three sciatic nerve myelin triplicates (Figure 4-15A), thereby significantly expanding the currently known PNS-myelin proteome of about 550 proteins (Patzig et al. 2011). When comparing the identifications of both datasets, there was a large congruency (Figure 4-15B). The majority (387 of 546 = ~71%) of the proteins identified in the published dataset were also found in the present study.

To see possible changes in the sciatic nerve myelin proteome composition, the results were further processed analogous to the brain myelin analysis (see: p.64). This reduced the protein list to 830 quantified protein groups, which was additionally filtered for significantly changed protein groups at each of the three assessed timepoints (6, 13 and 17M). Finally, this led to the identification of 96 protein groups significantly changed at at least one timepoint.

Similar to the CNS-myelin analysis, the expression differences of major PNS-myelin between FA2H-KO and WT proteins was assessed first. Therefore, the log2 fold changes of major PNS-myelin proteins

were plotted against the animal ages (Figure 4-16). Two horizontal doted black lines mark the area, within which log2 fold changes are considered not relevant. Note that MaxQuant assigned different sequence variants of periaxin, derived from different mouse strains, into two separate protein groups: PRX (C57BL/6) and PRX (129Sv/Ola). This was likely the case, because the older mice still had a mixed genetic background of 129/Ola and C57BL/6 (see 3.1.8 Mice strains).

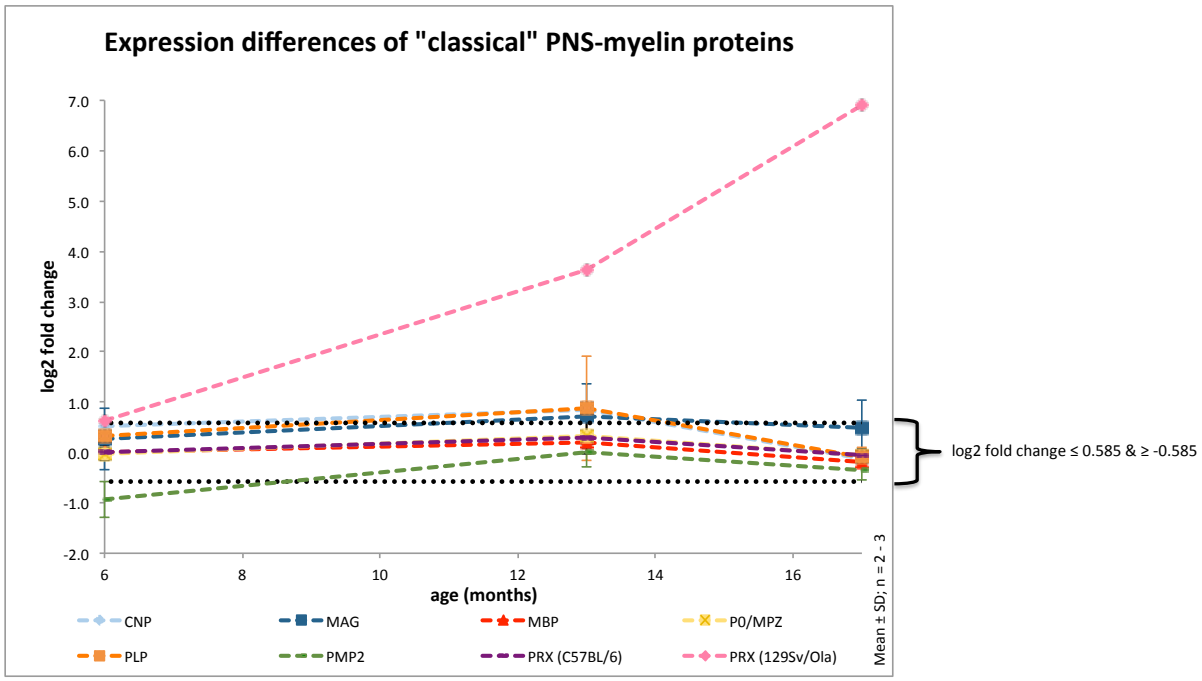

Figure 4-16: Expression differences of major PNS-myelin proteins between FA2H-KO and WT mice in sciatic nerve myelin. Each protein group's mean log2 transformed KO/WT expression ratios (log2 fold change) are plotted against the mice age in month. For each line the standard deviation at each time point is given by error bars, if it was calculable (n = 2-3). Horizontal doted black lines mark the borders for relevant, i.e. sufficiently large enough, log2 fold changes (log2 fold change ≥ 0.585 & ≤ -0.585). Note that MaxQuant assigned distinctive Periaxin-sequence variants derived from different mouse strains to two separate protein group entries, with all had significantly different mean log2 fold changes. CNP = cyclic nucleotide phosphodiesterase; MAG = myelin-associated glycoprotein; MBP = myelin basic protein; P0/MPZ = myelin protein zero; PLP = proteolipid protein; PMP2 = myelin P2 protein; PRX = periaxin.

At the most timepoints, major PNS-myelin proteins were not extensively changed in sciatic nerve myelin between both genotypes. Only for the protein groups MAG, PMP2 (myelin P2 protein) or PLP, some of the mean log2 fold changes also laid outside the borders marking sufficiently changed groups. But these changes were not significant, as became obvious when taking into account their large standard deviations. Interestingly, one of the two periaxin protein groups, PRX (129Sv/Ola), showed a very extensive upregulation (~120-fold) at timepoints 13 and 17M, while the second group, PRX (C57BL/6) did not. Moreover, the silver-stain gel analysis of PNS-myelin (Figure 4-2D) also had shown no difference in periaxin's expression between WT and FA2H-KO mice. Thus, to clarify the expression of periaxin in FA2H-KO animals, its protein level was analyzed by WB using whole nerve lysates from another independent group of four WT and three FA2H-KO animals of advanced age (21 - 23 months).

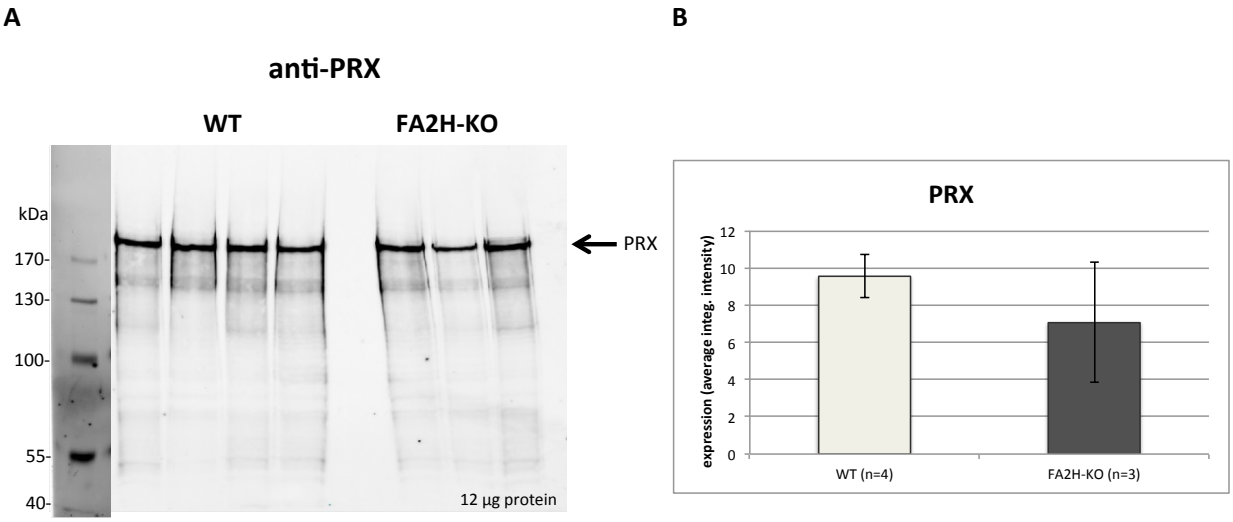

Figure 4-17: Analysis of periaxin protein levels in sciatic nerves of 21- to 23-month-old WT and FA2H-KO mice by WB. The indicated amount (protein content) of sciatic nerve lysate from each animal was concentrated by $CHCl_3$/MeOH-precipitation, resuspended in 2X Laemmli buffer, separated by SDS-PAGE and blotted onto PVDF. Afterwards, periaxin (PRX) was detected using an anti-periaxin primary antibody (α-PRX N-term, rabbit, 1:20,000, 4°C, ON) in combination with a fluorescent secondary goat-α-rabbit-DyLight800 antibody (1:5000, 45 min, RT). Signals were visualized and quantified using the near-infrared Odyssey detection system. Expression differences were statistically evaluated by Student's t-test. **(A)** WB image of periaxin in sciatic nerves of WT and FA2H-KO mice. Periaxin is indicated by a black arrow. **(B)** Bar chart depicting the quantification results for the PRX protein band. Note that the protein was not significantly changed between both genotypes.

In the WB periaxin (PRX) became visible as a protein signal with a molecular weight >170 kDa. Quantification of the signal showed that the expression of PRX was not significantly different between WT and FA2H-KO animals, thereby clarifying the conflicting result of the mass spectrometric analysis. Accordingly, it could be concluded that the major PNS-myelin proteins were not changed between both genotypes. The very extensive overexpression of periaxin measured by mass spectrometry was an artificial result, likely caused by the fact that by chance only the old KO animals expressed the 129SV/Ola sequence variant of periaxin. In theory, a similar influence of the mice strain could also have affected the quantification of other protein groups. But since the majority of proteins should not differ substantially in their amino acid sequence between mice strains, the influence of this effect is probably small.

Thus, all of the identified 96 protein groups significantly changed in FA2H-KO PNS-myelin were still evaluated in more detail (Figure 4-18). It became obvious, that at the early timepoints (6 and 13M) mainly significant upregulations, but almost no downregulations were present in PNS-myelin of FA2H-KO mice. While only a single protein group was downregulated at both timepoints, 35 or 11 were upregulated. In contrast, the most significant protein changes were observable at timepoint 17M with 28 down- and 22 upregulations, respectively. Interestingly, this high number of 50 changes correlates with the fact that the PNS-pathology was only observed in very old FA2H-KO animals (≥18 months).

	Up*	Down**
6 months	35	1
13 months	11	1
17 months	22	28

*Upregulated in KO = log2 fold change ≥ 0.585 & -log10 p-value > 1.301
**Downregulated in KO = log2 fold change ≤ 0.585 & -log10 p-value > 1.301

Figure 4-18: 96 protein groups significantly up- and downregulated in FA2H-KO sciatic nerve myelin.
Number of significantly up- and downregulated protein groups at each time point. Note that the same proteins can be changed at more than one timepoint.

In addition, for assessing the persistence of a protein group expression change, the identifications of the upregulated protein groups were compared to each other between the three timepoints. This comparison clearly showed almost no congruency between the significantly upregulated protein groups. There was only a congruency of 2 protein groups at timepoint 13 and 17M, hinting at a high degree of biological variability. Thus, some protein groups were potentially changed at more then one timepoint, but filtered out according to the applied p-value threshold. Thus, for a more detailed view of the significantly up- and downregulated protein groups, they are depicted in two separate tables (Table 4-3 and Table 4-4). In the tables the significant log2 fold changes are indicated by color shading. These tables showed that some of the protein groups had non-significant log2 fold changes at the other timepoints, which passed the criterium for a relevant change (log2 fold change ≥ 0.585 or ≤-0.585). Accordingly, these proteins might have been changed more constantly.

Table 4-3: Protein groups significantly upregulated in sciatic nerve myelin at at least one timepoint.
The table contains the proteins groups, indicated by their respective gene games, which showed a significant upregulation at one timepoint or more. Next to each gene name the log2 fold change (log2 ratio FA2H-KO/WT) is given for each timepoint. Significant changes (log2 fold change ≥ 0.585 & -log10 p > 1.301) are shaded in red. In addition, protein groups potentially changed at more that one timepoint are highlighted in bold.

Gene names	log2 fold change 6M	log2 fold change 13M	log2 fold change 17M	Gene names	log2 fold change 6M	log2 fold change 13M	log2 fold change 17M
Aldh1a1;Aldh1a7	0.7458	0.3614	-0.3449	Lyz1	0.6435	0.5410	1.5422
Aoc3	0.3152	**1.2030**	**1.7538**	Map1b	-0.4230	0.2745	-0.5373
Arf1;Arf3;Arf2	0.6607	-0.1374	-0.1833	Mif	0.6618	0.0509	-0.2833
Arf5	1.0884	0.0503	-0.3965	Mpp6	0.3816	-0.0133	0.6416
Ca3	-0.8108	2.0841	-0.3282	Mras	0.7056	-0.3389	0.0228
Cadm4	0.4947	0.0010	0.6080	Myh9	0.2899	0.5331	0.6757
Calb2	0.9536	-0.4999	-0.1689	Napg	0.9044	-0.0753	-0.3692
Cat	-0.1388	1.0159	0.1170	Nars	0.6022	-0.5758	-0.3375
Cd36	0.0440	**1.2747**	**1.8291**	Nedd4l	0.6082	0.1371	-0.1547
Cdh1	0.6125	-0.2669	0.2309	Ola1	0.8036	-0.3030	-0.1230
Ces1d	-0.2911	**2.4419**	**1.3073**	Pfkl	0.2432	0.6032	-0.1309
Cmtm5	-0.5606	0.2052	0.8544	Pfn2	0.8944	-0.3632	-0.1176
Ctnna1	0.3467	**0.6749**	**0.8268**	Phpt1	1.4332	-0.3146	-0.9006
Ddost	-0.2480	0.7186	0.4159	Plg	0.7654	-0.0880	-0.4177
Eif5a2;Eif5a	1.3881	0.0598	-0.4546	**Plin1**	0.1494	**0.9510**	**1.4792**

Entpd2	-0.1333	0.1342	0.9926	**Por**	0.0089	**0.9354**	**0.6637**
Epb41l2	0.3938	-0.0496	0.5945	Ppia	0.8250	-0.1071	-0.0169
Etfb	-0.0271	0.5978	0.3332	**Prx**	0.3137	**1.9547**	**6.8462**
Fam213a	-0.2442	0.7995	0.3780	Psap	0.6151	0.1777	0.0293
Fbn1	-0.5481	0.0922	0.8802	Rpl14	0.5220	0.6726	-0.2304
Fkbp1a	0.6657	-0.1790	-0.3025	Sfn	0.5876	-0.2769	0.0210
Gmfb	0.7212	-0.4018	-0.2959	Sh3bgrl3	0.5864	-0.0581	-0.1553
H2-K1;H2-Q4;H2-D1;H2-Q7;H2-Q10;H2-Q6;H2-Q8;H2-Q1;H2-L;Gm8909	0.3478	0.8448	1.2740	**Slc27a1**	-0.1520	**1.1278**	**0.9321**
H3f3a;Hist1h3b;Hist1h3a;H3f3c	-0.9270	0.3071	0.9981	Tuba1a;Tuba1c;Tuba3a;Tuba8	0.6135	-0.3046	-0.0391
Hagh	0.8233	0.2771	-0.4650	Tuba4a	0.6569	-0.5561	-0.2197
Hbb-b1	3.0594	0.3689	0.0117	Tubb2a	0.9108	-0.3937	-0.0559
Hbb-b2	3.0499	0.7280	-0.1449	Tubb3	0.7540	-0.4070	-0.0984
Hist1h1d;Hist1h1e	-0.2985	**0.7345**	**0.8436**	Tubb4a	1.0310	-0.4425	-0.1501
Hist1h2bp;Hist1h2bk;Hist1h2bb;Hist1h2bf;Gm13646;Hist3h2ba;Hist3h2bb;Hist1h2bc;Hist2h2bb;Hist1h2bh;Hist1h2bm;Hist1h2ba;Hist2h2be	-0.6878	0.3831	0.8346	Tubb4b;Tubb4b-ps1	0.6675	-0.3565	-0.0543
Hist1h4a	-1.1001	0.7419	1.0788	Tubb5	0.8640	-0.5981	-0.1452
Itgb6	-0.3327	0.0401	1.1889	Txn	1.0622	0.2652	-0.1932
Lgals3	0.5747	**0.9390**	**1.1667**	Uchl1	0.6595	-0.0959	-0.3411
Lin7c;Lin7a	0.3966	-0.0130	0.6037	Ywhaq	0.6798	-0.0378	-0.1323
Lxn	0.8072	-0.0094	-0.0731				

The table emphasized that the only two protein groups exhibiting a constant significant upregulation at timepoints 13 and 17M contained histone proteins (Hist1h4a; H2-K1…). Considering also non-significant, but large enough log2 fold changes (≥ 0.585), no protein group that was significantly changed at timepoint 6M showed a relevant degree of upregulation at the later timepoints. In contrast, 10 protein groups exhibited a potential upregulation at both later timepoints (highlighted in bold). These were amine oxidase copper containing 3 (Aoc3), platelet glycoprotein 4 (Cd36), carboxylesterase 1D (Ces1d), catenin alpha-1 (Ctnna1), histones (Hist1h1d/e), galectin 3 (Lgals3), perilipin (Plin1), NADPH-cytochrome P450 reductase (Por), periaxin (Prx) and Slc27a1 (solute carrier family 27 member 1).

Table 4-4: Protein groups significantly downregulated in sciatic nerve myelin at at least one timepoint.
The table contains the proteins groups, indicated by their respective gene games, which showed a significant downregulation at one timepoint or more. Next to each gene name the log2 fold changes (log2 ratio FA2H-KO/WT) for each timepoint are given. Significant changes (log2 fold change ≤ 0.585 & -log10 p > 1.301) are shaded in green. In addition, protein groups potentially changed at more that one timepoint are highlighted in bold.

Gene names	log2 fold change 6M	log2 fold change 13M	log2 fold change 17M	Gene names	log2 fold change 6M	log2 fold change 13M	log2 fold change 17M
Atp6v1c1	0.3182	-0.0344	-0.8649	Prelp	-0.6200	0.2474	-0.1466
Atpif1	0.3614	0.2107	-0.6507	**Prnp**	-0.2175	**-0.8843**	**-0.5892**
Cacybp	-0.1720	0.2130	-0.6303	**Rab6b**	0.2329	**-0.9942**	**-1.1359**
Cfh	0.3548	0.9513	-0.9888	**S100b**	1.0783	**-0.8920**	**-0.9166**
Chmp1b2;Chmp1b1	-0.2626	-0.0121	-1.1573	Sbds	-0.2634	-0.4987	-1.1183
Cst3	-0.2777	0.0653	-0.6068	**Serf1;Serf2**	0.1914	**-0.7458**	**-0.5933**
Eef1a1	-0.4326	-0.2638	-0.6327	Slc4a1	-0.1976	1.0789	-1.3713
Eef1a2	-1.2212	-0.0080	-0.8551	Stk10	0.5149	-0.1280	-0.6872
Fam213b	-0.4982	-0.5936	-0.1663	**Svip**	0.0599	**-1.0607**	**-0.8819**
Fkbp3	-0.3242	**-0.6214**	**-1.1188**	**Tma7**	-0.2545	**-0.9634**	**-0.6264**
Fsd1	0.1414	-0.0395	-0.7791	Tmod1	-0.2073	-0.3371	-0.5992
Ist1	0.1953	0.2656	-0.6884	Tppp	-0.1606	-0.3736	-1.1166
Map7d2	-0.2048	**-0.6719**	**-0.7621**	**Tppp3**	-0.3707	**-0.7085**	**-1.1668**
Mapt	0.1929	-0.1960	-0.6002	**Vsnl1**	0.5659	**-0.6144**	**-0.6665**
Ppp1r1c	0.1724	-0.3234	-1.1159				

Table 4-4 underlined the observation that almost all protein downregulations in PNS-myelin of FA2H-KO mice were exclusively found at timepoint 17M. When taking into account also non-significant, but large enough log2 fold changes (≤-0.585), 10 of these protein groups may have been downregulated already at timepoint 13M (highlighted in bold). These were FK506-binding protein 3 (Fkbp3), MAP7 domain-containing protein 2 (Map7d2), prion protein (Prnp), Rab6b, S100 calcium binding protein B (S100b), small EDRK-rich factors 1 and 2 (Serf1 and Serf2), small VCP/p97-interacting protein (Svip), translation machinery associated 7 homolog (Tma7), tubulin polymerization-promoting protein 3 (Tppp3) and visinin-like 1 (Vsnl1).

Taken together, the comparative PNS-myelin analysis revealed that almost all major PNS-myelin proteins were largely unchanged. Of them, only periaxin was potentially elevated, but this was disproved by a subsequent WB analysis. Moreover, other protein groups were also significantly changed, but usually at a single timepoint only. Of all timepoints the majority were present at the latest timepoint (17M), which is in line with the late onset of the PNS-pathology. In addition, the expression of many protein groups varied heavily between the three timepoints. Still, a few other interesting protein groups, like CD36, Por, Prnp etc., might had been altered already at timepoint 13M, but since not all of their log2 fold changes were significant, this cannot be said for sure. Accordingly, further experiments are needed to verify these putative PNS-myelin protein changes.

4.2 Identification of FA2H interaction partners

After the comparative proteomic CNS- and PNS-myelin analyses of FA2H-KO mice, the second part of this thesis focused on the discovery of FA2H interaction partners. This was done, because the pathology found in FA2H-KO mice potentially is not caused by the absence of 2-OH sphingolipids, but rather the loss of certain protein interactions of FA2H.

The most widely used method to identify a protein's interaction partners is co-immunoprecipitation (Co-IP) followed by Western blotting (WB) and/or mass spectrometry. The proteins are usually precipitated by using an antibody together with Protein G/A-coupled beads or, alternatively, via an affinity tag based purification system. Of the available affinity tags the Twin-Strep-tag was chosen, because it has a very high affinity to its binding partner StrepTactin and thus allows a fast and specific one-step IP of the bait protein. Moreover, a tag-based system has the general advantage that the bait proteins have a good accessibility, because they are usually tagged at their termini. Antibodies on the other hand may also bind to more central, less accessible regions, limiting an efficient IP.

As a second approach, the recently published BioID (biotin identification) method was used (Roux et al. 2012). Its working principle is the fusion of a permanently active mutant Biotin-ligase from *E.coli* (BirA*) to the bait protein. This ligase biotinylates the proteins in the vicinity of the bait protein, thereby allowing their identification by mass spectrometry after selective enrichment using biotin-affinity purification.

In the process of this assay, the tagged-mFA2H enzymes were first cloned, followed by an assessment of their expression and functionality. Then the presence of FA2H-containing protein complexes in mammalian cells was proven by initial BlueNative PAGE and PFA-crosslinking experiments. After this initial positive result, potential FA2H-interacting proteins were then identified in different screening experiments using quantitative mass spectrometry. Finally, a selection of these newly identified putative interaction partners was verified by WB and bimolecular fluorescence complementation (BiFC).

4.2.1 Cloning, expression and functionality assessment of mFA2H-bait constructs

4.2.1.1 Cloning, expression and purification of Twin-Strep-FA2H

FA2H was tagged with a Twin-StrepTag, allowing its precipitation with StrepTactin-coated polymer beads. In addition, a shortened Twin-Strep-tagged mFA2H, consisting only of its N-terminal cytosolic part (mFA2H1-163), was initially produced as well. The shortened protein was produced for the identification of proteins, which interact with FA2H's via its N-terminus. But since the experiments with the full-length protein were successful, this approach was not further pursued in this thesis.

First, full-length and the N-terminal cytosolic part (amino acids 1-163) of murine FA2H was cloned into both mammalian Twin-Strep vectors (pESG-IBA103 [C-terminal tag] and pESG-IBA105 [N-terminal tag]) contained in the StarGate® Twin-Strep® mammalian cloning kit (IBA lifesciences). The cloning was done according to the manufacturers instructions via a DNA-recombinase dependent process (see 3.2.6.8 StarGate® cloning). Afterwards, the vectors were transiently transfected into HeLa cells and the constructs expression and their solubility evaluated in a mild detergent-containing lysis buffer by anti-FA2H and anti-StrepTag WBs (Figure 4-19).

A

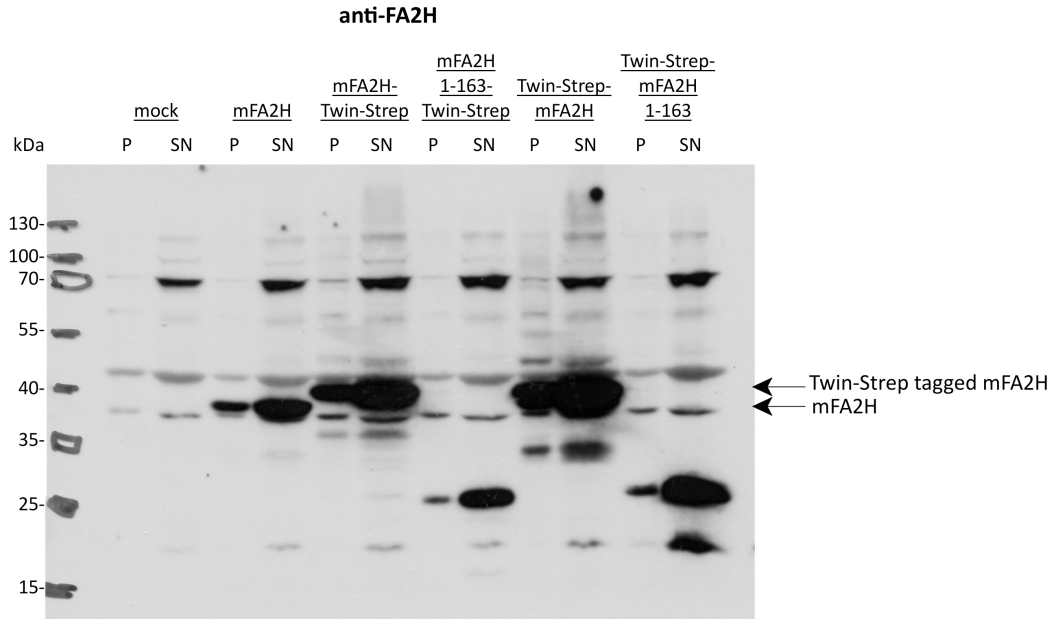

B

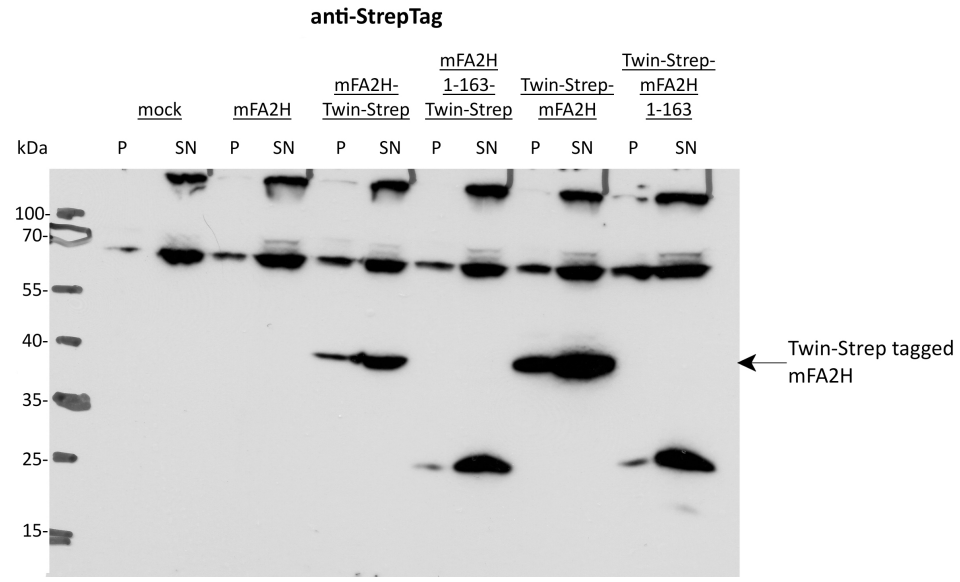

Figure 4-19: Expression and solubility analysis of Twin-Strep FA2H-constructs in HeLa cells. HeLa cells were transfected with mock (pcDNA3), untagged mFA2H, mFA2H-Twin-Strep, mFA2H1-163-Twin-Strep, Twin-Strep-mFA2H and Twin-Strep-mFA2H1-163 using Turbofect. After 24 h, cells were harvested, lysed in 50 µl StrepTag lysis buffer (cont. 1% TX-100), and centrifuged to obtain an insoluble pellet (P) and soluble supernatant (SN) fraction. The pellet was resuspended in 50 µl 1X Laemmli and 20 µl of both fractions separated via SDS-PAGE. Subsequently, both fractions were evaluated by WB with chemiluminescent detection. The expected protein sizes were: mFA2H = 38 kDa; mFA2H-Twin-Strep/Twin-Strep-mFA2H = 40 kDa; mFA2H1-163-Twin-Strep/Twin-Strep-mFA2H1-163 = 25 kDa. **(A)** FA2H blot obtained by incubation with FA2H antiserum #2 (dilution 1:800, ON, 4 °C) followed by goat-anti-rabbit-HRP secondary antibody incubation (dilution 1:5000, 1.5 h, RT). Twin-Strep-tagged and untagged mFA2H signals are indicated by arrows. **(B)** StrepTag blot developed by applying StrepTactin-HRP substrate (dilution 1:5000, 1.5 h, RT). Twin-Strep tagged mFA2H signals are indicated by an arrow.

The WB against FA2H showed specific FA2H-signals, corresponding with the expected molecular weights of the transfected constructs (mFA2H = 38 kDa; mFA2H-Twin-Strep/Twin-Strep-mFA2H = 40 kDa; mFA2H1-163-Twin-Strep/Twin-Strep-mFA2H1-163 = 25 kDa). In all samples the FA2H-signal was stronger in the supernatant (SN), than in the pellet fraction, showing an efficient protein solubilization by the applied StrepTag lysis buffer. Moreover, the strongest FA2H-signal was observable in the SN-sample transfected with N-terminally tagged Twin-Strep-mFA2H. Furthermore, there were some unspecific background bands present in all samples and fractions, with the most intense ones at ~38, 45 and 70 kDa.

The StrepTag-WB gave a similar result. As expected, only the Twin-Strep-tagged mFA2H-constructs were detectable at their predicted molecular weights (Twin-Strep mFA2H = 40 kDa, Twin-Strep mFA2H1-163 = 25 kDa), while untagged mFA2H was not. Again, each Twin-Strep-mFA2H signal was more intense in the supernatant, than in the pellet fraction and the strongest signal was visible for full length Twin-Strep-mFA2H. Moreover, in all samples background bands were present at ~70 and >100 kDa.

Taken together, all tagged mFA2H-constructs could be detected after transient expression in mammalian cells. Furthermore, the majority of each protein, including the full length ones, could be efficiently solubilized in lysis buffer, which is a prerequisite for subsequent affinity purifications.

At the next step, the functionality of the tagged mFA2H-constructs was evaluated by analyzing the sphingolipid profile of transfected HeLa cells (Figure 4-20). Overexpression of active FA2H should lead to an increase in 2-OH sphingolipids, which can be detected via thin layer chromatography (TLC).

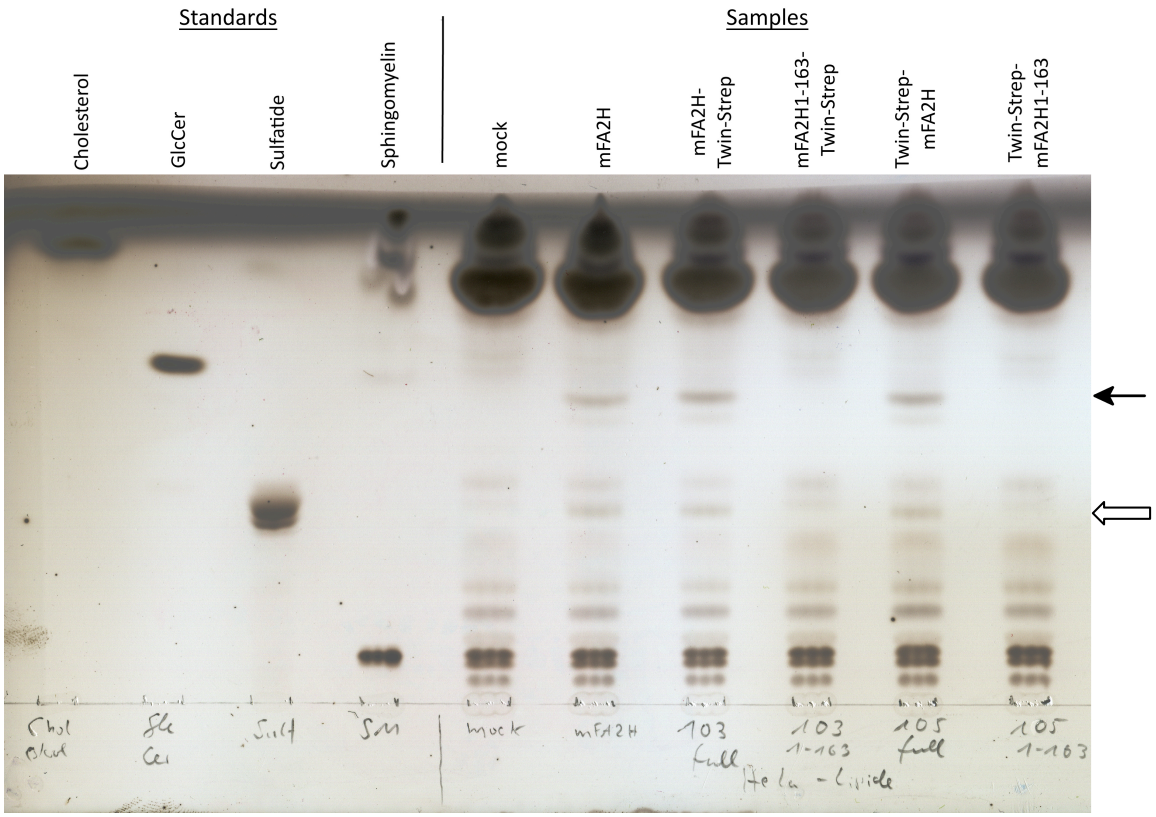

Figure 4-20: Sphingolipid analysis of HeLa cells transfected with Twin-Strep mFA2H-constructs. HeLa cells were transfected with mock (pcDNA3), untagged mFA2H, mFA2H-Twin-Strep, mFA2H1-163-Twin-Strep, Twin-Strep-mFA2H and Twin-Strep-mFA2H1-163 using Turbofect. After 24 h, cells were harvested and lipids extracted by the modified Bligh-Dyer-method followed by phospholipid degradation by alkaline methanolysis. The extracts and lipid standards (cholesterol, GlcCer, sulfatide, sphingomyelin) were applied to a HPTLC-silica plate and separated by a mobile phase of 70/30/4 $CHCl_3/CH_3OH/H_2O$. Lipid bands were made visible by copper sulfate charring. The filled arrow points at 2-OH cerebrosides, which have a slightly lower retardation factor (R_f) value, than their non-hydroxy counterparts. The non-filled arrow indicates another band, which becomes more intense in FA2H-transfected cells and might reflect 2-OH lactosylceramide.

As becomes clear from Figure 4-20, only the overexpression of full-length, but not shortened, mFA2H-constructs led to the appearance of an extra band (filled arrow) running slightly below GlcCer, which was used as a lipid standard. Based on its retardation factor (R_f), this substance probably represented hydroxylated GlcCer or GalCer. The intensity of this signal was of similar strength for all FA2H-constructs, thereby demonstrating that the presence of the Twin-StrepTag is not substantially affecting the proteins enzymatic activity. Furthermore, another band (non-filled arrow), probably representing 2-OH lactosylceramide, was significantly more intense in all samples expressing full-length mFA2H-constructs. This further proved the activity of the full-length proteins.

At this point it was clear that enzymatically active mFA2H, tagged N- or C-terminally with a Twin-StrepTag, could be expressed successfully in an immortalized human cell line. Since N-terminally tagged mFA2H was expressed at a slightly higher amount and C-terminal tagging could possibly mask FA2H's ER-retention signal, it was decided to use N-terminally tagged Twin-Strep-mFA2H for all following experiments.

At the next step, Twin-Strep-mFA2Hs precipitation by StrepTag-affinity purification was tested. Thus, Twin-Strep-mFA2H was transiently transfected into HEK293-T cells, the cells lysed and the affinity purification performed. The precipitation result was thereafter tested by a StrepTag WB of all fractions. This analysis, shown in Figure 4-21, demonstrated the successful and complete precipitation of Twin-Strep-mFA2H from the cell lysate and its subsequent almost complete elution.

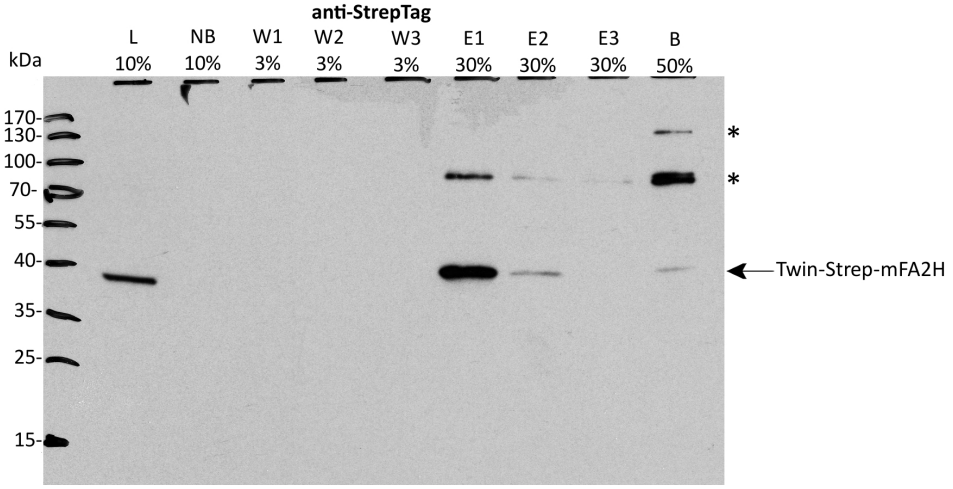

Figure 4-21: Affinity purification of Twin-Strep-mFA2H transiently expressed in HEK293-T. Twin-Strep-mFA2H was transfected using the $CaPO_4$-method and expressed for 48 h. Subsequently, the cells were lysed in StrepTag lysis buffer and centrifuged to obtain a cleared lysate (L). Then StrepTactin MacroPrep beads were added and the sample incubated overnight at 4 °C under constant agitation. Afterwards, the lysate containing the not binding proteins (NB) was removed, the beads washed three times with StrepTag washing buffer (W1-3) and the bound proteins eluted in three fractions of StrepTag elution buffer (E1-3). In addition, to assess elution efficiency, the MacroPrep beads (B) were afterwards boiled with 1X Laemmli. All fractions were subsequently separated via SDS-PAGE and analyzed by a StrepTag WB using StrepTactin-HRP substrate (dilution 1:5000, 2 h, RT). The following amounts of each fraction were loaded: lysate (L) 10%, non-bound lysate (NB) 10%, wash fractions (W1-3) 3%, eluates (E1-3) 30% and boiled beads (B) 50%. A black arrow indicates Twin-Strep-mFA2H (~40 kDa) and a black star(*) unspecific background bands.

The strongest Twin-Strep-mFA2H signals (~40 kDa) were present in the lysate (L) and the first elution fraction (E1). Furthermore, no Twin-Strep-mFA2H was detectable in the non-bound (NB) and wash fractions (W1 – W3), and only a small amount in the beads fraction (B). Taken together, this proved the accessibility of Twin-Strep-mFA2H to StrepTactin-affinity purification, a prerequisite for subsequent mass spectrometry-based interaction partner identifications.

4.2.1.2 Cloning, expression and functionality assessment of BirA-mFA2H*

FA2H was subcloned into the BioID-vector, downstream of the BirA*-sequence, after adding compatible restriction sites via PCR-amplification. Following sequence verification by DNA-sequencing, the construct was transfected into cells to assess its expression and functionality. Therefore, control (pcDNA3), BirA* (pcDNA3.1-mycBioID) and BirA*-mFA2H (pcDNA3.1-mycBioID-mFA2H) vectors were transiently transfected into HEK293-T cells grown in low-biotin medium (DMEM + 10% FCS) in four replicates each. DMEM itself contains no biotin, thus the only endogenous

biotin-source is FCS. 24 h after transfection, biotin was added to one half of the replicates, while the other half was left untreated. After another 24 h the cells were harvested, lysed and evaluated by a Streptavidin-HRP WB (Figure 4-22).

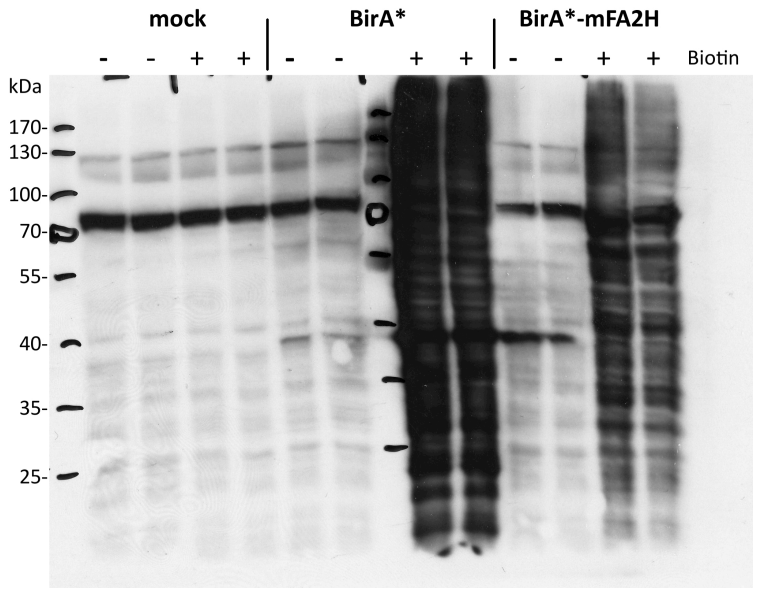

Figure 4-22: Expression and functionality analysis of BirA*-mFA2H. HEK293-T cells were transfected using $CaPO_4$ with either mock (pcDNA3), BirA* (pcDNA3.1-mycBioID) or BirA*-mFA2H (pcDNA3.1-mycBioID-mFA2H) in four replicates each. 24 h later, one half of the replicates were supplemented with 50 µM biotin and all cells grown for another 24 h. Subsequently, the cells were harvested, lysed in StrepTag lysis buffer and the protein amounts determined. Finally, 50 µg of total protein from each sample were separated by SDS-PAGE (10% gel) and analyzed via a Streptavidin-HRP WB (dilution 1:15,000, 1 h, RT). Since milk contains biotin, a BSA-solution (2.5% BSA, 0.4% TX-100 in PBS) was used for blocking and antibody incubation.

The WB showed the successful expression and functionality of the BirA*-mFA2H fusion protein. The samples from cells transfected with an empty vector (mock) exhibited only one intense major band of ~80 kDa and only a weak staining of other bands, regardless of the addition of biotin. The samples derived from cells transfected with pcDNA3.1-mycBioID (BirA*) or pcDNA3.1-mycBioID-mFA2H (BirA*-mFA2H) had a similar staining pattern when no additional biotin was present, but a significantly different one in the presence of 50 µM biotin. Without its addition, only one additional intense band of ~40 kDa appeared and the whole lane staining increased slightly. In contrast, the presence of 50 µM biotin led to an intense staining of various proteins over the whole lane, indicating the biotinylation of various proteins by the biotin ligase. This staining was more pronounced in the BirA* compared to the BirA*-mFA2H samples. In addition, both samples, BirA* and BirA*-mFA2H, differed in their staining patterns.

In summary, the results of this assay led to three conclusions. First, regardless of the addition of external biotin, the amount of biotinylated proteins within HEK293-T cells not expressing a BirA*-enzyme is low. Second, even in the presence of BirA*, the normal amount of biotin in the medium was not sufficient for widespread cellular biotinylation of various proteins proximal to the enzyme.

Therefore, the assay is inducible by the addition of external biotin. Third, cells transfected with pcDNA3.1-mycBioID-mFA2H exhibited a less intense and divergent staining pattern compared to pcDNA3.1-mycBioID-transfected ones. This was expected, since both proteins have a distinct localization and thus different biotinylation targets. While the BirA*-protein alone is localized in the cytosol, the fusion enzyme is integral to the ER-membrane via its FA2H part, with its biotin-ligase part facing the cytosol.

4.2.2 Identification of a FA2H-containing protein complex

Before starting the analysis of Twin-Strep-mFA2H precipitates for interaction partners by mass spectrometry, the presence of such a complex/complexes should be confirmed. Accordingly, cells expressing Twin-Strep-mFA2H were analysed by BlueNative PAGE and a PFA-cross linking assay.

4.2.2.1 BlueNative PAGE

Cell lysate of HEK293-T cells, transiently transfected with Twin-Strep-mFA2H, was separated via BlueNative PAGE followed by StrepTag WB detection (Figure 4-23) to assess if FA2H is part of one or more multiprotein complexes.

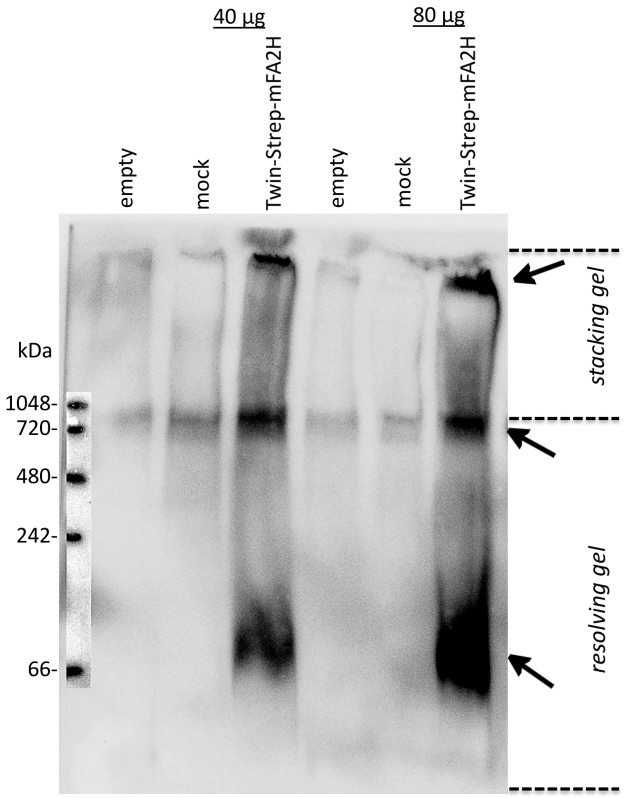

Figure 4-23: BlueNative PAGE analysis of Twin-Strep-mFA2H. HEK293-T cells were transfected with pcDNA3 (mock) or Twin-Strep-mFA2H via the $CaPO_4$-method. After 48 h the cells were harvested and lysed in 1% TX-100 lysis buffer. Then 40 and 80 µg of total protein were separated using BlueNative PAGE, blotted onto a PVDF membrane, and analyzed by a StrepTag WB using StrepTactin-HRP substrate (dilution 1:5000, 2 h, RT) and subsequent chemiluminescent detection. Note that empty lanes were left between samples. Areas of the blot corresponding to the original stacking and resolving gel are indicated on the right. Regions with very intense staining, hinting at the existence of a protein complex, are marked with an arrow.

The anti-StrepTag WB revealed the existence of three major Twin-Strep-mFA2H containing complexes: a small one of ~80 kDa, a medium one of ~750 - 900 kDa at the border of stacking and resolving gel, and a large one of >1000 kDa at the border between the SDS-gel pockets and the stacking gel. While the small signal was exclusively observed in the Twin-Strep-mFA2H sample, the two larger ones were also present in the mock sample. It can be therefore assumed that all protein complexes to large to pass one of these borders were arrested there. Obviously, the StrepTactin-HRP substrate had bound to some of these complexes unspecifically, leading to a signal in all samples. But since their intensities were much stronger in the Twin-Strep-mFA2H sample, compared to the control, it can be concluded that specific FA2H-containing complexes were also present there. In addition, because of its approximate size of 80 kDa, corresponding to about two times the size of FA2H, the smallest complex might have represented FA2H-homodimers.

4.2.2.2 PFA-crosslinking

Another complementary method employed to visualize a FA2H-protein complex is PFA-crosslinking. The advantage of this method is that it allows the identification of less-stable and transient

complexes, which are normally lost during cell lysis. Unfortunately, it has to be considered, that not all complexes detected by this method are specific, because it can also lead to the appearance of unspecifically crosslinked proteins.

The optimal amount of PFA necessary for efficient crosslinking varies, depending on the target protein and the cells used for expression. Thus, it had to be elucidated by titration. Consequently, HEK293-T cells, transiently transfected with mock (pcDNA3) or Twin-Strep-mFA2H, were treated (after 24 h) with increasing amounts of PFA (0 – 1% in 1X PBS) for 20 min at 37 °C. After the crosslinking was stopped by the addition of ice-cold glycine solution, the cells were lysed in RIPA-buffer and analyzed by a StrepTag WB (Figure 4-24).

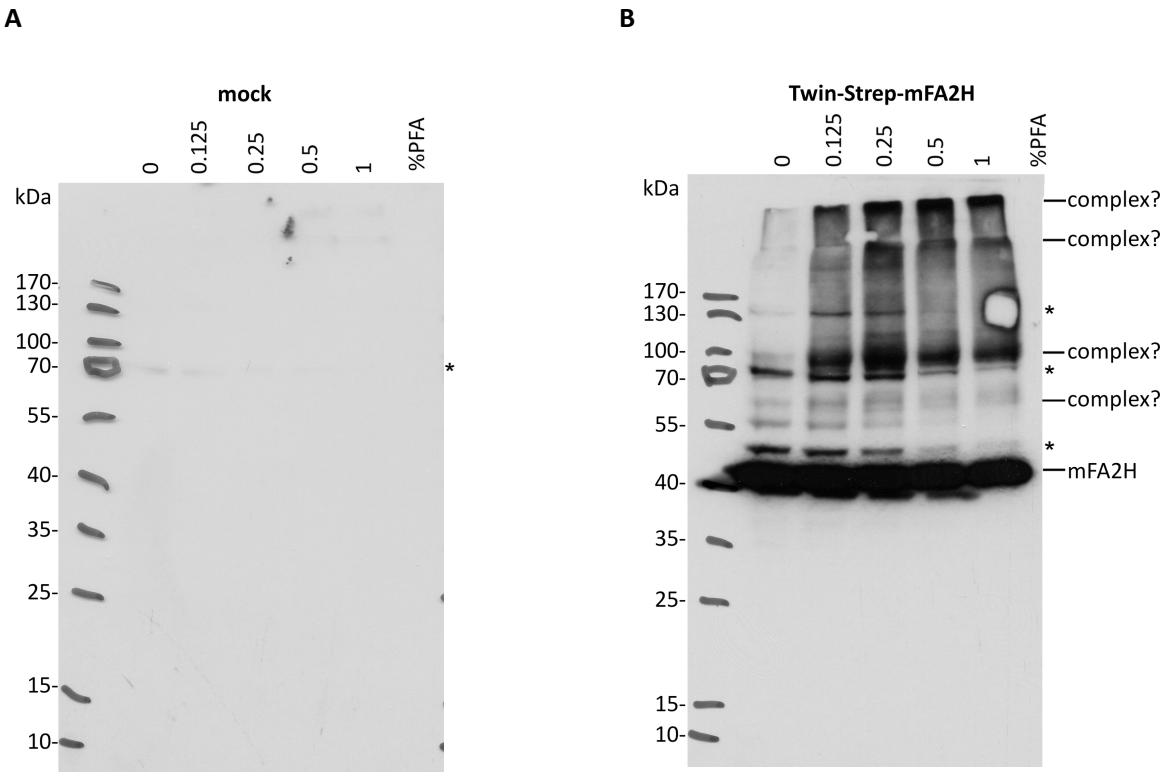

Figure 4-24: Evaluation of PFA-concentration needed for Twin-Strep-mFA2H crosslinking. Mock (pcDNA3) or Twin-Strep-mFA2H was transiently expressed in HEK293-T cells grown in 6-well plates for 24 h. Afterwards, they were washed with PBS and treated for 20 min with 0 – 1% (v/v) PFA (in 1 XPBS) at 37 °C. Crosslinking was stopped by the addition of 1.25 M ice-cold glycine. Cells were then harvested, washed once in PBS and subjected to lysis in RIPA buffer. Of each lysate 15 µg of total protein were mixed with Laemmli buffer (without boiling), separated via SDS-PAGE and analyzed by anti-StrepTag WB (dilution 1:5000, 2 h, RT). Potential FA2H-containing protein complexes are marked with "complex?" and unspecific background bands with a black star (*). **(A)** No StrepTag-mFA2H signal could be detected in samples originating from cells transfected with an empty vector. **(B)** Samples derived from cells expressing Twin-Strep-mFA2H exhibited intense staining in anti-StrepTag WB. First a strong Twin-Strep-mFA2H signal (~40 kDa) can be observed in all samples. Moreover, samples treated with PFA showed several additional signals at higher molecular weights marked with "complex?". Note that an airbubble was accidentialy introduced during blotting in the 1% PFA sample. Thus, no signals were visible at ~130 kDa.

The treatment of Twin-Strep-mFA2H expressing HEK293-T cells with increasing concentrations of PFA led to the appearance of several additional StrepTag WB signals besides the Twin-Strep-mFA2H signal

(~40 kDa). This effect was not found in the mock-transfected cells, which exhibited just very weakly the 70 kDa background signal (*) present in all anti-StrepTag WBs (see: Figure 4-19 or Figure 4-21). In contrast, three very prominent background signals of 50, 70 and 130 kDa (*) were observable in the Twin-Step-mFA2H sample, even without PFA-crosslinking. Furthermore, four additional signals became visible, ~60 kDa, ~80 kDa and two larger ones of >170 kDa, which probably reflected FA2H-containing protein complexes. With approximately two times the molecular weigth of FA2H the ~80 kDa complex might have reflected FA2H homodimers. Furthermore, there was a generally more intense staining over the whole lane, possibly derived from various less abundant proteins proximal to Twin-Strep-mFA2H. All of these signals appeared even at the lowest concentration of PFA and did not increase in intensity, when using more than 0.25% PFA. Moreover, some signals, especially background ones, became even weaker at higher PFA-concentrations, probably due to protein insolubility caused by excessive crosslinking. Thus, the end it was decided to use 0.5% PFA in all further PFA-crosslinking experiments, because at this concentration the potential complexes were still visible, while the background ones were significantly reduced in intensity.

As the next step, the accessibility of the crosslinked complexes by StrepTactin-affinity purification was assessed. Twin-Strep-mFA2H was again expressed transiently in HEK293-T cells. After 48 h, the cells were treated with 0.5% PFA for 20 min, the crosslinking stopped with ice-cold glycine solution and the cells lysed in RIPA-buffer. Afterwards, the lysates were subjected to StrepTactin-affinity purification. Finally, all purification fractions were evaluated by anti-StrepTag WB analysis (Figure 4-25).

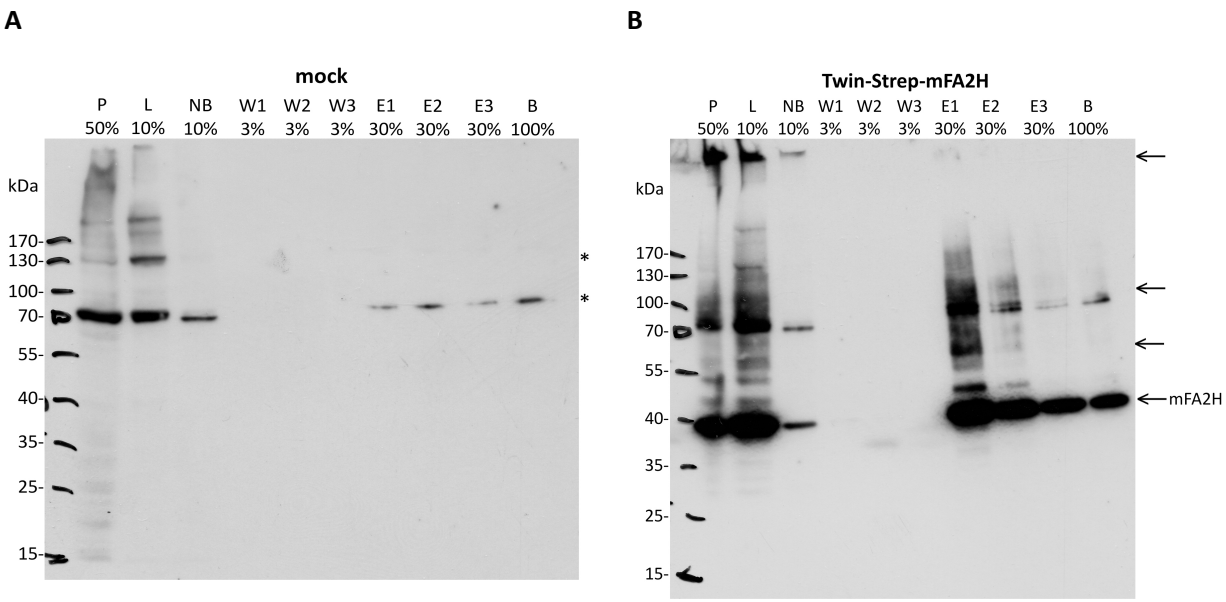

Figure 4-25: Purification of Twin-Strep-mFA2H after PFA-crosslinking. Either mock (pcDNA3) or Twin-Strep-mFA2H was expressed for 48 h in one 10 cm plate of HEK293-T cells. Afterwards, cells were washed two times in PBS, fixed for 20 min with 0.5% PFA, and finally washed twice with ice-cold glycine stopping solution. Subsequently, the cells were lysed in 150 µl RIPA buffer (incl. proteinase inhib.) for 30 min at 4 °C and centrifuged 30 min at 20,000 g. While the pellet (P) was resuspended in 40 µl 1X Laemmlli, the cleared lysate (L) was incubated with 50 µl StrepTactin-MacroPrep beads under constant agitation at 4 °C overnight. Then the beads were washed thrice with 500 µl RIPA buffer (W1-3) and bound proteins eluted three times with 50 µl 2.5 mM biotin in RIPA buffer (E1-3). In addition, the beads (B) were boiled in 20 µl 1X Laemmli. Thereafter, all fractions were separated by SDS-PAGE and evaluated by anti-StrepTag WB (dilution 1:5000, 2 h, RT). Of each fraction the following amounts were loaded: pellet (P) 50%, lysate (L) 10%, non-bound lysate (NB) 10%, wash fractions (W1-3) 3%, eluates (E1-3) 30% and boiled beads (B) 100%. **(A) StrepTag WB of mock transfected cells.** The purification fractions showed only a background signals at 70 and 130 kDa, marked with black stars (*), but no Twin-Strep-mFA2H signal. While the 70 kDa signal could be observed in all except the wash fractions, the 130 kDa signal was only visible in the pellet and lysate fraction. **(B) StrepTag WB of Twin-Strep-mFA2H transfected cells**. All except the wash fractions displayed differentially intense protein bands in the WB. Besides the 40 kDa FA2H-signal, there were three prominent protein bands at higher molecular weights marked with black arrows.

While the fractions, obtained from mock-transfected cells, showed mainly the 70 and 130 kDa background signals (*) previously seen in StrepTag WBs (see: Figure 4-19), the Twin-Strep-mFA2H expressing cells showed similar signals as before (see: Figure 4-24). Besides the strong 40 kDa FA2H-signal, in all but the washing fractions, there were putative complexes at ~60, ~80 and >170 kDa (black arrows). Furthermore, the general background staining, derived from less abundant proteins crosslinked to FA2H, was also present. When looking closely at the fractions, it became evident that besides FA2H only the ~60 and ~80 kDa complexes, as well as the less abundant crosslinked proteins, were purified. In contrast, the >170 kDa complex did not. This could be partly explained by the fact that a part of it did not bind to the affinity matrix (see signal in non-bound fraction). Still, the remaining amounts of this complex were not present in the elution fractions (E1 – E3), which might reflect a strong unspecific binding to the StrepTactin-beads. Interestingly, the ~60 kDa complex seemed to have been enriched by the purification process, which became apparent as a strong signal in the first elution fraction. This complex could almost not be discerned from the background signals, when looking at the lysate fraction. Taken together, Twin-Strep-mFA2H and some of crosslinked proteins could be purified by StrepTactin-affinity purification.

4.2.3 Determination of FA2H-protein complex constituents

With the existence of a FA2H-containing protein complex proven, the next step was to elucidate its composition. Therefore, two mass spectrometry based screening approaches were applied, Twin-StrepTag pulldown and BioID (in-vivo protein biotinylation). In both approaches, FA2H and interacting proteins were first enriched by an affinity purification step. The identity of putative FA2H-interacting proteins was then revealed by mass spectrometry using a high resolution Orbitrap Velos mass spectrometer.

4.2.3.1 SILAC Twin-StrepTag pulldown & MS-analysis

For the first approach, StrepTactin-affinity purification was used in combination with stable isotope labeling of cells (SILAC). In SILAC, all proteins of a cell are metabolically labeled with light or heavy amino acids containing light or heavy isotopes. This permits robust relative protein quantification between the differentially labeled cells by mass spectrometry. The combination of SILAC with immunoprecipitation or affinity purification, also called SILAC IP (see review by Ong & Mann (Ong & Mann 2005)), then helps to identify real interacting proteins and distinguishing them from proteins binding unspecifically to the affinity matrix (Figure 4-26A). Hence, an empty control plasmid and one coding for the bait protein (for example: Twin-Strep-mFA2H) are transfected in differently isotopically labeled cells. After 1 – 2 days of transgene expression, both cell types are subjected to lysis and protein determination. Then both lysates are mixed at a 1:1 protein ratio and StrepTactin-affinity purification is performed. Afterwards, the proteins in the eluate are enzymatically digested to peptides, allowing their identification and quantification by mass spectrometry. The quantitative information now directly allows separating proteins binding unspecifically to the affinity matrix (background) from interacting proteins. While background proteins, contributed by both samples, will exhibit heavy and light peptide signals of equal intensity, selectively enriched interacting proteins will have significantly larger heavy peptide signals.

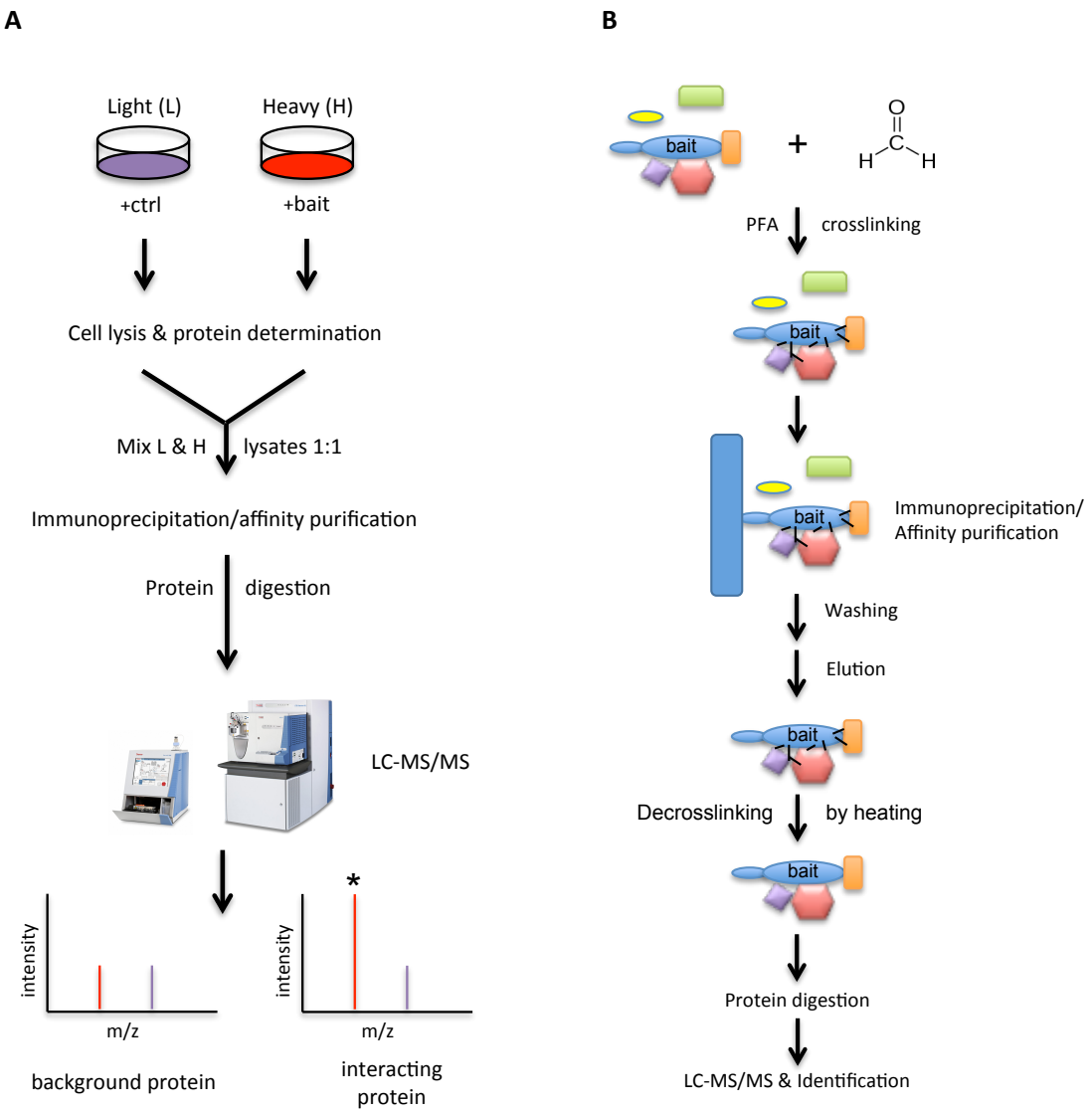

Figure 4-26: SILAC-IP. (A) General overview of SILAC-IP procedure. Control and bait-coding plasmids are transfected into cells labeled with light or heavy SILAC-medium. After protein expression, cells are lysed, their protein amount determined and the lysates mixed at a 1:1 ratio. Subsequently, immunoprecipitation/affinity purification of the bait protein is performed followed by protein digestion and LC-MS/MS analysis. While peptides derived from unspecific binding proteins exhibit equal light and heavy intensities, specific interaction partners are identifiable by higher intensities for the heavy peptides. **(B) Schematic workflow of PFA-crosslinking assisted IP.** Cells expressing the bait protein of interest are treated with formaldehyde/PFA chemically crosslinking proteins in close vicinity of each other. Afterwards, the cells are lysed and subjected to immunoprecipitation or affinity purification of the bait protein. During subsequent washing steps not binding proteins are washed away. Then the protein with its crosslinked partners is eluted. After removing the crosslinks by heating and protein digestion, the complex constituents can be identified by mass spectrometry.

In a variation of this method an additional PFA-crosslinking step (Vasilescu et al. 2004; Klockenbusch & Kast 2010) is added before cell lysis (Figure 4-26B). Hence, proteins, which are in close vicinity of each other, are covalently linked. On the one hand this facilitates the identification of medium and weak interactors, which are normally lost during the washing steps of the affinity purification. On the other hand this also inevitably increases the number of false positive identifications, due to proteins becoming crosslinked, which are just randomly located in the vicinity of the bait. Additionally, some

indirect interactions, i.e. ones facilitated by one ore more additional proteins, will also be captured by this method. But these disadvantages of PFA-crosslinking have to be accepted, if also weak and transient interactors should be identified. Moreover, since most random interactions should happen at low rates, a high H/L-ratio should help to distinguish them from true interactors at least partially.

4.2.3.1.1 Twin-Strep pulldown of transiently-overexpressed mFA2H

For the first SILAC Twin-StrepTag pulldown experiment (Figure 4-27A), HEK293-T cells labeled with light or heavy SILAC-medium, were transiently transfected with an empty control vector (pcDNA3) or with Twin-Strep-mFA2H (pESG-IBA105-mFA2H) and grown for 48 h. Afterwards, the cells were lysed, StrepTactin-affinity purification performed and the samples processed for the subsequent mass spectrometric analysis. Finally, the mass spectrometric data were analyzed by MaxQuant and Perseus. While MaxQuant was used for protein identification and quantification, Perseus was used for the following statistical analysis including a one-sample t-test (different from 0) and the generation of a Volcano plot. The results are depicted in Figure 4-27B and Table 4-5. Moreover, the MS raw data and the unprocessed as well as the processed MaxQuant result files can be found on the DVD accompanying this thesis. Note again that MaxQuant did not present the identifications as single proteins, but protein groups.

A

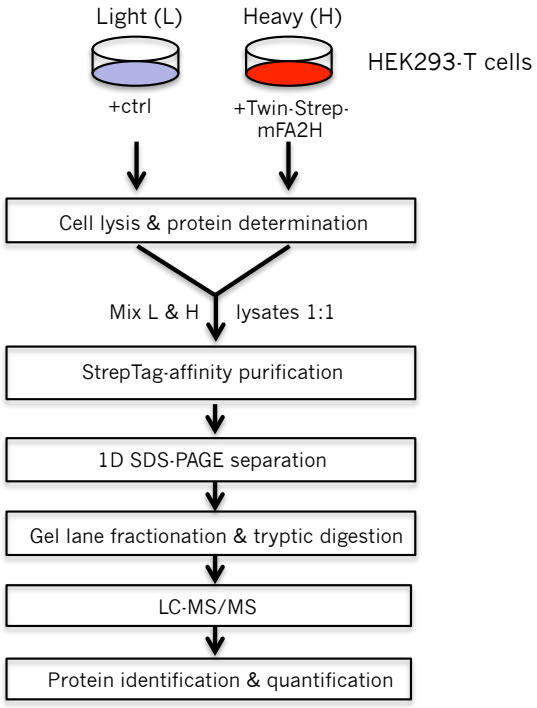

B

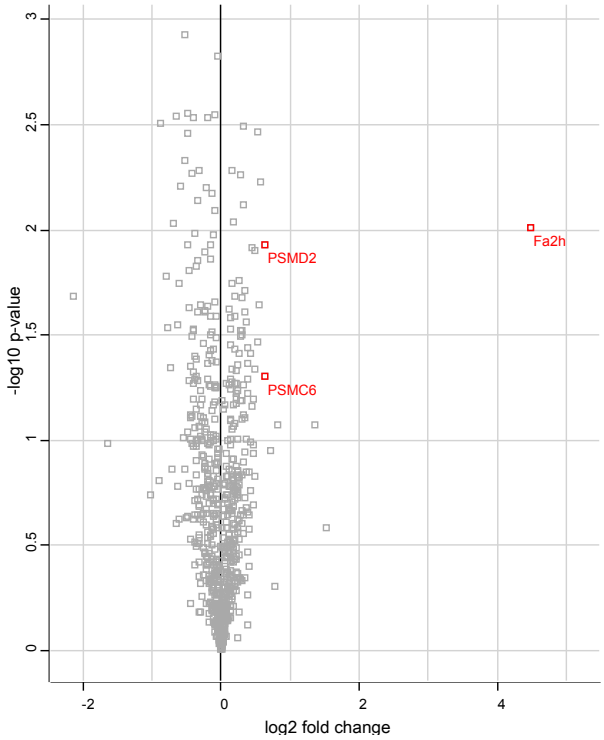

Figure 4-27: Twin-Strep-mFA2H interaction partner analysis after overexpression in HEK293-T cells.
(A) Workflow diagram illustrating the assay procedure. Twelve 15 cm dishes of HEK293-T cells (6x light and 6x heavy SILAC-labeled) were transiently transfected with either empty control (pcDNA3) or Twin-Strep-mFA2H vector (pESG-IBA105-mFA2H). After 48 h, cells were harvested, thereby pooling two dishes of equally labeled and transfected cells. The cells were lysed in StrepTag-lysis buffer followed by protein amount determination. Subsequently each empty vector-lysate was mixed with a differentially labeled Twin-Strep-mFA2H lysate at a protein ratio of 1:1. The resulting three replicates were then subjected to StrepTactin-affinity purification. The resulting eluates of each purification were pooled, concentrated by $CHCl_3$/MeOH-precipitation, separated by SDS-PAGE and Coomassie-stained. Thereafter, the complete protein lane of each replicate was cut into fractions of equal protein amount and processed by tryptic in-gel digestion. Finally, the resulting peptides were cleaned using StageTips and analyzed by LC-MS/MS. This was followed by protein identification (human Uniprot database +mFA2H), quantification and ratio-normalization by MaxQuant and statistical evaluation using Perseus. **(B) Volcano plot of all protein groups identified and quantified in at least two replicates.** After a one-sample t-test against 0, the resulting –log10-transformed p-values (-log10 p-value) of each protein group were plotted against their log2-transformed average H/L-ratio (log2 fold change). Significantly enriched protein groups having a log2 fold change ≥ 0.585 (fold change ≥ 1.5) and –log10 p-value > 1.301 (p-value < 0.05) are highlighted in red.

Overall, 716 protein groups were identified and quantified in at least two replicates (Complete protein list can be found on the accompanying DVD). After performing a one-sample t-test they can be depicted in a volcano plot (Figure 4-27B), comparing the log2-transformed average H/L-ratio (log2 fold change) of each identified and quantified protein group with its –log10-transformed p-value (-log10 p-value). This plot is a frequently used method to visualize the results of an interaction partner search. Protein groups enriched in the bait-containing sample should have a high log2 fold change (=enrichment) in combination with a large –log10 p-value (=significance), therefore appearing in the upper right part of the plot. In contrast, background proteins contributed by both samples (control & bait) should cluster around a log2 fold change of 0. In all SILAC-IP experiments presented in this thesis the thresholds for a protein group to be considered significantly enriched were: log2 fold change ≥ 0.585 (fold change ≥ 1.5) and –log10 p-value > 1.301 (p-value < 0.05)

As becomes evident for this pulldown analysis, only three protein groups, containing FA2H and two proteasomal proteins, 26S proteasome non-ATPase regulatory subunit 2 (PSMD2) and 26S protease regulatory subunit 10B (PSMC6), passed the criteria for significant enrichment. The majority of the proteins clustered around the y-axis, having only a low level of enrichment. Also when looking at all protein groups with a log2 fold change ≥ 0.585 (see Table 4-5), the number of potential FA2H interaction partners did not increase drastically.

Table 4-5: Protein groups significantly enriched in Twin-Strep-mFA2H-containing samples after pulldown from transiently transfected HEK293-T cells. Shown are all protein groups identified with a log2 fold change ≥ 0.585. The protein groups are given by their corresponding gene name and sorted by their –log10 p-value. Groups associated with protein quality control processes are highlighted in red.

	Gene names	log2 fold change	-log10 p-value		Gene names	log2 fold change	-log10 p-value
1	Fa2h	4.4894	2.0110	8	SMARCA4;SMARCA2	0.7752	0.3034
2	PSMD2	0.6296	1.9286	9	TOP2A	1.1422	0.0000
3	PSMC6	0.6266	1.3054	10	AIFM1	1.1391	0.0000
4	HAX1	0.8132	1.0709	11	BAG2	0.8654	0.0000
5	UBB;RPS27A;UBC;UBA52;UBBP4	1.3620	1.0696	12	SEC24A	0.7250	0.0000
6	ESYT1	0.7239	0.9522	13	CACYBP	0.6805	0.0000
7	TFRC	1.5195	0.5825				

Considering protein groups with lower p-values only slightly extended the list. The largest amount (6/13 ≈ 46%) of protein groups, like ubiquitin or the above mentioned proteasomal subunits, are involved in protein quality control processes. In general, finding such proteins is not unexpected, since most cellular proteins have a limited lifetime and are subjected to normal cellular turnover mechanims. Still, the large amount of these proteins may argue for an artificial effect caused by FA2H's overexpression. According to this, the majority of the overexpressed Twin-Strep-mFA2H was ubiquitinated, exported from the ER and afterwards degraded by the proteasome. This in turn then might have impeded the identification of other proteins associated with FA2H.

4.2.3.1.2 PFA-assisted Twin-Strep pulldown of transiently-overexpressed mFA2H

As mentioned above, PFA-crosslinking can help to identify weak and transient interactions. Therefore, the assay was also done with the inclusion of an additional PFA-crosslinking step between cell harvesting and lysis. In addition, since the crosslinking should preserve and strengthen even weak protein-protein interactions, a more stringent washing and elution buffer (RIPA) was used. Finally, a decrosslinking-step had to be included after elution to remove the PFA-derived covalent protein-protein bridges. The results obtained after subsequent processing with MaxQuant, Perseus and GOrilla are depicted in Figure 4-28B, Table 4-6, Table 4-7 and Table 4-8.

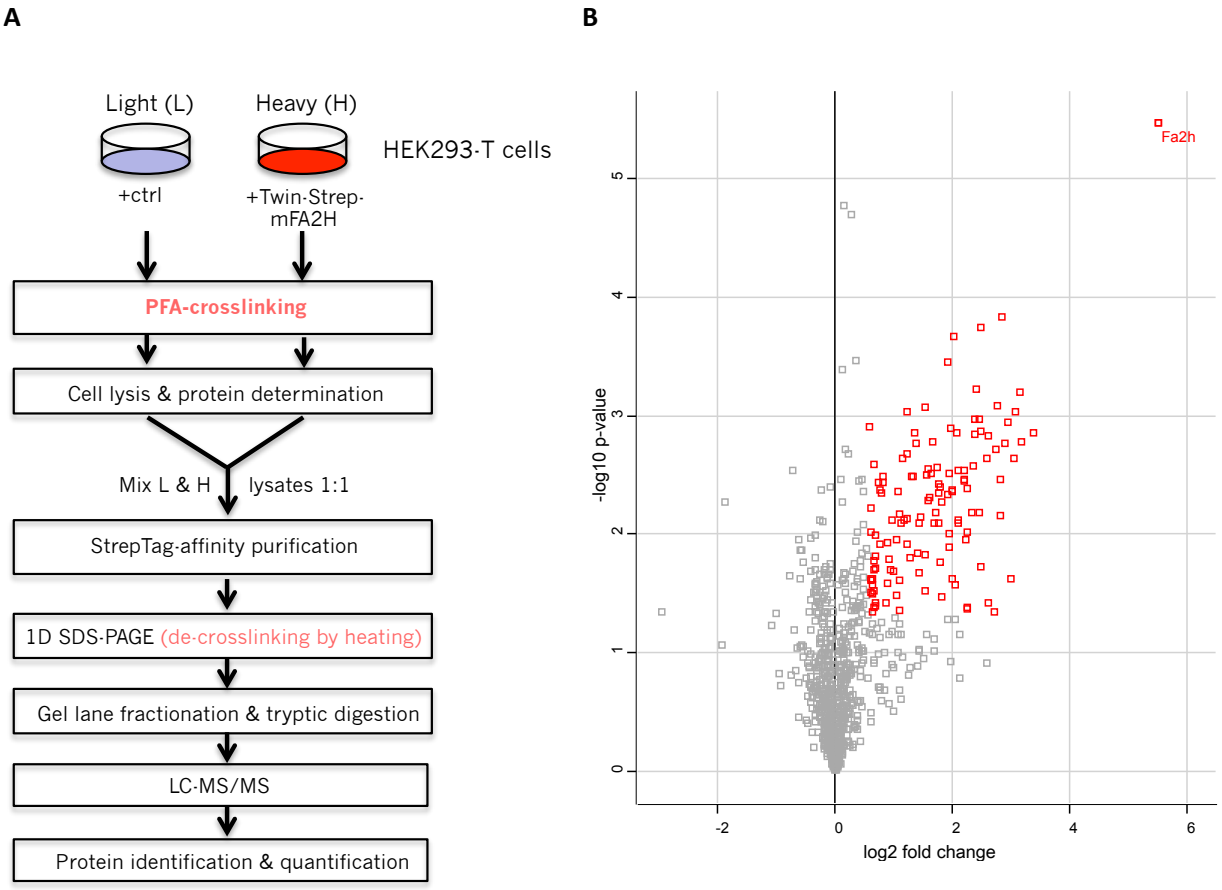

Figure 4-28: PFA-assisted Twin-Strep-mFA2H interaction partner analysis after overexpression.
(A) Workflow of the performed analysis. Twelve 15 cm dishes of HEK293-T cells (6x light and 6x heavy SILAC-labeled) were transiently transfected with either empty control (pcDNA3) or Twin-Strep-mFA2H vector (pESG-IBA105-mFA2H). After 48 h, the cells were harvested thereby always pooling two dishes of equally labeled and transfected cells. Then all six cell pellets were fixed for 20 min with 0.5% PFA at room temperature. The fixations were stopped by the addition of ice-cold 1.25 M glycine solution. Subsequently, each pellet was lysed in RIPA buffer followed by protein amount determination. Thereafter, each light-labeled lysate was mixed with one heavy-labeled lysate at a protein ratio of 1:1. The resulting three replicates were subsequently subjected to StrepTactin-affinity purification using RIPA-buffer. The eluate fractions of each purification were pooled, concentrated by $CHCl_3$/MeOH-precipitation, resuspended and reduced in 2X Laemmli buffer (95 °C, 10 min), separated by SDS-PAGE and Coomassie-stained. Then the complete protein lane of each replicate was cut into fractions of equal protein amount and processed by tryptic in-gel digestion. In the end, the resulting peptides were cleaned using StageTips and analyzed by LC-MS/MS, followed by protein identification (human Uniprot database +mFA2H), quantification and ratio-normalization by MaxQuant. Finally, the resulting protein groups were statistically evaluated with Perseus and GOrilla. **(B) Volcano plot of all protein groups identified and quantified in at least two replicates.** After performing a one-sided t-test against 0, the resulting –log p-values of each protein group were plotted against their log2-transformed average H/L-ratio (log2 fold change). Significantly enriched protein groups having a log2 fold change ≥ 0.585 (fold change ≥ 1.5) and –log10 p-value > 1.301 (p-value < 0.05) are highlighted in red.

In this analysis 840 protein groups could be identified and quantified in at least two replicates. Of these 125 exhibited a log2 fold change ≥ 0.585 together with a good level of confidence (–log10 p-value > 1.301). These protein groups sorted by their log2 fold change are given in Table 4-6. For the complete protein group list consult the supplemental DVD.

Table 4-6: Protein groups significantly enriched in Twin-Strep-mFA2H-containing samples after pulldown from transiently transfected and PFA-crosslinked HEK293-T cells. Shown are all protein groups identified in at least two replicates with a log2 fold change ≥ 0.585 (fold change ≥ 1.5) and –log10 p-value > 1.301 (p-value < 0.05). Protein groups are given by their respective gene names and sorted by their log2 fold change in descending order. Proteins groups associated with protein quality control processes are highlighted in red and with (sphingo-)lipid metabolism in **bold**.

N°	Gene names	log2 fold change	-log10 p-value	N°	Gene names	log2 fold change	-log10 p-value
1	**Fa2h**	**5.4958**	**5.4827**	64	TMPO	1.6111	2.3139
2	UBB;RPS27A;UBC;UBA52;UBBP4	3.3651	2.8557	65	TOR1AIP1	1.5902	2.2823
3	LRRC59	3.1670	2.7849	66	RPN2	1.5854	2.5481
4	ERLIN2	3.1417	3.2035	67	RAB8A;RAB8B;RAB13	1.5479	2.4963
5	GOLGA2	3.0727	3.0404	68	COPA	1.5385	1.8321
6	EMC2	3.0275	2.6455	69	CAPZA1	1.5359	1.5248
7	**OSBPL8**	**2.9854**	**1.6175**	70	RAB1A	1.5202	3.0729
8	SRPRB	2.9262	2.9514	71	RAB14	1.4368	2.1397
9	ESYT1	2.8924	2.7621	72	RAB2A	1.4226	1.6727
10	CKAP4	2.8293	3.8363	**73**	**CYB5R3**	**1.4125**	**2.0875**
11	STIM1	2.8183	2.1622	74	TMEM109	1.3949	1.8409
12	SEC22B	2.7978	2.4560	75	RAB1B;RAB1C	1.3735	2.7733
13	**SPTLC1**	**2.7454**	**3.0873**	76	DNAJA1	1.3480	2.8504
14	**SPTLC2**	**2.7327**	**2.7170**	77	NCLN	1.3230	2.4832
15	STX18	2.7006	1.3384	**78**	**HSD17B12**	**1.2913**	**2.4890**
16	KTN1	2.6016	1.4226	79	TMED1	1.2727	1.8053
17	ERLIN1	2.6010	2.8339	80	DPM1	1.2242	3.0326
18	**POR**	**2.5668**	**2.6340**	81	HSPA8	1.2225	1.9162
19	HMOX2	2.4849	1.7230	82	HSPA6;HSPA7	1.2177	2.6754
20	RPN1	2.4811	3.7498	83	RAB11B;RAB11A	1.2144	2.1319
21	CCDC47	2.4724	2.8743	84	RAB5C	1.1743	2.1232
22	MIA3	2.4404	2.9753	85	SND1	1.1323	2.6438
23	BCAP31	2.4400	2.1806	86	PDIA3	1.1079	2.0923
24	ATP2A2	2.3959	3.2260	87	HSPA5	1.0890	2.1675
25	**VAPA**	**2.3748**	**2.9680**	88	PCYOX1	1.0887	1.3520
26	**SLC27A4**	**2.3607**	**2.8470**	89	PPIB	1.0821	1.6068
27	**VAPB**	**2.3508**	**2.5712**	90	SURF4	1.0770	2.3657
28	**SACM1L**	**2.3110**	**2.1876**	91	TOLLIP	1.0373	1.4804
29	PTPN1	2.2487	1.3647	92	PDIA3	1.0306	1.9473
30	TMED9	2.2460	2.3799	93	PSMC4	0.9820	1.6857
31	**ACSL3**	**2.2416**	**2.0170**	**94**	**HSD17B7**	**0.9531**	**2.1170**
32	PTRH2	2.2392	1.3850	**95**	**LBR**	**0.9433**	**1.6940**
33	SPCS2	2.2144	1.9552	96	PSMD6	0.9011	1.7816
34	RDH11	2.1961	2.4627	97	RPL14	0.8837	1.9330
35	TFRC	2.1897	2.4552	98	PSMD11	0.8750	1.5857
36	EPHX1	2.1857	2.5343	99	PSMD2	0.8716	1.4179
37	TMX1	2.1012	2.1208	100	GNB2;GNB4	0.8207	2.4884
38	SDCBP	2.1001	2.0992	101	ATP1A1;ATP1A3	0.7979	2.4411
39	SSR4	2.0929	2.5328	102	RHOT2	0.7935	2.3484

40	RAB6A	2.0774	2.8583	103	DNAJC7	0.7696	1.9204
41	NOMO2;NOMO3;NOMO1	2.0330	1.5703	104	RPL7	0.7626	2.3759
42	**NSDHL**	**2.0248**	**3.6691**	105	RPL10A	0.7216	2.4374
43	ZW10	1.9876	2.3597	106	RPL13	0.6907	1.4209
44	LMAN1	1.9858	1.6262	107	AMOT	0.6845	1.9892
45	SCFD1	1.9845	2.3757	108	ATP6V0D1	0.6785	1.3905
46	**ALDH3A2**	**1.9656**	**2.8884**	109	YIPF5	0.6755	1.8147
47	NSF	1.9427	2.0021	110	PDIA4	0.6744	1.7131
48	**DHCR7**	**1.9388**	**2.5147**	111	RPL8	0.6672	1.5207
49	**PLD3**	**1.9272**	**1.8886**	112	HYOU1	0.6619	1.6970
50	CANX	1.9132	2.3357	113	SEC23A	0.6596	2.5929
51	DDOST	1.9121	3.4491	114	PSMC3	0.6517	1.3750
52	AAAS	1.8152	1.4704	115	RPL27	0.6461	1.7736
53	**PTPLAD1**	**1.8122**	**2.2742**	116	NCL	0.6412	1.4936
54	VCP	1.7863	1.7622	117	PSMC5	0.6398	1.5693
55	FAF2	1.7843	2.4030	118	RPLP0;RPLP0P6	0.6394	1.6239
56	STT3A	1.7683	2.0973	119	FLOT1	0.6289	1.3431
57	**PGRMC1**	**1.7594**	**2.3419**	120	PDIA6	0.6135	2.0210
58	RAB7A	1.7463	2.4234	121	ERP29	0.6106	1.5141
59	EMD	1.7331	2.5587	122	DNAJB1	0.6091	1.6038
60	NAPA	1.6985	2.1838	123	P4HB	0.6009	2.2157
61	HSPA1A	1.6758	2.0928	124	PSMC6	0.5944	1.6244
62	**PGRMC2**	**1.6514**	**2.7803**	125	RPL23A	0.5877	2.9015
63	APMAP	1.6203	2.5128				

The results cleary showed that, by applying PFA-crosslinking, the number of significantly enriched protein groups increased dramatically compared to the pulldown without PFA. 125 protein groups presented with sufficient degree of enrichment (log2 fold change ≥ 0.585) together with a good level of confidence (–log10 p-value > 1.301). Similar to the experiment before (4.2.3.1.1 Twin-Strep pulldown of transiently-overexpressed mFA2H), a significant number of protein groups were general (e.g. proteasomal subunits, chaperones) as well as ER-specific (e.g. ER-associated protein degradation proteins) components of the protein quality control machinery. In this experiment they constituted about 22% (28 of 125) of all putative FA2H interaction partners. Since the expression conditions were not changed, this was expected. Nevertheless, there was also a large number of other proteins present of which many were associated with lipid metabolism (highlighted in bold). While some protein groups are directly involved in sphingolipid metabolism (SPTLC1 and SPTLC2 = serine palmitoyl transferase long chain 1 and 2), others are linked to cholesterol metabolism (12HSD17B12 = hydroxysteroid 17-beta dehydrogenase, HSD17B7 = hydroxysteroid 17-beta dehydrogenase 7, DHCR7 = 7-dehydrocholesterol reductase, NSDHL = NAD(P) dependent steroid dehydrogenase-like, LBR = lamin B receptor). In addition, protein groups were present linked to lipid transport (VAPA/B = vesicle-associated membrane protein-associated protein A and B, OSBPL8 = oxysterol binding

protein-like 8, SLC27A4 = solute carrier family 27 A4), as well as fatty acid metabolism (PTPLAD1 = protein tyrosine phosphatase-like A domain containing 1, ALDH3A2 = aldehyde dehydrogenase 3A2, ACSL3 = acyl-CoA synthetase long-chain 3). Last but not least, some of the identified proteins are regulators of lipid metabolism (SACM1L = SAC1 suppressor of actin mutations 1-like) or phospholipid metabolism (PLD3 = phospholipase D3). There were also two reductases enriched known to be involved in lipid metabolism (POR = NADPH-cytochrome P450 reductase, CYB5R3 = cytochrome b5 reductase 3) and the cyt_{b5}-containing proteins progesterone receptor membrane component 1 and 2 (PGRMC1 and PGRMC2), which are implicated in regulating the activities of various metabolic enzymes. In addition, a substantial number of ribosomal protein groups were significantly enriched as well, like ribosomal protein L (RPL7, RPL13, and RPL14), nucleolin (NCL) and signal recognition particle receptor B (SRPRB). Moreover, vesicular transport-related protein groups e.g. Rab-proteins (RAB7A, RAB5C,…), Sec-proteins SEC22B and SEC23A, coatomer protein alpha (COPA) and N-ethylmaleimide-sensitive factor (NSF) also showed a significant enrichment.

To further evaluate the dataset, the 125 significantly enriched protein groups were analyzed for enrichment of GO-terms (GeneOntology) with GOrilla (Gene Ontology enRIchment anaLysis and visuaLizAtion tool). For this the 125 protein groups (target list) were compared to the whole set of 840 identified protein groups (ID list). The “Biological Process” (BP) and “Cellular Component” (CC) categories of GO-terms were assessed separately. As identifiers for the GOrilla analysis the first major gene name of each protein group was used. The output of both enrichment analyses is given in tables (Table 4-7, Table 4-8), containing the enriched GO-terms sorted by their significance of enrichment (p-value), which were calculated by hypergeometric testing (see 3.2.4.14.2.2 GOrilla). Note that entries with p-values > 0.001 were filtered out. Tables comprising the complete GOrilla results, including false-discovery rate-corrected p-values (FDR q), enrichments factors and the protein groups contributing to each GO-term, can be found on the accompanying DVD. Table 4-7 gives the results for the “Biological Process” GO-category.

Table 4-7: “Biological Process” GO-enrichment analysis results for protein groups significantly enriched after Twin-Strep-mFA2H pulldown from PFA-treated HEK293-T cells. The set of 125 significantly enriched protein groups (target list) was analyzed for GO-term enrichment by comparing it with the whole set of identified 840 protein groups (ID list) using GOrilla. As identifier the first major gene name for each protein group was imputed into GOrilla. GOrilla could assign terms to 123 (of 125) and 833 (of 840) gene names. Each terms degree of enrichment is given by an uncorrected p-value calculated by hypergeometric testing. The list is sorted by p-values in ascending order. Entries with p-values > 0.001 were filtered out.

GO Term	Description	P-value
GO:0015031	protein transport	3.07E-08
GO:0045184	establishment of protein localization	1.07E-07
GO:0016192	vesicle-mediated transport	1.66E-07
GO:0007165	signal transduction	1.02E-06
GO:0071702	organic substance transport	2.07E-06

GO:0018196	peptidyl-asparagine modification	2.10E-06
GO:0018279	protein N-linked glycosylation via asparagine	2.10E-06
GO:0006487	protein N-linked glycosylation	2.10E-06
GO:0034976	response to endoplasmic reticulum stress	5.21E-06
GO:0050789	regulation of biological process	5.41E-06
GO:0035556	intracellular signal transduction	6.05E-06
GO:0050794	regulation of cellular process	6.81E-06
GO:0048193	Golgi vesicle transport	7.55E-06
GO:0044765	single-organism transport	7.82E-06
GO:0051649	establishment of localization in cell	8.92E-06
GO:0006810	transport	1.04E-05
GO:0050896	response to stimulus	1.26E-05
GO:0065007	biological regulation	1.27E-05
GO:0006486	protein glycosylation	1.29E-05
GO:0043413	macromolecule glycosylation	1.29E-05
GO:0070085	glycosylation	1.29E-05
GO:0051234	establishment of localization	1.88E-05
GO:0006888	ER to Golgi vesicle-mediated transport	2.06E-05
GO:0043687	post-translational protein modification	2.66E-05
GO:0007264	small GTPase mediated signal transduction	2.80E-05
GO:0006984	ER-nucleus signaling pathway	5.38E-05
GO:0046907	intracellular transport	5.46E-05
GO:0008610	lipid biosynthetic process	5.57E-05
GO:0051716	cellular response to stimulus	5.70E-05
GO:0006986	response to unfolded protein	7.26E-05
GO:0035966	response to topologically incorrect protein	7.26E-05
GO:1902582	single-organism intracellular transport	9.44E-05
GO:0046165	alcohol biosynthetic process	1.07E-04
GO:0030163	protein catabolic process	1.12E-04
GO:0018193	peptidyl-amino acid modification	1.18E-04
GO:0016482	cytoplasmic transport	1.22E-04
GO:0002474	antigen processing and presentation of peptide antigen via MHC class I	1.57E-04
GO:0019941	modification-dependent protein catabolic process	1.69E-04
GO:0006066	alcohol metabolic process	1.74E-04
GO:0010498	proteasomal protein catabolic process	2.40E-04
GO:0043161	proteasome-mediated ubiquitin-dependent protein catabolic process	2.40E-04
GO:0019882	antigen processing and presentation	2.45E-04
GO:0043632	modification-dependent macromolecule catabolic process	2.49E-04
GO:0006695	cholesterol biosynthetic process	3.46E-04
GO:0046467	membrane lipid biosynthetic process	3.46E-04
GO:0006511	ubiquitin-dependent protein catabolic process	3.59E-04
GO:0048002	antigen processing and presentation of peptide antigen	3.59E-04
GO:0051603	proteolysis involved in cellular protein catabolic process	3.59E-04
GO:0031401	positive regulation of protein modification process	6.86E-04
GO:0019725	cellular homeostasis	7.08E-04

GO:0002478	antigen processing and presentation of exogenous peptide antigen	7.46E-04
GO:0019884	antigen processing and presentation of exogenous antigen	7.46E-04
GO:0034620	cellular response to unfolded protein	8.30E-04
GO:0030968	endoplasmic reticulum unfolded protein response	8.30E-04
GO:0035967	cellular response to topologically incorrect protein	8.30E-04
GO:0048518	positive regulation of biological process	9.00E-04

Gorilla could assign GO-terms for 833 of the 840 imputed gene names on the ID-list and for 123 of the 125 on the target list. The following enrichment-analysis revealed a couple of things. Regarding the "Biological Process"–terms, it became obvious that many of the enriched proteins are associated with cellular transport (GO:0006810 transport, GO:0015031 protein transport, GO:0045184 establishment of protein localization, GO:0016192 vesicle-mediated transport, …). In addition, there were enriched BP-terms related to protein quality control (GO:0006487 protein N-linked glycosylation, GO:0034976 response to ER stress, GO:0030968 ER-unfolded protein response, GO:0043161 proteasome-mediated ubiquitin-dependent protein catabolic process, …). This was similar to the results obtained before (see 4.2.3.1.1 Twin-Strep pulldown of transiently-overexpressed mFA2H). FA2H-overexpression may have led to aggregation of the enzyme causing an ER stress response. However, an enrichment of terms linked to lipid metabolism (GO:0008610 lipid biosynthetic process, GO:0006695 cholesterol biosynthetic process, GO:0046467 membrane lipid biosynthetic process) was also observable, showing that a significant number of protein groups identified in this experiment are associated with lipid metabolism.

The results for the "Cellular Component" category are shown in Table 4-8.

Table 4-8: "Cellular Component" GO-enrichment analysis results for protein groups significantly enriched after Twin-Strep-mFA2H pulldown from PFA-treated HEK293-T cells. The set of 125 significantly enriched protein groups (target list) was analyzed for GO-term enrichment by comparing it with the whole set of identified 840 protein groups (ID list) using GOrilla. As identifier the first major gene name for each protein group was imputed into GOrilla. GOrilla could assign terms to 123 (of 125) and 833 (of 840) gene names. Each terms degree of enrichment is given by an uncorrected p-value calculated by hypergeometric testing. The list is sorted by p-values in ascending order. Entries with p-values > 0.001 were filtered out.

GO Term	Description	P-value
GO:0044432	endoplasmic reticulum part	1.42E-39
GO:0005789	endoplasmic reticulum membrane	1.03E-37
GO:0098588	bounding membrane of organelle	1.61E-36
GO:0098589	membrane region	2.06E-35
GO:0016021	integral component of membrane	2.95E-23
GO:0044425	membrane part	1.87E-19
GO:0031090	organelle membrane	1.19E-15
GO:0005783	endoplasmic reticulum	3.57E-14
GO:0016020	membrane	1.05E-13
GO:0031410	cytoplasmic vesicle	1.88E-08
GO:0000139	Golgi membrane	6.40E-08

GO:0016023	cytoplasmic membrane-bounded vesicle	2.86E-07
GO:0044446	intracellular organelle part	3.13E-07
GO:0044422	organelle part	4.22E-07
GO:0042470	melanosome	1.14E-06
GO:0048770	pigment granule	1.14E-06
GO:0044431	Golgi apparatus part	4.34E-06
GO:0033116	endoplasmic reticulum-Golgi intermediate compartment membrane	9.26E-06
GO:0005811	lipid particle	2.06E-05
GO:0005774	vacuolar membrane	2.66E-05
GO:0005793	endoplasmic reticulum-Golgi intermediate compartment	1.23E-04
GO:0005765	lysosomal membrane	1.23E-04
GO:0008250	oligosaccharyltransferase complex	4.56E-04
GO:0044437	vacuolar part	6.33E-04
GO:0022625	cytosolic large ribosomal subunit	8.30E-04

Considering the “Cellular Component”-category, a very strong enrichment of terms related to the ER (GO:0044432 endoplasmic reticulum part, GO:0005789 endoplasmic reticulum membrane, …), membrane or membrane-associated proteins (GO:0098589 membrane region, GO:0016021 integral component of membrane, GO:0044425 membrane part) and to the Golgi apparatus (GO:0000139 Golgi membrane, GO:0044431 Golgi apparatus part) was observable. This indicated that most of the proteins co-precipitated with FA2H were ER or Golgi or associated proteins, respectively.

Taken together, while many of FA2H potential interaction partners were again linked to protein quality control processes, the use of PFA-crosslinking allowed the identification of additional protein groups. However, because I could not be exluded that the transient overexpression had caused a cellular stress response, at least in some of the transfected cells, they were repeated with a stable cell line. Furthermore, the interaction with quality control proteins might impede the identification of less abundant interaction partners by competing with their binding to FA2H.

4.2.3.1.3 Twin-Strep pulldown of stably transfected mFA2H

The assay was performed as before (see: 4.2.3.1.1 Twin-Strep pulldown of transiently-overexpressed mFA2H) with some minor changes. First, HEK293 stably transfected with Twin-Strep-FA2H were used, because HEK293-T cells are not compatible with stable-transfection. Second, non-transfected and not mock-transfected HEK293 cells, labeled with light SILAC medium, were used as control samples. Third, the mixing of each light control sample with one heavy Twin-Strep-mFA2H sample was done one step later, after the affinity purification. This should ensure that high H/L-ratios, indicating true interactors, are not lost due to protein exchanges between complexes from differentially labeled cells. The results of the analysis are depicted in Figure 4-29, Table 4-9, Table 4-10 and Table 4-11.

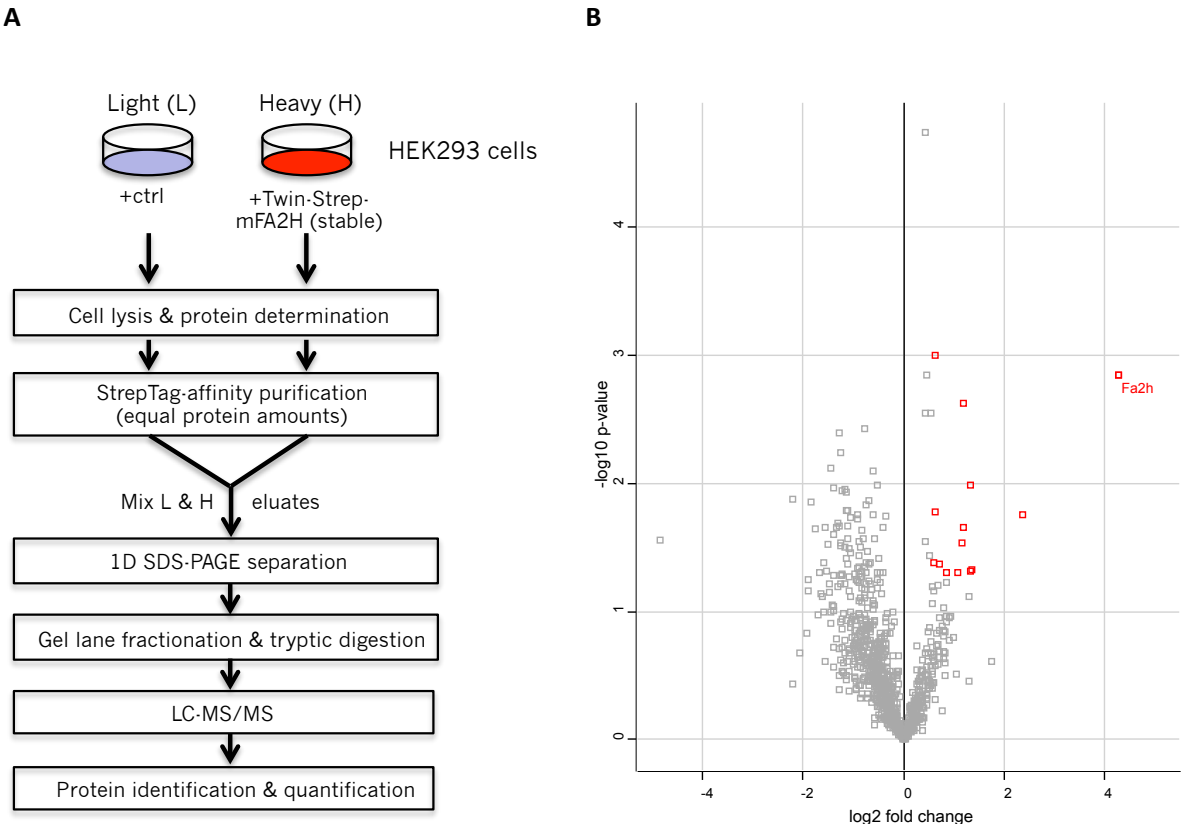

Figure 4-29: Identification of FA2H interaction partners via Twin-Strep-FA2H pulldown from stably transfected HEK293.
(A) Workflow diagram illustrating the assay procedure. HEK293 cells (ctrl.; light SILAC-labeled) and of HEK293 stably expressing pESG-IBA105-mFA2H (+Twin-Strep-mFA2H; heavy SILAC-labeled) were seeded on six 15 cm dishes each and grown to confluency. Afterwards, they were harvested, thereby pooling two dishes of equally labeled and transfected cells. The cells were lysed in StrepTag-lysis buffer followed by protein amount determination. Subsequently, StrepTactin-affinity purification was performed with each lysate separately using equal protein amounts. Then the eluates from each light ctrl-sample were combined with one heavy Twin-Strep-mFA2H sample, concentrated by $CHCl_3$/MeOH-precipitation, separated by SDS-PAGE and Coomassie-stained. Thereafter, the complete protein lane of each replicate was cut into fractions of equal protein amount and processed by tryptic in-gel digestion. Finally, the resulting peptides were cleaned using StageTips and analyzed by LC-MS/MS. This was followed by protein identification (human Uniprot database +mFA2H), quantification and ratio-normalization by MaxQuant and statistical evaluation using Perseus. **(B) Volcano plot of all protein groups identified and quantified in at least two replicates**. After performing a one-sample t-test against 0, the resulting –log p-values of each protein group were plotted against their log2-transformed average H/L-ratio (log2 fold change). Significantly enriched protein groups (log2 fold change ≥ 0.585 (fold change ≥ 1.5); –log p-value > 1.301 (p-value < 0.05)) are highlighted in red.

In this analysis 992 protein groups could be identified and quantified in at least two replicates. Of these, 27 exhibited a log2 fold change ≥ 0.585 together with a good level of confidence (–log p-value > 1.301). Note that the unprocessed and processed results can be found on the supplemental DVD.

Table 4-9: Protein groups significantly enriched after pulldown from HEK293 cells stably transfected with Twin-Strep-mFA2H. Shown are the all protein groups identified in at least two replicates with a log2 fold change ≥ 0.585 (fold change ≥ 1.5) and a –log10 p-value > 1.301 (p-value < 0.05). Protein groups are given by their respective gene names and sorted by their log2 fold change in descending order. Proteins groups associated with protein quality control processes are highlighted in red and with (sphingo-)lipid metabolism in **bold**.

N°	Gene names	log2 fold change	-log10 p-value	N°	Gene names	log2 fold change	-log10 p-value
1	**Fa2h**	**4.293**	**2.520**	15	ARPC3	0.846	1.447
2	MYO1E	2.468	2.318	16	NOP58	0.829	2.148
3	VCP	1.495	1.487	17	HSPA1A	0.800	1.569
4	SNX33	1.491	2.136	18	AP2A2	0.766	1.611
5	PTK7	1.264	2.262	**19**	**SPTLC1**	**0.726**	**2.600**
6	TFRC	1.190	1.939	20	WDR67	0.704	1.647
7	RACGAP1	0.984	1.369	21	AP2S1	0.690	1.332
8	FXR1	0.979	1.423	22	NEDD4L	0.670	1.572
9	ARPC2	0.977	1.608	23	CTTN	0.660	1.314
10	SSX2IP	0.977	1.550	24	PELP1	0.659	1.642
11	FAF2	0.918	1.313	25	PEG10	0.620	2.122
12	HAX1	0.886	1.493	26	LAS1L	0.614	1.374
13	ARPC1A	0.877	1.611	27	EPN1	0.587	1.668
14	TJP2	0.866	1.842				

Only a small number of the identified protein groups exhibited a significant enrichment (log2-fold change ≥ 0.585 and –log10 p-value > 1.301), as was the case in the previous experiment without PFA-crosslinking (4.2.3.1.1 Twin-Strep pulldown of transiently-overexpressed mFA2H). Again, the highest enrichment was seen for the bait protein FA2H. Furthermore, there was one co-purification of a sphingolipid metabolism enzyme, SPTLC1, which catalyzes the first step in sphingolipid synthesis. In addition, there were again some protein groups present, which are related to protein quality control processes (VCP = valosin containing protein, FAF2 = Fas associated factor family member 2, HAX1 = HCLS1 associated protein X-1, HSPA1A = heat shock 70kDa protein 1A, NEDD4L = neural precursor cell expressed developmentally down-regulated 4-like). They made up about 19% (5 of 27) of the significantly enriched protein groups.

To further functionally assess the co-purified 27 protein groups, a GO-enrichment analysis was performed with GOrilla, comparing them to the whole set of 992 identified protein groups. Each protein group's major gene name was used as identifier. The GO-subcategories "Biological Process", "Cellular Component" and "Molecular Function" were analyzed. The results are depicted in Table 4-10 and Table 4-11. The complete GO-term result tables can be found on the supplemental data DVD.

Table 4-10: "Biological Process" GO-enrichment analysis results for protein groups significantly enriched after Twin-Strep-mFA2H pulldown from stably transfected HEK293 cells. The set of 27 significantly enriched protein groups (target list) was analyzed for GO-term enrichment by comparing it with the whole set of identified 992 protein groups (ID list) using GOrilla. As identifier the first major gene name for each protein group was imputed into GOrilla. GOrilla could assign terms to 26 (of 27) and 963 (of 992) gene names. Each terms degree of enrichment is given by an uncorrected p-value calculated by hypergeometric testing. The list is sorted by p-values in ascending order. Entries with p-values > 0.001 were filtered out.

GO Term	Description	P-value
GO:0006897	endocytosis	1.43E-04
GO:0043254	regulation of protein complex assembly	7.33E-04

Table 4-11: Molecular Function GO-enrichment analysis results for protein groups significantly enriched after Twin-Strep-mFA2H pulldown from stably transfected HEK293 cells. The set of 27 significantly enriched protein groups (target list) was analyzed for GO-term enrichment by comparing it with the whole set of identified 992 protein groups (ID list) using GOrilla. As identifier the first major gene name for each protein group was imputed into GOrilla. GOrilla could assign terms to 26 (of 27) and 963 (of 992) gene names. Each terms degree of enrichment is given by an uncorrected p-value calculated by hypergeometric testing. The list is sorted by p-values in ascending order. Entries with p-values > 0.001 were filtered out.

GO Term	Description	P-value
GO:0008289	lipid binding	5.74E-04

GOrilla could assign GO-terms to 963 of the 992 imputed gene names and found only a small number of enriched terms in the "Biological Process"- and "Molecular Function"-category, but not in the "Cellular Component"-category. The low number of enriched terms was expected since the target list, containing the significantly enriched proteins, was very small. It seemed that the proteins co-purified with FA2H are mainly involved in endocytosis (AP2A2 = adaptor-related protein complex 2 alpha 2 subunit, SNX33 = sorting nexin 33, TFRC = transferrin receptor, AP2S1 = adaptor-related protein complex 2 sigma 1 subunit, EPN1 = epsin 1, MYO1E = myosin IE) and the regulation of protein complex assembly (ARPC1A = actin related protein complex subunit 1A, ARPC2 = actin related protein complex subunit 2, ARPC3 = actin related protein complex subunit 3, VCP, HAX1). Within the later group the ARPC-genes indicate that the major complex for regulation of actin-filament polymerization was co-purified along with FA2H. Furthermore, 6 proteins (AP2A2, SNX33, EPN1, MYO1E, VCP, RACGAP1 = Rac GTPase activating protein 1) have a known lipid binding activity (GO:0008289). The exact definition of this GO-term is: Interacting selectively and non-covalently with a lipid.

Taken together, the pulldown of stably expressed Twin-Strep-mFA2H showed two positive changes in comparison to the previous one utilizing transiently transfected cells. First, while protein quality control protein groups were still present, proteins unrelated to this process could also be co-purified. In the experiment with transiently transfected HEK293-T the majority of co-purified proteins was associated with protein quality control processes. In contrast, such proteins constituted only ~20% in

this approach, which is significantly less. Moreover, since protein quality control proteins should examine all proteins imported into the ER, a certain amount of these will always be identified in interaction partner screenings. The second change was that SPTLC1, an enzyme working in the same metabolic pathway as FA2H, was now identifiable also without the use of PFA-crosslinking.

4.2.3.1.4 PFA-assisted Twin-Strep pulldown of stably transfected FA2H

Analogous to the experiment with transiently transfected cells (4.2.3.1.2 PFA-assisted Twin-Strep pulldown of transiently-overexpressed mFA2H), PFA-crosslinking was used together with stably transfected cells to identify weak or minor interactors, which are otherwise lost during the pulldown process. Therefore, a PFA-crosslinking step was added between cell harvesting and cell lysis. In addition, samples had to be decrosslinked after elution. Figure 4-30B, Table 4-12, Table 4-13 and present the results of this analysis.

A

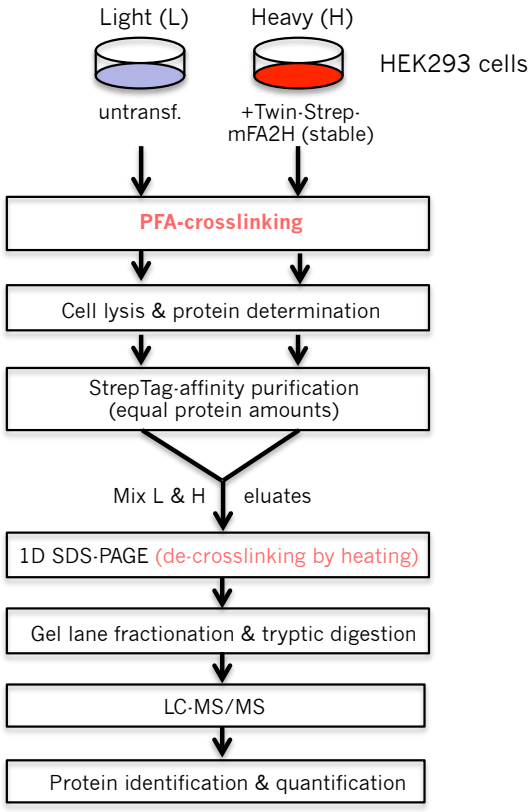

B

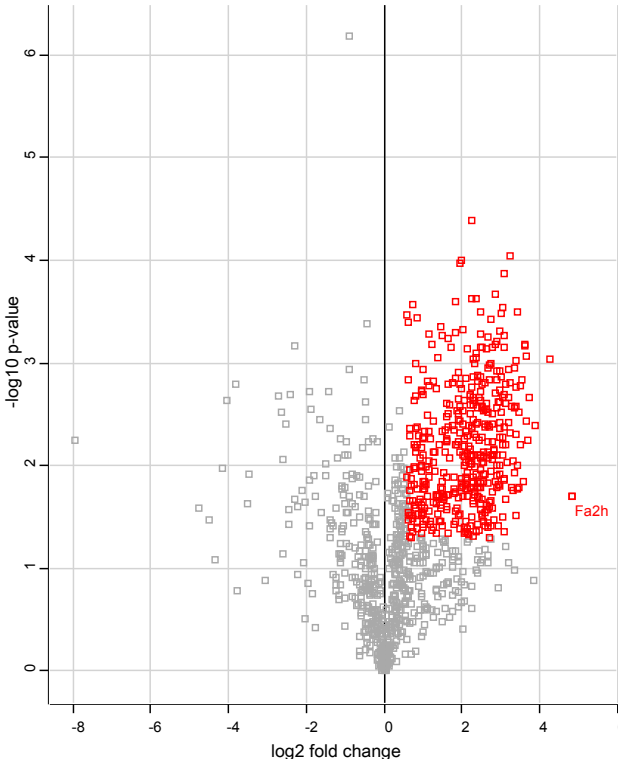

Figure 4-30: PFA-assisted interaction partner analysis of stably transfected Twin-Strep-mFA2H.
(A) Workflow of the performed analysis. Six 15 cm dishes each of untransfected HEK293 grown in SILAC light (control) and stably expressing Twin-Strep-mFA2H HEK293 grown in heavy SILAC medium were used. Always two equal plates were pooled, thereby leading to three replicates of untransfected and stably transfected cells, fixed for 20 min with 0.5% PFA and stopped by icecold 1.25 M glycine buffer addition. Afterwards, all cells were lysed in RIPA buffer and the protein amounts determined. StrepTactin-affinity purification was performed on equal protein amounts of each lysate individually. Subsequently, each light-labeled control eluate was mixed with one heavy-labeled stably expressing Twin-Strep-mFA2H eluate. Each combined eluate was then concentrated by $CHCl_3$/MeOH-precipitation, resuspended in 2X Laemmli, reduced and decrosslinked by heating to 95 °C for 10 min and separated by SDS-PAGE. After Coomassie-staining, each lane was separated into fractions of equal protein amount and subjected to tryptic in-gel digestion. The resulting peptides were cleaned via C18-StageTipps and finally analyzed by LC-MS/MS. Protein identification (human Uniprot database +mFA2H) and quantification was performed with MaxQuant and statistical evaluation with Perseus and GOrilla. **(B) Volcano plot of all protein groups identified and quantified in at least two replicates.** After performing a one-sided t-test against 0, the resulting –log p-values of each protein group were plotted against their log2-transformed average H/L-ratio (log2 fold change). Proteins with a log2 fold change ≥ 0.585 (fold change ≥ 1.5) and a –log p-value > 1.301 (p-value < 0.05) are considered significantly enriched and highlighted in red.

With this approach, 1062 protein groups were identified and quantified in at least two replicates. Of these a very high number, 437, were significantly enriched exhibiting a log2 fold change ≥ 0.585 and a -log10 p-value > 1.301. 375 protein groups showed even a very high degree of enrichment (log2 fold change ≥ 1). The 50 protein groups with the highest degree of enrichment are shown below (Table 4-12). For the comprehensive protein group list with all 437 entries see to the supplementary DVD.

Table 4-12: 50 most highly enriched protein groups after PFA-assisted Twin-Strep-mFA2H pulldown from stably transfected HEK293 cells. Depicted are the 50 protein groups identified with the highest log2 fold change. All protein groups were found in at least two replicates and had a -log10 p-value > 1.301 (p-value < 0.05). Protein groups are given by their respective gene names and sorted by their log2 fold change in descending order. Protein groups associated with protein quality control processes are highlighted in red, and with (sphingo-)lipid metabolism in **bold**.

N°	Gene names	log2 fold change	-log10 p-value	N°	Gene names	log2 fold change	-log10 p-value
1	**Fa2h**	**4.8168**	**1.6974**	26	SEC62	3.3296	1.9376
2	UBB;RPS27A;UBC;UBA52;UBBP4	4.2411	3.0434	27	SEC22B	3.3174	2.0514
3	LRRC59	3.8879	2.3980	28	AMFR	3.3059	1.7645
4	**PTPLAD1**	**3.7153**	**2.6568**	**29**	**SPTLC1**	**3.2840**	**2.5805**
5	**LBR**	**3.7036**	**2.2442**	30	APLP2	3.2789	1.7938
6	SURF4	3.6677	3.0665	31	RAB10	3.2461	2.3173
7	TMEM161A	3.6552	2.4273	32	ATP2A2	3.2292	2.8144
8	TNFRSF10B	3.6294	3.1774	33	RPN1	3.2155	4.0398
9	STT3A	3.5966	3.1653	34	KCT2	3.2111	2.9395
10	ANTXR1	3.5880	1.8430	**35**	**TECR**	**3.2079**	**2.6661**
11	**OSBPL8**	**3.5339**	**2.8360**	36	TOLLIP	3.1759	2.4233
12	SEC63	3.5101	2.7854	37	RAB6A	3.1691	2.0366
13	**VAPA**	**3.4946**	**2.1985**	38	AUP1	3.1206	1.6761
14	**DHCR7**	**3.4427**	**1.7817**	39	GOLIM4	3.1179	2.2114
15	RDH11	3.4424	2.5201	40	EMD	3.1096	2.7882
16	**ELOVL5**	**3.4310**	**1.7753**	41	TMED2	3.1023	2.6106
17	EMC10	3.4266	3.5028	42	GOSR1	3.0956	2.3715

18	SDCBP	3.4039	2.0016	43	RAB14	3.0888	2.6959
19	SRPR	3.3962	2.7603	44	SLC20A1	3.0866	1.3557
20	EMC1	3.3830	3.0258	45	SSR1	3.0814	3.2738
21	MFSD10	3.3731	2.5739	46	TM9SF3	3.0731	3.8667
22	TMEM30A	3.3677	1.5093	47	NEDD4L	3.0703	1.8659
23	KIAA2013	3.3653	2.2982	**48**	**UGCG**	**3.0697**	**1.8757**
24	STT3B	3.3563	2.5675	49	RAB1B	3.0640	3.1481
25	RAB1A	3.3448	2.9493	50	SRPRB	3.0595	1.5005

The inclusion of a PFA-crosslinking step into the analysis workflow again largely increased the number of significantly enriched protein groups after Twin-Strep-mFA2H pulldown. With 437 out of 1062 (≈41%) protein groups this number is very high. In addition, with 559 out of 1062 (~47%) the number of background protein groups (log2 fold change between 0.58 and -0.58) was quite low, compared to the PFA-crosslinking experiment with transiently transfected cells (709/840 ≈ 85%). Normally, the majority of the non-interacting background protein groups should cluster around a log2 fold change of 0, being equally contributed by the control and bait-containing sample. This indicates that the PFA-fixation lasted too long, leading to more background proteins becoming crosslinked to FA2H. Thus, the putative interaction candidates identified in this experiment probably contained a larger amount of false positive identifications.

Looking only at the 50 protein groups with the highest enrichment (Table 4-12), as observed before, about 18% (9 of 50) were known to be involved in protein quality control (UBB = ubiquitin B, TNFRSF10B = tumor necrosis factor receptor superfamily member 10b, STT3A = STT3A subunit of the oligosaccharyltransferase complex, EMC10 = ER membrane protein complex subunit 10, …). The amount was similar, when considering all significantly enriched 437 protein groups (76 of 437 ≈ 17%). Moreover, within the 50 protein groups there were also 10 groups present linked to lipid metabolism processes. For example, these were proteins involved in sphingolipid anabolism (SPTLC1, UGCG = glucosylceramide synthase), cholesterol metabolism (DHCR7), lipid transport (VAPA; OSBPL8) and fatty acid metabolism (PTPLAD1 = protein tyrosine phosphatase-like A domain containing 1, ELOVL5 = ELOVL fatty acid elongase 5). Interestingly, many of those have been also identified in the previous pulldown experiment including a PFA-crosslinking step (Table 4-6).

To further characterize the large amount of 437 significantly enriched protein groups, a GO-term analysis was performed with GOrilla. Again, the enriched protein groups (target list) were compared to the whole number of 1062 identified and quantified protein groups (background list). As identifiers the first gene name associated with a protein group was used. The results for the GO-categories “Biological Process” and “Cellular Component” are shown below in Table 4-13 and Table 4-14. Complete tables, containing also the gene names associated with each GO-term, can be found on the supplemental DVD.

Table 4-13: "Biological Process" GO-enrichment analysis results for protein groups significantly enriched after Twin-Strep-mFA2H pulldown from stably transfected & PFA-treated HEK293 cells. The set of 437 significantly enriched protein groups (target list) was analyzed for GO-term enrichment by comparing it with the whole set of identified 1062 protein groups (ID list) using GOrilla. As identifier the first major gene name for each protein group was imputed into GOrilla. GOrilla could assign terms to 432 (of 437) and 1049 (of 1062) gene names. Each terms degree of enrichment is given by an uncorrected p-value calculated by hypergeometric testing. The list is sorted by p-values in ascending order. Entries with p-values > 0.001 were filtered out.

GO Term	Description	P-value
GO:0006810	transport	9.14E-16
GO:0051234	establishment of localization	9.10E-15
GO:0044765	single-organism transport	1.24E-13
GO:0071702	organic substance transport	3.63E-12
GO:0015031	protein transport	4.00E-10
GO:1902582	single-organism intracellular transport	5.05E-10
GO:0045184	establishment of protein localization	2.33E-09
GO:0046907	intracellular transport	1.17E-08
GO:0051649	establishment of localization in cell	3.44E-07
GO:0007264	small GTPase mediated signal transduction	4.12E-07
GO:0006886	intracellular protein transport	1.09E-06
GO:0006605	protein targeting	1.41E-06
GO:0006184	GTP catabolic process	1.49E-06
GO:0006811	ion transport	1.88E-06
GO:0009203	ribonucleoside triphosphate catabolic process	2.87E-06
GO:0009207	purine ribonucleoside triphosphate catabolic process	2.87E-06
GO:0009146	purine nucleoside triphosphate catabolic process	2.87E-06
GO:0009143	nucleoside triphosphate catabolic process	2.87E-06
GO:0016482	cytoplasmic transport	3.25E-06
GO:0055085	transmembrane transport	3.85E-06
GO:0072594	establishment of protein localization to organelle	4.03E-06
GO:1901069	guanosine-containing compound catabolic process	4.47E-06
GO:0046039	GTP metabolic process	4.47E-06
GO:0048193	Golgi vesicle transport	5.18E-06
GO:0009261	ribonucleotide catabolic process	5.82E-06
GO:0009154	purine ribonucleotide catabolic process	5.82E-06
GO:0016050	vesicle organization	6.28E-06
GO:1901136	carbohydrate derivative catabolic process	6.45E-06
GO:0007165	signal transduction	9.88E-06
GO:0006152	purine nucleoside catabolic process	1.14E-05
GO:0006195	purine nucleotide catabolic process	1.14E-05
GO:1901292	nucleoside phosphate catabolic process	1.14E-05
GO:1901658	glycosyl compound catabolic process	1.14E-05
GO:0072523	purine-containing compound catabolic process	1.14E-05
GO:0042454	ribonucleoside catabolic process	1.14E-05
GO:0046130	purine ribonucleoside catabolic process	1.14E-05
GO:0009166	nucleotide catabolic process	1.14E-05
GO:0009164	nucleoside catabolic process	1.14E-05
GO:0035556	intracellular signal transduction	1.20E-05
GO:0006901	vesicle coating	1.54E-05

GO:0048205	COPI coating of Golgi vesicle	2.17E-05
GO:0048200	Golgi transport vesicle coating	2.17E-05
GO:0046434	organophosphate catabolic process	2.29E-05
GO:0016192	vesicle-mediated transport	2.78E-05
GO:1901068	guanosine-containing compound metabolic process	2.98E-05
GO:0061024	membrane organization	3.41E-05
GO:0090150	establishment of protein localization to membrane	3.42E-05
GO:0006820	anion transport	3.71E-05
GO:0009205	purine ribonucleoside triphosphate metabolic process	4.32E-05
GO:0009144	purine nucleoside triphosphate metabolic process	4.32E-05
GO:0006613	cotranslational protein targeting to membrane	4.38E-05
GO:0045047	protein targeting to ER	4.38E-05
GO:0072599	establishment of protein localization to endoplasmic reticulum	4.38E-05
GO:0006612	protein targeting to membrane	6.61E-05
GO:0006614	SRP-dependent cotranslational protein targeting to membrane	8.03E-05
GO:0009199	ribonucleoside triphosphate metabolic process	1.25E-04
GO:0023051	regulation of signaling	1.57E-04
GO:0010646	regulation of cell communication	2.15E-04
GO:0006890	retrograde vesicle-mediated transport, Golgi to ER	3.61E-04
GO:0019439	aromatic compound catabolic process	4.84E-04
GO:0044270	cellular nitrogen compound catabolic process	7.01E-04
GO:0009141	nucleoside triphosphate metabolic process	7.88E-04
GO:0046467	membrane lipid biosynthetic process	9.15E-04
GO:1901361	organic cyclic compound catabolic process	9.34E-04

Table 4-14: "Cellular Component" GO-enrichment analysis results for protein groups significantly enriched after Twin-Strep-mFA2H pulldown from stably transfected & PFA-treated HEK293 cells. The set of 437 significantly enriched protein groups (target list) was analyzed for GO-term enrichment by comparing it with the whole set of identified 1062 protein groups (ID list) using GOrilla. As identifier the first major gene name for each protein group was imputed into GOrilla. GOrilla could assign terms to 432 (of 437) and 1049 (of 1062) gene names. Each terms degree of enrichment is given by an uncorrected p-value calculated by hypergeometric testing. The list is sorted by p-values in ascending order. Entries with p-values > 0.001 were filtered out.

GO Term	Description	P-value
GO:0016021	integral component of membrane	1.04E-46
GO:0044425	membrane part	2.15E-41
GO:0098588	bounding membrane of organelle	8.18E-28
GO:0031090	organelle membrane	3.68E-23
GO:0016020	membrane	2.70E-22
GO:0044432	endoplasmic reticulum part	3.72E-17
GO:0005789	endoplasmic reticulum membrane	2.67E-16
GO:0098589	membrane region	2.10E-15
GO:0044431	Golgi apparatus part	1.76E-11
GO:0000139	Golgi membrane	6.54E-11
GO:0005887	integral component of plasma membrane	1.24E-09
GO:0005783	endoplasmic reticulum	3.78E-09
GO:0044446	intracellular organelle part	3.69E-07

GO:0044422	organelle part	2.32E-06
GO:0005886	plasma membrane	2.72E-06
GO:0044459	plasma membrane part	3.19E-06
GO:0030139	endocytic vesicle	1.54E-05
GO:0005794	Golgi apparatus	2.08E-04
GO:0030659	cytoplasmic vesicle membrane	2.89E-04
GO:0031410	cytoplasmic vesicle	6.27E-04
GO:0031965	nuclear membrane	7.21E-04
GO:0012506	vesicle membrane	7.88E-04

GOrilla found GO-terms for 1049 gene identifiers on the ID-list and 432 on the target-list. The results for the Biological Process GO-category showed a significant enrichment of various terms. The by far largest amount of terms was again related to transport processes (GO:0006810 transport, GO:0051234 establishment of localization, …) of various substrates (GO:0015031 protein transport, GO:0071702 organic substance transport, GO:0006811 ion transport, …). Furthermore, there were also many terms enriched, which are linked to GTP-metabolism and small GTPase signaling (GO:0007264 small GTPase mediated signal transduction, GO:0006184 GTP catabolic process, GO:0046039 GTP metabolic process).

Nonetheless, there was also an enrichment of a GO-term indicating the presence of lipid metabolism-related proteins co-purifying with Twin-Strep-mFA2H. The gene names corresponding to the protein groups within this enriched term (GO:0046467 membrane lipid biosynthetic process) are given in the table below.

Table 4-15: Genes associated with enriched GO-term GO:0046467 membrane lipid biosynthetic process.
P-value = enrichment p-value calculated by hypergeometric testing

GO:0046467 membrane lipid biosynthetic process (P-value= 9.15E-04)
DPM1 - dolichyl-phosphate mannosyltransferase polypeptide 1, catalytic subunit
SGPL1 - sphingosine-1-phosphate lyase 1
SMPD4 - sphingomyelin phosphodiesterase 4, neutral membrane (neutral sphingomyelinase-3)
UGCG - udp-glucose ceramide glucosyltransferase
SPTLC1 - serine palmitoyltransferase, long chain base subunit 1
SPTLC2 - serine palmitoyltransferase, long chain base subunit 2
DEGS1 - delta(4)-desaturase, sphingolipid 1
VAPA - vamp (vesicle-associated membrane protein)-associated protein a 33kda
VAPB - vamp (vesicle-associated membrane protein)-associated protein b and c
CERS2 - ceramide synthase 2

Table 4-15 illustrated that the majority of the proteins are related to sphingolipid metabolism (SGPL1, SMPD4, UGCG, SPTLC1, SPTLC2, DEGS1, VAPA/B, CERS2). Only DPM1 (dolichyl-phosphate mannosyltransferase polypetide 1) is involved in the synthesis of the modified phospholipid glycophosphatidylinositol (GPI).

The “Cellular Component” GO-category result (Table 4-14) again showed that the majority of the significantly enriched protein groups contained ER (GO:0044432 endoplasmic reticulum part, …) and/or Golgi-localized proteins (GO:0044431 Golgi apparatus part, GO:0000139 Golgi membrane, …). In addition, many enclosed membrane or membrane-related proteins (GO:0016021 integral component of membrane, GO:0044425 membrane part, GO:0098588 bounding membrane of organelle, GO:0031090 organelle membrane, …).

Considering the above results, the inclusion of PFA-crosslinking step again enabled the identification of substantially more putative FA2H-interacting proteins, when compared to the experiment without. Moreover, while there was certainly some error due to extensive crosslinking leading to a larger amount of false-positive identifications, a significant amount of the enriched protein groups were linked to lipid, especially sphingolipid, metabolism.

4.2.3.2 SILAC BioID-FA2H-assay

Analogous to the SILAC IP experiments, the identification of mFA2H interaction partners using the BioID-method (see 3.2.4.1 Proximity-dependent protein biotinylation & identification (BioID), was carried out in combination with SILAC-labeling. Again, the addition of quantitative information should help to distinguish true interacting from unspecific background-binding proteins. Still, because of the random biotinylation by the fused biotin ligase, this screening method will unavoidably also lead to some false-positive identifications. As for the PFA-crosslinking, this bias has to be accepted when aiming to capture also weak and transient interactions.

Thus, HEK293-T cells grown in SILAC-media were either transiently transfected with the plasmid coding for biotin ligase BirA* alone (pcDNA3.1-myc-BioID) or the fusion protein BirA*-mFA2H (pcDNA3.1-myc-BioID-mFA2H). BirA*-transfected cells were grown in light and BirA*-mFA2H-transfected in heavy SILAC-medium. 24h after transfection, biotinylation of proximal proteins by BirA* was induced by the addition of biotin to the culture media followed by another 24h-incubation. Thereafter, cells were harvested, lysed, protein amounts determined and NeutrAvidin-affinity purification performed. Subsequently, bound proteins were tryptically digested directly on the beads and the resulting peptides solutions of each light BirA*-sample combined with one heavy BirA*-mFA2H sample. The combined peptides were then desalted, fractionated by OFFGEL, analyzed by LC-MS/MS, and the raw data processed by MaxQuant. Finally, identified and quantified protein groups were statistical evaluated by Perseus and GOrilla (see Figure 4-31, Table 4-16 and Table 4-17). The experiment was done in triplicates.

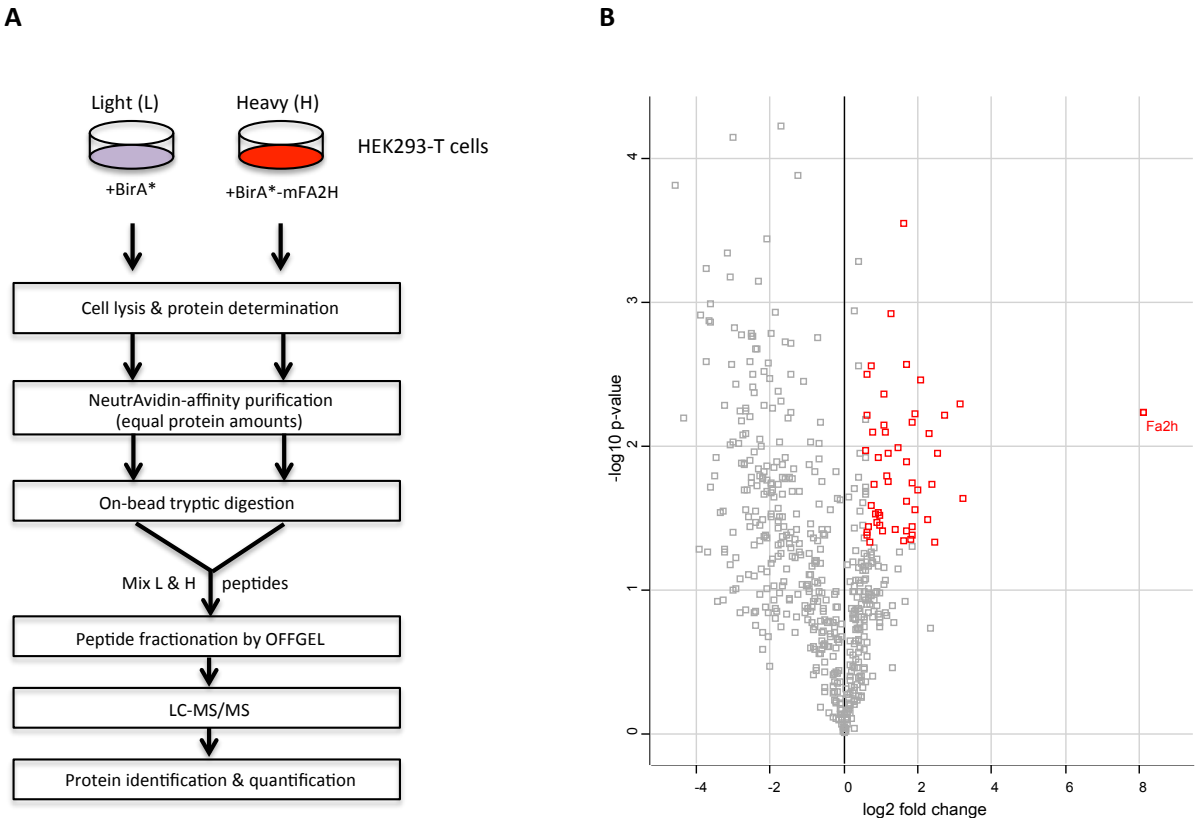

Figure 4-31: Identification of FA2H-interactors by the SILAC BioID-FA2H-assay.
(A) Workflow diagram of the SILAC BioID-FA2H-assay. Twelve 15 cm dishes of HEK293-T each, labeled with SILAC culture medium, were transfected with pcDNA3.1-mycBioID (light) or pcDNA3.1-mycBioID-mFA2H (heavy) respectively. 24 h later, biotinylation was induced by adding 50 µM biotin to the medium and the cells grown for another 24 h. Then cells were harvested, thereby always pooling two dishes of equally labeled and transfected cells. Thereafter, cells were lysed, protein amounts determined and biotinylated proteins affinity purified from each lysate separately using NeutrAvidin. Afterwards, by adding trypsin directly to the beads, proteins bound to the affinity matrix were digested overnight. Then the resulting peptide digests were aspirated and remaining peptides reextracted with 5% ACN 0.1% FA. Subsequently, each light BirA* digest was combined with one heavy BirA*-mFA2H digest. Afterwards, the combined samples (n=3) were desalted using Oasis HLB cartridges, followed by fractionation into 12 fractions via isoelectric focusing (OFFGEL). Finally, after peptide desalting by C18-StageTips, all fractions were analyzed by LC-MS/MS, proteins identified (human Uniprot database +mFA2H) and quantified by MaxQuant and statistical analysis performed by Perseus and GOrilla. **(B) Volcano plot of all protein groups identified in at least two replicates.** The resulting –log10 p-values of each protein group (one-sample t-test against 0) were plotted against their log2-transformed average H/L-ratio (log2 fold change). Proteins exhibiting a log2 fold change ≥ 0.585 (fold change ≥ 1.5) and a –log10 p-value > 1.301 (p-value < 0.05) are highlighted in red.

In this experiment, 546 protein groups were identified and quantified in at least two replicates. Of these only a small number of 24 protein groups showed a significant enrichment (log2 fold change ≥ 0.585; –log10 p-value > 1.301) for the BirA*-mFA2H sample. These are given in Table 4-16. The original unprocessed MaxQuant results can and the processed protein group list can be found on the supplemental DVD.

Table 4-16: Significantly enriched protein groups in BirA*-mFA2H sample.Depicted are all protein groups identified in at least two replicates with a log2 fold change ≥ 0.585 and a –log10 p-value > 1.301. Protein groups are given by their respective gene names and sorted by their log2 fold change in descending order. Proteins groups associated with protein quality control processes are highlighted in red, and with (sphingo)lipid metabolism in **bold**.

	Gene names	log2 fold change	-log10 p-value		Gene names	log2 fold change	-log10 p-value
1	**Fa2h**	**5.696**	**4.273**	**13**	SRPR	1.393	2.627
2	CCDC47	2.229	2.650	**14**	**LBR**	**1.333**	**1.866**
3	**PGRMC2**	**2.126**	**3.036**	**15**	STBD1	1.353	1.835
4	PTPN1	2.021	3.186	**16**	**SPTLC1**	**1.310**	**1.351**
5	TOR1AIP1	1.867	3.545	17	LRRC59	1.144	1.712
6	**SMPD4**	**1.669**	**2.166**	18	LEMD3	1.147	1.686
7	SRPRB	1.835	2.399	19	TMPO	1.102	2.112
8	**VAPA**	**1.770**	**2.988**	20	NUP155	0.902	1.771
9	**VAPB**	**1.740**	**2.440**	21	FAF2	0.958	1.952
10	STIM1	1.617	1.638	22	NSDHL	0.857	1.678
11	**ALDH3A2**	**1.643**	**2.044**	23	ESYT1	0.888	1.807
12	CDKAL1	1.350	3.093	24	MTDH	0.591	1.382

As expected, the bait protein FA2H itself showed the highest degree of enrichment (log2 fold change), thereby proving the assay principle. Inspecting the other protein groups in detail revealed mainly groups linked to lipid metabolism processes. For example, the sphingolipid metabolizing enzymes SMPD4 and SPTLC1, as well as lipid transport (VAPA/B) and fatty acid metabolizing enzymes (ALDH3A2). Moreover, LBR (Lamin B receptor), which has known cholesterol desaturase activity, and PGRMC2, whose paralog PGRMC1 is implicated in the activity regulation of various metabolic enzymes, were also significantly enriched. In addition, two protein groups (~8% of all identifications) related to protein-quality control processes (CCD47, FAF2) were also present. This indicated that at least parts of the transiently expressed BirA*-FA2H fusion protein were processed by the protein quality control machinery.

To additionally characterize these protein groups, GO-term enrichment analysis was performed with GOrilla comparing the 25 significantly enriched against the 546 identified proteins. The main GO-categories “Biological Process” and “Cellular Component” were assessed. The results are shown below in Table 4-17 and Table 4-18.

Table 4-17: "Biological Process" GO-enrichment analysis results for protein groups significantly in BirA*-mFA2H sample. The set of 25 significantly enriched protein groups (target list) was analyzed for GO-term enrichment by comparing it with the whole set of identified 546 protein groups (ID list) using GOrilla. As identifier the first major gene name for each protein group was imputed into GOrilla. GOrilla could assign terms to 24 (of 25) and 501 (of 546) gene names. Each terms degree of enrichment is given by an uncorrected p-value calculated by hypergeometric testing. The list is sorted by p-values in ascending order. Entries with p-values > 0.001 were filtered out.

GO Term	Description	P-value
GO:0006643	membrane lipid metabolic process	1.65E-07
GO:0006665	sphingolipid metabolic process	1.65E-07
GO:0006066	alcohol metabolic process	3.24E-06
GO:0030148	sphingolipid biosynthetic process	4.10E-06
GO:0046467	membrane lipid biosynthetic process	4.10E-06
GO:1901615	organic hydroxy compound metabolic process	1.82E-05
GO:0008610	lipid biosynthetic process	4.70E-05
GO:0006629	lipid metabolic process	1.58E-04
GO:0034976	response to endoplasmic reticulum stress	1.64E-04
GO:0006984	ER-nucleus signaling pathway	3.58E-04
GO:0046165	alcohol biosynthetic process	3.76E-04
GO:0044255	cellular lipid metabolic process	7.67E-04
GO:1901617	organic hydroxy compound biosynthetic process	9.11E-04

Table 4-18: "Cellular Component" GO-enrichment analysis results for protein groups significantly in BirA*-mFA2H sample. The set of 25 significantly enriched protein groups (target list) was analyzed for GO-term enrichment by comparing it with the whole set of identified 546 protein groups (ID list) using GOrilla. As identifier the first major gene name for each protein group was imputed into GOrilla. GOrilla could assign terms to 24 (of 25) and 501 (of 546) gene names. Each term's degree of enrichment is given by an uncorrected p-value calculated by hypergeometric testing. The list is sorted by p-values in ascending order. Entries with p-values > 0.001 were filtered out.

GO Term	Description	P-value
GO:0016021	integral component of membrane	6.76E-18
GO:0044425	membrane part	5.59E-16
GO:0044432	endoplasmic reticulum part	1.73E-12
GO:0005789	endoplasmic reticulum membrane	1.84E-12
GO:0098589	membrane region	2.07E-10
GO:0031090	organelle membrane	1.08E-08
GO:0016020	membrane	1.69E-07
GO:0098588	bounding membrane of organelle	2.02E-07
GO:0005783	endoplasmic reticulum	4.46E-05
GO:0005637	nuclear inner membrane	9.11E-04

The GO-enrichment analysis further supported the observations made when manually evaluating the enriched protein groups. The terms enriched within Biological Process category were mainly related to lipid, especially sphingolipid, metabolism (GO:0006643 membrane lipid metabolic process, GO:0006665 sphingolipid metabolic process, …) and to protein quality control (GO:0034976 response to endoplasmic reticulum stress).

The Cellular Compartment category proved the assay functionality by showing a strong enrichment of ER (GO:0044432 endoplasmic reticulum part, GO:0005789 endoplasmic reticulum membrane) and membrane protein containing protein groups (GO:0016021 integral component of membrane, GO:0044425 membrane part, …). Since FA2H is an ER-membrane protein, the majority of its interactors should be such proteins.

4.2.3.3 Comparison of the screening results

The different screening methods for protein interaction partners of FA2H revealed a large amount of possible candidates. As mentioned before, PFA and BioID screenings inevitably lead to some false positive identifications. Therefore, each candidate has to be verified by additional assays. Since this is not feasible for all of the candidates, the results of the different approaches were compared to find proteins identified in two or three approaches. Moreover those were also more likely true interactors of FA2H. For this comparison, the list of significantly enriched protein groups from the two PFA-assisted Twin-StrepTag pulldowns, transient (PFA PD transient) and stable (PFA PD stable), and the BioID-FA2H-assay (BioID) were used. The results are depicted in the Venn diagram below. In this a circle, whose size is proportional to the number of significantly enriched protein groups, represents each experiment. Overlapping areas between the circles resemble the amount of protein groups shared between experiments. Note that the two non-PFA experiments were not considered, because they showed only small numbers of putative interaction partners.

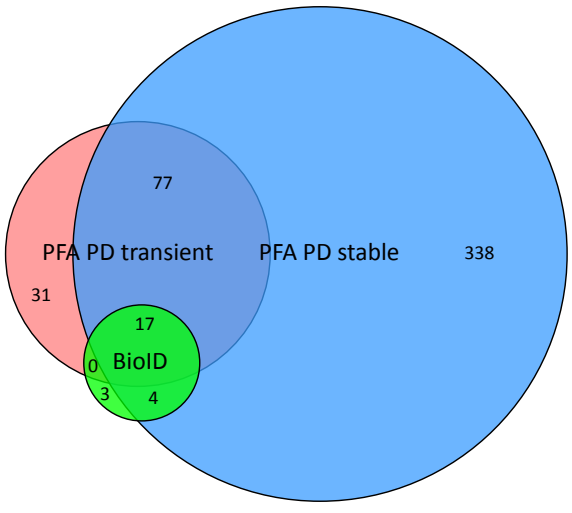

Figure 4-32: Venn diagram showing the overlap in protein group identifications between three mFA2H interaction partner screenings. PFA PD transient = PFA-assisted Twin-Strep pulldown of transiently-overexpressed mFA2H; PFA PD stable = PFA assisted Twin-Strep pulldown of stably transfected mFA2H; BioID = BioID-FA2H-assay

The three mFA2H interaction partner screenings showed a good degree of congruency. Only in the PFA PD stable experiment a huge amount of identifications was present, which were not identified

in any of the other two experiments (338). But this was not surprising, since this experiment exhibited a very high number of significantly enriched proteins (437) likely including many false-positives. Overall, 17 protein groups were consistently identified in all three experiments. In addition, 77 protein groups were exclusively enriched in the two PFA-experiments and 4 only in PFA PD stable and BioID. A table containing the protein identifications corresponding to each overlapping area of the Venn diagram is given in Table 4-19.

Table 4-19: Protein groups identified and significantly enriched in two or three screenings. The protein groups, which were significantly enriched in two or three of the indicated screening approaches, PFA pulldown transient (P_T), PFA pulldown stable (P_S) or BioID (B), are given by their respective gene and protein names. The presence of a protein group in the respective screening is indicated by a plus sign.

Gene names	Protein names	P_T	P_S	B	Gene names	Protein names	P_T	P_S	B
ACSL3	Long-chain-fatty-acid--CoA ligase 3	+	+		**PSMC5**	26S protease regulatory subunit 8	+	+	
ALDH3A2	Fatty aldehyde dehydrogenase	+	+	+	**PSMD2**	26S proteasome non-ATPase regulatory subunit 2	+	+	
ATP1A1; ATP1A3	Sodium/potassium-transporting ATPase subunit alpha-1; subunit alpha-3	+	+		**PSMD6**	26S proteasome non-ATPase regulatory subunit 6	+	+	
ATP2A2	Sarcoplasmic/endoplasmic reticulum calcium ATPase 2	+	+		**PTPLAD1**	Very-long-chain (3R)-3-hydroxyacyl-[acyl-carrier protein] dehydratase 3	+	+	
BCAP31	B-cell receptor-associated protein 31	+	+		**PTPN1**	Tyrosine-protein phosphatase non-receptor type 1	+	+	+
CANX	Calnexin	+	+		**PTRH2**	Peptidyl-tRNA hydrolase 2, mitochondrial	+	+	
CCDC47	Coiled-coil domain-containing protein 47	+	+	+	**RAB11A; RAB11B**	Ras-related protein Rab-11A; 11B	+	+	
CKAP4	Cytoskeleton-associated protein 4	+	+		**RAB13; RAB8A; RAB8B**	Ras-related protein Rab-13; 8A; 8B	+	+	
COPA	Coatomer subunit alpha	+	+		**RAB14**	Ras-related protein Rab-14	+	+	
CYB5R3	NADH-cytochrome b5 reductase 3	+	+		**RAB1A**	Ras-related protein Rab-1A	+	+	
DDOST	Dolichyl-diphosphooligosaccharide--protein glycosyltransferase 48 kDa subunit	+	+		**RAB1B; RAB1C**	Ras-related protein Rab-1B; 1C	+	+	
DHCR7	7-dehydrocholesterol reductase	+	+		**RAB2A**	Ras-related protein Rab-2A	+	+	
DNAJC7	DnaJ homolog subfamily C member 7	+	+		**RAB5C**	Ras-related protein Rab-5C	+	+	
DPM1	Dolichol-phosphate mannosyltransferase	+	+		**RAB6A**	Ras-related protein Rab-6A	+	+	
EMC2	ER membrane protein complex subunit 2	+	+		**RAB7A**	Ras-related protein Rab-7a	+	+	
EMD	Emerin	+	+		**RDH11**	Retinol dehydrogenase 11	+	+	
EPHX1	Epoxide hydrolase 1	+	+		**RPLP0; RPLP0P6**	60S acidic ribosomal protein P0; P0-like	+	+	
ERLIN1	Erlin-1	+	+		**RPN1**	Dolichyl-diphosphooligosaccharide--protein glycosyltransferase subunit 1	+	+	

ESYT1	Extended synaptotagmin-1	+	+	+	**RPN2**	Dolichyl-diphosphooligosaccharide--protein glycosyltransferase subunit 2	+	+	
Fa2h	Fatty acid 2-hydroxylase	+	+	+	**RPS27A; UBA52; UBB; UBBP4; UBC**	Ubiquitin-60S ribosomal protein L40;Ubiquitin;60S ribosomal protein L40;Ubiquitin-40S ribosomal protein S27a;Ubiquitin;40S ribosomal protein S27a;Polyubiquitin-B;Ubiquitin;Polyubiquitin-C;Ubiquitin	+	+	
FAF2	FAS-associated factor 2	+	+	+	**SACM1L**	Phosphatidylinositide phosphatase SAC1	+	+	
HMOX2	Heme oxygenase 2	+	+		**SCFD1**	Sec1 family domain-containing protein 1	+	+	
HSD17B12	Estradiol 17-beta-dehydrogenase 12	+	+		**SDCBP**	Syntenin-1	+	+	
HSD17B7	3-keto-steroid reductase	+	+		**SEC22B**	Vesicle-trafficking protein SEC22b	+	+	
HSPA1A	Heat shock 70 kDa protein 1A/1B	+	+		**SEC23A**	Protein transport protein Sec23A	+	+	
HSPA5	78 kDa glucose-regulated protein	+	+		**SLC27A4**	Long-chain fatty acid transport protein 4	+	+	
HSPA6; HSPA7	Heat shock 70 kDa protein 6;Putative heat shock 70 kDa protein 7	+	+		**SMPD4**	Sphingomyelin phosphodiesterase 4		+	+
HSPA8	Heat shock cognate 71 kDa protein	+	+		**SND1**	Staphylococcal nuclease domain-containing protein 1	+	+	
HYOU1	Hypoxia up-regulated protein 1	+	+		**SPCS2**	Signal peptidase complex subunit 2	+	+	
KTN1	Kinectin	+	+		**SPTLC1**	Serine palmitoyltransferase 1	+	+	+
LBR	Lamin-B receptor	+	+	+	**SPTLC2**	Serine palmitoyltransferase 2	+	+	
LMAN1	Protein ERGIC-53	+	+		**SRPR**	Signal recognition particle receptor subunit alpha		+	+
LRRC59	Leucine-rich repeat-containing protein 59	+	+	+	**SRPRB**	Signal recognition particle receptor subunit beta	+	+	+
MTDH	Protein LYRIC		+	+	**SSR4**	Translocon-associated protein subunit delta	+	+	
NAPA	Alpha-soluble NSF attachment protein	+	+		**STIM1**	Stromal interaction molecule 1	+	+	+
NCLN	Nicalin	+	+		**STT3A**	Dolichyl-diphosphooligosaccharide--protein glycosyltransferase subunit STT3A	+	+	
NOMO1; NOMO2; NOMO3	Nodal modulator 1; 2; 3	+	+		**STX18**	Syntaxin-18	+	+	
NSDHL	Sterol-4-alpha-carboxylate 3-dehydrogenase, decarboxylating	+	+	+	**SURF4**	Surfeit locus protein 4	+	+	
NSF	Vesicle-fusing ATPase	+	+		**TFRC**	Transferrin receptor protein 1	+	+	
NUP155	Nuclear pore complex protein Nup155		+	+	**TMED9**	Transmembrane emp24 domain-containing protein 9	+	+	
OSBPL8	Oxysterol-binding protein-related protein 8	+	+		**TMEM109**	Transmembrane protein 109	+	+	
PDIA3	Thioredoxin	+	+		**TMPO**	Lamina-associated polypeptide 2, isoforms beta/gamma; Thymopoietin;	+	+	+
PDIA3	Protein disulfide-	+	+		**TMX1**	Thioredoxin-related	+	+	

	isomerase A3					transmembrane protein 1			
PGRMC1	Membrane-associated progesterone receptor component 1	+	+		**TOLLIP**	Toll-interacting protein	+	+	
PGRMC2	Membrane-associated progesterone receptor component 2	+	+	+	**TOR1AIP 1**	Torsin-1A-interacting protein 1	+	+	+
PLD3	Phospholipase D3	+	+		**VAPA**	Vesicle-associated membrane protein-associated protein A	+	+	+
POR	NADPH-cytochrome P450 reductase	+	+		**VAPB**	Vesicle-associated membrane protein-associated protein B/C	+	+	+
PPIB	Peptidyl-prolyl cis-trans isomerase B	+	+		**VCP**	Transitional endoplasmic reticulum ATPase	+	+	
PSMC4	26S protease regulatory subunit 6B	+	+		**YIPF5**	Protein YIPF5	+	+	

The majority of the protein groups concurrently identified and significantly enriched in two or three assays are linked to lipid metabolism, protein folding and degradation, and cellular transport process. Examples for lipid metabolism-related proteins are: sphingolipid metabolism proteins (SACM1L, SMPD4, SPTLC1, SPTLC2, VAPA, VAPB), electron transferring proteins (CYB5R3, POR), or cholesterol metabolizing enzymes (DHCR7, HSD17B7, LBR, NSDHL). Furthermore, PGRMC1 and PGRMC2 were identified repeatedly, which are both known to be involved in regulating the activity of various metabolic enzymes. Enriched proteins linked to protein folding and degradation machinery are proteasomal subsunits (PSMC5, PSMD6, PSMD6), ubiquitin (UBB, UBC), chaperones (CANX, HSPA1A, HSPA6, HSPA7), olichyl-diphosphooligosaccharide-protein glycotransferase (DDOST, RPN1, RPN2) and ERAD-components (FAF2, ERLIN1, EMC2). Examples for proteins involved in cellular transport processes are various Rab-proteins (RAB1A, RAB1B, RAB5C, RAB7A), vesicular transport proteins (COPA, SEC22B, SEC23A, SCFD1, STX18, TMED9), and ER-protein import components (SRPR, SRPRB, SSR4).

4.2.4 Verification of FA2H interaction partners

With quite a large number of possible FA2H interaction partners identified in the different mass spectrometry based screening approaches, a selection of promising candidates was tested by two other assay methods. In the first method Twin-Strep-mFA2H was affinity purified after PFA-crosslinking as in the respective screenings, since most interactors were not identifiable without a crosslinking step. Subsequently, the co-precipitation of putative interactors was evaluated via WB. For the second method bimolecular fluorescence complementation assays (BiFC) were conducted, which allow the monitoring of protein interactions in living cells. In BiFC two fragments of a fluorescent protein are fused to putative interacting proteins. Co-expressed in the same cells the interaction of the candidate proteins can lead to the complementation of a functional fluorescent

protein, which can be visualized and quantified subsequently (see 3.2.4.16 Bimolecular fluorescence complementation (BiFC)).

4.2.4.1 TWIN-StrepTag pulldown & Western blot

The interactions of FA2H with SACM1L, ACSL3, PGRMC1, ALDH3A2 and SPTLC1 were evaluated by Co-IP and WB. Thus, Twin-Strep-mFA2H was expressed in HEK293-T cells (transient) or HEK293 (stable). Afterwards, PFA-crosslinking was applied, the cells lysed and Twin-Strep-mFA2H precipitated by StrepTactin-affinity purification. The presence of putative interaction partners in the lysate (input) and the eluate fraction was then tested by WB. For some proteins two additional fractions were examined: unbound = lysate after bead incubation; beads = not-eluted proteins. The WBs using transiently transfected cells are shown in Figure 4-33 and the WBs using stably transfected cells in Figure 4-34.

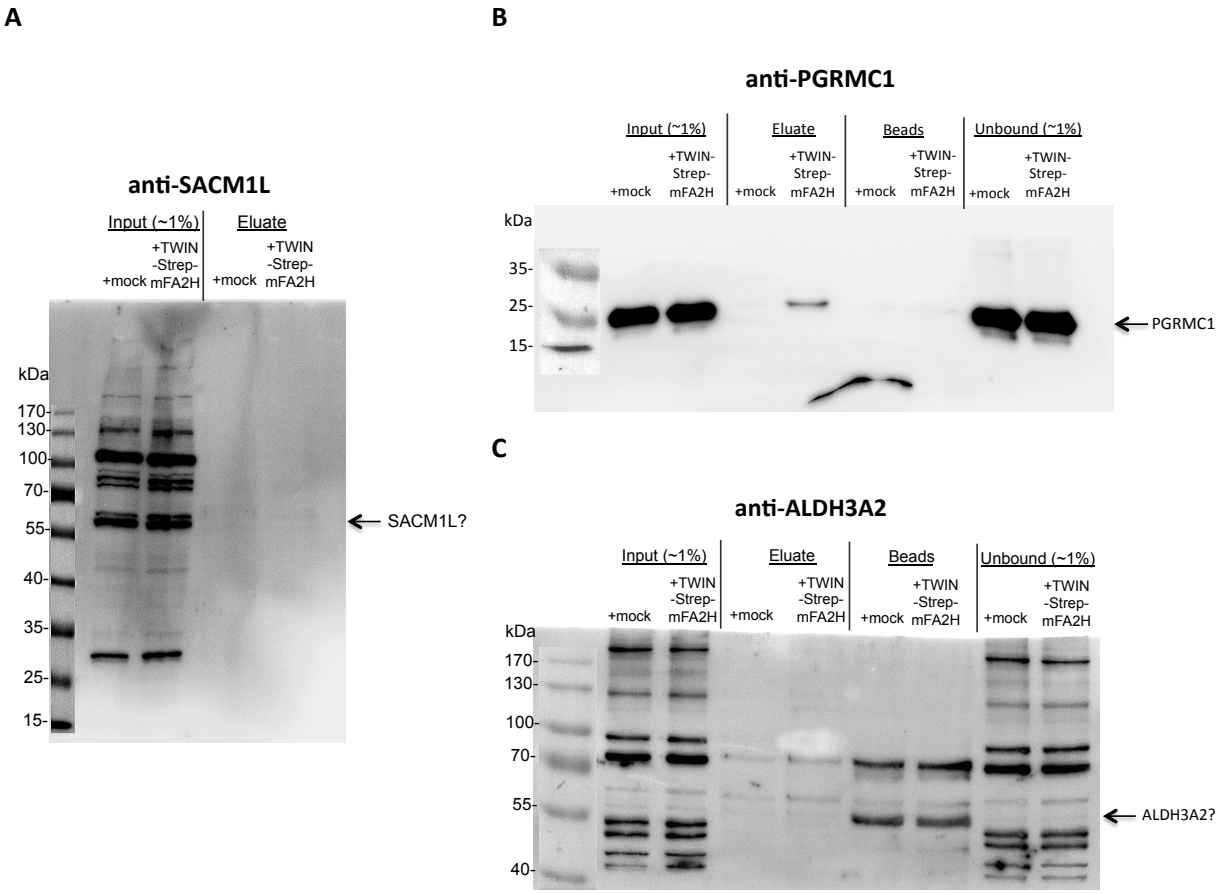

Figure 4-33: FA2H interaction partner verification by WB (transiently transfected cells). Either mock (pcDNA3) or Twin-Strep-mFA2H (pESG-IBA105-mFA2H) plasmids were transfected into HEK293-T cells (2x15 cm plate each). After 48 h, cells were harvested, thereby combining equally transfected cells. Then the cells were fixed for 20 min with 0.5% PFA, which was stopped by the addition of icecold 1.25 M glycine buffer. Cell lysis was achieved in RIPA buffer followed by protein amount determination. A small amount of each lysate (1% (v/v)) was removed for later analysis (Input (1%)) and the remaining lysate subjected to StrepTactin-affinity purification. Subsequently, each eluate was concentrated by CHCl3/MeOH-precipitation, resuspended in 2X Laemmli buffer (Eluate). In some cases two additional samples were prepared. One, representing the proteins not bound to the affinity matrix (Unbound (1%)), taken from the lysate after affinity-purification. The other, signifying non-eluted proteins (Beads), was produced by boiling the beads in 2X Laemmli after elution. Finally, all samples were heated to 95 °C for 10 min, separated by SDS-PAGE, transferred to a PVDF-membrane and analyzed by WB. Goat-anti-rabbit-HRP was used as secondary antibody (dilution 1:5000, 1 h, RT). **(A)** SACM1L detected by anti-SACM1L antibody incubation (dilution 1:500, ON, 4 °C). **(B)** PGRMC1 detected with anti-PGRMC1 antibody (dilution 1:1000, ON, 4 °C). **(C)** ALDH3A2 detected with anti-ALDH3A2 antibody (dilution 1:1000, ON, 4 °C).

The SACM1L-WB (Figure 4-33A) showed many proteins of different sizes with very prominent ones at ~30, ~60 and ~110 kDa, arguing against the antibodies specificity. According to the literature, SACM1L should have given a protein signal corresponding to its molecular mass of 67 kDa. Thus, the 60 kDa-signal possibly represented SACM1L running a little lower than expected in the used gel system. Accordingly, one could speculate that the larger protein-band at ~110 kDa represented SACM1L-dimers. But both signals were only present in the input and not in the eluate fractions regardless of the presence of Twin-Strep-mFA2H. Therefore, the SACM1L-FA2H interaction could not be verified by WB with the used antibody.

The PGRMC1-WB (Figure 4-33B) showed a single band at ~25 kDa corresponding with the proteins predicted molecular weight (22 kDa). This band was strongly visible in both input and unbound fractions. Furthermore, a weaker PGRMC1 signal was solely present in the +Twin-Strep-mFA2H, but not in the mock eluate fraction, proving the specific interaction between FA2H and PGRMC1. Together with the strong PGRMC1-signals in the unbound fraction this further showed that only a small fraction of PGRMC1 is interacting with FA2H. Lastly, there was no PGRMC1-signal in the bead fractions, demonstrating no residual PGMC1-binding to the beads.

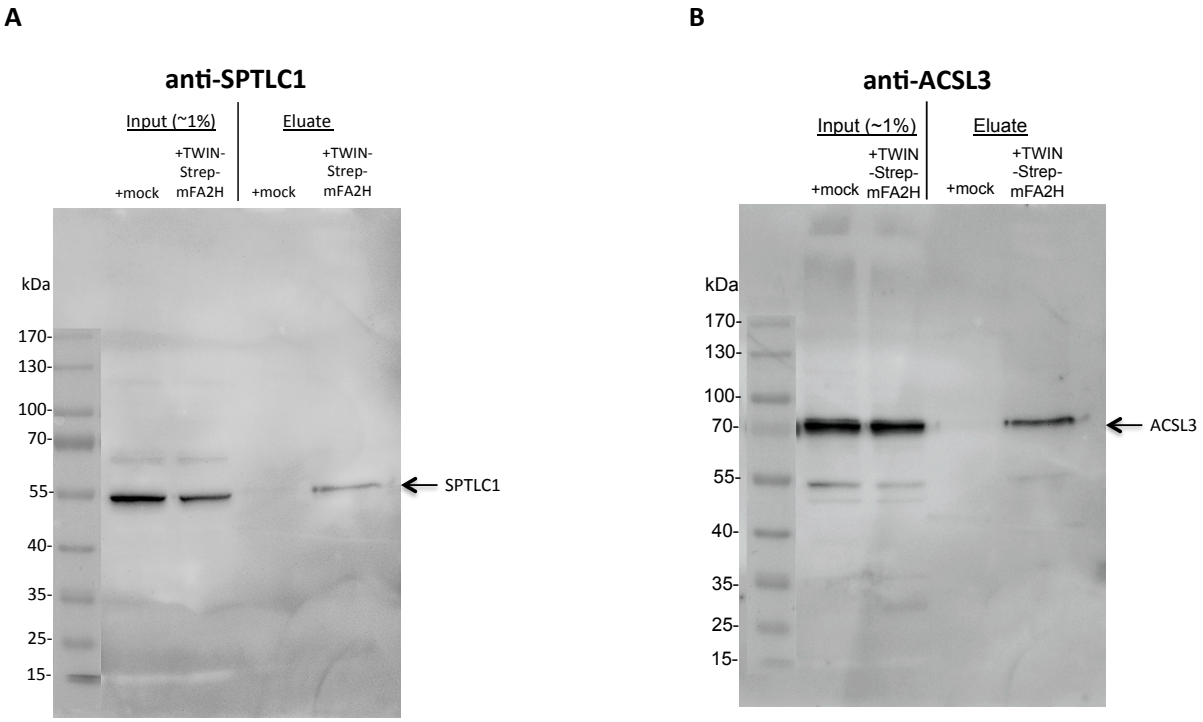

Figure 4-34: FA2H interaction partner verification by WB (stably transfected cells). HEK293 cells, untransfected (mock) or stably transfected with Twin-Strep-mFA2H (+Twin-Strep-mFA2H), were grown until reaching confluence on two 15 cm plates each. Afterwards, cells were harvested, equal cells from two plates combined, pellets fixed in 0.5% PFA for 20 min and the fixation stopped by adding icecold 1.25 M glycine solution. Cell lysis was achieved in RIPA buffer followed by protein amount determination. A small amount of each lysate (1% (v/v)) was removed for later analysis (Input (1%)) and the remaining lysate subjected to StrepTactin-affinity purification. Subsequently, each eluate was concentrated by CHCl3/MeOH-precipitation, resuspended in 2X Laemmli buffer (Eluate). Finally, all samples were heated to 95 °C for 10 min, separated by SDS-PAGE, transferred to a PVDF-membrane and analyzed by WB. Anti-rabbit-HRP was used as secondary antibody (dilution 1:5000, 1.5 h, RT). For the detection of more than one protein the membrane was stripped and reprobed. **(A)** SPTLC1 was detected by incubating with the respective antibody (dilution 1:2000, 2 h, RT). **(B)** ACSL3 detected with anti-ACSL3 antibody after membrane stripping (dilution 1:1000, ON, 4 °C). Note the very weak protein signal at 55 kDa, representing residual anti-SPTLC1 antibody not removed by the stripping step.

The SPTLC1-WB (Figure 4-34A) displayed one major signal at ~54 kDa, fitting the expected molecular weight of SPTLC1 (53 kDa), together with two very weak background bands of greater sizes. The major band was visible within both input fractions, but just in the +Twin-Strep-mFA2H eluate fraction, thereby successfully proving the FA2H-SPTLC1 interaction. Moreover, its intensity was

higher in the input, than in the eluate fraction. Considering this difference in signal intensity and the fact that only ~1% of the total lysate were analyzed, it became obvious that only a small fraction of SPTLC1 interacted with FA2H.

The ACSL3-WB (Figure 4-34B) exhibited mainly one prominent protein band at ~75 - 80 kDa, which was in line with ACSL3's predicted molecular weight (80 kDa). As for SPTLC1, it was present with a high intesity in both input and with less intensity in the +Twin-Strep-mFA2H eluate fraction, thereby verifying the interaction between FA2H and ACSL3. Furthermore, this difference in signal intensity, together with the fact that only ~1% of the total lysate were analyzed, proved that only a small fraction of ACSL3 was interacting with FA2H.

In summary, PGRMC1, SPTLC1 and ACSL3 could be verified as FA2H interaction partners by WB, showing a signal in the eluate fraction derived from the Twin-Strep-mFA2H sample, but not from the control sample. In addition, it became clear for all three that that only a small fraction of each protein was part of the interaction with FA2H.

4.2.4.2 Bimolecular fluorescence complementation

Verification of protein interaction in living cells was done using bimolecular fluorescence complementation (BiFC) for the interactions with PGRMC1, CersS2, ACSL3 and SPTLC1. Therefore, cells were transiently transfected with plasmids coding for Split-YFP-tagged putative interaction partners. The complementation of functional fluorescent proteins was then qualitatively evaluated by fluorescence microscopy (Figure 4-35). As a positive control for successful BiFC, cells were also co-transfected with plasmids coding for cYFP1- and YFP2-tagged ER-Golgi intermediate compartment 53 kDa protein (ERGIC53), which is known to produce a strong BiFC-signal due to protein oligomerization. As a potential second positive control CerS2 recently discovered dimerization was also tested by BiFC (Laviad et al. 2012). After this initial experiments, two interactions were further assessed in quantitative competition assays using fluorescence intensity measurements in a plate reader (Figure 4-36).

For the qualitative evaluation, BHK cells were seeded on coverslips and subsequently transfected with the respective constructs. 24 h after transfection, the cells were PFA-fixed, permeabilized, DAPI-stained and mounted on coverslides. Representative fluorescent images of each interaction tested are shown below.

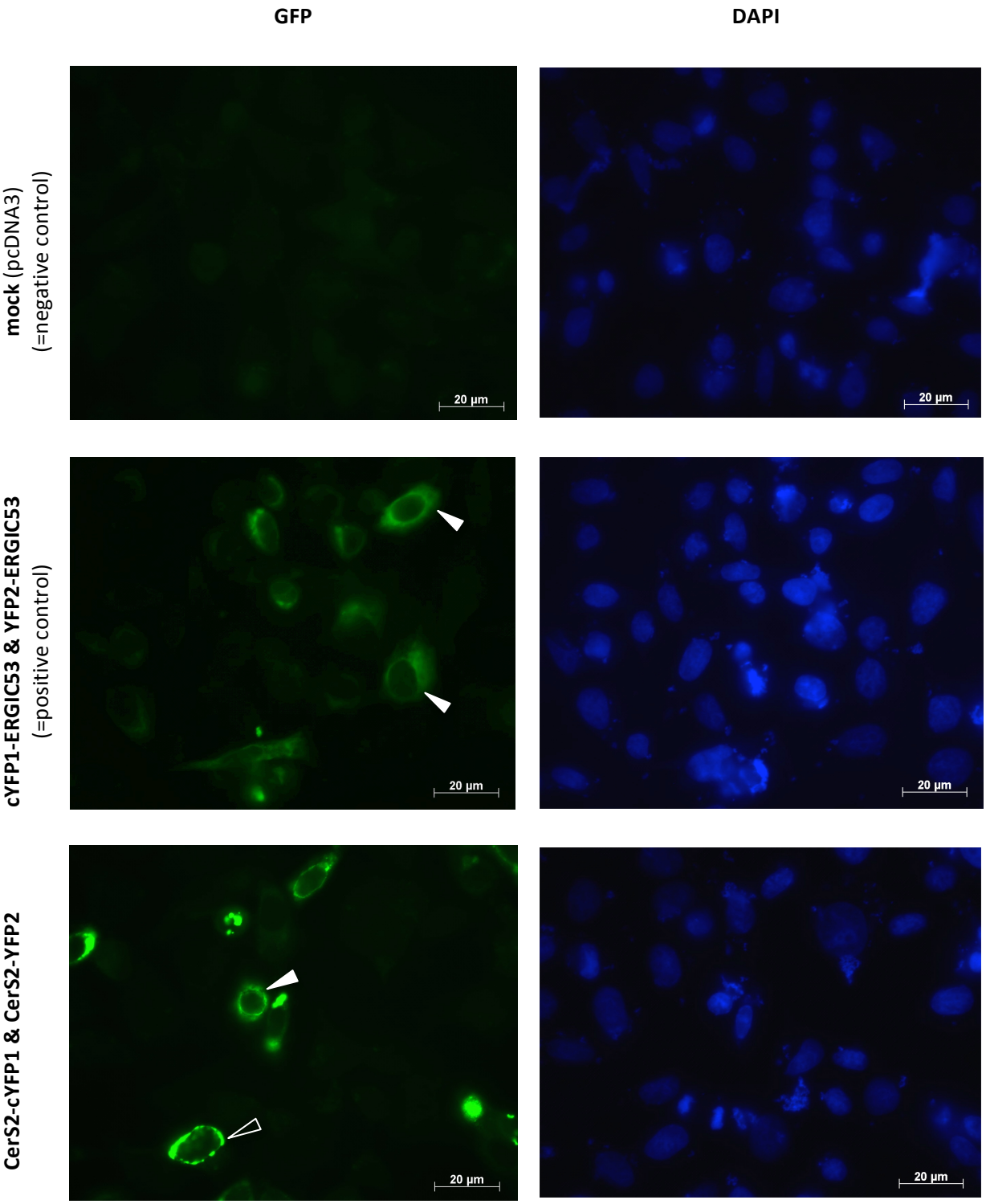
GFP
DAPI
mock (pcDNA3)
(=negative control)
cYFP1-ERGIC53 & YFP2-ERGIC53
(=positive control)
CerS2-cYFP1 & CerS2-YFP2
20 µm
20 µm
20 µm
20 µm
20 µm
20 µm

FA2H-YFP2 & PGRMC1-cYFP1

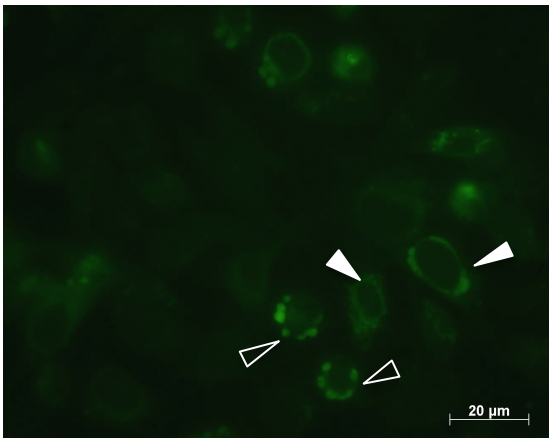

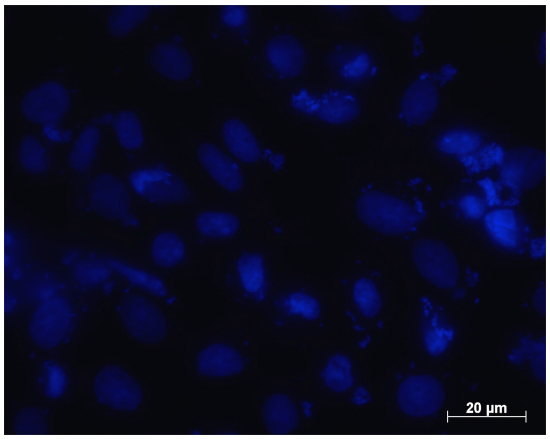

FA2H-cYFP1 & CerS2-YFP2

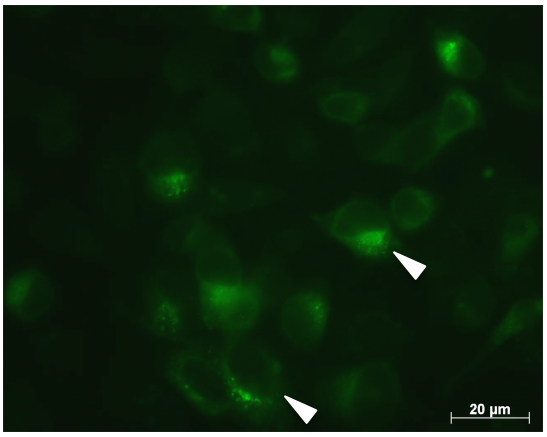

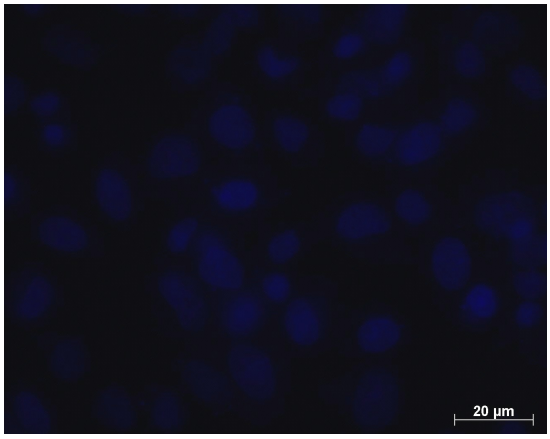

FA2H-YFP2 & ACSL3-cYFP1

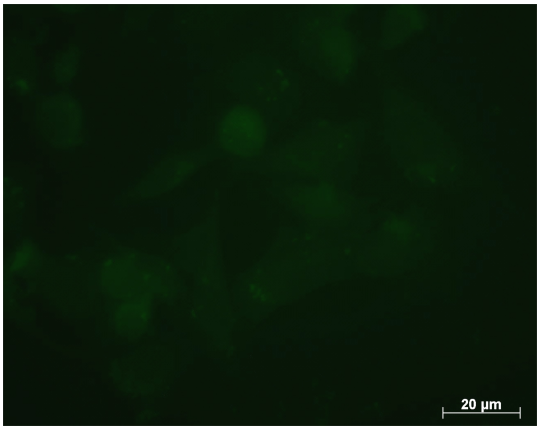

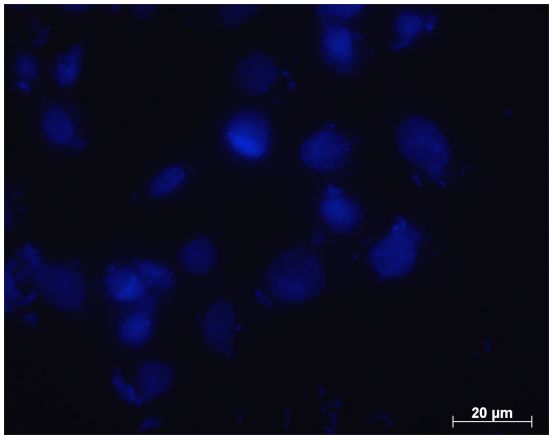

FA2H-YFP1 & SPTLC1-YFP2

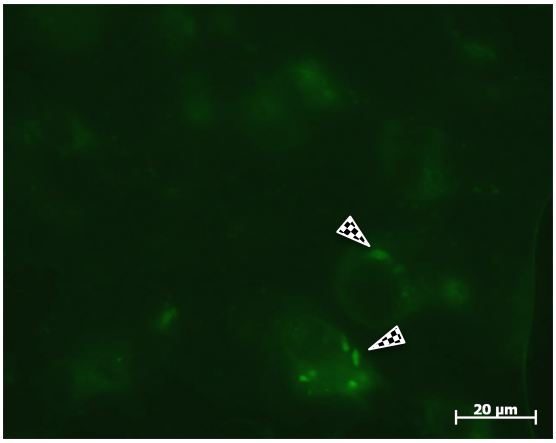

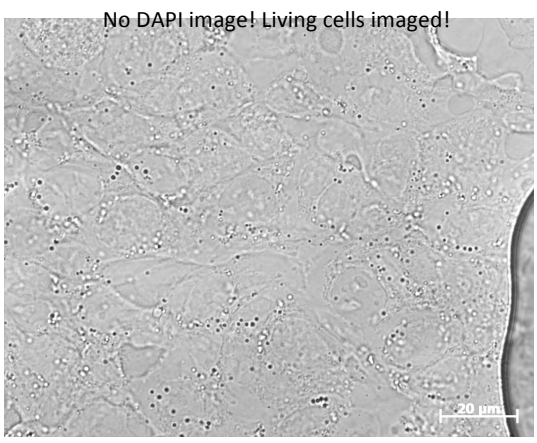

Figure 4-35: Fluorescent microscopy of BiFC-tested protein-protein interactions. BHK cells were seeded on glass coverslips in a 24-well plate. 24h later they were transfected with 1 µg total plasmid DNA (0.5 µg of each BiFc-plasmid) using TurboFect. **(A) – (F)** After another 24 h, the cells were washed, fixed with PFA, permeabilized with TX-100 and nuclei stained with DAPI. Following subsequent washing steps, all coverslips were mounted on coverslides and fluorescent microscopy performed using 63X magnification and immersion oil. Since no YFP-filters were available, the constructs were visualized in the GFP-channel. The YFP1-ERGIC53-YFP2-ERGIC dimerization was used as positive control. White arrowheads indicate cells exhibiting an ER & Golgi-like staining pattern. Unfilled arrowheads indicate cells with a circular staining pattern. Note that the circular assemblies seem to be composed of smaller rounder structures. **(G)** Because of unstable YFP-constructs PFA-fixation, permeabilization and DAPI-staining were omitted. Living cells were mounted on coverslides in PBS and directly visualized using the same microscope settings as above. Checkered arrowheads point at cells, which exhibit an ER & Golgi-like staining pattern in combination with strongly staining punctuate structures.

As expected, no GFP-signals were visible in the negative control (mock), but strong signals in the positive control (cYFP1-ERGIC53 + YFP2-ERGIC53). The majority of the cells transfected with the different interaction partner candidates showed signals, which varied in intensity and shape. The oligomerization of ERGIC53 showed strong signals with a typical ER & Golgi-like staining pattern (white arrowheads), corresponding with the expected protein localization. Interestingly, BiFC was also able to verify the recently published oligomerization of CerS2, thus further demonstrating the validity of the method. Moreover, while some cells co-transfected with CerS2-cYFP1 and CerS2-YFP2 also exhibited ER & Golgi-like signals, many others showed a very different signal shape. In those the fluorescent signal was observable as thin circular assemblies composed of smaller round structures (unfilled arrowheads). The interaction of FA2H with PGRMC1 was also observable by BiFC. Intriguingly, it presented with the same two distinct staining patterns as the CerS-dimerization. Moreover, the FA2H-CerS2 interaction was verified by BiFC, showing an ER & Golgi-like staining pattern similar to the ERGIC53-dimerization. In contrast, no signal was observable for the FA2H-ACSL3-interaction. This was also the case when other YFP-tag combinations, e.g. FA2H-YFP1 & ACSL3-YFP2, were used (data not shown). This negative result does not disprove the interaction, because some protein-protein interactions are not accessible by BiFC due to steric constraints. If the two YFP-fragments do not come into close contact, no functional fluorescent protein is complemented and thus no signal measurable. Alternatively, the interaction may be indirect i.e. facilitated by an additional protein and therefore not provable using BiFC. Lastly, the interaction of FA2H and SPTLC1 was also shown using BiFC. While the fluorescent signals were very weak, an ER & Golgi-like staining pattern in combination with strongly staining punctuate structures could still be discerned (checkered arrowheads). In summary, the assay showed the complementation of functional fluorescent proteins for three of the four putative FA2H interaction partners tested (PGRMC1, CerS2, SPTLC1), thereby further supporting the validity of each interaction.

To further support the specificity of the interactions two of them, FA2H & PGRMC1 and FA2H & SPTLC1, were also assayed in BiFC competition assays. Accordingly, BHK cells were seeded in 6 well plates, transiently transfected with the respective BiFC-constructs and grown for 48 h. For the

competition, samples were included in which untagged FA2H, PGRMC1 or SPTLC1 were co-expressed together with their BiFC-counterparts. If the interactions are really specific the untagged proteins should lead to a fluorescence intensity reduction, since complexes composed of tagged and untagged protein are not fluorescent. Note that a complete reduction will not be achieved, since the complemented fluorescent protein is very stable once it has been formed. Thus, the competitors can only sequester target proteins, which are not already interacting with their respective BiFC-partner. After transfection, the cells were harvested by trypsinization, washed and resuspended in PBS, and finally transferred to a black 96 well plate. Subsequently, fluorescence intensities were measured using a plate reader. For each interaction three independent experiments were conducted. Since the measured absolute intensities differed strongly between independent experiments, due to variations in transfection efficiency, all values were normalized to the dimerization of cYFP1-ERGIC53 with YFP2-ERGIC53 (=positive control). Figure 4-36 shows the results for both interactions.

A

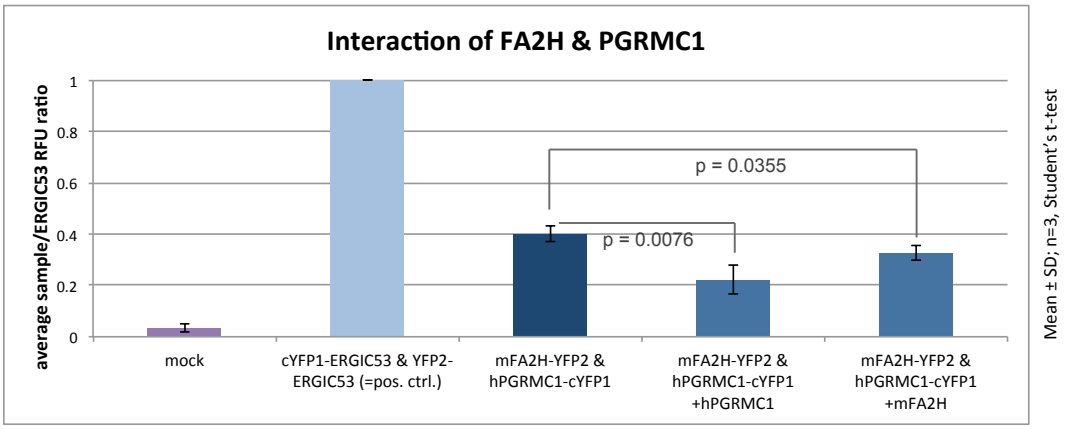

B

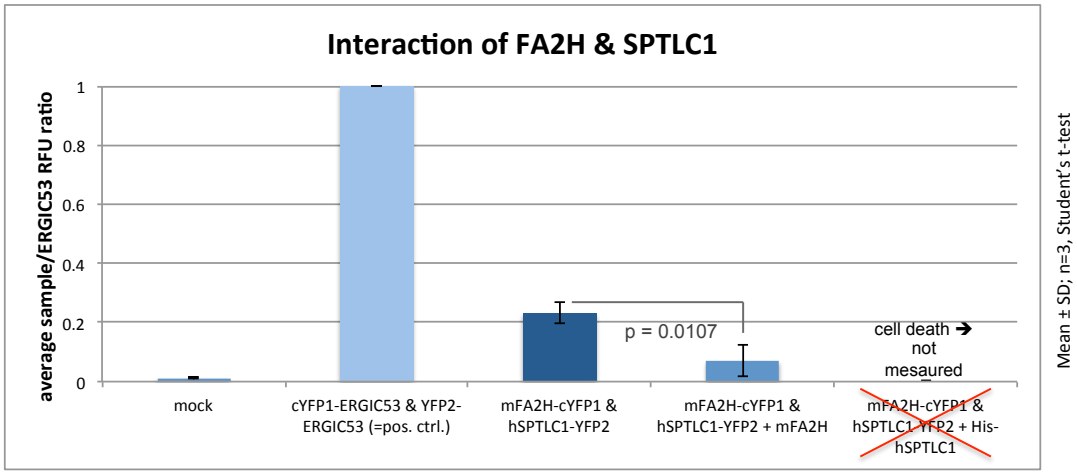

Figure 4-36: BiFC competition assay of the interaction FA2H-PGRMC1 and FA2H-SPTLC1. BHK cells were seeded in 6 well plates. 24 h later they were transfected with a total plasmid DNA amount of 4 µg (0.25 µg of each BiFC-plasmids filled up to 4 µg total plasmid amount with pcDNA3). To further support the specificity of the interaction, competition samples were included by co-expressing high amounts of untagged FA2H or the respective interaction partner (3.5 µg of plasmid). The cYFP1-ERGIC53 + YFP2-ERGIC53 sample was included as a positive control. Following a medium exchange 24 h after transfection, the cells were grown another 24 h before harvesting by trypsinization. Subsequently, the cells were washed twice in 1 ml PBS, resuspended in 200 µl PBS, transferred to a black 96 well plate and their fluorescence measured in a plate reader. Each experiment was done in three replicates (n=3) and values are given as mean +/- standard deviation. P-values were obtained by Student's t-test. To correct for intensity variations, caused by differences in transfection efficiency, intensities are given relatively to the cYFP1-ERGIC53 + YFP2-ERGIC53 positive control (average sample/ERGIC53 RFU ratio). **(A) FA2H-PGRMC1 interaction.** Measured with Mithras LB 940 plate reader. **(B) FA2H-SPTLC1 interaction.** Measured with Infinite 200 PRO plate reader.

The FA2H-PGRMC1 interaction was repetitively measurable by BiFC (Figure 4-36A). Furthermore, the specificity of the interaction could be confirmed by competition samples, in which excess amounts of non-tagged hPGRMC1 or mFA2H were co-expressed with the BiFC-partners. While the co-expression of hPGRMC1 significantly reduced the average sample/ERGIC53 RFU ratio by 40%, co-expression of mFA2H, however, led only to a significant reduction of 15%. The less efficient competition with mFA2H might be explained by the observation made before, that FA2H may functions as a dimer (see ~80 kDa complex in: 4.2.2.1 BlueNative PAGE and 4.2.2.2 PFA-crosslinking). If FA2H-PGRMC1 complexes also contained two FA2H molecules, a strong BiFC competition was only possible when both FA2H-molecules were replaced by untagged ones. Conversely, the competition with PGRMC1, presumably present in the complex as a monomer, was much more efficient.

A similar result was apparent for the FA2H-SPTLC1 interaction (Figure 4-36B). This interaction could be almost completely diminished by competing with untagged FA2H, thereby significantly reducing ($p = 0.0107$) the average sample/ERGIC53 RFU ratio by 70%. Unfortunately, the competition with SPTLC1 led to massive cell death, thereby not allowing a BiFC measurement. Thus, it should be repeated with lower plasmid amounts of untagged SPTLC1.

Taken together, the competition experiments confirmed the specific interaction of FA2H with PGRMC1 and with SPTLC1.

5 Discussion

5.1 Comparative quantitative myelin proteome analysis of FA2H-KO mice

The first part of this thesis focused on the discovery of potential changes in the myelin protein composition of FA2H-KO in comparison to WT mice by mass spectrometry based proteomics. Finding differences might help to explain the observed pathology. Interestingly, the initial analysis of young (~5 month) FA2H-KO mice by WB showed no differences for some major CNS-myelin proteins, like MBP, CNP and L-MAG (Zöller et al. 2008). But this does not excludes that other myelin proteins are changed. Moreover, some changes might be only minimal in young animals and become more prominent over time. This would be in line with the late occurrence (~18 month) of histological-observable myelin changes. Thus, a systematic and comprehensive evaluation of both CNS- and PNS-myelin from animals of different ages should clarify the contribution of proteomic changes to the myelin pathology. The general feasibility of a mass spectrometry based screening approach has been shown before in other publications using mouse models of demyelination e.g. CGalT-KO (Taylor et al. 2004), PLP-KO (Werner et al. 2007), CGalT-KO and CST-KO (Fewou et al. 2010) and prion protein-KO (Prnp-KO) mice (Patzig et al. 2011). While the first three publications concentrated on CNS-myelin, the fourth one investigated PNS-myelin. In all recent approaches, two dimensional differential gel electrophoresis (2D DIGE) (Rozanas & Loyland 2008) was used to measure the proteome changes. While it is a well-established method, by now it has been increasingly replaced by shotgun proteomics in combination with label-free or label-based protein quantification (Lambert et al. 2005; Brewis & Brennan 2010). In these approaches, proteins are digested to peptides, afterwards separated by multidimensional liquid chromatography-based systems, and subsequently directly analyzed in a mass spectrometer. These systems are usually more sensitive, allowing a greater number of peptide and protein identifications and are also better applicable for highly charged and hydrophobic proteins, which present a challenge for gel-based systems. In addition, the use of certain labeling techniques, like the isobaric TMT or iTRAQ-tags, allows for more complex multiplexing (Wu et al. 2006). While only up to three samples can be measured simultaneously with DIGE, the newest generation of TMT-tags permits the quantification of up to ten samples in one mass spectrometric measurement (McAlister et al. 2012).

CNS- and PNS-myelin from WT and KO-animals of three different ages (6, 13 and 17 months) were each compared using a gel-free mass spectrometry-based relative-quantification approach, including isobaric TMT 6-plex peptide labeling. Furthermore, the assays were conducted in three biological replicates. Subsequently, a selection of changed proteins was independently verified by quantitative

WBs in brain lysates and myelin obtained from another group of very old (21 – 23 months) WT and FA2H-KO animals.

Initially, myelin was purified from both tissues using a well-established density gradient method. Afterwards, myelin purity and the consistency of purification were successfully confirmed by 1D-SDS-PAGE and silver staining. Moreover, it showed no obvious protein abundance differences between KO and WT animals in both tissues. At the next step, the proteomic analyses were conducted.

5.1.1 CNS-myelin

Considering CNS-myelin, 1682 protein groups could be identified. This significantly exceeded (~30%) the number of about 1300 proteins constituting the reference list compiled by de Monasterio-Schrader and colleagues from all articles published about the CNS-myelin proteome until 2012 (de Monasterio-Schrader et al. 2012). This was even more drastic considering that in each single study comprising the compendium not more than ~1000 proteins were reported. Nevertheless, about 2/3 (829) of the reference CNS-myelin proteins were also identified in this study. This is a very good overlap and in agreement with observations made by the authors of the reference list, which calculated that only 52% of myelin proteins were found in more than one experiment, while 48% were identified once. The reasons for this are that each study differed in aspects like sample preparation (myelin amount, delipidation, digestion method), protein and/or peptide fractionation, the mass spectrometer (type, generation, settings) and the mode of data analysis (software, database, stringency settings). Especially the availability of the newest generation of high resolution and fast scanning MS-devices allows for the identification of significantly more proteins than found in older studies. Another aspect is data analysis search stringency. Some of the studies used a cutoff of 2 unique peptides to deem an identification specific. In contrast, in this study a false discovery rate-based (FDR-based) approach was used, taking even proteins with one razor peptide (peptide shared by different proteins comprising a group) into account. The FDR is calculated by comparing the peptide sequence information to a decoy database besides the normal database. The decoy database is a sequence-reversed version of the normal database and thus all peptides found in the reversed database should be false positive identifications. Afterwards, the search algorithm dynamically adjusts the peptide score significance threshold to a value, where a predefined amount of the protein identifications are false positives (=FDR-treshold). In this study this FDR-threshold was set to 0.01 (1% false positive identifications). But even when filtering this dataset for two razor peptides, 1233 protein groups remain, which are still about 20% more identifications than in any of the single studies analyzing mouse myelin before. Furthermore, within the identified 1682 protein groups, a significant amount of protein groups was present, which are not regarded “classical” myelin proteins. This is expected and consistent with myelin proteome analyses published before, especially the most

recent ones using more sensitive mass spectrometers (de Monasterio-Schrader et al. 2012). There are always contaminations with mitochondria and synaptic vesicles, which are co-purified in the myelin preparation process. Besides, residual axonal membranes, which are directly bound to the myelin sheath, are also inevitably co-enriched. Still, since some reported protein locations found in public database are incorrect and a protein may have more than one localization, these identifications are usually not excluded (de Monasterio-Schrader et al. 2012).

As the next step, FA2H-KO/WT ratios were calculated and the 1682 protein groups filtered in a way, that only those remained, which had at least two expression ratios at one timepoint. This reduced the list to 1205 protein groups, which were afterwards analyzed by a separate one-sample t-test for each timepoint, to find protein groups significantly changed between both genotypes. Overall, there were protein groups both up- and/or downregulated at all three timepoints, together making up 145 significant changes. None of the major CNS-myelin proteins were significantly changed, which is in line with the previous WB analyses of major myelin proteins (Zöller et al. 2008). Only the data for MBP was inconsistent, possibly because of the large amounts of different MBP-isoforms. Thus, its expression was further examined by WB in myelin and whole brain lysates of very old animals (21 – 23 months). The WB clarified that no expression difference existed for all detectable MBP-isoforms in brain myelin, which was consistent with the protein bands seen in the silver stained 1D gel. In contrast, MBP was significantly reduced in the whole brain of FA2H-KO mice, which is contradictory to the results of the initial FA2H-KO mice characterization. But both experiments cannot be compared completely, because the animals assessed back then were much younger (10 days - 12 weeks). Furthermore, the previous quantification was based on an ECL-WB, whereas an infrared fluorescent WB (LICOR) was used in this study, whose quantification results are more reliable. In summary, these results suggest that while the major composition of myelin was not changed, its total amount became reduced in KO-animals during aging. This is further supported by the observation made in our group that the amount of compact myelin, obtained from FA2H-KO animals, appeared to be reduced by 25 – 30% (Meixner 2009). Furthermore, this has a general consequence for the quantification of myelin-protein changes in FA2H-KO mice solely based on whole brain lysates. Total brain lysates are usually normalized by loading the same protein amounts, but the lysates from KO-mice contain less myelin. Hence, protein upregulations will be reduced or even masked, while protein downregulations will be exaggerated.

Analyzing the 145 significantly changed protein groups there was an interesting observation. While the number of upregulated protein groups increased (15 -> 11 -> 61), the number of downregulated decreased (35 -> 19 -> 10) over time. In addition, only a small number of protein groups were constantly significantly changed. In detail, considering the upregulated proteins, some permanent

changes existed, which appeared already at 6 months or 13 months of age. In contrast, the downregulated proteins were less consistently changed, with many reverting back to WT-levels in 17-month-old KO-animals. Only when considering not significant changes, a small number of protein groups seemed to display a persistent change. Nevertheless, for some protein groups this seemingly not permanent change was possibly just a result of a high biological variability. One has to consider that using 18 mice varying in their genetic background purity certainly caused a high degree of biological variability. This in turn resulted in higher p-values, which were filtered out by the applied significance threshold. In summary, these results indicated that the pathology of FA2H-deficiency is aggravating over time with more proteins becoming upregulated in KO-mice. Furthermore, they suggested that many protein changes were strongly compensated by the KO-animals organism, thus restoring the amounts of affected proteins to WT levels.

The 145 significantly changed protein groups were also analyzed by an automated GO-annotation analysis, which gave inconclusive results. The protein groups, up- and downregulated in FA2H-KO mice, had very diverse cellular localizations and functions. The only striking observation was the considerably large number of upregulated protein groups at each timepoint, which were linked to the cytoskeleton or the immune system. Moreover, the number of proteins found in both categories increased over time.

Since the strongest CNS-myelin proteome changes were upregulations at timepoint 17M, involving mainly cytoskeletal and immune system-related protein groups, a selection of these were studied in more detail by WBs. Upregulated cytoskeletal-related proteins were microtubule-associated protein tau (MAPT), glial fibrillary acidic protein (GFAP) and neurofilament heavy (NF-H). Furthermore, the immunological complement proteins C1qb and C4b, the cholesterol-transport protein apolipoprotein E (ApoE), which is also involved in immunological processes, and the structural myelin membrane protein Opalin were analyzed. All of these seven protein groups had at least a ~2-fold upregulation at timepoint 17M according to the mass spectrometric analysis. Moreover, except for Opalin, all of these are often not considered classical myelin proteins. Still, they have all been identified repeatedly in systematic myelin analyses (de Monasterio-Schrader et al. 2012). Cytoskeletal proteins for example are often closely linked to cell membranes of neural and glial origin and become co-purified during myelin preparation. Thus, a measured upregulation in myelin might reflect an upregulation in the whole brain. Accordingly, the WB analyses were conducted on myelin, but also whole brain lysates, of another group of old WT and FA2H-KO mice (21 – 23 month).

Microtubule-associated protein tau is a cellular protein, binding to microtubule and thereby stabilizing them. While it is usually considered a neuronal protein being responsibly for axonal tubulin stabilization, it has also been shown to be expressed and function in other neural cells e.g.

oligodendrocytes (LoPresti et al. 1995; LoPresti 2002). Interestingly, in oligodendrocytes it showed a similar cellular distribution as MBP, suggesting a role in myelination (LoPresti et al. 1995). Furthermore, under certain circumstances, tau can become hyperphophorylated and forms intracellular fibrillary tangle aggregates in a still not fully discovered process. These aggregates have been first described in Alzheimer's disease (MIM 104300), but by now they have also been found in a variety of other neurodegenerative diseases, which are therefore collectively called tauopathies (MIM: 157140) (Spillantini & Goedert 2013). Excitingly, in many tauopathies, brain iron accumulation has been observed as well (Haraguchi et al. 2011; Lei et al. 2012), which is a feature also found in some FA2H-deficient patients (Schneider & Bhatia 2010). Intriguingly, the mass spectrometric analysis showed a ~2-fold increase of microtubule-associated protein tau in myelin of FA2H-KO mice, which could be verified by WB (~3-fold). In contrast, the total tau amount in the whole brain seemed was not statistically significantly changed. The meaning of the myelin-restriced increase of tau cannot be explained conclusively, but it might reflect a relocalization of oligodendrocyte-expressed tau. Thus, the strong overexpression of myelin-associated tau in FA2H-KO animals opens the possibility that FA2H deficiency is a tauopathy. But to clarify this issue, an aggregation of tau in FA2H-KO mice has to be shown first. If such an aggregation exists, it might explain some of the neurodegenerative features seen in FA2H-deficient patients. Moreover, since tau has also been implicated to be involved in myelination (LoPresti et al. 1995) and oligodendrocyte maturation (LoPresti 2002), the increase in tau may indicate remyelination in FA2H-KO mice. Alternatively, the larger tau amounts in FA2H-KO myelin might have been only a consequence of the axon and myelin sheath degeneration found in FA2H-KO animals. The degeneration potentially led to increased amounts of cellular debris, which might had been co-purified in the myelin preparation, becoming evident in higher amounts of certain cellular proteins.

Glial fibrillary acidic protein (GFAP) is not a classical myelin protein, but usually co-purified during myelin purification (de Monasterio-Schrader et al. 2012). Thus, it can be considered a contamination of myelin with astroglial cellular material. GFAP is one of the major cytoskeletal intermediate filament proteins of astrocytes, thought to be important for maintaining mechanical strength, cell shape and motility (Middeldorp & Hol 2011). Still, its precise functions are largely unknown. Furthermore, increased levels of GFAP are a marker for astrogliosis, the strong increase in activated and reactive astrocytes, following different types of CNS injury. The activated astrocytes proliferate and secrete various factors to repair the tissue damage (Karimi-Abdolrezaee & Billakanti 2012). But if the CNS damage is extremely severe, the effects caused by the activated astrocytes can be more detrimental than helpful, leading to neuronal death and eventually glial scaring. Accordingly, astrogliosis is a feature of many neuroinflammatory and neurodegenerative diseases, like multiple sclerosis, prion associated spongiform encephalopathies, Alzheimer's disease and Parkinson's disease

(Kurz et al. 2012; Nagele et al. 2004; Eng & Ghirnikar 1994; Linker et al. 2009). Interestingly, the GFAP signal was more prominent in FA2H-KO myelin, as became evident by the mass spectrometric analysis, showing a ~2.5-fold upregulation of GFAP. This indicated that astrogliosis was occurring in brains of FA2H-KO mice, becoming evident in higher amounts of co-purified GFAP. Presumably, the axonal and myelin sheath degeneration led to brain tissue lesions, which were populated by proliferating astrocytes. Interestingly, this expands the pathology of FA2H deficiency, for which astrogliosis has not been described before. To verify this assumption, quantitative WB-analyses were performed on myelin and whole brain lysates of very old (21 – 23 month) WT and FA2H-KO animals. The WB-analyses successfully confirmed the astrogliosis, showing even a ~6-fold higher GFAP-amount in myelin and a ~2-fold GFAP-upregulation in the whole brain. The stronger GFAP-increase in myelin in the WB-analysis compared to the mass spectrometric analysis might be explained by fact, that the animals use for the WB-analysis were 4 – 6 months older than the ones measured by mass spectrometry. Consequently, it could be speculated that the proposed astrogliosis is aggravating.

Neurofilament proteins are not classical myelin proteins, but usually co-purified probably because of their association with axonal membranes. Neurofilament heavy (NF-H) is the largest of the three major neuronal intermediate filaments. Largely abundant in axons, they are responsible for axonal structural integrity and transport (Collard et al. 1995). In addition, NF-H seems to be especially important for the development of large-caliber myelinated axons (Elder et al. 1998). Intriguingly, neurofilaments are linked to various neurodegenerative diseases e.g. amyotrophic lateral sclerosis (ALS), Charcot-Marie-Tooth (CMT) disease, neurofilament inclusion disease (NFID), giant axonal neuropathy (GAN), diabetic neuropathy and spastic paraplegia (Yuan et al. 2012; Szaro & Strong 2010). Consequently, the ~2-fold increase of NF-H, measured by mass spectrometry in 17-month-old FA2H-KO, might capitulate the late occurring axonal degeneration. To confirm this, NF-H's expression was also analyzed by WB-analyses of total brain and myelin. But both WBs showed no significant difference in the protein's expression between both genotypes. This implies that NF-H has to be considered a contamination, becoming co-purified during myelin purification in an inconsistent manner.

Besides cytoskeletal proteins, two immune-related proteins showed an upregulation according to the mass spectrometric analysis: C1qb (~4-fold) and C4b (~5-fold). Both are components of the complement cascade system and thus major mediators of inflammatory responses. C1q is a key component of the multiprotein C1-complex, mediating the first step in the classical component activation cascade in the context of an antibody-mediated response. In contrast, C4b is part of the C4-complex, which itself becomes activated through proteolytic cleavage by the C1-complex, thereby representing the second step in classical component activation (Kindt et al. 2007). Accordingly, the

proteins' upregulation in FA2H-KO mice points at a previously unknown involvement of aberrant neuroinflammatory processes in the pathogenesis of FA2H deficiency. Since no pathogens or autoimmune response are known to be involved in FA2H deficiency, this result was rather surprising. But there is an increase in research, documenting a antibody-independent activation of the complement system in other CNS-pathologies like Alzheimer's disease (Aiyaz et al. 2012; Shen et al. 2013) and brain or spinal cord injury (Qiao et al. 2006; Pasinetti et al. 1992). Remarkably, in Alzheimer's disease it seems that aggregating Aβ-itself binds and activates the C1-complex (Rogers et al. 1992), and there is also evidence showing the same for tau (Shen et al. 2001). As for the other candidates, C1q's expression was also evaluated by WB-analyses in myelin and whole brain. Besides the expected C1q-signal, the used antibody produced a strong additional and probably unspecific signal, which did not correspond to the proteins normal size. Therefore, the whole antibody might be unspecific, casting doubt on the quantification results. While a significant ~2-fold upregulation was observable in myelin, no significant change was measurable in the whole brain. Accordingly, C1q should be verified with another antibody to be sure of its upregulation. Alternatively, the expression of other complement factors could be examined to clarify the contribution of neuroinflammation to the pathology of FA2H deficiency. Moreover, in the myelin WB-analysis the measured change was only ~2-fold and thus substantially smaller than in the MS-analysis (~4-fold). Since the animals used in the WB were significantly older, the opposite result had been expected. Older animals should show at least a similar or even a higher degree of neuroinflammation. An explanation may be that the neuroinflammation is occurring in episodes, and thus the C1q-level is fluctuating over time.

In accordance with the upregulation of complement proteins, apolipoprotein E (ApoE) exhibited an increase (~2-fold) in FA2H-KO myelin as well. This protein, being the essential apolipoprotein of chylomicrons and very low-density lipoproteins, has been known and studied extensively regarding its role in cholesterol transport. In addition, by now it has been proven to play roles in neurodegenerative diseases like Alzheimer's disease (Kim et al. 2009; Kanekiyo et al. 2014). Likewise, ApoE is also involved in immunoregulation processes as has been shown in Alzheimer's, but also in other diseases like multiple sclerosis and Guillain-Barré syndrome (Zhang et al. 2011; Zhang et al. 2010). Intriguingly, ApoE seems to modulate microglial and macrophage activation by switching them from a pro- to an anti-inflammatory state (Baitsch et al. 2011). For the FA2H-KO mice the upregulation of ApoE therefore strengthens the observation that neuroinflammation was present in the diseased animals brains. Presumably, the organism tried to attenuate this neuroinflammation by increasing its ApoE amounts. Again, the upregulation of ApoE found in the mass spectrometric screening could also be verified by WB in whole brain and myelin. While a similar increase of ~2-fold could be measured and quantified in the whole brain, the myelin WB result allowed no quantitative evaluation. Nevertheless, because ApoE became visible with a strong protein signal in all four KO-

animals, but with a weak signal in only a single WT-animal, its upregulation in myelin of FA2H-KO mice was clearly verified.

Lastly, the mass spectrometric analysis also revealed the ~2-fold upregulation of the myelin membrane protein Opalin, for which only a small amount of information is available. Moreover, the upregulation could also be verified using quantitative WBs in myelin (~5-fold) and whole brain (~3-fold). Initially, Opalin, also called transmembrane protein 10 (Tmem10), was discovered in a chromosome locus associated with temporal lobe epilepsy and spastic paraplegia (Nobile et al. 2002). Later research revealed Opalin to be an oligodendrocyte specific transmembrane sialylglycoprotein, which starts being expressed during early myelination and becoming later mainly located in myelin paranodal loops. There it is speculated to have an intermembranous connective or signaling function (Aruga et al. 2007; Kippert et al. 2008; Golan et al. 2008; Yoshikawa et al. 2008). Furthermore, recent research results showed that it is largely found in mature oligodendrocytes, becoming expressed after the typical early myelin proteins MBP and MAG (Jiang et al. 2013). In the same article, the authors further showed that, Opalin was reduced in a hypomyelination mouse model. This is in line with an earlier publication, which revealed a reduced expression of Opalin and other major myelin proteins like myelin-associated glycoprotein (MAG) and myelin and lymphocyte protein (MAL) in a canine model of the lysosomal storage disease fucosidosis (Fletcher et al. 2011). On the contrary, in a Parkinson's disease related LRRK2-KO mouse model Opalin was found to be increased significantly (Dorval et al. 2014). Furthermore, my own results also showed an upregulation of Opalin in myelin and whole brain of FA2H-KO mice. Since Opalin may have a function in myelin stability maintenance, the upregulation could explain the long-term myelin instability caused by FA2H deficiency. Moreover, the higher amounts of Opalin in FA2H-KO myelin can be explained by different mechanisms. First, Opalins transport may be dependent on 2-OH sphingolipids. Since these lipids are missing in FA2H-KO mice, the protein may become mislocalized from its normal localization, the paranodes, to compact myelin. Potentially, the cells try to counteract this by producing higher amounts of the protein, thereby leading to an overall increase of Opalin in the whole brain. Alternatively, the transport of Opalin is not affected. Instead the protein's increase in myelin might reflect a stronger gene expression of Opalin. But to clarify this, further studies have to be conducted.

5.1.2 PNS-myelin

Besides CNS-myelin, PNS-myelin derived from the same animals was analyzed as well. While the protein composition of FA2H-KO PNS-myelin has not been investigated so far, the PNS-pathology observed in some very old (~18 month) mice argues for a systematic evaluation (Zöller et al. 2008). Thus, PNS-myelin was analyzed by the same analytical setup, leading to the identification of 1309

protein groups. This largely extended the currently known PNS-myelin proteome (550 PNS-myelin proteins (Patzig et al. 2011)) by ~160%. While at the first glance this number seems to be extensively large, one has to consider that the reference study was actually the first systematic mass spectrometry study conducted on PNS-myelin so far. Comparatively, in CNS-myelin the number of identifications was also increasing with every new publication, starting with about 100 in the 2004 publication by Taylor and colleagues (Taylor et al. 2004) and reaching ~1000 in the recent publication by Gopalakrishnan and colleagues (Gopalakrishnan et al. 2013). The reasons for this increase over time are the same discussed for the CNS-myelin above e.g. improved sample preparation and mass spectrometry instrumentation. But for the same reasons it also has to be assumed that a certain amount of the newly identified proteins are contaminants, becoming detactable by the more sensitive instruments. Nevertheless, a comparison of the 1309 identifications with the 550 previously reported identifications supported the validity of this study by showing a huge congruency. 387 (~70%) of the previously identified proteins were present in our study as well.

Afterwards, analogous to the CNS-myelin analysis, FA2H-KO/WT ratios were calculated for the three timepoints. Subsequently the protein groups were filtered in a way that only those remained, which exhibited at least two expression ratios at one timepoint. This reduced the protein list to 830 entries. Thereafter, significantly changed protein groups were calculated by one-sample t-tests, which resulted in a list of 95 protein groups being significantly changed at at least one timepoint. Interestingly, none of the major PNS-myelin proteins were part of the significant changes, except periaxin. Because of the mixed genetic background of the analyzed mice, it was unclear if periaxin was upregulated in 17-month-old FA2H-KO animals. Therefore, periaxin's expression status had to be additionaly clarified by WB. This analysis showed that periaxin, like the other major PNS-myelin proteins, was not significantly changed between WT and FA2H-KO animals.

Moreover, when considering all 95 significantly changed protein groups, most were not consistently changed. Overall, the majority of these changes were found in the 17-month-old animals, which is in line with the observed late on-set of the PNS-pathology. In addition, when looking at the average FA2H-KO/WT ratios regardless of their significance, the expression of many varied strongly between the three timepoints, indicating a high degree of biological variability. Still, a few protein groups might have been altered more constantly, having similar average expression ratios at more than one timepoint. Accordingly, about 20 protein groups existed, which were significantly changed exclusively at timepoint 13 or 17M, but had a second expression value at the other timepoint that was not significant. Therefore, to confirm these potential consistent changes, the experiment should be repeated with additional animals. Besides, complementary experiments, like WBs or immunofluorescence stainings, should be done as well. Furthermore, it has to be considered that

some protein alterations may manifest at late stages of the disease progression and thus cannot be measured in young animals. Consequently, the mass spectrometry screening should be also conducted with old animals starting at ~17 month of age. Likewise, it should be mentioned that the PNS-pathology in general is very variable between individual mice regarding onset and severity. From observations made in our group (not published), this seems to be particularly affected by the animals' genetic background. While many of the initially analyzed very old mixed-background (129Ola/C57BL/6) mice developed a progressing hindlimb paralysis, this was not the case for a small number of the animals backcrossed to a C57BL/6 background. Thus, it would be an option to selectively analyze only FA2H-KO mice, which have already developed the paralysis, to get clearer results.

Still, the potentially changed protein groups contained some promising proteins. Considering the upregulated protein groups the most interesting changes were upregulations of CD36 and galectin 3. CD36 is an integral plasma membrane scavenger receptor, which has been shown to bind various ligands, e.g. anionic phospholipids, collagen, oxidized low-density lipoproteins and thrombospondin. Moreover, it is involved in the binding and transport of long-chain fatty acids. Accordingly, it has been described to be involved in various processes, like angiogenesis, atherosclerosis, metabolism and immunity. For example, it has been shown to promote adipocyte differentiation (Christiaens et al. 2012). In this regard a captivating link exist to FA2H. In a cell culture model of adipocyte differentiation the siRNA-mediated knock-down of FA2H inhibited the differentiation and led to decreased levels of CD36 mRNA (Guo et al. 2010). Moreover, studies using CD36-KO mice have shown, that its presence on the surface of macrophage is important for the phagocytosis of degraded myelin after nerve injury (Eto et al. 2003). Thus, CD36-KO mice exhibited a delayed clearance of myelin debris, which in turn led to a delayed remyelination. As a consequence, the upregulation in PNS-myelin indicates, that the demyelination observed in FA2H-KO mice is potentially accompanied by myelin phagocytosis and remyelination.

The also upregulated lectin galectin 3 (Lgals3) is involved in similar processes. Galectin 3 binds to various oligosaccharide chains of glycosylated PM or extracellular matrix proteins. The protein has been shown to play an important role in inflammatory diseases. For example, galectin 3 is upregulated in experimental autoimmune encephalomyelitis and it's KO drastically reduces the disease severity (Jiang et al. 2009). Moreover, in the CNS it has been shown to promote oligodendrocyte differentiation, which is needed for myelination. Accordingly, Lgals3-KO mice showed signs of demyelination (Pasquini et al. 2011). In the PNS it has been shown to be upregulated in Schwann cells after PNS injury and inhibits the cells' proliferation (Gustavsson et al. 2007). Therefore, its upregulation in myelin of old FA2H-KO mice might represent similar processes.

Regarding the downregulated protein groups, the potentially most interesting one was prion protein (Prnp). Prion protein is a glycosylphosphatidylinositol-anchored membrane glycoprotein targeted to lipid rafts (Taylor et al. 2009). It can exist in different isoforms, most notably the normal cellular PrP^{C} and the misfolded and aggregating PrP^{SC}. The later is the disease-causing agent in so-called prion diseases, like Creutzfeldt-Jakob disease, bovine spongiform encephalopathis or scrapie (OMIM: 176640). The normal functions of Prp^{C} are still not completely understood, but it seems to be involved in a couple of processes e.g. iron uptake and homeostasis (Singh et al. 2009), neuronal development (Steele et al. 2006), synaptic plasticity (Laurén et al. 2009), and PNS myelin sheath maintenance (Bremer et al. 2010). Evidence for the last function came from studies with PrP^{C}-KO mice. The animals developed a chronic demyelinating polyneuropathy (CDP) in the PNS. Intriguingly, similar to FA2H-KO mice, the PrP^{C}-KO animals had a normal initial myelin development, but its long-term stability was impaired. Furthermore, CDP only occurred if the gene was deleted in neurons, but not in Schwann cells. This suggests that neuronal PrP^{C} is involved in the directed communication between axons and Schwann cells and this communication seems to be essential for maintaining myelin stability. Hence, the reduction of PrP^{C} in PNS-myelin of FA2H-KO mice may explain the long-term myelin instability. A possible mechanism could be that the loss of 2-OH sphingolipids from lipid rafts is interfering with PrP^{C}'s localization. But to clarify this assumption, further experiments are needed. First of all the mass spectrometry result should be confirmed by WB. Afterwards, a potential PrP^{C}-mislocalization could be confirmed by immunostainings in isolated nerves and cell culture models of FA2H deficiency.

Another downregulated protein group contained the small VCP/p97-interacting protein (Svip). Svip was initially identified as a cofactor of the ATPase VCP, which is an essential component of ER-associated degradation (ERAD) (Nagahama et al. 2003). Further studies showed that it functions as a negative regulator of ERAD (Ballar et al. 2007) and that its expression is largely restricted to the CNS and PNS, where it co-localizes with VCP in neuronal cell bodies (Wang et al. 2011). Intriguingly, recent findings showed that it is also localized to compact myelin independent of VCP (Wu et al. 2013). There it might be important for myelin compaction, because of certain structural characteristics similar to MBP, as the authors of this study suggested. As a consequence, it could be speculated that its reduction leads to the long-term myelin instability observed in FA2H-deficient mice.

5.1.3 Conclusion

In summary, the proteomic analysis of CNS- and PNS-myelin of FA2H-KO mice revealed some interesting protein changes, of which some may be essential in understanding the pathology of FA2H deficiency. In the CNS the most prominent ones were upregulations of C1qb, C4b, ApoE, GFAP and

tau, hinting at previously unknown roles of inflammation, astrogliosis and tau aggregation in the pathology of FA2H deficiency. Moreover, Opalin, a structural myelin membrane protein potentially involved in myelin stability maintenance, was also upregulated. Accordingly, it might account for the long-term myelin instability found in FA2H-KO mice, but this has to be verified by further experiments. In the PNS the analysis results were less consistent, but there was still evidence for some noteworthy protein changes. For example, CD36 and galectin 3 seem to be upregulated, which is indicative of processes like myelin debris clearance and remyelination. In addition, there seemed to be a reduction of PrP^C ans Svip in FA2H-KO myelin. Similar to Opalin in the CNS, both proteins may be been necessary for myelin stability and thus might explain the long-term PNS-myelin instability.

5.2 Interaction partners of FA2H

The second part of this thesis focused on the discovery of protein interactions partners of mFA2H. Identifying them might give insights into the regulation of sphingolipid metabolism and possibly the pathology of FA2H deficiency, which may not only be caused by loss of 2-OH sphingolipids synthesis, but the loss of certain protein interactions of FA2H. Evidence for this assumption is given by the observation that some FA2H mutations found in SPG35 patients retained high or WT-levels of FA2H activity (Dick et al. 2010; Kruer et al. 2010). For the discovery of interaction partners two types of affinity tag-based Co-IP experiments were done in combination with quantitative mass spectrometry. The two affinity systems used were the Twin-StrepTag-StrepTactin system and the BioID-system. In the first system interactors were directly co-purified with recombinantly expressed Twin-Strep-mFA2H. In contrast, in the second system a fusion protein of a biotin-ligase and mFA2H was expressed, leading to the biotinylation of proteins proximal to FA2H. These were then purified using biotin-specific NeutrAvidin-affinity purification. Furthermore, quantitative mass spectrometry, using SILAC-labeling, was included to reduce the number of false interaction partner identifications, caused by proteins unspecifically bound to the affinity-matrix material.

5.2.1 Initial detection of FA2H-containing protein complexes

In the beginning, mFA2H was cloned into expression vectors for both systems. Afterwards, the expression of constructs and functionality of both systems could be verified in initial experiments using immortalized human cell lines (HeLa and HEK293-T). These cell lines were chosen, because they allow the efficient transfection of large cell numbers needed for the affinity purification process and thus have been often used in similar studies. Since FA2H is highly conserved between human and mouse, with the murine enzyme being active in human cells, this should not reduce validity of the Co-IP experiments. At the next step, the presence of a FA2H-containing complex was tested by BlueNative PAGE and PFA-crosslinking in conjunction with anti-StrepTag-WB, using Twin-Strep-mFA2H transiently expressed in HEK293-T cells. The BlueNative PAGE showed the presence of three FA2H-containing complexes of ~80, ~750 – 900 and >1000 kDa. The PFA-crosslinking experiments revealed four major complexes at ~60, ~80 and two more at >170 kDa. Whether these two were the same as the ones seen in the BlueNative experiment could not be determined. In a follow up experiment, showing the applicability of StrepTactin-affinity purification after PFA-crosslinking, only the ~60 and ~80 kDa complexes were still visible in the eluate. Interestingly, the 80 kDa signal might resemble FA2H homodimers, since FA2H itself has a molecular weight of about 40 kDa. Potentially, such a dimerization could be a prerequisite for FA2H to be fully functional, as it is for example the case for CerS-enzymes (Laviad et al. 2012). Thus, additional experiments should be done to clarify the identity of the 80 kDa signal. In summary, the results showed that only the relatively small complexes containing crosslinked FA2H could be enriched by affinity purification. Following this initial

experiments, the affinity tag-based SILAC Co-IP experiments including mass spectrometric analyzes were conducted.

5.2.2 Identification of FA2H interacting proteins by mass spectrometry

The first attempt of identifying interaction partners of FA2H after StrepTactin-affinity purification did only lead to the identification of a few co-purified proteins. While FA2H itself was significantly enriched, thereby proving a successful and efficient SILAC-IP, only two other protein groups showed a significant co-purification. The proteins corresponding to the groups were components of the proteasome (PSMD2; PSMC6). Even when lowering the threshold for a significant enrichment, the majority of groups (45%) contained manly other proteins related to protein quality control processes, for example chaperones, ubiquitin, ubiquitin ligases etc. This indicated that the overexpression of FA2H was probably too strong. Since the ER's capacity is limited, probably the majority of the transiently expressed FA2H was targeted and processed by the ER-associated protein degradation (ERAD) machinery.

In parallel, the same experiment was conducted with the inclusion of a PFA-crosslinking step to strengthen weak interactions normally lost during sample processing and possibly also capture transient interactions. This enlarged the number of significantly enriched protein groups to 125. Manual inspection and an automated GO-term enrichment analysis revealed, that many of the enriched proteins had a putative ER and/or membrane localization. Since FA2H itself is an ER protein, its interaction partners are expected to be ER or ER-associated proteins. In addition, the GO analysis also proved an enrichment of Golgi apparatus-related protein groups, but since the ER and the Golgi apparatus are closely linked, with many proteins shuttling between both compartments, this was not unexpected. Regarding protein function, many of the 125 protein groups were again linked to protein quality control processes, but their amount in regard to all identifications was only ~20%. In detail, components of the protein folding system as well as the ERAD machinery (Christianson et al. 2012) were present. Significantly enriched ERAD subcompenents for example were: EMC2, which is part of the ER membrane complex, ERLIN1 and ERLIN2, which are involved in ubiquitin ligation and VCP, which is needed for the extraction of proteins from the ER. Overall, this result was not surprising, since the expression conditions of FA2H were not different from the ones used in the other experiment. Nonetheless, now additional protein groups, mainly associated with cellular transport and lipid metabolism, were identified as FA2H interaction partners as well. The cellular transport processes included direct protein transport as well as general vesicular transport processes. In detail, these were parts of the ribosome-ER protein translocation complex, like ribosomal structural components (RPL7, RPL13 and RPL14) or the signal recognition particle receptor B (SRPRB). Since newly synthesized FA2H had to be inserted into the ER, finding such interaction partners was not

surprising. In addition, many protein groups involved in vesicular transport, for example RAB-proteins (RAB7A, RAB5C), SNARE-proteins (SEC22B, SEC23A), a vesicle-fusing ATPase (NSF) and a coatomer subunit (COPA), were present. However, because some are highly abundant ER-proteins, it cannot be excluded that some were just randomly crosslinked to FA2H and thus not real interaction partners. Last but not least, a significant number of enriched protein groups was linked to lipid metabolism. Among these were protein groups involved in fatty acid (PTPLAD1, ALDH3A2, ACSL3), phospholipid (PLD3), sphingolipid (SPTLC1 and SPTLC2), as well as cholesterol metabolism (HSD17B12, HSD17B7, DHCR7, NSDHL, LBR). Others are responsible for lipid transport processes (VAPA, VAPB, OSBPL8, SLC27A4) and the regulation of lipid metabolism (SACM1L). Furthermore, two reductases, shown to be involved in lipid metabolism (POR, CYB5R3), and the cytochrome b5 ($cytb_5$)-containing proteins PGRMC1 and PGRMC2, which are implicated in regulating the activities of various metabolic enzymes, were present.

Although the inclusion of PFA-crosslinking allowed the identification of more and other than just protein quality control-related FA2H interaction partners, both experiments were repeated with a stable cell line. According to the literature (Gibson et al. 2013), stable cell lines, expressing the gene of interest at near-physiological levels, should be chosen in favour of transient transfected ones, because overexpression can cause various unwanted effects. Normally, the amount of a protein in different complexes within a cell is tightly regulated and balanced. Large amounts of a protein may perturb stoichiometric balances within complexes, lead to wrong cellular localization, induce unspecific non-natural occurring interactions and cause protein misfolding and aggregation. Furthermore, transient transfections often show a high variance in efficiency between experiments. Last but not least, the expression of FA2H at lower levels might allow for the identification of less abundant proteins, which may have been lost due to a displacement by quality control proteins. Besides the mode of transfection, the experimental sample processing was also slightly altered by performing the sample mixing step of control and Twin-Strep-mFA2H samples after the affinity-purification step. The intention for this was to prevent protein exchanges between complexes from differentially labeled cells. Such exchanges can lead to the loss of high H/L-ratios, thereby making some interaction partners undetectable.

When looking at the results of the Co-IP of stably expressed Twin-Strep-mFA2H without crosslinking, only a small number (27) of the total number of identified protein groups was significantly enriched including FA2H. Nevertheless, these were substantially more compared to the experiment with transiently transfected cells. GO-term enrichment analysis showed that they were largely related to endocytosis processes and the regulation of protein complex assembly. For example, vesicular adaptor proteins (AP2A2, AP2S1), a motor protein (MYO1E), a membrane-curvature inducing protein

(EPN1) and parts of the actin-polymerization machinery co-purified (ARPC1A, ARPC2, ARPC3) were present, which are known to facilitate vesicular budding processes. The identification of such proteins very likely reflects FA2H transport between the ER and early Golgi system. As an ER-membrane protein, FA2H is also partly transported to the early Golgi apparatus. From there it is transported back by retrograde transport processes, involving its C-terminal ER-retention signal. Besides the transport related protein goups, the sphingolipid metabolizing enzyme SPTLC1, previously identified in the Co-IP from transiently-transfected and PFA-crosslinked cells, was also identified as FA2H interaction partner. In addition, despite the use of stable transfection, 20% of all protein groups were still related to protein quality control. While this amount was drastically lower compared to the experiment with transiently transfected cells, it was of a similar magnitude as seen in the PFA-assisted pulldown experiment. This implied that the improvement described above was mainly caused by the postponement of the sample mixing step and likely not the mode of protein expression. Obviously, the expression of FA2H was still too high, thus causing the enzyme's degradation by the ERAD machinery.

Repeating the PFA-assisted Co-IP with stably expressed Twin-Strep-mFA2H led to the identification of 437 significantly enriched protein groups. Thus, with 1062 identifications in total, about 41% were putative interaction partners. Together with the observation, that only ~47% of the identified proteins were background proteins (log2 fold change between 0.58 and -0.58), compared to ~85% in the PFA-crosslinking experiment with transiently transfected cells, this pointed at an experimental error. Very likely, the stopping of the crosslinking reaction was incomplete, thereby resulting in excessive crosslinking. Accordingly, some of the potential interaction partners may just be false positive identifications and the results of this analysis should be interpreted with caution. But since this experiment was only intended to be a large screening approach and interesting interaction partners were later confirmed in detail by follow-up experiments, its results were still taken into account. Interestingly, they were quite similar to the results obtained with the transiently transfected and PFA-treated cells. First, the majority of the potential interaction partners had a known ER and/or Golgi apparatus localization, thereby suggesting the correct targeting of the bait protein. Second, GO-analyses again revealed an enrichment of protein groups related to cellular transport processes, like protein, vesicular and ion transport. Third, proteins involved in lipid metabolism were present, with a strong focus on sphingolipid-related proteins. Fourth, the amount of significantly enriched protein quality control-related protein groups was again about 20%. As discussed above, this repeatedly proved that changing the mode of transfection had not led to the expected reduction in FA2H's degradation. Last, unlike before, the GO analysis proved the enrichment of protein groups linked to GTP-metabolism and small GTPase signaling. But inspecting them closely revealed that these were largely RAB-proteins facilitating cellular transport processes.

Obviously, while some of them were also identified in the assays before, their abundance was especially high in this experiment.

Using the BioID-method, 24 protein groups were significantly enriched. As expected, the highest enrichment was observed for the bait protein itself, thus proving its strong biotinylation by the fused biotin ligase. Moreover, manual inspection and GO-analyses showed that the majority of the identified protein groups had known ER and/or membrane-localization, again hinting at the correct targeting of the bait protein. Further, the enriched protein groups were largely linked to lipid, especially sphingolipid metabolism, but some were also associated with protein quality control processes. In detail, there was a significant enrichment of the sphingolipid metabolizing enzymes SMPD4 and SPTLC1, as well as lipid transport (VAPA/B) and fatty acid metabolizing enzymes (ALDH3A2). Moreover, LBR (Lamin B receptor), which has known cholesterol desaturase activity and PGRMC2, which, similar to its paralog PGRMC1, is implicated in the activity regulation of various metabolic enzymes (Wendler & Wehling 2013), were enriched as well.

5.2.3 Comparison of the FA2H interaction partner screening results

In summary, the different screening experiments allowed insights into the largely unknown protein-protein interaction network of mammalian FA2H. While the initial experiment with transiently expressed Twin-Step-mFA2H resulted only in the identification of a few interaction partners, all other experiments revealed significantly more. Many of these were either proteins involved in the same metabolic context as FA2H i.e. lipid metabolism, or in cellular transport processes. In addition, because FA2H was probably present in larger amounts than under physiological conditions, there was a significant amount (~20%) of protein quality control related proteins identified as well. Consequently, the expression level of FA2H should be further lowered to a near-physiological level by changing the transfection method. Methods to achieve such a near-physiological expression are for example possible by bacterial artificial chromosome transfection or direct genetical manipulation methods (CRISPR/Cas9-system, TALE-system, ...). Alternatively, an antibody has to be generated, which is capable of precipitating endogenous FA2H, thereby omitting the need for any kind of cellular manipulation.

Nevertheless, some interesting and likely FA2H interaction partner candidates were identified. Of these, especially the ones found multiple times had a higher probability to be true interactors. Therefore, a comparison of the three experiments with the most interaction partners, both PFA-assisted and the BioID-experiment, was conducted. The comparison showed 16 protein groups besides FA2H itself, which were constantly significantly enriched. Furthermore, there were 81 protein groups shared between two experiments only. Not surprisingly, as seen in each individual assay, many of these are linked to the same biological process FA2H is involved in i.e. lipid

metabolism. Thus, a selection of the most interesting interaction partners, identified in 2 or more screenings, are discussed in more detail below. It should be noted, that not all these have to interact functionaly with FA2H, because for some proteins the interaction may only be physical.

Most notably, the serine palmitoyl transferases 1 and 2 (SPTLC1 and SPTLC2) were identified repeatedly, which are the essential components of the serine palmitoyl transferase (SPT) complex. Importantly, SPTLC1 was also identified by SILAC-IP without PFA-crosslinking. This suggested that the interaction with FA2H is first relatively strong, and second not an artifact of unspecific protein crosslinking. The SPT-complex catalyzes the first step of sphingolipid synthesis (Hornemann et al. 2007). This is especially interesting, because the product of this reaction, dihydrosphingosine, and the product of FA2H, 2-OH fatty acids, are used by ceramide synthases (CerS) to form ceramides (Mizutani et al. 2008). Intriguingly, CerS2, specific for generating very long-chain ceramides, was also identified in one screening assay. In addition, the repeatedly discovered acyl-CoA synthetase long-chain 3 (ACSL3) also fits into this process, because CerS-enzymes need activated fatty acids as substrates. Hence, the interaction of ACSL3 and FA2H potentially ensures that alpha-hydroxylated fatty acids are directly activated after synthesis and thus efficiently incorporated into sphingolipids. Excitingly, the fatty acid elongase ELOVL5, which is involved in the generation of long and very long fatty acids (Leonard et al. 2000), was also discovered once. Taken together, these findings hint at a functional coupling of the proteins involved in the early steps of 2-OH sphingolipid synthesis, possibly allowing an efficient substrate transfer and interregulation of the enzymes involved.

Likewise, there were other identified proteins, which are known to be involved in additional areas of sphingolipid metabolism. One has to keep in mind that it is not clear, if all of them are truly direct interaction partners of FA2H. Since many proteins are part of relatively large protein complexes, some interactions may just be indirect. One such protein was aldehyde dehydrogenase 3A2 (ALDH3A2), which links sphingolipid synthesis to sphingolipid degradation (Nakahara et al. 2012). The enzyme catalyzes the oxidation of hexadecenal to hexadecenoic acid, which is generated during breakdown of sphingosine 1-phosphate (S1P) by S1P-lyase. Hexadecenoic acid is then further converted to palmitoyl-CoA involving an activation step by ACSL-enzymes. The generated palmitoyl-CoA could subsequently be reused, for example by the SPT-complex. Since ALDH3A2 works on a sphingolipid degradation product, whose N-linked fatty acid chain has been removed already, a direct functional relationship with FA2H seems unlikely. Presumably ALDH3A2 is rather associated with ACSL-enzymes, and thus was co-purified with them. Similarly, the repeatedly identified sphingomyelin phosphodiesterase 4 (SMPD4), which hydrolyses sphingomyelin to ceramide and phosphocholine, may have been soley co-purified because of an interaction with CerS-enzymes.

Other identified interactors, like vesicle-associated membrane protein-associated proteins A and B (VAPA/B) and oxysterol binding protein-like 8 (OSBPL8), are involved in lipid transport processes and the interplay between cholesterol and sphingolipid metabolism. The ER-resident proteins VAPA/B facilitate ER-Golgi trafficking of proteins, but also non-vesicular lipid transport. The later process is thought to be achieved by recruiting transport proteins like CERT and OSBPs to VAPs via a specific FFAT-peptide motif present in both protein types (Hanada et al. 2007; Raychaudhuri & Prinz 2010). While CERT is responsible for sphingolipid intermembrane transfer, OSBPs probably facilitate sterol transport processes. In addition, OSBP seems to be able to facilitate CERTs binding to VAP, thereby activating ceramide transfer from ER to the Golgi apparatus and finally leading to an upregulation of sphingomyelin synthesis (Perry & Ridgway 2006). Surprisingly, the OSBP found as potential FA2H interaction partner, OSBPL8, misses the FFAT-motif needed for VAP-binding. One could therefore speculate that this interaction represents a previously unknown direct linkage between 2-OH sphingolipid synthesis and sterol metabolism. Intriguingly, evidence for a co-regulation between both pathways has already been discovered in the analyses of yeast mutants (Swain et al. 2002; Guan et al. 2009). Alternatively, these interactions might be less specific than assumed, since VAPA, VAPB and OSBPL8 have recently been identified as parts of the mammalian ERAD network (Christianson et al. 2012). Therefore, finding them in a complex with FA2H may solely be caused by the enzyme's overexpression.

The potential interaction partner, SACM1L, is a known regulator of sphingolipid synthesis. This protein is called suppressor of actin mutations 1-like protein (SACM1L) after its initially discovered yeast homolog SAC1. It is a phosphoinositide phosphatase that primarily dephosphorylates phosphatidylinositol 4-phosphate (PI4P), the predominant phosphoinositide of the Golgi apparatus (Hughes et al. 2000; Foti et al. 2001). In yeast it has been shown to be part of the SPOTS-complex, whose other major components are the yeast serine palmitoyltransferase (LCB1 and 2), the regulatory Orm proteins (ORM1 and ORM2), the accessory protein TSC3 and SAC1 (Breslow et al. 2010). Remarkably, the Orm proteins and SAC1 both seem to negatively regulate serine palmitoyltransferase. This was shown in yeast mutant of both protein types, which exhibited a significant increase in cellular sphingoid base amounts (Breslow et al. 2010). Also interesting is the fact, that SACM1L's substrate PI4P further presents a link to the regulation of lipid transport processes. This is the case, because lipid transport proteins like CERT, FAPP2 and most OSBPs contain a PI4P-binding pleckstrin homology (PH) domain, which targets them to the Golgi apparatus (Breslow & Weissman 2010). But how SACM1L, which is an ER-membrane protein, acts on the mainly Golgi-localized PI4P is still an open question. Attractively, there is also evidence for a functional relationship between yeast FA2H (SCS7) and SACM1L , as shown by Tani and Kuge (Tani & Kuge

2010). Obviously, yeast double-deficient for SCS7 and SAC1, but not for SAC1 alone, exhibit a severe growth defect.

The two endoplasmatic-localized oxidoreductases, cytochrome b5 reductase 3 (CYB5R3) and NADPH-cytochrome P450 reductase (POR), were also identified. Both are responsible for the transfer of electrons from reduction equivalents, NADH (CYB5R3) or NADPH (POR), to metabolic enzymes. CYB5R3, as it name implies, reduces $cytb_5$ and $cytb_5$-domain containing proteins. POR, in contrast, transfers electrons mainly to P450 enzymes, but it can also supply them to heme oxygenases and $cytb_5$. Interestingly, POR is also the reductase used in in-vitro fatty acid 2-hydroxylation assays (Alderson et al. 2004; Alderson et al. 2005). Since FA2H needs a supply of electrons for hydroxylating fatty acids, identifying both in the interaction partner screenings strengthens the validity of the assays functionality.

Two other enzymes, identified as potential FA2H interaction partners, were the highly sequence-homologous membrane-associated progesterone receptor component 1 and 2 (PGRMC1 and PGRMC2). Both proteins contain a $cytb_5$ heme-binding domain similar to FA2H's. Furthermore, there is a large amount of research, proving that PGRMC1 binds and regulates the activity of various cytochrome P450, including sterol synthesizing, enzymes (Hughes et al. 2007; Debose-Boyd 2007). Interestingly, the regulation can be negative and positive depending on the respective binding-partner. Taken together, this hints at a potential regulatory interaction between FA2H and the PGRMC proteins. In addition, PGRMC1 is also involved in other processes, like tumor growth regulation (Peluso, Liu, et al. 2008; Crudden et al. 2005; Ahmed et al. 2010) and progesterone signaling (Meyer et al. 1996; Peluso, Romak, et al. 2008). Moreover, PGRMC1 has been shown to interact with insulin-induced gene 1 protein (Insig1) and sterol regulatory element-binding protein cleavage-activating protein (SCAP), important regulators of cholesterol homeostasis (Suchanek et al. 2005). Stimulatingly, Insig1 has just lately been shown to facilitate ERAD of the sphingolipid synthesizing enzyme CGalT in collaboration with the sigma-1 receptor chaperone (Sig-1R) in a sterol-dependent matter (Hayashi et al. 2012) to regulate the cellular enzyme-amount. Together with the observation that PGRMC1 has been proven to be the elusive sigma-2 receptor, this strongly argues for a similar ERAD-function of PGRMC1 (Xu et al. 2011). Regarding the interaction with FA2H, this opens the possibility that PGRMC1 negatively regulates FA2H's activity by inducing the protein's degradation. But this remains to be proven experimentally. Moreover, it also hints at a close cross-regulation between sterol and sphingolipid metabolism. Considering PGRMC2, much less is known so far, but recent research showed that it shares PGRMC1's binding to cytochrome enzymes (Albrecht et al. 2012) and therefore may have similar regulatory function. Fittingly, it was recently identified as

part of the mammalian ERAD system in a complex systematic approach combining proteomics, functional genomics and transcriptional data (Christianson et al. 2012).

In regard to the ERAD system, two other of its components, ER lipid raft associated 1 and 2 (ERLIN1 and ERLIN2), were identified as well. While ERLIN1 was identified in two screenings, ERLIN2 was just identified once. Henceforth, they were initially dismissed as specific FA2H interaction partners. While their association with FA2H may solely be an artifact of FA2H's overexpression, the fact that mutations in both genes can cause hereditary spastic paraplegias (ERLIN1 ➔ SPG18; ERLIN2 ➔ SPG62) hints at a more specific connection. Functionally, both proteins form a complex with various target proteins, thereby initializing their degradation by the ERAD pathway (Pearce et al. 2009; Jo et al. 2011; Christianson et al. 2012). Intriguingly, they also seem to interact with and regulate proteins of the cholesterol-sensing machinery, like Insig1, SCAP and sterol regulatory element binding protein (SREBP). Moreover, it was shown that both ERLINs also interact directly with cholesterol (Huber et al. 2013). In summary, analogous to PGRMC1 and PGRMC2, FA2H's interaction with ERLIN1 and ERLIN2 suggests, that FA2H and thus 2-OH sphingolipid synthesis may be negatively regulated by the ERAD system. In addition, it seems to be closely linked to cholesterol metabolism, which apparently is regulated by the same protein degradation machinery. In this regard it could be speculated that the spastic paraplegias, linked to mutations in both ERLIN-genes, are potentially caused by the loss of FA2H's protein level regulation.

5.2.4 Verification of FA2H interaction partners by Western blot and bimolecular fluorescence complementation

To confirm some of the discovered potential interaction partners, the interactions of FA2H with ACSL3, ALDH3A2, CerS2, SACM1L, SPTLC1 and PGRMC1 were afterwards tested by Co-IP + WB and/or BiFC experiments. PGRMC1, ACSL3 and SPTLC1 could be verified as FA2H-interactors by Co-IP + WB (including PFA-crosslinking). In contrast, ALDH3A2 and SACM1L could not, because the antibodies used seemed not be specific. Therefore, the assays should be repeated with different antibodies. In addition, both assays should then further be conducted with the stable cell line, to exclude potential overexpression artifacts affecting the WB. Regarding BiFC, the interactions of FA2H with PGRMC1, SPTLC1 and CerS2 could be confirmed also in living cells. Additionally, BiFC competition experiments, employing co-expressed untagged versions of the interaction partners as competitors, lend further credibility to the interactions of FA2H with PGRMC1 and with SPTLC1. Only the competition with untagged SPTLC1 was not successful and should be repeated with lower plasmid amounts, because the protein's overexpression caused massive cell death. In contrast, the ACSL3-FA2H interaction could not be validated with BiFC. This can be attributed to the fact that not all protein-protein interactions are accessible by BiFC-assays, because certain steric constraints can impair the formation

of functional fluorescent protein. In many cases this can be solved by varying the attachment site (N- or C-terminal) of the fluorescent fragments and trying all possible combinations of both putative interactions partners (Kerppola 2008). For ACSL3 this still led to no measurable BiFC-signal (data not shown). But since FA2H's termini are both located in the cytosol and ACSL3's N-terminus in the ER-lumen, not all interaction partner combinations could be experimentally tested using this approach. Furthermore, even if all combinations are available, steric constraints may still exist. In conclusion this generally emphasizes an inherent disadvantage of BiFC. While a positive BiFC-result is indicative of a protein-protein interaction, a negative result neither proves nor disproves it. An alternative explanation for the negative BiFC-results lies in the fact that some protein-protein interactions, identified with the used screening approaches, may be indirect, i.e. facilitated by an additional protein. Accordingly, the fluorescent fragments cannot come in the close contact needed for BiFC.

5.2.5 Conclusion

In summary, the conducted analysis revealed a substantial number of potential FA2H interaction partners of which many were linked to sphingolipid metabolism. Thus, a pathway diagram of sphingolipid metabolism can be generated, in which the identified proteins are highlighted in color. Moreover, proteins additionaly identified with another method (Co-IP + WB or BiFC), are indicated in bold (Figure 5-1). The pathway diagram shows that the majority of these interaction partners are either potentially involved in the alpha-hydroxylation of fatty acids, like the reductases POR or CYB5R3, or in other early steps of sphingolipid synthesis. The most notable identifications were subunits of the SPOTS-complex, which catalyzes the initial step of sphingolipid synthesis, ACSL3, which activates fatty acid chains, and CerS2, which incorporates fatty acyl-CoAs into sphingolipids. Therefore, it seems, that the early sphingolipid synthesizing enzymes are part of a multiprotein complex, implying a tight coupling of the enzymatic reactions. Accordingly, products of one enzymatic reaction can be easily transported from one enzyme to the next, allowing a very efficient and potentially fast synthesis of sphingolipids. In addition, the coupling also opens up the possibility of efficient interregulation between the different synthesis steps.

Interestingly, SMPD4 and ALDH3A2 were also identified, which might suggest that sphingolipid synthesis and degradation are closely linked, thereby open up the possibility of interregulation between both pathways. Furthermore, the identification of lipid transport proteins, like VAPA, VAPB and OSBBPL, connects sphingolipid metabolism and lipid transport. Last but not least, PGRMC1 and PGRMC2 were repeatedly identified. So far, both proteins have not been connected to sphingolipid metabolism, but since they are known to regulate the activity of various enzymes, they might are regulators of FA2H's activity.

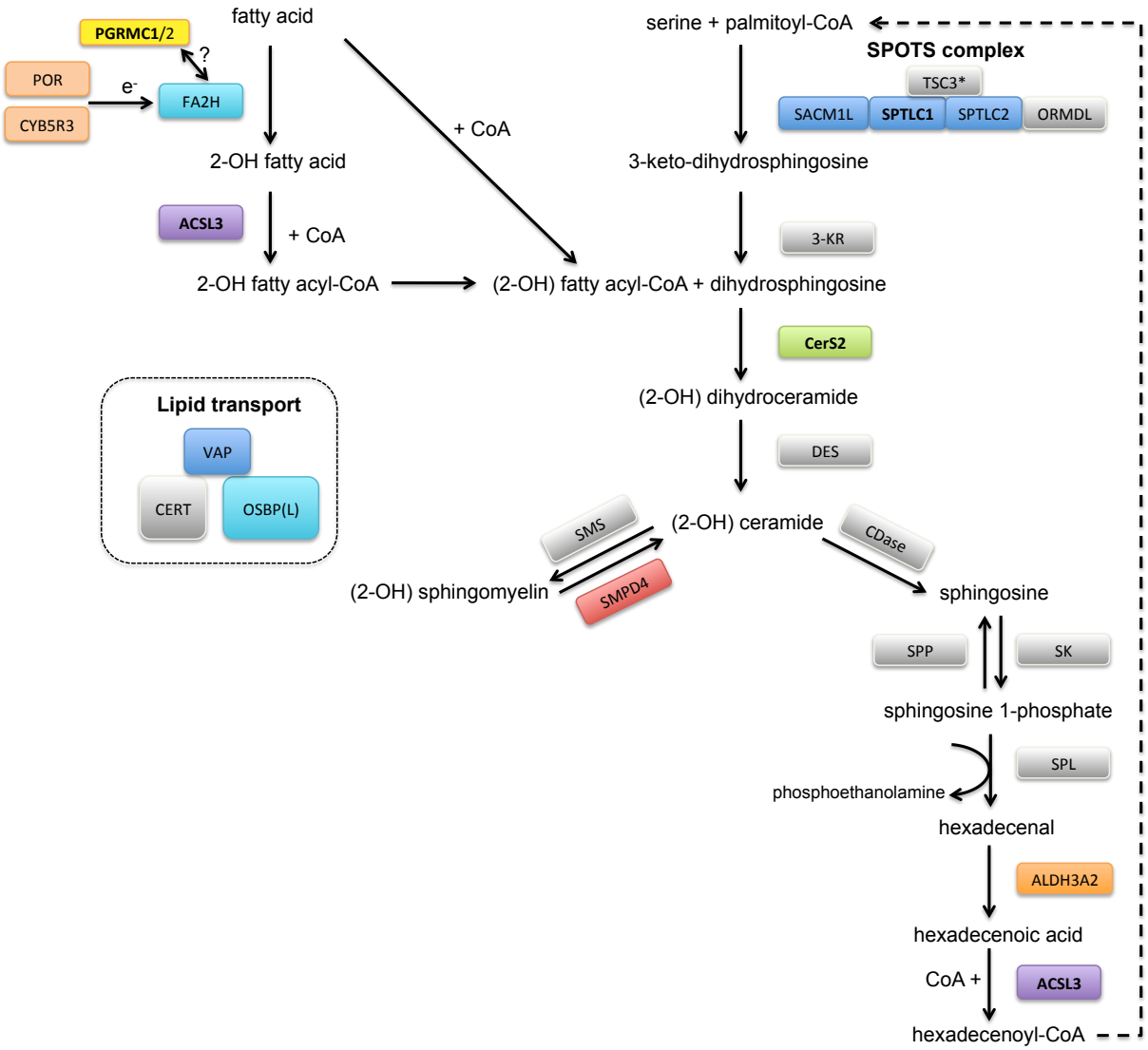

Figure 5-1: Discovered putative FA2H interaction partners and their position in sphingolipid metabolism. Colored boxes highlight proteins discovered in screenings as potential FA2H interaction partners, while all other important proteins are depicted in grey boxes. Proteins verified in another assay besides mass spectrometry (WB, BiFC) are highlighted in bold. 3-KR = 3-keto-dihydrosphingosine reductase; ACSL3 = acyl-CoA synthetase long-chain 3; ALDH3A2 = aldehyde dehydrogenase 3 A2; CerS2 = ceramide synthase 2; CDase = ceramidase; CERT = ceramide transfer protein; CYB5R3 = cytochrome b5 reductase 3; DES = desaturase; FA2H = fatty acid 2-hydroxylase; OSBP(L) = oxysterol binding protein like; PGRMC1/2 = progesterone receptor membrane component 1/2; SK = sphingosine kinase; SACM1L = suppressor of actin mutations 1-like (*S. cerevisiae*); SMS = sphingomyelin synthase; SMPD4 = sphingomyelin phosphodiesterase 4; SPL = sphingosine 1-phosphate lyase; SPOTS = SPTLC, Orm1/2, Tsc3, Sac1; SPP = sphingosine 1-phosphate phosphatase; SPTLC1/2 = serine palmitoyltransferase 1/2; TSC3 = temperature-sensitive CSG2 supressor (*S. cerevisiae*) (existence of human homolog in SPOTS-complex unknown); ORMDL = Orm1-like (*S. cerevisiae*); POR = NADPH-cytochrome P450 reductase; VAP = vesicle-associated membrane protein (consists of VAPA and VAPB).

6 References

Ahmed, I.S., Rohe, H.J., Twist, K.E., Mattingly, M.N. & Craven, R.J., 2010. Progesterone Receptor Membrane Component 1 (Pgrmc1): A Heme-1 Domain Protein That Promotes Tumorigenesis and Is Inhibited by a Small Molecule. *The Journal of Pharmacology and Experimental Therapeutics*, 333(2), pp.564–73.

Aiyaz, M., Lupton, M.K., Proitsi, P., Powell, J.F. & Lovestone, S., 2012. Complement activation as a biomarker for Alzheimer's disease. *Immunobiology*, 217(2), pp.204–15.

Albrecht, C., Huck, V., Wehling, M. & Wendler, A., 2012. In vitro inhibition of SKOV-3 cell migration as a distinctive feature of progesterone receptor membrane component type 2 versus type 1. *Steroids*, 77(14), pp.1543–50.

Alderson, N.L. & Hama, H., 2009. Fatty acid 2-hydroxylase regulates cAMP-induced cell cycle exit in D6P2T schwannoma cells. *Journal of Lipid Research*, 50(6), pp.1203–8.

Alderson, N.L., Rembiesa, B.M., Walla, M.D., Bielawska, A., Bielawski, J. & Hama, H., 2004. The human FA2H gene encodes a fatty acid 2-hydroxylase. *The Journal of Biological Chemistry*, 279(47), pp.48562–8.

Alderson, N.L., Walla, M.D. & Hama, H., 2005. A novel method for the measurement of in vitro fatty acid 2-hydroxylase activity by gas chromatography-mass spectrometry. *Journal of Lipid Research*, 46(7), pp.1569–75.

Arana, L., Gangoiti, P., Ouro, A., Trueba, M. & Gómez-Muñoz, A., 2010. Ceramide and ceramide 1-phosphate in health and disease. *Lipids in Health and Disease*, 9(1), p.15.

Aruga, J., Yoshikawa, F., Nozaki, Y., Sakaki, Y., Toyoda, A. & Furuichi, T., 2007. An oligodendrocyte enhancer in a phylogenetically conserved intron region of the mammalian myelin gene Opalin. *Journal of Neurochemistry*, 102, pp.1533–1547.

Baitsch, D., Bock, H.H., Engel, T., Telgmann, R., Müller-Tidow, C., Varga, G., Bot, M., Herz, J., Robenek, H., von Eckardstein, A. & Nofer, J.-R., 2011. Apolipoprotein E induces antiinflammatory phenotype in macrophages. *Arteriosclerosis, Thrombosis, and Vascular Biology*, 31(5), pp.1160–8.

Ballabio, A. & Gieselmann, V., 2009. Lysosomal disorders: from storage to cellular damage. *Biochimica et Biophysica Acta*, 1793(4), pp.684–96.

Ballar, P., Zhong, Y., Nagahama, M., Tagaya, M., Shen, Y. & Fang, S., 2007. Identification of SVIP as an endogenous inhibitor of endoplasmic reticulum-associated degradation. *The Journal of Biological Chemistry*, 282(47), pp.33908–14.

Benjamini, Y. & Hochberg, Y., 1995. Controlling the False Discovery Rate: A Practical and Powerful Approach to Multiple Testing. *Journal of the Royal Statistical Society. Series B (Methodological)*, 57(1), pp.289–300.

Bligh, E.G. & Dyer, W.J., 1959. A rapid method of total lipid extraction and purification. *Canadian Journal of Biochemistry and Physiology*, 37(8), pp.911–917.

Bodennec, J., Koul, O., Aguado, I., Brichon, G., Zwingelstein, G. & Portoukalian, J., 2000. A procedure for fractionation of sphingolipid classes by solid-phase extraction on aminopropyl cartridges. *Journal of Lipid Research*, 41(9), pp.1524–1531.

Boggs, J.M., Koshy, K.M. & Rangaraj, G., 1988. Influence of structural modifications on the phase behavior of semi-synthetic cerebroside sulfate. *Biochimica et Biophysica Acta*, 938(3), pp.361–72.

Bremer, J., Baumann, F., Tiberi, C., Wessig, C., Fischer, H., Schwarz, P., Steele, A.D., Toyka, K. V, Nave, K.-A., Weis, J. & Aguzzi, A., 2010. Axonal prion protein is required for peripheral myelin maintenance. *Nature Neuroscience*, 13(3), pp.310–8.

Breslow, D.K., Collins, S.R., Bodenmiller, B., Aebersold, R., Simons, K., Shevchenko, A., Ejsing, C.S. & Weissman, J.S., 2010. Orm family proteins mediate sphingolipid homeostasis. *Nature*, 463(7284), pp.1048–53.

Breslow, D.K. & Weissman, J.S., 2010. Membranes in balance: mechanisms of sphingolipid homeostasis. *Molecular Cell*, 40(2), pp.267–79.

Brewis, I.A. & Brennan, P., 2010. Proteomics technologies for the global identification and quantification of proteins. *Advances in Protein Chemistry and Structural Biology*, 80, pp.1–44.

Cao, L., Huang, X.-J., Chen, C.-J. & Chen, S.-D., 2013. A rare family with Hereditary Spastic Paraplegia Type 35 due to novel FA2H mutations: a case report with literature review. *Journal of the Neurological Sciences*, 329(1-2), pp.1–5.

Caroni, P. & Schwab, M.E., 1988. Two membrane protein fractions from rat central myelin with inhibitory properties for neurite growth and fibroblast spreading. *The Journal of Cell Biology*, 106(4), pp.1281–1288.

Christiaens, V., Van Hul, M., Lijnen, H.R. & Scroyen, I., 2012. CD36 promotes adipocyte differentiation and adipogenesis. *Biochimica et Biophysica Acta*, 1820(7), pp.949–56.

Christianson, J.C., Olzmann, J.A., Shaler, T.A., Sowa, M.E., Bennett, E.J., Richter, C.M., Tyler, R.E., Greenblatt, E.J., Harper, J.W. & Kopito, R.R., 2012. Defining human ERAD networks through an integrative mapping strategy. *Nature Cell Biology*, 14(1), pp.93–105.

Coetzee, T., Fujita, N., Dupree, J., Shi, R., Blight, A., Suzuki, K., Suzuki, K. & Popko, B., 1996. Myelination in the Absence of Galactocerebroside and Sulfatide: Normal Structure with Abnormal Function and Regional Instability. *Cell*, 86(2), pp.209–219.

Collard, J.F., Côté, F. & Julien, J.P., 1995. Defective axonal transport in a transgenic mouse model of amyotrophic lateral sclerosis. *Nature*, 375(6526), pp.61–4.

Cox, J. & Mann, M., 2012. 1D and 2D annotation enrichment: a statistical method integrating quantitative proteomics with complementary high-throughput data. *BMC Bioinformatics*, 13 Suppl 1(Suppl 16), p.S12.

Cox, J. & Mann, M., 2008. MaxQuant enables high peptide identification rates, individualized p.p.b.-range mass accuracies and proteome-wide protein quantification. *Nature Biotechnology*, 26(12), pp.1367–1372.

Cox, J., Neuhauser, N., Michalski, A., Scheltema, R. a, Olsen, J. V & Mann, M., 2011. Andromeda: a peptide search engine integrated into the MaxQuant environment. *Journal of Proteome Research*, 10(4), pp.1794–805.

Crudden, G., Loesel, R. & Craven, R.J., 2005. Overexpression of the cytochrome p450 activator hpr6 (heme-1 domain protein/human progesterone receptor) in tumors. *Tumour Biology*, 26(3), pp.142–6.

D'Angelo, G., Polishchuk, E., Di Tullio, G., Santoro, M., Di Campli, A., Godi, A., West, G., Bielawski, J., Chuang, C.-C., van der Spoel, A.C., Platt, F.M., Hannun, Y. a, Polishchuk, R., Mattjus, P. & De Matteis, M.A., 2007. Glycosphingolipid synthesis requires FAPP2 transfer of glucosylceramide. *Nature*, 449(7158), pp.62–7.

Debose-Boyd, R.A., 2007. A helping hand for cytochrome p450 enzymes. *Cell Metabolism*, 5(2), pp.81–3.

Dick, K.J., Al-Mjeni, R., Baskir, W., Koul, R., Simpson, M.A., Patton, M.A., Raeburn, S. & Crosby, A.H., 2008. A novel locus for an autosomal recessive hereditary spastic paraplegia (SPG35) maps to 16q21-q23. *Neurology*, 71(4), pp.248–52.

Dick, K.J., Eckhardt, M., Paisán-Ruiz, C., Alshehhi, A.A., Proukakis, C., Sibtain, N. a, Maier, H., Sharifi, R., Patton, M. a, Bashir, W., Koul, R., Raeburn, S., Gieselmann, V., Houlden, H. & Crosby, A.H., 2010. Mutation of FA2H underlies a complicated form of hereditary spastic paraplegia (SPG35). *Human Mutation*, 31(4), pp.E1251–60.

Donkervoort, S., Dastgir, J., Hu, Y., Zein, W.M., Marks, H., Blackstone, C. & Bönnemann, C.G., 2014. Phenotypic variability of a likely FA2H founder mutation in a family with complicated hereditary spastic paraplegia. *Clinical Genetics*, 85(4), pp.393–5.

Dorval, V., Mandemakers, W., Jolivette, F., Coudert, L., Mazroui, R., De Strooper, B. & Hébert, S.S., 2014. Gene and MicroRNA transcriptome analysis of Parkinson's related LRRK2 mouse models. *PloS ONE*, 9(1), p.e85510.

Dupree, J.L. & Pomicter, A.D., 2010. Myelin, DIGs, and membrane rafts in the central nervous system. *Prostaglandins & Other Lipid Mediators*, 91(3-4), pp.118–29.

Eckhardt, M., Yaghootfam, A., Fewou, S.N., Zöller, I. & Gieselmann, V., 2005. A mammalian fatty acid hydroxylase responsible for the formation of alpha-hydroxylated galactosylceramide in myelin. *The Biochemical Journal*, 388(Pt 1), pp.245–54.

Eden, E., Navon, R., Steinfeld, I., Lipson, D. & Yakhini, Z., 2009. GOrilla: a tool for discovery and visualization of enriched GO terms in ranked gene lists. *BMC Bioinformatics*, 10(1), p.48.

Edvardson, S., Hama, H., Shaag, A., Gomori, J.M., Berger, I., Soffer, D., Korman, S.H., Taustein, I., Saada, A. & Elpeleg, O., 2008. Mutations in the fatty acid 2-hydroxylase gene are associated with leukodystrophy with spastic paraparesis and dystonia. *American Journal of Human Genetics*, 83(5), pp.643–648.

Eikelenboom, P., Hack, C.E., Rozemuller, J.M. & Stam, F.C., 1989. Complement activation in amyloid plaques in Alzheimer's dementia. *Virchows Arch B Cell Pathol Incl Mol Pathol*, 56, pp.259–262.

Elder, G.A., Friedrich, V.L., Kang, C., Bosco, P., Gourov, A., Tu, P.H., Zhang, B., Lee, V.M. & Lazzarini, R.A., 1998. Requirement of heavy neurofilament subunit in the development of axons with large calibers. *The Journal of Cell Biology*, 143(1), pp.195–205.

Eng, L.F. & Ghirnikar, R.S., 1994. GFAP and astrogliosis. *Brain Pathology (Zurich, Switzerland)*, 4(3), pp.229–37.

Eto, M., Yoshikawa, H., Fujimura, H., Naba, I., Sumi-Akamaru, H., Takayasu, S., Itabe, H. & Sakoda, S., 2003. The role of CD36 in peripheral nerve remyelination after crush injury. *European Journal of Neuroscience*, 17(12), pp.2659–2666.

Fewou, S.N., Fernandes, A., Stockdale, K., Francone, V.P., Dupree, J.L., Rosenbluth, J., Pfeiffer, S.E. & Bansal, R., 2010. Myelin protein composition is altered in mice lacking either sulfated or both sulfated and non-sulfated galactolipids. *Journal of Neurochemistry*, 112(3), pp.599–610.

Fletcher, J.L., Kondagari, G.S., Wright, A.L., Thomson, P.C., Williamson, P. & Taylor, R.M., 2011. Myelin genes are downregulated in canine fucosidosis. *Biochimica et Biophysica Acta - Molecular Basis of Disease*, 1812, pp.1418–1426.

Foti, M., Audhya, A. & Emr, S.D., 2001. Sac1 lipid phosphatase and Stt4 phosphatidylinositol 4-kinase regulate a pool of phosphatidylinositol 4-phosphate that functions in the control of the actin cytoskeleton and vacuole morphology. *Molecular Biology of the Cell*, 12(8), pp.2396–411.

Foulon, V., Sniekers, M., Huysmans, E., Asselberghs, S., Mahieu, V., Mannaerts, G.P., Van Veldhoven, P.P. & Casteels, M., 2005. Breakdown of 2-hydroxylated straight chain fatty acids via peroxisomal 2-hydroxyphytanoyl-CoA lyase: a revised pathway for the alpha-oxidation of straight chain fatty acids. *The Journal of Biological Chemistry*, 280(11), pp.9802–12.

Garone, C., Pippucci, T., Cordelli, D.M., Zuntini, R., Castegnaro, G., Marconi, C., Graziano, C., Marchiani, V., Verrotti, A., Seri, M. & Franzoni, E., 2011. FA2H-related disorders: a novel c.270+3A>T splice-site mutation leads to a complex neurodegenerative phenotype. *Developmental Medicine and Child Neurology*, 53(10), pp.958–961.

Gibson, T.J., Seiler, M. & Veitia, R.A., 2013. The transience of transient overexpression. *Nature Methods*, 10(8), pp.715–21.

Gieselmann, V. & Krägeloh-Mann, I., 2010. Metachromatic leukodystrophy--an update. *Neuropediatrics*, 41(1), pp.1–6.

Golan, N., Adamsky, K., Kartvelishvily, E., Brockschnieder, D., Möbius, W., Spiegel, I., Roth, A.D., Thomson, C.E., Rechavi, G. & Peles, E., 2008. Identification of Tmem10/Opalin as an oligodendrocyte enriched gene using expression profiling combined with genetic cell ablation. *Glia*, 56(11), pp.1176–86.

Gopalakrishnan, G., Awasthi, A., Belkaid, W., De Faria, O., Liazoghli, D., Colman, D.R. & Dhaunchak, A.S., 2013. Lipidome and proteome map of myelin membranes. *Journal of Neuroscience Research*, 91(3), pp.321–34.

Guan, X.L., Souza, C.M., Pichler, H., Dewhurst, G., Schaad, O., Kajiwara, K., Wakabayashi, H., Ivanova, T., Castillon, G.A., Piccolis, M., Abe, F., Loewith, R., Funato, K., Wenk, M.R. & Riezman, H., 2009. Functional interactions between sphingolipids and sterols in biological membranes regulating cell physiology. *Molecular Biology of the Cell*, 20(7), pp.2083–95.

Guo, L., Zhou, D., Pryse, K.M., Okunade, A.L. & Su, X., 2010. Fatty acid 2-hydroxylase mediates diffusional mobility of Raft-associated lipids, GLUT4 level, and lipogenesis in 3T3-L1 adipocytes. *The Journal of Biological Chemistry*, 285(33), pp.25438–47.

Gustavsson, P., Linsmeier, C.E., Leffler, H. & Kanje, M., 2007. Galectin-3 inhibits Schwann cell proliferation in cultured sciatic nerve. *Neuroreport*, 18(7), pp.669–73.

Halter, D., Neumann, S., van Dijk, S.M., Wolthoorn, J., de Mazière, A.M., Vieira, O. V, Mattjus, P., Klumperman, J., van Meer, G. & Sprong, H., 2007. Pre- and post-Golgi translocation of glucosylceramide in glycosphingolipid synthesis. *The Journal of Cell Biology*, 179(1), pp.101–15.

Hama, H., 2010. Fatty acid 2-Hydroxylation in mammalian sphingolipid biology. *Biochimica et Biophysica Acta*, 1801(4), pp.405–14.

Hanada, K., 2003. Serine palmitoyltransferase, a key enzyme of sphingolipid metabolism. *Biochimica et Biophysica Acta*, 1632(1-3), pp.16–30.

Hanada, K., Kumagai, K., Tomishige, N. & Kawano, M., 2007. CERT and intracellular trafficking of ceramide. *Biochimica et Biophysica Acta*, 1771(6), pp.644–53.

Hanada, K., Kumagai, K., Yasuda, S., Miura, Y., Kawano, M., Fukasawa, M. & Nishijima, M., 2003. Molecular machinery for non-vesicular trafficking of ceramide. *Nature*, 426(6968), pp.803–9.

Haraguchi, T., Terada, S., Ishizu, H., Yokota, O., Yoshida, H., Takeda, N., Kishimoto, Y., Katayama, N., Takata, H., Akagi, M., Kuroda, S., Ihara, Y. & Uchitomi, Y., 2011. Coexistence of TDP-43 and tau pathology in neurodegeneration with brain iron accumulation type 1 (NBIA-1, formerly Hallervorden-Spatz syndrome). *Neuropathology : Official Journal of the Japanese Society of Neuropathology*, 31(5), pp.531–9.

Hartline, D. & Colman, D., 2007. Rapid conduction and the evolution of giant axons and myelinated fibers. *Current Biology*, 17(1), pp.29–35.

Hartline, D.K., 2008. What is myelin? *Neuron Glia Biology*, 4(2), pp.153–63.

Hayashi, T., Hayashi, E., Fujimoto, M., Sprong, H. & Su, T.-P., 2012. The lifetime of UDP-galactose:ceramide galactosyltransferase is controlled by a distinct endoplasmic reticulum-associated degradation (ERAD) regulated by sigma-1 receptor chaperones. *The Journal of Biological Chemistry*, 287(51), pp.43156–69.

Heukeshoven, J. & Dernick, R., 1986. Neue Ergebnisse zum Mechanismus der Silberfärbung. *B.J. Radla (Ed.), Elektrophorese Forum '86, Technische Universität, München*, pp.22–27.

Hornemann, T., Wei, Y. & von Eckardstein, A., 2007. Is the mammalian serine palmitoyltransferase a high-molecular-mass complex? *The Biochemical Journal*, 405(1), pp.157–64.

Huber, M.D., Vesely, P.W., Datta, K. & Gerace, L., 2013. Erlins restrict SREBP activation in the ER and regulate cellular cholesterol homeostasis. *The Journal of Cell Biology*, 203(3), pp.427–36.

Hughes, A.L., Powell, D.W., Bard, M., Eckstein, J., Barbuch, R., Link, A.J. & Espenshade, P.J., 2007. Dap1/PGRMC1 binds and regulates cytochrome P450 enzymes. *Cell Metabolism*, 5(2), pp.143–9.

Hughes, W.E., Woscholski, R., Cooke, F.T., Patrick, R.S., Dove, S.K., McDonald, N.Q. & Parker, P.J., 2000. SAC1 encodes a regulated lipid phosphoinositide phosphatase, defects in which can be suppressed by the homologous Inp52p and Inp53p phosphatases. *The Journal of Biological Chemistry*, 275(2), pp.801–8.

Huitema, K., van den Dikkenberg, J., Brouwers, J.F.H.M. & Holthuis, J.C.M., 2004. Identification of a family of animal sphingomyelin synthases. *The EMBO Journal*, 23(1), pp.33–44.

Jahn, O., Tenzer, S. & Werner, H.B., 2009. Myelin Proteomics: Molecular Anatomy of an Insulating Sheath. *Molecular Neurobiology*, 40(1), pp.55–72.

Jeckel, D., Karrenbauer, A., Burger, K.N., van Meer, G. & Wieland, F., 1992. Glucosylceramide is synthesized at the cytosolic surface of various Golgi subfractions. *The Journal of Cell Biology*, 117(2), pp.259–67.

Jiang, H.-R., Al Rasebi, Z., Mensah-Brown, E., Shahin, A., Xu, D., Goodyear, C.S., Fukada, S.Y., Liu, F.-T., Liew, F.Y. & Lukic, M.L., 2009. Galectin-3 deficiency reduces the severity of experimental autoimmune encephalomyelitis. *Journal of Immunology (Baltimore, Md. : 1950)*, 182(2), pp.1167–73.

Jiang, W., Yang, W., Yang, W., Zhang, J., Pang, D., Gan, L., Luo, L., Fan, Y., Liu, Y. & Chen, M., 2013. Identification of Tmem10 as a novel late-stage oligodendrocytes marker for detecting hypomyelination. *International Journal of Biological Sciences*, 10(1), pp.33–42.

Jo, Y., Sguigna, P. V & DeBose-Boyd, R.A., 2011. Membrane-associated ubiquitin ligase complex containing gp78 mediates sterol-accelerated degradation of 3-hydroxy-3-methylglutaryl-coenzyme A reductase. *The Journal of Biological Chemistry*, 286(17), pp.15022–31.

Kanekiyo, T., Xu, H. & Bu, G., 2014. ApoE and Aβ in Alzheimer's disease: accidental encounters or partners? *Neuron*, 81(4), pp.740–54.

Karimi-Abdolrezaee, S. & Billakanti, R., 2012. Reactive astrogliosis after spinal cord injury-beneficial and detrimental effects. *Molecular Neurobiology*, 46(2), pp.251–64.

Kerppola, T.K., 2008. Bimolecular fluorescence complementation (BiFC) analysis as a probe of protein interactions in living cells. *Annual Review of Biophysics*, 37, pp.465–87.

Kerppola, T.K., 2006. Design and implementation of bimolecular fluorescence complementation (BiFC) assays for the visualization of protein interactions in living cells. *Nature Protocols*, 1(3), pp.1278–86.

Kihara, A. & Igarashi, Y., 2004. FVT-1 is a mammalian 3-ketodihydrosphingosine reductase with an active site that faces the cytosolic side of the endoplasmic reticulum membrane. *The Journal of Biological Chemistry*, 279(47), pp.49243–50.

Kim, J., Basak, J.M. & Holtzman, D.M., 2009. The role of apolipoprotein E in Alzheimer's disease. *Neuron*, 63(3), pp.287–303.

Kindt, T.J., Goldsby, R.A. & Osborne, B.A., 2007. *Kuby Immunology* 6th ed., W. H. Freeman & Company.

Kippert, A., Trajkovic, K., Fitzner, D., Opitz, L. & Simons, M., 2008. Identification of Tmem10/Opalin as a novel marker for oligodendrocytes using gene expression profiling. *BMC Neuroscience*, 9, p.40.

Klockenbusch, C. & Kast, J., 2010. Optimization of Formaldehyde Cross-Linking for Protein Interaction Analysis of Non-Tagged Integrin 1. *Journal of Biomedicine and Biotechnology*, 2010.

Klugmann, M., Schwab, M.H., Pühlhofer, A., Schneider, A., Zimmermann, F., Griffiths, I.R. & Nave, K.-A., 1997. Assembly of CNS Myelin in the Absence of Proteolipid Protein. *Neuron*, 18(1), pp.59–70.

Kohlschütter, A., Bley, A., Brockmann, K., Gärtner, J., Krägeloh-Mann, I., Rolfs, A. & Schöls, L., 2010. Leukodystrophies and other genetic metabolic leukoencephalopathies in children and adults. *Brain & Development*, 32(2), pp.82–9.

Kota, V., Dhople, V.M., Fullbright, G., Smythe, N.M., Szulc, Z.M., Bielawska, A. & Hama, H., 2013. 2'-hydroxy c16-ceramide induces apoptosis-associated proteomic changes in c6 glioma cells. *Journal of Proteome Research*, 12(10), pp.4366–75.

Kruer, M.C., Paisán-Ruiz, C., Boddaert, N., Yoon, M.Y., Hama, H., Gregory, A., Malandrini, A., Woltjer, R.L., Munnich, A., Gobin, S., Polster, B.J., Palmeri, S., Edvardson, S., Hardy, J., Houlden, H. & Hayflick, S.J., 2010. Defective FA2H leads to a novel form of neurodegeneration with brain iron accumulation (NBIA). *Annals of Neurology*, 68(5), pp.611–8.

Kurz, A., May, C., Schmidt, O., Müller, T., Stephan, C., Meyer, H.E., Gispert, S., Auburger, G. & Marcus, K., 2012. A53T-alpha-synuclein-overexpression in the mouse nigrostriatal pathway leads to early increase of 14-3-3 epsilon and late increase of GFAP. *Journal of Neural Transmission (Vienna, Austria : 1996)*, 119(3), pp.297–312.

Kyogashima, M., Tadano-Aritomi, K., Aoyama, T., Yusa, A., Goto, Y., Tamiya-Koizumi, K., Ito, H., Murate, T., Kannagi, R. & Hara, A., 2008. Chemical and apoptotic properties of hydroxy-ceramides containing long-chain bases with unusual alkyl chain lengths. *The Journal of Biological Chemistry*, 144(1), pp.95–106.

Lambert, J.P., Ethier, M., Smith, J.C. & Figeys, D., 2005. Proteomics: From gel based to gel free. *Analytical Chemistry*, 77, pp.3771–3787.

Larocca, J.N. & Norton, W.T., 2007. Isolation of myelin. *Current Protocols in Cell Biology*, Chapter 3, p.Unit3.25.

Laurén, J., Gimbel, D.A., Nygaard, H.B., Gilbert, J.W. & Strittmatter, S.M., 2009. Cellular prion protein mediates impairment of synaptic plasticity by amyloid-beta oligomers. *Nature*, 457(7233), pp.1128–32.

Laviad, E.L., Kelly, S., Merrill, A.H. & Futerman, A.H., 2012. Modulation of ceramide synthase activity via dimerization. *The Journal of Biological Chemistry*, 287(25), pp.21025–33.

Lei, P., Ayton, S., Finkelstein, D.I., Spoerri, L., Ciccotosto, G.D., Wright, D.K., Wong, B.X.W., Adlard, P.A., Cherny, R.A., Lam, L.Q., Roberts, B.R., Volitakis, I., Egan, G.F., McLean, C.A., Cappai, R., Duce, J.A. & Bush, A.I., 2012. Tau deficiency induces parkinsonism with dementia by impairing APP-mediated iron export. *Nature Medicine*, 18(2), pp.291–5.

Leonard, A.E., Bobik, E.G., Dorado, J., Kroeger, P.E., Chuang, L.T., Thurmond, J.M., Parker-Barnes, J.M., Das, T., Huang, Y.S. & Mukerji, P., 2000. Cloning of a human cDNA encoding a novel enzyme involved in the elongation of long-chain polyunsaturated fatty acids. *The Biochemical Journal*, 350 Pt 3, pp.765–70.

Linker, R.A., Brechlin, P., Jesse, S., Steinacker, P., Lee, D.H., Asif, A.R., Jahn, O., Tumani, H., Gold, R. & Otto, M., 2009. Proteome Profiling in Murine Models of Multiple Sclerosis: Identification of Stage Specific Markers and Culprits for Tissue Damage. *PLoS ONE*, 4(10), p.e7624.

LoPresti, P., 2002. Regulation and differential expression of tau mRNA isoforms as oligodendrocytes mature in vivo: implications for myelination. *Glia*, 37(3), pp.250–7.

LoPresti, P., Szuchet, S., Papasozomenos, S.C., Zinkowski, R.P. & Binder, L.I., 1995. Functional implications for the microtubule-associated protein tau: localization in oligodendrocytes. *Proceedings of the National Academy of Sciences of the United States of America*, 92(22), pp.10369–73.

Maceyka, M., Harikumar, K.B., Milstien, S. & Spiegel, S., 2012. Sphingosine-1-phosphate signaling and its role in disease. *Trends in Cell Biology*, 22(1), pp.50–60.

Maier, H., Meixner, M., Hartmann, D., Sandhoff, R., Wang-Eckhardt, L., Zöller, I., Gieselmann, V. & Eckhardt, M., 2011. Normal fur development and sebum production depends on fatty acid 2-hydroxylase expression in sebaceous glands. *The Journal of Biological Chemistry*, 286(29), pp.25922–34.

Maldonado, E.N., Alderson, N.L., Monje, P. V, Wood, P.M. & Hama, H., 2008. FA2H is responsible for the formation of 2-hydroxy galactolipids in peripheral nervous system myelin. *Journal of Lipid Research*, 49(1), pp.153–61.

Mao, C. & Obeid, L.M., 2008. Ceramidases: regulators of cellular responses mediated by ceramide, sphingosine, and sphingosine-1-phosphate. *Biochimica et Biophysica Acta*, 1781(9), pp.424–34.

McAlister, G.C., Huttlin, E.L., Haas, W., Ting, L., Jedrychowski, M.P., Rogers, J.C., Kuhn, K., Pike, I., Grothe, R.A., Blethrow, J.D. & Gygi, S.P., 2012. Increasing the multiplexing capacity of TMTs using reporter ion isotopologues with isobaric masses. *Analytical Chemistry*, 84(17), pp.7469–78.

Meixner, M., 2009. Untersuchungen zur Funktion der alpha-hydroxylierten Sphingolipide im Nervensystem und in der Haut.

Meyer, C., Schmid, R., Scriba, P.C. & Wehling, M., 1996. Purification and partial sequencing of high-affinity progesterone-binding site(s) from porcine liver membranes. *European Journal of Biochemistry / FEBS*, 239(3), pp.726–31.

Mi, H., Muruganujan, A., Casagrande, J.T. & Thomas, P.D., 2013. Large-scale gene function analysis with the PANTHER classification system. *Nature Protocols*, 8(8), pp.1551–66.

Michel, C., van Echten-Deckert, G., Rother, J., Sandhoff, K., Wang, E. & Merrill, A.H., 1997. Characterization of ceramide synthesis. A dihydroceramide desaturase introduces the 4,5-trans-double bond of sphingosine at the level of dihydroceramide. *The Journal of Biological Chemistry*, 272(36), pp.22432–7.

Middeldorp, J. & Hol, E.M., 2011. GFAP in health and disease. *Progress in Neurobiology*, 93(3), pp.421–43.

Mizutani, Y., Kihara, A., Chiba, H., Tojo, H. & Igarashi, Y., 2008. 2-Hydroxy-ceramide synthesis by ceramide synthase family: enzymatic basis for the preference of FA chain length. *Journal of Lipid Research*, 49(11), pp.2356–64.

De Monasterio-Schrader, P., Jahn, O., Tenzer, S., Wichert, S.P., Patzig, J. & Werner, H.B., 2012. Systematic approaches to central nervous system myelin. *Cellular and Molecular Life Sciences*, 69(17), pp.2879–94.

Mullen, T.D., Hannun, Y.A. & Obeid, L.M., 2012. Ceramide synthases at the centre of sphingolipid metabolism and biology. *The Biochemical Journal*, 441(3), pp.789–802.

Nagahama, M., Suzuki, M., Hamada, Y., Hatsuzawa, K., Tani, K., Yamamoto, A. & Tagaya, M., 2003. SVIP is a novel VCP/p97-interacting protein whose expression causes cell vacuolation. *Molecular Biology of the Cell*, 14(1), pp.262–73.

Nagano, M., Ihara-Ohori, Y., Imai, H., Inada, N., Fujimoto, M., Tsutsumi, N., Uchimiya, H. & Kawai-Yamada, M., 2009. Functional association of cell death suppressor, Arabidopsis Bax inhibitor-1, with fatty acid 2-hydroxylation through cytochrome b. *The Plant Journal*, 1, pp.122–134.

Nagele, R.G., Wegiel, J., Venkataraman, V., Imaki, H., Wang, K.-C. & Wegiel, J., 2004. Contribution of glial cells to the development of amyloid plaques in Alzheimer's disease. *Neurobiology of Aging*, 25(5), pp.663–74.

Nakahara, K., Ohkuni, A., Kitamura, T., Abe, K., Naganuma, T., Ohno, Y., Zoeller, R. a & Kihara, A., 2012. The Sjögren-Larsson syndrome gene encodes a hexadecenal dehydrogenase of the sphingosine 1-phosphate degradation pathway. *Molecular Cell*, 46(4), pp.461–71.

National Library of Medicine, 2014. Niemann-Pick disease. Available at: http://ghr.nlm.nih.gov/condition/niemann-pick-disease [Accessed March 11, 2014].

Nobile, C. et al., 2002. Identification and characterization of a novel human brain-specific gene, homologous to S. scrofa tmp83.5, in the chromosome 10q24 critical region for temporal lobe epilepsy and spastic paraplegia. *Gene*, 282(1-2), pp.87–94.

Nyfeler, B., Michnick, S.W. & Hauri, H.-P., 2005. Capturing protein interactions in the secretory pathway of living cells. *Proceedings of the National Academy of Sciences of the United States of America*, 102(18), pp.6350–5.

Ong, S.-E., Blagoev, B., Kratchmarova, I., Kristensen, D.B., Steen, H., Pandey, A. & Mann, M., 2002. Stable isotope labeling by amino acids in cell culture, SILAC, as a simple and accurate approach to expression proteomics. *Molecular & Cellular Proteomics*, 1(5), pp.376–386.

Ong, S.-E. & Mann, M., 2005. Mass spectrometry-based proteomics turns quantitative. *Nature Chemical Biology*, 1(5), pp.252–262.

Pascher, I., 1976. Molecular arrangements in sphingolipids Conformation and hydrogen bonding of ceramide and their implication on membrane stability and permeability. *Biochimica et Biophysica Acta (BBA) - Biomembranes*, 455(2), pp.433–451.

Pasinetti, G.M., Johnson, S.A., Rozovsky, I., Lampert-Etchells, M., Morgan, D.G., Gordon, M.N., Morgan, T.E., Willoughby, D. & Finch, C.E., 1992. Complement C1qB and C4 mRNAs responses to lesioning in rat brain. *Experimental Neurology*, 118(2), pp.117–125.

Pasquini, L.A., Millet, V., Hoyos, H.C., Giannoni, J.P., Croci, D.O., Marder, M., Liu, F.T., Rabinovich, G.A. & Pasquini, J.M., 2011. Galectin-3 drives oligodendrocyte differentiation to control myelin integrity and function. *Cell Death and Differentiation*, 18(11), pp.1746–56.

Patzig, J. et al., 2011. Quantitative and Integrative Proteome Analysis of Peripheral Nerve Myelin Identifies Novel Myelin Proteins and Candidate Neuropathy Loci. *The Journal of Neuroscience*, 31(45), pp.16369–16386.

Pearce, M.M.P., Wormer, D.B., Wilkens, S. & Wojcikiewicz, R.J.H., 2009. An endoplasmic reticulum (ER) membrane complex composed of SPFH1 and SPFH2 mediates the ER-associated degradation of inositol 1,4,5-trisphosphate receptors. *The Journal of Biological Chemistry*, 284(16), pp.10433–45.

Peluso, J.J., Liu, X., Saunders, M.M., Claffey, K.P. & Phoenix, K., 2008. Regulation of ovarian cancer cell viability and sensitivity to cisplatin by progesterone receptor membrane component-1. *The Journal of Clinical Endocrinology and Metabolism*, 93(5), pp.1592–9.

Peluso, J.J., Romak, J. & Liu, X., 2008. Progesterone receptor membrane component-1 (PGRMC1) is the mediator of progesterone's antiapoptotic action in spontaneously immortalized granulosa cells as revealed by PGRMC1 small interfering ribonucleic acid treatment and functional analysis of PGRMC1 m. *Endocrinology*, 149(2), pp.534–43.

Perry, R.J. & Ridgway, N.D., 2006. Oxysterol-binding protein and vesicle-associated membrane protein-associated protein are required for sterol-dependent activation of the ceramide transport protein. *Molecular Biology of the Cell*, 17(6), pp.2604–16.

Poliak, S. & Peles, E., 2003. The local differentiation of myelinated axons at nodes of Ranvier. *Nature Reviews Neuroscience*, 4(12), pp.968–980.

Potter, K. a, Kern, M.J., Fullbright, G., Bielawski, J., Scherer, S.S., Yum, S.W., Li, J.J., Cheng, H., Han, X., Venkata, J.K., Khan, P.A.A., Rohrer, B. & Hama, H., 2011. Central nervous system dysfunction in a mouse model of FA2H deficiency. *Glia*, 59(7), pp.1009–21.

Pyne, S. & Pyne, N.J., 2000. Sphingosine 1-phosphate signalling in mammalian cells. *The Biochemical Journal*, 349(Pt 2), pp.385–402.

Qiao, F., Atkinson, C., Song, H., Pannu, R., Singh, I. & Tomlinson, S., 2006. Complement plays an important role in spinal cord injury and represents a therapeutic target for improving recovery following trauma. *The American Journal of Pathology*, 169(3), pp.1039–47.

Rappsilber, J., Mann, M. & Ishihama, Y., 2007. Protocol for micro-purification, enrichment, pre-fractionation and storage of peptides for proteomics using StageTips. *Nature Protocols*, 2(8), pp.1896–906.

Raychaudhuri, S. & Prinz, W.A., 2010. The diverse functions of oxysterol-binding proteins. *Annual Review of Cell and Developmental Biology*, 26, pp.157–77.

Readhead, C. & Hood, L., 1990. The dysmyelinating mouse mutations shiverer (shi) and myelin deficient (shimld). *Behavior Genetics*, 20(2), pp.213–34.

Rogers, J., Cooper, N.R., Webster, S., Schultz, J., McGeer, P.L., Styren, S.D., Civin, W.H., Brachova, L., Bradt, B. & Ward, P., 1992. Complement activation by beta-amyloid in Alzheimer disease. *Proceedings of the National Academy of Sciences of the United States of America*, 89(21), pp.10016–20.

Roux, K.J., Kim, D.I., Raida, M. & Burke, B., 2012. A promiscuous biotin ligase fusion protein identifies proximal and interacting proteins in mammalian cells. *The Journal of Cell Biology*, 196(6), pp.801–810.

Rozanas, C.R. & Loyland, S.M., 2008. Capabilities using 2-D DIGE in proteomics research : the new gold standard for 2-D gel electrophoresis. *Methods in Molecular Biology (Clifton, N.J.)*, 441, pp.1–18.

Rupps, R., Hukin, J., Balicki, M., Mercimek-Mahmutoglu, S., Rolfs, A. & Dias, C., 2013. Novel Mutations in FA2H-Associated Neurodegeneration: An Underrecognized Condition? *Journal of Child Neurology*, 28(11), pp.1500–1504.

Sakai, N., 2009. Pathogenesis of leukodystrophy for Krabbe disease: molecular mechanism and clinical treatment. *Brain & Development*, 31(7), pp.485–7.

Schmidt, T.G.M., Batz, L., Bonet, L., Carl, U., Holzapfel, G., Kiem, K., Matulewicz, K., Niermeier, D., Schuchardt, I. & Stanar, K., 2013. Development of the Twin-Strep-tag® and its application for purification of recombinant proteins from cell culture supernatants. *Protein Expression and Purification*, 92(1), pp.54–61.

Schneider, S.A. & Bhatia, K.P., 2010. Three Faces of the Same Gene : FA2H Links Neurodegeneration with Brain Iron Accumulation , Leukodystrophies , and Hereditary Spastic Paraplegias. *Annals of Neurology*, pp.575–577.

Schulze, H. & Sandhoff, K., 2011. Lysosomal lipid storage diseases. *Cold Spring Harbor Perspectives in Biology*, 3(6), p.a004804–.

Shanklin, J. & Cahoon, E.B., 1998. Desaturation and related modifications of fatty acids. *Annual Review of Plant Physiology and Plant Molecular Biology*, 49, pp.611–641.

Shen, Y., Lue, L.-F., Yang, L.-B., Roher, A., Kuo, Y.-M., Strohmeyer, R., Goux, W.J., Lee, V., Johnson, G.V.., Webster, S.D., Cooper, N.R., Bradt, B. & Rogers, J., 2001. Complement activation by neurofibrillary tangles in Alzheimer's disease. *Neuroscience Letters*, 305, pp.165–168.

Shen, Y., Yang, L. & Li, R., 2013. What does complement do in Alzheimer's disease? Old molecules with new insights. *Translational Neurodegeneration*, 2(1), p.21.

Siegel, G.M.D., Albers, R.W.P.., Brady, S.P.., Price, D.M.D. & Neurochem, A.S. for, 2005. *Basic Neurochemistry: Molecular, Cellular and Medical Aspects* 7th ed., Academic Press.

Simons, M. & Trotter, J., 2007. Wrapping it up : the cell biology of myelination. *Current Opinion in Neurobiology*, pp.533–540.

Singh, A., Kong, Q., Luo, X., Petersen, R.B., Meyerson, H. & Singh, N., 2009. Prion Protein (PrP) Knock-Out Mice Show Altered Iron Metabolism: A Functional Role for PrP in Iron Uptake and Transport J. El Khoury, ed. *PLoS ONE*, 4(7), p.e6115.

Spillantini, M.G. & Goedert, M., 2013. Tau pathology and neurodegeneration. *Lancet Neurology*, 12(6), pp.609–22.

Steele, A.D., Emsley, J.G., Ozdinler, P.H., Lindquist, S. & Macklis, J.D., 2006. Prion protein (PrPc) positively regulates neural precursor proliferation during developmental and adult mammalian neurogenesis. *Proceedings of the National Academy of Sciences*, 103(9), pp.3416–3421.

Suchanek, M., Radzikowska, A. & Thiele, C., 2005. Photo-leucine and photo-methionine allow identification of protein-protein interactions in living cells. *Nature Methods*, 2(4), pp.261–7.

Swain, E., Baudry, K., Stukey, J., McDonough, V., Germann, M. & Nickels, J.T., 2002. Sterol-dependent regulation of sphingolipid metabolism in Saccharomyces cerevisiae. *The Journal of Biological Chemistry*, 277(29), pp.26177–84.

Szaro, B.G. & Strong, M.J., 2010. Post-transcriptional control of neurofilaments: New roles in development, regeneration and neurodegenerative disease. *Trends in Neurosciences*, 33(1), pp.27–37.

Szulc, Z.M., Bai, A., Bielawski, J., Mayroo, N., Miller, D.E., Gracz, H., Hannun, Y.A. & Bielawska, A., 2010. Synthesis, NMR characterization and divergent biological actions of 2'-hydroxy-ceramide/dihydroceramide stereoisomers in MCF7 cells. *Bioorganic & Medicinal Chemistry*, 18(21), pp.7565–79.

Tafesse, F.G., Ternes, P. & Holthuis, J.C.M., 2006. The multigenic sphingomyelin synthase family. *The Journal of Biological Chemistry*, 281(40), pp.29421–5.

Tani, M. & Kuge, O., 2010. Requirement of a specific group of sphingolipid-metabolizing enzyme for growth of yeast Saccharomyces cerevisiae under impaired metabolism of glycerophospholipids. *Molecular Microbiology*, 78(2), pp.395–413.

Taylor, C.M., Marta, C.B., Claycomb, R.J., Han, D.K., Rasband, M.N., Coetzee, T. & Pfeiffer, S.E., 2004. Proteomic mapping provides powerful insights into functional myelin biology. *Proceedings of the National Academy of Sciences of the United States of America*, 101(13), pp.4643–4648.

Taylor, D.R., Whitehouse, I.J. & Hooper, N.M., 2009. Glypican-1 mediates both prion protein lipid raft association and disease isoform formation. *PLoS Pathogens*, 5(11), p.e1000666.

Tonelli, A., D'Angelo, M.G., Arrigoni, F., Brighina, E., Arnoldi, A., Citterio, A., Bresolin, N. & Bassi, M.T., 2012. Atypical adult onset complicated spastic paraparesis with thin corpus callosum in two patients carrying a novel FA2H mutation. *European journal of neurology : the official journal of the European Federation of Neurological Societies*, 19(11), pp.e127–9.

Uchida, Y., Hama, H., Alderson, N.L., Douangpanya, S., Wang, Y., Crumrine, D. a, Elias, P.M. & Holleran, W.M., 2007. Fatty acid 2-hydroxylase, encoded by FA2H, accounts for differentiation-associated increase in 2-OH ceramides during keratinocyte differentiation. *The Journal of Biological Chemistry*, 282(18), pp.13211–9.

Vasilescu, J., Guo, X. & Kast, J., 2004. Identification of protein-protein interactions using in vivo cross-linking and mass spectrometry. *Proteomics*, pp.3845–3854.

Wang, Y., Ballar, P., Zhong, Y., Zhang, X., Liu, C., Zhang, Y.-J., Monteiro, M.J., Li, J. & Fang, S., 2011. SVIP induces localization of p97/VCP to the plasma and lysosomal membranes and regulates autophagy. *PloS ONE*, 6(8), p.e24478.

Wendler, A. & Wehling, M., 2013. PGRMC2, a yet uncharacterized protein with potential as tumor suppressor, migration inhibitor, and regulator of cytochrome P450 enzyme activity. *Steroids*, 78(6), pp.555–8.

Werner, H.B., Kuhlmann, K., Shen, S., Uecker, M., Schardt, A., Dimova, K., Orfaniotou, F., Dhaunchak, A., Brinkmann, B.G., Mobius, W., Guarente, L., Casaccia-Bonnefil, P., Jahn, O. & Nave, K.-A., 2007. Proteolipid Protein Is Required for Transport of Sirtuin 2 into CNS Myelin. *Journal of Neuroscience*, 27(29), pp.7717–7730.

Wu, J., Peng, D., Voehler, M., Sanders, C.R. & Li, J., 2013. Structure and expression of a novel compact myelin protein - small VCP-interacting protein (SVIP). *Biochemical and Biophysical Research Communications*, 440(1), pp.173–8.

Wu, W.W., Wang, G., Baek, S.J. & Shen, R.-F., 2006. Comparative study of three proteomic quantitative methods, DIGE, cICAT, and iTRAQ, using 2D gel- or LC-MALDI TOF/TOF. *Journal of Proteome Research*, 5(3), pp.651–8.

Xu, J., Zeng, C., Chu, W., Pan, F., Rothfuss, J.M., Zhang, F., Tu, Z., Zhou, D., Zeng, D., Vangveravong, S., Johnston, F., Spitzer, D., Chang, K.C., Hotchkiss, R.S., Hawkins, W.G., Wheeler, K.T. & Mach, R.H., 2011. Identification of the PGRMC1 protein complex as the putative sigma-2 receptor binding site. *Nature Communications*, 2, p.380.

Yoshikawa, F., Sato, Y., Tohyama, K., Akagi, T., Hashikawa, T., Nagakura-Takagi, Y., Sekine, Y., Morita, N., Baba, H., Suzuki, Y., Sugano, S., Sato, A. & Furuichi, T., 2008. Opalin, a transmembrane sialylglycoprotein located in the central nervous system myelin paranodal loop membrane. *The Journal of Biological Chemistry*, 283(30), pp.20830–40.

Yuan, A., Rao, M. V, Veeranna & Nixon, R.A., 2012. Neurofilaments at a glance. *Journal of Cell Science*, 125(Pt 14), pp.3257–63.

Zhang, H., Wu, J. & Zhu, J., 2010. The role of apolipoprotein E in Guillain-Barré syndrome and experimental autoimmune neuritis. *Journal of Biomedicine & Biotechnology*, 2010, p.357412.

Zhang, H., Wu, L.-M. & Wu, J., 2011. Cross-talk between apolipoprotein E and cytokines. *Mediators of Inflammation*, 2011, p.949072.

Zöller, I., Meixner, M., Hartmann, D., Büssow, H., Meyer, R., Gieselmann, V. & Eckhardt, M., 2008. Absence of 2-hydroxylated sphingolipids is compatible with normal neural development but causes late-onset axon and myelin sheath degeneration. *The Journal of Neuroscience*, 28(39), pp.9741–54.

7 Figure Index

8 Table Index

9 Abbreviations

ACN	acetonitrile	MBP	myelin basic protein
ACSL3	acyl-CoA synthetase long-chain 3	MCFD2	multiple coagulation factor deficiency 2
ALDH3A2	aldehyde dehydrogenase 3 family, member A2	mFA2H	murine fatty acid 2-hydroxylase
ApoE	apolipoprotein E	NF-H	neurofilament heavy
BHK	baby hamster kidney cells	MS	mass spectrometry
BiFC	bimolecular fluorescence complementation	ON	overnight
BioID	proximity-dependent protein biotinylation and identification	P0	myelin protein P0
BirA*	constitutively active *E.coli* biotin ligase	PAGE	polyacrylamide gel electrophoresis
C1qb	complement C1q subcomponent subunit B	PBS	phosphate buffered saline
C4b	complement 4-B	PCR	polymerase chain reaction
Cer	ceramide	PFA	paraformaldehyde
CerS	ceramide synthase	PGRMC1	progesterone receptor membrane component 1
CERT	ceramide transfer protein	PLP	myelin proteolipid protein
CHO	chinese hamster ovary cells	PM	plasma membrane
CGT	ceramide galactosyl transferase	PMP2	myelin P2 protein
CNP	2',3'-cyclic-nucleotide 3'-phosphodiesterase	PNS	peripheral nervous system
CNS	central nervous system	Prp^C	prion protein
ddH_2O	double destilled water	PPI	protein-protein interaction(s)
DAPI	4',6-diamidino-2-phenylindole	PRX	periaxin
DMEM	Dulbecco's modified Eagle's medium	PVDF	polyvinylidene fluoride
DMSO	dimethyl sulfoxide	RT	room temperature
DTT	dithiothreitol	SACM1L	SAC1 suppressor of actin mutations 1-like (yeast)
EDTA	ethylenediaminetetraacetic acid	SAG	Schwann cell membrane glycoprotein
ER	endoplasmic reticulum	SDS	sodium dodecyl sulfate
ERAD	ER-associated degradation	SILAC	stable isotope labeling by amino acids in cell culture
ERGIC53	ER-Golgi intermediate compartment 53 kDa protein	SPE	solid phase extraction
FA	formic acid	SM	sphingomyelin
FA2H	fatty acid 2-hydroxylase	SMPD	sphingomyelin phosphodiesterase
FCS	fetal calf serum	SN	supernatant
GalCer	galactosylceramide	SPTLC	serine palmitoyltransferase
GFAP	glial fibrillary acidic protein	StageTips	stop-and-go-extraction tips
GlcCer	glucosylceramide	TAE	Tris-acetate-EDTA buffer
GSL	glycosphingolipid	TBS	TRIS buffered saline
HEK	human embryonic kidney cells	TBS-T	TRIS buffered saline + Tween 20
HeLa	Henrietta Lacks cells (immortal cell line)	TEAB	triethylammonium bicarbonate buffer
IP	immunoprecipitation	TFA	trifluoroacetic acid
KO	knock-out	TMT	tandem mass tag
LB	lysogeny broth	TOF	time of flight
MAG	myelin-associated glycoprotein	ULCFA	ultra long-chain fatty acids
MALDI	matrix-assisted laser desorption/ionization	VLCFA	very long-chain fatty acids
MAPT	microtubule-associated protein tau	WB	Western blot

10 Supplements

10.1 Plasmid maps

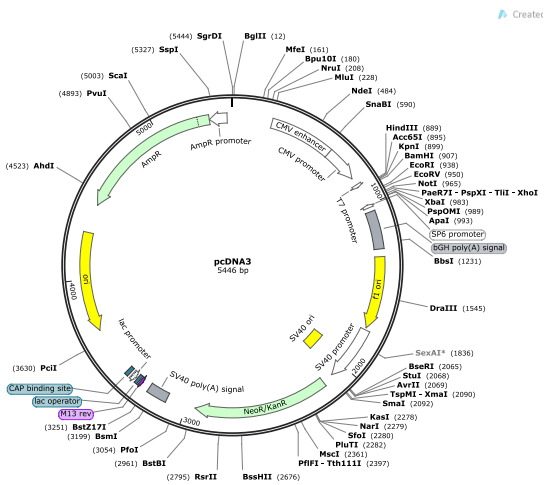

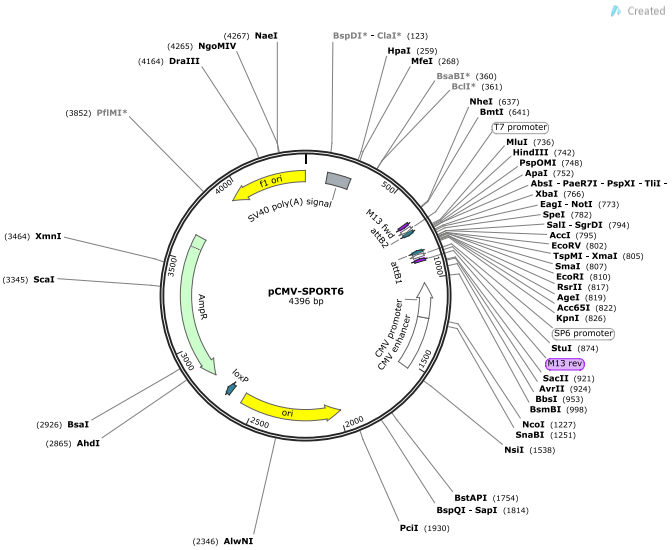

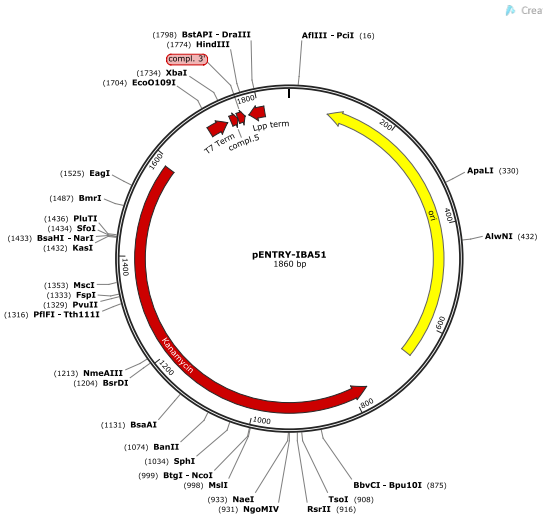

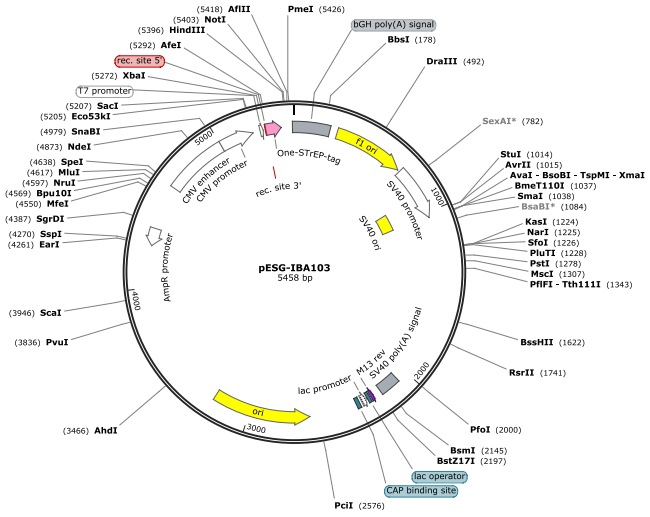

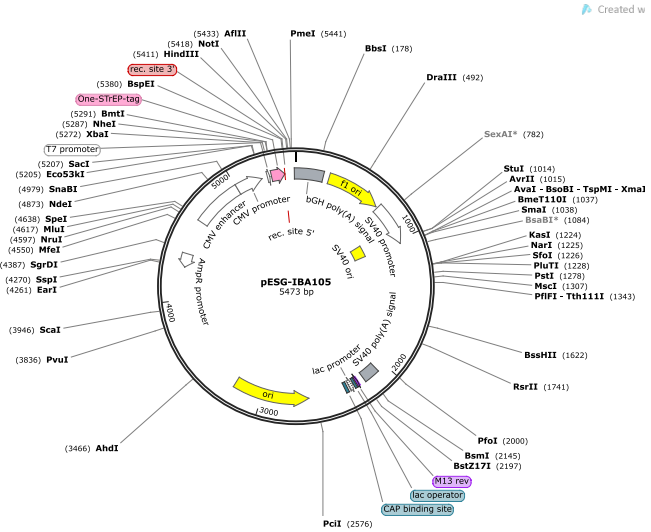
pESG-IBA105
5473 bp
CMV enhancer
CMV promoter
rec. site 5'
f1 ori
bGH poly(A) signal
SV40 Promoter
SV40 ori
SV40 poly(A) signal
lac promoter
ori
AmpR promoter
rec. site 3'
One-STrEP-tag
T7 promoter
(5433) AflII
(5418) NotI
(5411) HindIII
(5380) BspEI
(5291) BmtI
(5287) NheI
(5272) XbaI
(5207) SacI
(5205) Eco53kI
(4979) SnaBI
(4873) NdeI
(4638) SpeI
(4617) MluI
(4597) NruI
(4550) MfeI
(4387) SgrDI
(4270) SspI
(4261) EarI
(3946) ScaI
(3836) PvuI
(3466) AhdI
PmeI (5441)
BbsI (178)
DraIII (492)
SexAI* (782)
StuI (1014)
AvrII (1015)
AvaI - BsoBI - TspMI - XmaI
BmeT110I (1037)
SmaI (1038)
BsaBI* (1084)
KasI (1224)
NarI (1225)
SfoI (1226)
PluTI (1228)
PstI (1278)
MscI (1307)
PflFI - Tth111I (1343)
BssHII (1622)
RsrII (1741)
PfoI (2000)
BsmI (2145)
BstZ17I (2197)
M13 rev
lac operator
CAP binding site
PciI (2576)

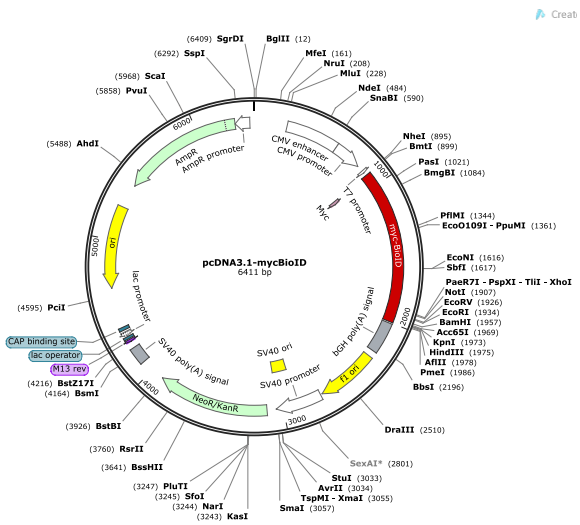
pcDNA3.1-mycBioID
6411 bp
CMV enhancer
CMV promoter
AmpR promoter
T7 promoter
Myc
myc-BioID
bGH poly(A) signal
f1 ori
SV40 ori
SV40 promoter
SV40 poly(A) signal
NeoR/KanR
lac promoter
ori
CAP binding site
lac operator
M13 rev
(6409) SgrDI
BglII (12)
(6292) SspI
MfeI (161)
NruI (208)
MluI (228)
(5968) ScaI
(5858) PvuI
NdeI (484)
SnaBI (590)
(5488) AhdI
NheI (895)
BmtI (899)
PasI (1021)
BmgBI (1084)
PflMI (1344)
EcoO109I - PpuMI (1361)
EcoNI (1616)
SbfI (1617)
PaeR7I - PspXI - TliI - XhoI
NotI (1907)
EcoRV (1926)
EcoRI (1934)
BamHI (1957)
Acc65I (1969)
KpnI (1973)
HindIII (1975)
AflII (1978)
PmeI (1986)
BbsI (2196)
DraIII (2510)
SexAI* (2801)
StuI (3033)
AvrII (3034)
TspMI - XmaI (3055)
SmaI (3057)
(3243) KasI
(3244) NarI
(3245) SfoI
(3247) PluTI
(3641) BssHII
(3760) RsrII
(3926) BstBI
(4164) BsmI
(4216) BstZ17I
(4595) PciI

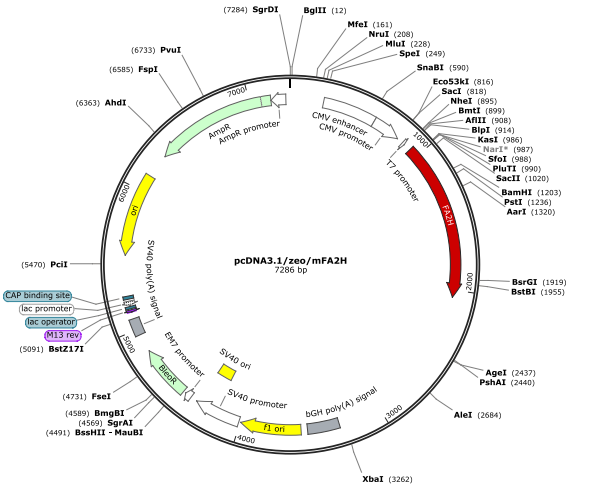
pcDNA3.1/zeo/mFA2H
7286 bp
AmpR promoter
CMV enhancer
CMV promoter
T7 promoter
mFA2H
bGH poly(A) signal
f1 ori
SV40 ori
SV40 promoter
SV40 poly(A) signal
EM7 promoter
BleoR
lac promoter
lac operator
M13 rev
CAP binding site
(7284) SgrDI
BglII (12)
MfeI (161)
NruI (208)
MluI (228)
SpeI (249)
SnaBI (590)
Eco53kI (816)
SacI (818)
NheI (895)
BmtI (899)
AflII (908)
BlpI (914)
KasI (986)
NarI* (987)
SfoI (988)
PluTI (990)
SacII (1020)
BamHI (1203)
PstI (1236)
AarI (1320)
BsrGI (1919)
BstBI (1955)
AgeI (2437)
PshAI (2440)
AleI (2684)
XbaI (3262)
(4491) BssHII - MauBI
(4569) SgrAI
(4589) BmgBI
(4731) FseI
(5091) BstZ17I
(5470) PciI
(6363) AhdI
(6585) FspI
(6733) PvuI

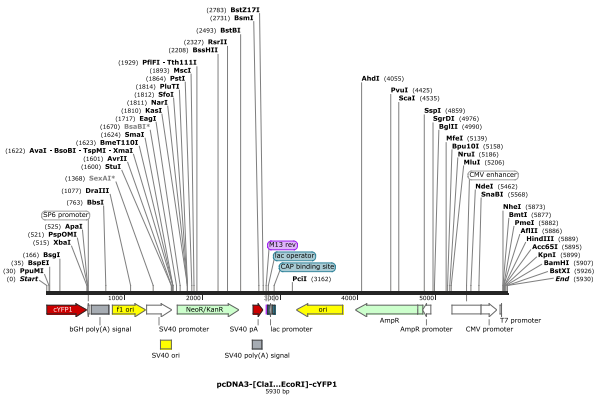
pcDNA3-[ClaI...EcoRI]-cYFP1
5930 bp
cYFP1
SP6 promoter
Start
BspEI
BsgI
PpuMI
ApaI
PspOMI
XbaI
BbsI
DraIII
SexAI*
StuI
AvaI - BsoBI - TspMI - XmaI
BmeT110I
SmaI
EagI
NarI
KasI
SfoI
PluTI
PstI
MscI
PflFI - Tth111I
BssHII
BstBI
BsmI
BstZ17I
AhdI
PvuI
ScaI
SspI
SgrDI
BglII
MfeI
Bpu10I
NruI
MluI
CMV enhancer
NdeI
SnaBI
NheI
BmtI
PmeI
AflII
HindIII
Acc65I
KpnI
BamHI
BstXI
End
M13 rev
lac operator
CAP binding site
PciI
bGH poly(A) signal
f1 ori
NeoR/KanR
SV40 promoter
SV40 pA
lac promoter
ori
AmpR
AmpR promoter
CMV promoter
T7 promoter
SV40 ori
SV40 poly(A) signal

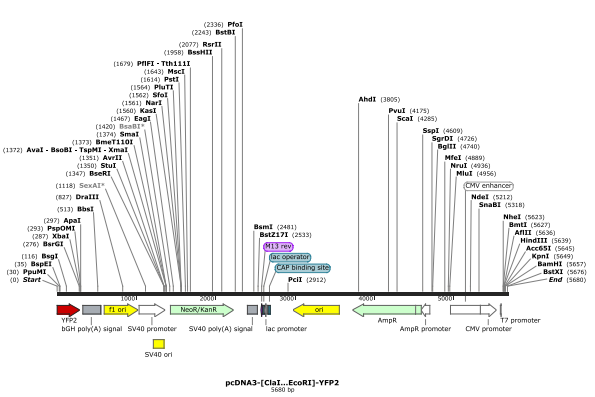
pcDNA3-[ClaI...EcoRI]-YFP2
5680 bp
YFP2
bGH poly(A) signal
f1 ori
NeoR/KanR
SV40 promoter
SV40 poly(A) signal
lac promoter
ori
AmpR
AmpR promoter
CMV promoter
T7 promoter
SV40 ori
M13 rev
lac operator
CAP binding site
PciI
BsmI
BstZ17I
AhdI
PvuI
ScaI
SspI
SgrDI
BglII
MfeI
NruI
MluI
CMV enhancer
NdeI
SnaBI
NheI
BmtI
AflII
HindIII
Acc65I
KpnI
BamHI
BstXI
End

10.2 Amino acid sequences

mFA2H

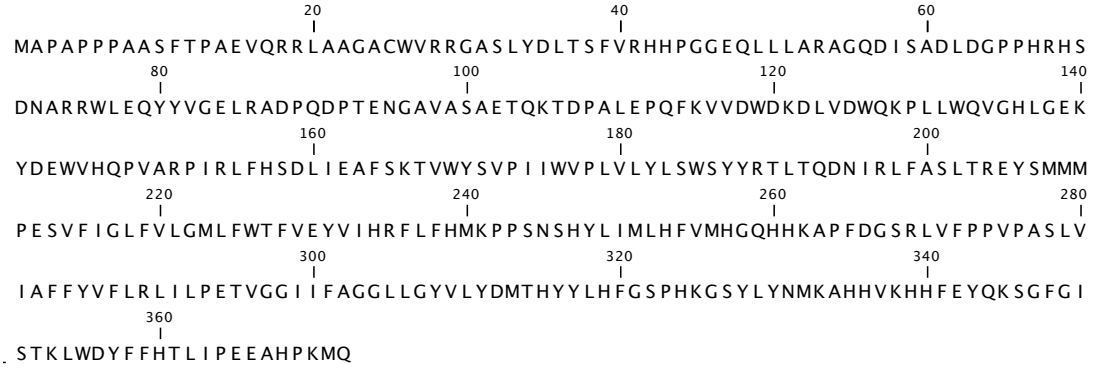

hPGRMC1

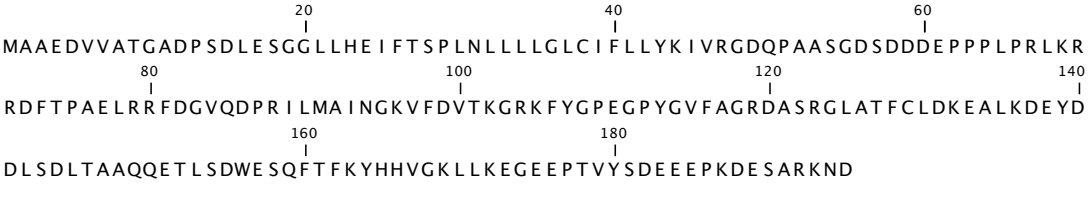

mCerS2

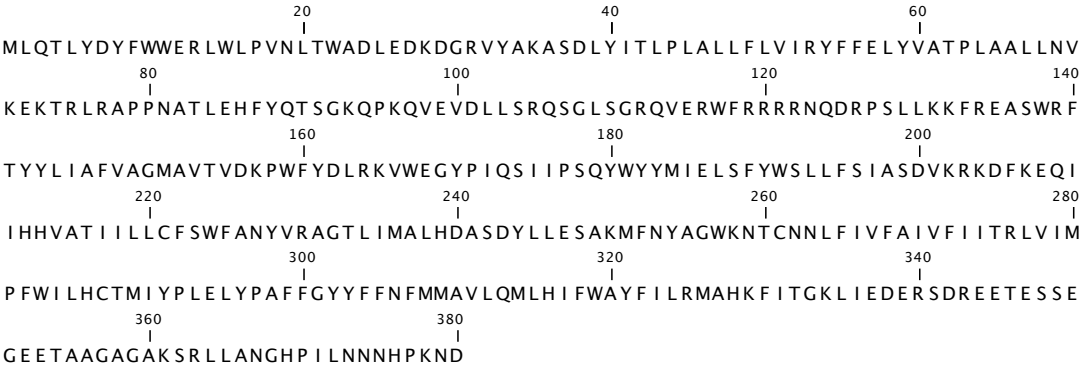

hSPTLC1

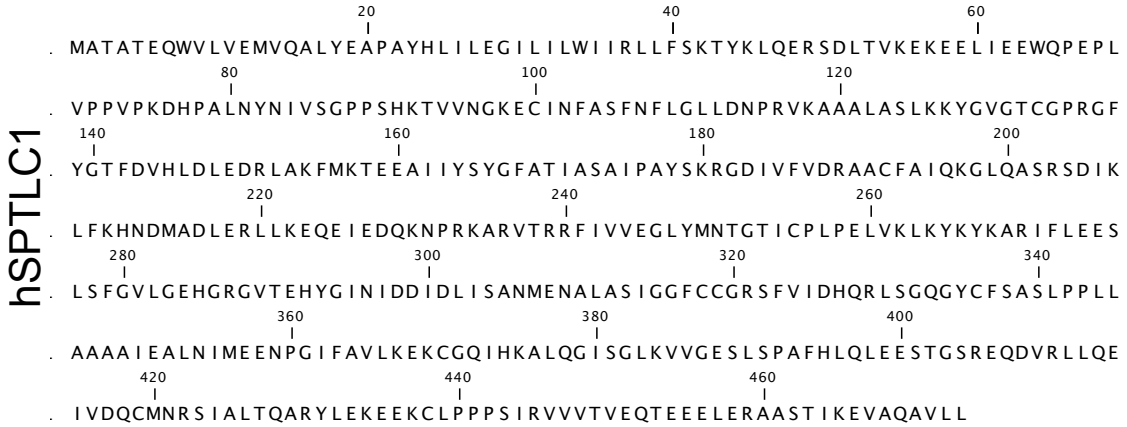


hACSL3
20
40
60
MNNHVSSKPSTMKLKHTINPILLYFIHFLISLYTILTYIPFYFFSESRQEKSNRIKAKPVNSKPDSAYRS
80
100
120
140
VNSLDGLASVLYPGCDTLDKVFTYAKNKFKNKRLLGTREVLNEEDEVQPNGKIFKKVILGQYNWLSYEDV
160
180
200
FVRAFNFGNGLQMLGQKPKTNIAIFCETRAEWMIAAQACFMYNFQLVTLYATLGGPAIVHALNETEVTNI
220
240
260
280
ITSKELLQTKLKDIVSLVPRLRHIITVDGKPPTWSEFPKGIIVHTMAAVEALGAKASMENQPHSKPLPSD
300
320
340
IAVIMYTSGSTGLPKGVMISHSNIIAGITGMAERIPELGEEDVYIGYLPLAHVLELSAELVCLSHGCRIG
360
380
400
420
YSSPQTLADQSSKIKKGSKGDTSMLKPTLMAAVPEIMDRIYKNVMNKVSEMSSFQRNLFILAYNYKMEQI
440
460
480
SKGRNTPLCDSFVFRKVRSLLGGNIRLLLCGGAPLSATTQRFMNICFCCPVGQGYGLTESAGAGTISEVW
500
520
540
560
DYNTGRVGAPLVCCEIKLKNWEEGGYFNTDKPHPRGEILIGGQSVTMGYYKNEAKTKADFFEDENGQRWL
580
600
620
CTGDIGEFEPDGCLKIIDRKKDLVKLQAGEYVSLGKVEAALKNLPLVDNICAYANSYHSYVIGFVVPNQK
640
660
680
700
ELTELARKKGLKGTWEELCNSCEMENEVLKVLSEAAISASLEKFEIPVKIRLSPEPWTPETGLVTDAFKL
720
KRKELKTHYQADIERMYGRK

10.3 Data files (DVD)

In the printed version of this thesis an envelope containing optical data media (DVDs) should be found here. They contain the following supplemental data files:

- Unprocessed MaxQuant result text files (txt-format)
- Processed protein groups lists (xxls-format)
- Annotation analysis result lists (xxls-format)

10.4 Acknowledgements

Conducting the research presented in this thesis was very exiting and fun, but certainly sometimes also hard and even frustrating. Still I was very lucky to have the constant encouragement and support of many people, which I want to thank here in detail.

First of all I my greatest amount of gratitude goes to my thesis supervisor PD. Dr. Matthias Eckhardt for giving me the opportunity to work on my thesis subjects in his workgroup. Matthias was always supportive of my ideas and gave me valuable suggestions how to process further. Despite limited time and other restrictions, he was constantly open for interesting and fruitful discussion, sometimes even lasting for hours.

Furthermore, I also feel especially grateful to Prof. Dr. Michael Hoch, from the LIMES-Institute, for being my secondary thesis supervisor. Additionally I want to thank him for his key role in the successful extension of the SFB645, throughout which my research was founded.

This said I also want to thank the DFG for the generous funding of my research provided through SFB645. Without it this thesis would not have been accomplished.

In addition, I like to express my gratitude to Prof. Dr. Volkmar Gieselmann, the head of the Arbeitskreis our workgroup is part of, for his indispensable support and advice.

Special thanks go also to Dr. Dominic Winter and Dr. Marc Sylvester for their excellent knowledge and advise in everything concerning mass spectrometry. I really learned a lot from them and we had many exciting, but also funny discussions.

In this regard I want thank all the superb colleagues in the AG Eckhardt, but also the whole Gieselmann group. We really had a superb time together both in science and in everyday life. I will really miss you all and the friendly working atmosphere we created together. Concretely my thanks go to: Frank “Pezzie” Matthes, Asis(i)a Saile, Isabell Zech, Lena Maier, Klaudia “Claudine” Brysch, Lihua Wang-Eckhardt, Tilman Schuster, Axel Stein, Debora Kaminski (+ Tim & Constantin), Annika Böckenhoff, Carmen Schoor, Sheeva Ahmadi, Alireza Dehghani and Markus Gödderz.

Moreover, for excellent technical and administrative support and more, I wholeheartedly want to thank Norbert Rösel, Karola Ragut, Elvira Thiessen, Claudia Wohlenberg and Heidi Simonis.

Finally I want to thank all my friends and my family. Especially my parents, which have always supported me through all my life and encouraged me to study the subject I really like by heart. They always believed in me and I am confident that this thesis proofs them right. Sadly my father passed

away two years ago and thus could not see the completion of this thesis. Still, I am sure he would be proud. In addition, I also want to thank my “little” brother Tobias.

Last but not least, my deepest gratitude goes to a very special person: Wilma. Without your love and relentless support this thesis would not exist today. I am very lucky to have you and the “second family” you brought into my life.

11 Declaration

I hereby declare that the whole of this Ph.D. thesis (Dissertation) titled “Consequence of Fatty Acid 2-Hydroxylase Deficiency and FA2H Interaction Partners Revealed by Proteomic Analyses” was carried out by me in the Institut für Biochemie und Molekularbiologie (IBMB) under the supervision of PD. Dr. M. Eckhardt. It is my own work, except where explicitly stated otherwise in the text or in the bibliography.

This work is submitted to the Mathematisch-Naturwissenschaftlichen Fakultät of the Rheinische Friedrich-Wilhelms Universität Bonn as a requirement for being awarded a Dr. rer. nat. degree in Molekulare Biomedizin. I declare that it has not been submitted in whole, or in part, for any other degree.

Bonn, February 13, 2015

_____

Robert Hardt